Forschungszentrum Karlsruhe
Technik und Umwelt

Wissenschaftliche Berichte
FZKA 6266

Proceedings of the Workshop "Monte Carlo Methods and Models for Applications in Energy and Technology"

Forschungszentrum Karlsruhe, May 12 – 14, 1998

Edited by U. Fischer

Institut für Neutronenphysik und Reaktortechnik
Projekt Kernfusion

März 1999

Forschungszentrum Karlsruhe

Technik und Umwelt
Wissenschaftliche Berichte

FZKA 6266

Proceedings of the Workshop „Monte Carlo Methods and Models for Applications in Energy and Technology“ Forschungszentrum Karlsruhe, May 12-14, 1998

Edited by U. Fischer
Institut für Neutronenphysik und Reaktortechnik
Projekt Kernfusion

Forschungszentrum Karlsruhe GmbH, Karlsruhe

1999

Als Manuskript gedruckt

Forschungszentrum Karlsruhe GmbH
Postfach 3640, 76021 Karlsruhe

Mitglied der Hermann von Helmholtz-Gemeinschaft
Deutscher Forschungszentren (HGF)

ISSN 0947-8620

Abstract

The workshop on "Monte Carlo Methods and Models for Applications in Energy and Technology" was held at Forschungszentrum Karlsruhe, May 12-14, 1998, with the objective to present an overview of the current research and development in Monte Carlo simulations for applications in nuclear and environmental technology areas and thereby provide the basis for the elaboration of a future European Monte Carlo research network. This report provides an overview of the workshop as well as a full documentation of the contributed presentations. It includes also a proposal for a network frame programme elaborated by J. Devooght, ULB, Brussels, on the basis of the workshop outcome.

Proceedings des Workshops "Monte Carlo Methods and Models for Applications in Energy and Technology" , Forschungszentrum Karlsruhe, 12. – 14. Mai 1998.

Zusammenfassung

Der Workshop "Monte Carlo Methods and Models for Applications in Energy and Technology" wurde vom 12. bis 14. Mai 1998 am Forschungszentrum Karlsruhe mit der Zielsetzung abgehalten, den gegenwärtigen Stand der Forschung und Entwicklung von Monte-Carlo-Simulationsverfahren für Anwendungen in Bereichen der Nuklear- und Umwelttechnologie darzustellen und damit die Grundlage für die Ausarbeitung eines künftigen Europäischen Monte-Carlo-Netzwerkes zu schaffen. Der Bericht gibt eine Übersicht zur Veranstaltung und beinhaltet eine vollständige Dokumentation der beigetragenen Präsentationen sowie einen von J. Devooght, ULB Brüssel, in der Folge ausgearbeiteten Vorschlag für ein Netzwerk-Rahmenprogramm.

CONTENTS

I. Introduction

The purpose of the Monte Carlo (MC) workshop was to bring together MC theorists, code developers and users to present an overview of the current research and development in Monte Carlo simulations with regard to applications in nuclear and environmental technology areas and thereby provide the basis for the elaboration of a potential European MC network co-operation.

The idea of establishing a European MC network was initiated in late 1996 by Kenneth Burn, ENEA Bologna, who organised a first network proposal with contributions from several EU and non-EU institutions. Although that first proposal has not been supported by the EU, it was felt by most of the participants that it would be beneficial to proceed with the network idea because

- There is an obvious need and interest by the user communities to further develop MC methods for various technology-oriented applications.
- Such a development can benefit very much from a well defined and co-ordinated co-operation between the various laboratories/institutions.
- Within a network there is the possibility of a close co-operation of MC theorists, code developers and users allowing for interaction and feedback.
- A network co-operation can be established in different ways, ranging from a collection of bilateral co-operations running in parallel (with almost no organisation) to a well organised net of multilateral co-operations with a clear overall objective.

The workshop on Monte Carlo Methods and Models for Applications in Energy and Technology held at Forschungszentrum Karlsruhe, May 12-14, 1998, has been organised with the main objective to discuss the possibility for establishing a European MC network co-operation, to define suitable development goals that could be achieved in such a framework and, finally, to agree on the further proceeding in developing the network.

The workshop has been organised in two parts:

- Part A: Presentations, to give an overview of current and future development lines in Monte Carlo theory, procedures and applications with regard to energy and technology related issues.
- Part B: Discussion, to define, on the basis of the given presentations, objectives for the further development, elaborate suitable development goals, procedures and recommendations for establishing a MC network co-operation.

A workshop web site has been made available at http:/inrwww.fzk.de/mc-workshop including all relevant information related to the workshop and displaying the submitted abstracts of the presentations as well.

II. Agenda

Tuesday, May 12, 1998

8.30	Pick-up at hotel	
9.00	Opening	U. Fischer

Part A: Presentations

Monte Carlo Method Development

9. 15	The Double Randomisation Technique in Monte Carlo Simulations	K. Sabelfeld
	The Direct Statistical Approach: Past, Present and Future	K. Burn

Implementation, Code Development & Interfaces

	On Geometry Generation for Monte Carlo Particle Transport Using CAD Systems	H. Tsige-Tamirat
	Monte Carlo Calculation of Point-Detector Sensitivities to Material Parameters	R. Perel
	Discussion of Methods for the Assessment of Uncertainties in Monte Carlo Particle Transport Calculations	B. Siebert
12.30	Lunch	

Applications in Energy & Technology

13.30	***Reliability Analysis***	
	Monte Carlo Methods in Dynamic Reliability	P. Labeau
	Weight Updating in Forced Monte Carlo Approach to Dynamic PSA	E. Zio
	Reactor & Shielding Analysis	
	Influence of the Photoneutrons on the Kinetics of Beryllium Reflected Core of the Budapest Research Reactor	G. Hordosy
	Application of MCNP to Accelerator Shielding Analysis	J. Rodenas
	Radio Nuclide Transport	
	Monte Carlo Simulation of Groundwater Contaminant Transport	E. Zio
	Point and Surface Activities of Radionuclide Chains in Porous Media by a Non Analog Monte Carlo Simulation	O. Smidts
17.30	Transfer to hotels	

Wednesday, May 13, 1998

Applications in Energy & Technology (cont'd)

9.00	***Fusion Related Applications***	
	Monte Carlo Applications in Fusion Neutronics	U. Fischer
	Monte Carlo Sensitivity Analysis of Deep-Penetration Benchmarks to Iron Cross Sections	R. Perel
	A Review of the Applications of MCNP in Neutronics for Fusion Technology at ENEA FRASCATI	L. Petrizzi
	Other Nuclear Applications	
	Monte Carlo Approach to Modelling of a Detection System for Gamma-Sources Embedded in Metal Truck Loads	E. Zio
	Simulation of Ge-Detector Calibration Using MCNP Code	J. Rodenas
	Medical Applications	
	Conceptual Design of Epithermal Neutron Beam for BNCT in the TRIGA Reactor Thermalizing Column	M. Maucec
12.30	Lunch	
13.30	Monte Carlo Calculation of Neutron Photo-Production in Radiotherapy Linear Accelerator High-Z Components	C. Ongaro
	Other Applications	
	Monte Carlo Simulation for Low Energy Electron Transport	A. Dubus

Part B: Working Group Discussion

15.00	**Method development**
17.00	**Implementation, codes & interfaces**
17.30	Transfer to hotels
19.30	Dinner

Thursday, May 14, 1998

9.00	**Implementation, codes & interfaces (cont'd)**
10.30	**Application areas in energy & technology**
12.30	Lunch
13.30	**Summary discussion & conclusion**
14.30	**Adjourn**

III. Participants

Name	Affiliation	e-mail
K. Burn	ENEA - ERG FISS, Via Martiri di Monte Sole 4, I- 40129 Bologna,	kburn@bologna.enea.it
F. Calvino	Universitat Politècnica de Catalunya, Dept. De Fisica i Enginyeria Nuclear, ETSEIB-UPC, Diagonal 647, E-08028 Barcelona	calvino@fen.upc.es
G. Cortes	Universitat Politècnica de Catalunya, Dept. De Fisica i Enginyeria Nuclear, ETSEIB-UPC, Diagonal 647, E-08028 Barcelona	cortes@inte.upc.es
J. Devooght	Universite Libre de Bruxelles, Service de Metrologie Nucleaire (CP 165), Avenue F.D.Roosevelt 50, B-1050 Bruxelles	josee@metronu.ulb.ac.be
A. Dubus	Universite Libre de Bruxelles, Service de Metrologie Nucleaire (CP 165), Avenue F.D.Roosevelt 50, B-1050 Bruxelles	adubus@metronu.ulb.ac.be
U. Fischer	Forschungszentrum Karlsruhe, Institut für Neutronenphysik u. Reaktortechnik, P.O.Box 3640, D-76021 Karlsruhe	ulrich.fischer@inr.fzk.de
G. Hordosy	KFKI Atomic Energy Research Institute, Reactor Analysis Department, H-2525 Budapest 114, POB 49	hordosy@sunserv.kfki.hu
P. E. Labeau	Universite Libre de Bruxelles, Service de Metrologie Nucleaire (CP 165), Avenue F.D.Roosevelt 50, B-1050 Bruxelles	pelabeau@metronu.ulb.ac.be
D. Leichtle	Forschungszentrum Karlsruhe, Institut für Neutronenphysik u. Reaktortechnik, P.O.Box 3640, D-76021 Karlsruhe	dieter.leichtle@inr.fzk.de
M. Maucec	Jozef Stefan Institute, Reactor Physics Division, Jamova 39, 1000 Ljubljana, Slovenia	marko.maucec@ijs.si
C. Ongaro	Universita' di Torino, Dip. Fisica Sperimentale, Via P.Giuria 1, I-10125 Torino	ongaro@to.infn.it
R. Perel	The Hebrew University of Jerusalem, Racah Institute of Physics, 91904 Jerusalem	perel@vms.huji.ac.il
L. Petrizzi	CRE ENEA Frascati, FUS ING NEUT, Via E. Fermi 27, I- 00044 Frascati (Roma)	petrizzi@frasacati.enea.it
K. Sabelfeld	Weierstraß-Institut für Angewandte Analysis und Stochastik (WIAS), Mohrenstrasse 39, D-10117 Berlin	sabelfel@wias-berlin.de
B. Siebert	Physikalisch-Technische Bundesanstalt, Postfach 3345, D-38023 Braunschweig	bernd.siebert@ptb.de
O. F. Smidts	Universite Libre de Bruxelles, Service de Metrologie Nucleaire (CP 165), Avenue F.D.Roosevelt 50, B-1050 Bruxelles	osmidts@metronu.ulb.ac.be
J. Rodenas	Universidad Politecnica de Valencia , Dpto. Ingenieria Nuclear, Apartado 22012, E-46071 Valencia	jrodenas@iqn.upv.es
H. Tsige-Tamirat	Forschungszentrum Karlsruhe, Institut für Neutronenphysik u. Reaktortechnik, P.O.Box 3640, D-76021 Karlsruhe	tsige@inr.fzk.de
P. Wilson	Forschungszentrum Karlsruhe, Institut für Neutronenphysik u. Reaktortechnik, P.O.Box 3640, D-76021 Karlsruhe	paul.wilson@inr.fzk.de
E. Zio	Politecnico di Milano, Dipartimento di Ingegneria Nucleare, Via Ponzio 34/3, I-20133 Milano	zio@ipmce7.cesnef.polimi.it

IV. Working Group Discussions

The objective of the working group discussions was to develop ideas for a suitable future network co-operation, to define possible development goals that could be achieved through a network co-operation and, finally, to elaborate a scheme for a network application proposal in the framework of the EU TMR (Training and Mobility of Researchers) programme.

A. MC Network Proposal

The idea of developing a MC network co-operation with support from the EU originates from Kenneth Burn who organised a first network proposal for application in the framework of the TMR programme in late 1996. The proposal, integrated to the network subject area „Mathematics and Information Sciences", was finally not approved by the EU. Nevertheless it was felt by most of the participants that it would be beneficial to proceed with the network idea.

At the workshop, it was agreed that another trial should be undertaken to develop a MC network co-operation with possible support from the European TMR programme. Consequently, a second network proposal has to be elaborated in time to be ready for the next call for network proposals expected with the beginning of the 5th EU framework programme.

It was agreed that the overall objective of the network should be to develop novel MC techniques and tools that allow to solve „engineering physics problems" in medical, environmental and energy technology applications. Consequently, the network proposal is application-oriented, i. e. driven by the needs and goals for MC methods/techniques and tools in the specified technology application areas.

An outline scheme for a network proposal as discussed at the workshop is given in section B below. It follows the guideline to enable through the network co-operation the development of novel/advanced MC calculational methods as well as corresponding computational tools with the ultimate goal to make available them for practical applications in the selected technology areas. To this end, the MC network is devoted to the development of methods and tools in the first place and deals, secondly, with the application of the novel methods and tools in the different technology areas. The latter is to show the importance/significance of the newly developed tools in practical applications and to demonstrate their applicability, capabilities and advantages as well. Thereby feed-back can be provided to the MC theorists and code developers. Through the network co-operation, MC theorists, code developers and users will therefore benefit very much from each other.

To make sure that the network proposal will be placed in the proper network area entitled „Engineering Sciences" (as agreed at the workshop) objectives, tasks and concept of the MC network should therefore follow this guideline.

B. Scheme for a MC Network Programme

At the workshop, possible schemes for a network programme have been discussed. Key issues of such a programme are outlined in the following.

Title of the Network

Advanced Monte Carlo Methods & Tools for Engineering Physics Applications

Objective of the Network

The objective is to develop advanced/novel Monte Carlo techniques and tools for solving engineering physics problems in medical, environmental and energy technology related applications.

The network is organised in two parts: Part A, the development of methods and tools, providing the basis for Part B, the application of the new tools in medical, environmental and energy technology.

Part A: Development of Methods and Tools

Objective: To develop and provide advanced methods and tools as needed in medical, environmental and energy technology related practical applications

Areas:

I. **Novel techniques for improving reliability & efficiency for calculations**

1. Double randomisation techniques (Sabelfeld)
2. Direct statistical approach (DSA) for variance reduction in particle transport (Burn)
3. Sensitivity/uncertainty calculus (Perel)
4. Geometry generation using CAD-systems (Tsige-Tamirat)

II. Optimisation & Inverse Problems (Devooght et al.)

Part B: Applications in medical, environmental and energy technology

Objective: To show the importance/significance of the newly developed tools and to demonstrate their applicability, capabilities and advantages in medical, environmental and energy technology related practical applications.

Areas:

I. Medical Physics

Medical & industrial imaging, Inverse Planing
(Calvino, Cortes, Maucec, Zio)

Photoneutrons in Shielding + Medical Physics Applications
(Calvino, Hordosy, Rodenas, Ongaro, Petrizzi,)

II. Environmental Technology

Contaminant Transport in the biosphere
(Smidts, Cortes, Zio, Sabelfeld, Jordenas)

Dynamic PSA of Industrial Processes
(Labeau, Zio)

Nano-particle technology (Sabelfeld)

III. Energy Technology (Radiation)

Assessment of sensitivities & uncertainties in particle transport
(Fischer, Perel, Petrizzi, Siebert)

Damage to reactor pressure vessel (Hordosy)

C. Schedule for the preparation of a proposal

As agreed at the workshop, the following actions will follow:

1. Distribution of the draft summary of working group discussion.
   Responsible: U. Fischer, FZK; due date: May 22, 1998

2. Comments, revisions etc.
   Responsible: All participants; due date: June 15, 1998

3. Concise "unified" network proposal.
   Responsible: J. Devooght, ULB; due date: July 31, 1998

4. Responses to the "unified" proposal.
   Responsible: All participants; due date: September 11, 1998

5. Final version of network proposal.
   Responsible: J. Devooght, ULB, U. Fischer, FZK
   Due date: September 30, 1998

D. Task co-ordination

It was agreed that a MC theorist should act as task co-ordinator. At the workshop there was no volunteer for this task. A solution might be achieved with Prof. Beauvens, Universite Libre de Bruxelles, who could be interested but was not present at the workshop. Prof. Devooght proposed to contact him.

E. Further co-operation

The idea of the MC network appeared to be beneficial and fruitful to the workshop participants. It was therefore agreed to proceed with the idea of the network co-operation independent from a success or failure with the application in the TMR programme. Co-operations can be established in many ways: formally and informally, bilateral and multilateral. In any case it is essential to have available a well organised MC network group that allows for easy and efficient communication and is open to new ideas and members.

To proceed with that, it was agreed to

- to exchange information, ideas etc. by e-mail (e. g. via the list server)
- to establish a forum on the net (make the workshop web-site to a permanent site that allows for communication; will be done by P. Wilson, FZK)
- to organise regular meetings, e. g. once a year, starting with a follow-up workshop by mid 1999.

V. Monte Carlo Network Proposal

Draft by J. Devooght , ULB, July 1998

Following the workshop, a concise proposal for a Monte Carlo network has been drafted by Prof. J. Devooght, ULB. It is anticipated that this draft will serve as general reference frame when preparing the final network proposal.

Draft for Monte-Carlo network proposal

J. Devooght (July 1998)

1 Terms of agreement

It is important to agree on a general philosophy about "advanced Monte-Carlo methods for engineering physics applications".

The applications of Monte-Carlo, dealt with by the participants of the Karlsruhe meetings, are so far : neutral and charges particle transport in fission and fusion reactors, photon transport in radiation shielding, contaminant transport in the biosphere including aerosols, dynamic PSA of industrial processes.

The common link between participants is the fact that the method used to treat the various problems is Monte-Carlo. Most of us do report our work in conferences and journals devoted to applications and not to the method. If we decide to cooperate, it is mostly because we want to share information on the method but not on the application, i.e. not because people interested in aerosols want to know all about PSA or on radiation shielding. To share knowledge and experience on Monte-Carlo techniques may be done at two levels :

(1) Improvement and implementation of existing methods, including standardized software shared by a large number of users. Improvements may range from better data to increased user-friendliness of software tools, etc.

(2) Development or implementation of new tools capable of solving a wider range of problems.

To participate in the network is meaningless if each one is not willing to invest some time in learning some new tool or method. The network is a process of give and take. It is not a short term investment where everyone could find an immediate answer concerning a problem in his application field. The future activity of a Monte-Carlo "network" may be twofold :

(1) Either we meet regularly and exchange information, each group continuing essentially his present work. In that case, the proposal given below is probably of little interest.

(2) Or we adopt a more ambitious stand in the perspective of introducing a research proposal, which means that everyone has agreed to develop (besides its usual Monte-Carlo application) or to implement innovative developments either developed by himself or by others. It is in that perspective that the text below has been written.

It may be that some groups may wish to opt out if (2) is followed and that others in Europe would wish to get in.

The draft, as agreed in Karlsruhe, is an invitation for comment, addition or correction and it is expected that as a result every group will be able to define his contribution.

2 A common frame of reference

So far, all applications treated by the participants amount to solve integral equation (or system of) of the second kind :

$$\phi(P) = \int K(P, P')\phi(P')dP' + Q(P) \tag{1}$$

The association of a Markov chain with (1) yields a Monte-Carlo algorithm for evaluation of a functional $< f(P), \phi(P) >$ when $< \ldots, \cdots >$ is some scalar product.

The basic problem is to define a random variable ξ such that $E\xi =< f, \phi >$. Since we have a finite sample, we want to minimize the variance $V(\xi)$ in order to minimize the computation time. Most of the literature on Monte-Carlo methods is essentially concerned with variance reduction using either a priori information or information gathered during the stochastic process. Among scientists using Monte-Carlo methods, those dealing with radiation transport by means of (1) are probably the most sophisticated in the development of non analog methods, not widely used in other fields. Finally we may end the characterization of Monte-Carlo by writing that it used to be a "last resort" method[1], that it is rather insensitive to the complexity of the problem solved or to the number of dimensions of the phase-space, where standard ! numerical methods fail.

All participants to the Karlsruhe workshop do solve generalized transport problems formulated by (1). Indeed we have neutrons, photons for the most part; accessorily electrons and other charged particles; "pollutant" molecules; "systems" for reliability and safety problems.

Table 1 subsumes the main characteristics of the four categories of problems. Dynamics of neutral particles is trivial (although the crossing of surfaces is not) but much more time consuming for systems.

[1] Much of the opposition to Monte-Carlo due to heavy computer load has been reduced by the tremendous improvement of workstations

"Particles"	Neutrons and photons	Electrons and other charged particles	"Systems"	Pollutants
Dynamics	Straight lines	Curves (in plasmas)	System dynamics	Imposed by fluid flow
Transition laws	Cross-sections	Cross-sections	Failure rates	Radioactive or biological decay rates
Piecewise determitic process	Yes	Yes	Yes	No (unless Langevin equation)
Phase space dimension	6	6	High (number of process variables)	6 or more
Linear equation	Yes	Yes (Vlasov)	Yes	No (in case of reactions)
Rare events	In many applications	Sometimes	Always	In many applications

Table 1: Categories of problems

In three cases we have piecewise-deterministic process i.e. deterministic trajectories interrupted by random events; the fourth is a diffusion-advection process unless one uses a Langevin equation technique. Equations are linear unless one studies interparticle reaction rates. Tracking rare events is a common characteristic of many problems treated by Monte-Carlo hence the drive for non analog methods. However not all problems need non analog treatment and direct simulation (in the second category) yields interesting results by a statistical analysis of events.

The topics that could be investigated by scientific groups with expertise in the field of Monte-Carlo and/or solution of the Boltzmann equation are for instance :

A. Fission and fusion reactor technologies

Up to now these topics have been the main source of problems and of standard software tools and need not be detailed since they are familiar to every participant. Although very important, there are obvious reasons why a shift of emphasis is likely to happen now and tomorrow as new topics are appearing in many nuclear research centers or departments.

B. Others topics

B.1. Radiation therapy

Problems (including geometry) are so complex that Monte-Carlo is the only practical solution. However the present need is for very fast calculation of radiation planning which is so far impossible or difficult with present day computers in order to replace existing methods. The potential market is very large and open to innovative Monte-Carlo techniques but experts claim that progress is unlikely without a close collaboration with users, i.e. medical doctors, a fact we should acknowledge.

B.2. Pollutant transport in complex uncertain media

Again the scientific market is large and difficulties are linked to the fact that multispecies transport in an uncertain medium taxes heavily standard numerical schemes and where Monte-carlo is ideally suited.

B.3. Safety and reliability studies

Industrial systems (like reactors) that obey a non linear dynamics $\frac{d\bar{x}}{dt} = \bar{f}_i(\bar{x})$, depending on the current state i of the hardware may shift, by failure, from one state to another and change in dynamics may lead to safety boundary crossing. These rare events lead to a "Boltzmann equation" with complex trajectories in a high dimension phase space and can only be studied by Monte-Carlo.

B.4. Instrumentation design and interpretation of experiments

This is not new but potential exists for development of optimization and stochastic programming (see § 5) in Monte-Carlo. When used as an analog simulation tool, statistical analysis of combination of events may lead to unsuspected physical phenomena and better or simplified modelization.

3 Variance reduction techniques

A good deal of current research work on Monte-Carlo for transport is devoted to the implementation of concepts invented long ago like splitting, russian roulette, patch stretching, direct statistical approach of splitting (DSA), etc. As it is well known to practitioners, the best schemes can go astray for lack of proper implementation. Although Monte-Carlo software does allow in general for variance reduction techniques the automatic timing of parameters of self-learning games, from observations gathered from the Monte-Carlo process is quite difficult, the even more so if it has to be done in an user-friendly way covering all possible circumstances. This theme is the principal workhorse of Monte-Carlo research and is likely to remain so.

Another category of problems, which cannot be classified as variance reduction but which contributes to the reduction of computation time, is the efficient treatment of surface crossings.

Both topics are been covered by expertise in the group (DSA and geometry generation by CAD-systems). Reduction of variance is also currently applied in Monte-Carlo of PRA.

4 Treatment of uncertainty

What are the less well known aspects which involve potential use of Monte-Carlo?

First of all, $K(P, P')$ may depend on :

(1) the geometry

(2) the composition of the domain

and in PSA

(3) the system dynamics.

Most realistic problems involve complex geometric (or dynamic) auxiliary problems and the efficient treatment of boundaries is not a trivial task. But many realistic problems involve usually uncertain data :

(a) geometry and composition may be uncertain (as for instance in geological media or in atmospheric physics) or known imperfectly (simplified geometry, reactor core with variable burnup)

(b) dynamics does depend on uncertain or unknown parameters, or changes in dynamics are subject to random delays

(c) cross-sections are known with limited accuracy.

Best estimate calculations (i.e. with "average" parameters) are less and less acceptable because designers or decision makers want to know confidence intervals for instance that $< f, \phi > < c$ with a given probability $p(c)$.

The nature of uncertainty may be different :

(a) boundaries of homogeneous regions are unknown or uncertain. This is for instance the case for "inverse" problems like tomography or for anatomical uncertainties in radiation therapy.

(b) the medium is described by a few parameters, say vector $\overline{a}$ whose distribution $\pi(\overline{a})$ is known

(c) the medium is described by "random fields", say $\chi_k(\overline{r})$, where $\chi_k(\overline{r})$ is a random function of the position $\overline{r}$. Usually, one makes the assumption of stationarity (translation invariance) and knowledge is reduced to $E[\chi_k(\overline{r})]$ and $E[\chi_k(\overline{r})\chi_\ell(\overline{r}')] = F_{k\ell}(|\overline{r} - \overline{r}'|)$. Alternatively the random field can be described by a large set of random variables sampled from a distribution characterized by average and covariance (or $F_{k\ell}$) [4]. Transport in random media is a topic where random fields are used and where Monte-Carlo is needed [8].

In all three cases we have problems characterized by a parameter vector $\overline{a}$. Equation (1) reads

$$\phi(P, \overline{a}) = \int K(P, P'|\overline{a})\, \phi(P, \overline{a})\, dP' + Q(P, \overline{a}) \tag{2}$$

Two cases are possible :

(1) we want to know

$$E_a \langle f(P), \phi(P, \overline{a}) \rangle = \int \pi(\overline{a}) \langle f(P), \phi(P, \overline{a}) \rangle\, d\overline{a} \tag{3}$$

(2) we want to estimate $\overline{a}$ given observations

$$c_k = \langle f_k(P), \phi(P, \overline{a}) \rangle \tag{4}$$

This is a problem of parametric estimation, i.e. $\overline{a}$ is fixed but unknown.

The first problem amounts to double randomization [3][4] where the algorithm reduces essentially to :

- sampling of n values $\overline{a}_i$ from $\pi(\overline{a})$
- obtain an estimate of $< f(P), \phi(P, \overline{a}_i) >$ by a Monte-Carlo sample of size N, and finally of $E_a < f(P), \phi(P, \overline{a}) > \simeq \frac{1}{n} \sum_{i=1}^{n} < f(P), \phi(P, \overline{a}_i) >$

such that the variance due to Monte-Carlo sampling of $\phi(P, \overline{a})$ is negligible compared to the intrinsic variance due to $\pi(\overline{a})$. In the second problem, we have many options. For the simplest case where the number of observations is equal to the number of parameters, a Newton-like method

$$\langle f_k(P), \phi(P, \overline{a}^n) \rangle + \sum_{\ell} \left(a_\ell^{n+1} - a_\ell^n\right) \left\langle f_k(P), \frac{\partial \phi(P, \overline{a}^n)}{\partial a_\ell^n} \right\rangle - c_k = 0$$

yields iterates $\overline{a}^n$ given $\overline{a}^o$ and the functionals $< f_k(P), \phi(P, \overline{a}^n) >$ and $\frac{\partial}{\partial a_\ell} < f_k(P), \phi(P, \overline{a}^n) >$ (importance coefficients) obtained by Monte-Carlo.

An associated problem to double randomization is the proper balance to give to each type of sampling. This is only one example of the minimization of computational costs that occur in Monte-Carlo [3].

5 Optimal design, inverse problems, stochastic programming

Although the first moment $E_a \phi(P, \overline{a})$ (or $E_a < f(P), \phi(P, \overline{a}) >$) is of crucial importance, it may not be enough.

For instance safety goals involve conditions like

$$Prob.\left(\overline{a} \middle| \langle f(P), \phi(P, \overline{a}) \rangle > \alpha\right) < \eta \tag{5}$$

This is the case for radiation protection, radioactive waste transport in the biosphere, or irradiation of a critical organ in a radiation therapy program. To find the distribution of $u \equiv < f(P), \phi(P, \overline{a}) >$ given that $\overline{a}$ has distribution $\pi(\overline{a})$ and $\phi(P, \overline{a})$ is solution of (2) is a challenging problem.

One option is to write the first order development

$$u \cong \langle f(P), \phi(P, \langle \overline{a} \rangle) \rangle + (\overline{a} - \langle \overline{a} \rangle) \left\langle f(P), \overline{\nabla}_a \phi(P, \langle \overline{a} \rangle) \right\rangle \tag{6}$$

which leads to importance coefficients $I_k \equiv < f(P), \frac{\partial}{\partial a_k} \phi(P, < \overline{a} >) >$: estimated by differential or perturbation Monte-Carlo. In many cases ("elliptic" distributions)

$$u - \langle f(P), \phi(P, \langle \overline{a} \rangle) \rangle \cong \sum_{k} (a_k - \langle a_k \rangle) I_k \tag{7}$$

is a random variable whose distribution is given in closed form, hence $Prob(u > \alpha)$.

What are the other options?

Problems are not only characterized by uncertain or unknown parameters $\overline{a}$ but also by design parameters $\overline{\theta}$. Design parameters are under control and we are free to chose them under certain constraints. They are for instance, a shield thickness, an irradiation duration, a burnable isotope concentration, a source location or intensity, etc. etc. Therefore (2) can be rewritten :

$$\phi\left(P,\overline{a}|\overline{\theta}\right)=\int K\left(P,P'|\overline{a},\overline{\theta}\right)\phi\left(P,\overline{a}|\overline{\theta}\right)dP'+Q\left(P,\overline{a}|\overline{\theta}\right) \tag{8}$$

and we may want to minimize the probability, i.e.

$$Min_{\overline{\theta}}Prob.\left(\overline{a}|\left\langle f\left(P,\overline{\theta}\right),\phi\left(P,\overline{a}|\overline{\theta}\right)\right\rangle>\alpha\right) \tag{9}$$

to which we may eventually add constraints like $Q_k(\overline{a},\overline{\theta})\leq 0$. This is typically the case for a radiotherapy program which one wishes to optimize duration and energy for each irradiation angle (in which case the maximization of expectation is enough) or the case of probabilistic risk assessment (PRA) where one wishes to optimize safety features ($\overline{\theta}$), such that the probability that the population dose $<f(P,\overline{\theta}),\phi(P,\overline{a}|\overline{\theta})>$ exceeds some value α_1, given uncertain parameters $\overline{a}$ (failure rates) is minimized. A problem of type (9) is a problem of stochastic programming [1][2] and an equivalent formulation is

$$Min_{\overline{\theta}}E_aH\left(\left\langle f\left(P,\overline{\theta}\right),\phi\left(P,\overline{a}|\overline{\theta}\right)\right\rangle-\alpha\right)$$

The optimal value of $\overline{\theta}$ is usually sought in a restricted domain $\mathcal{D}$ where the solution is acceptable. A succession of iterates $\overline{\theta}^n$ is obtained as follows :

(a) An estimate of $E_aH(<f(P,\overline{\theta}),\phi(P,\overline{a}|\overline{\theta})>-\alpha)=P_\alpha(\overline{\theta})$ is built by Monte-Carlo sampling;

(b) A stochastic gradient $\overline{\xi}^n$ is evaluated, where

$$E\left[\overline{\xi}^n|\overline{\theta}^n\right]=\overline{\nabla}_\theta P_\alpha\left(\overline{\theta}^n\right)$$

(c) The new value is computed by [5]

$$\begin{aligned}\overline{\theta}^{n+1}&=\arg\min\parallel\overline{\theta}^{n+1}-\overline{\theta}^n-\rho_n\overline{\xi}_n\parallel \qquad \text{if } \parallel\overline{\xi}_n\parallel \text{ is small enough}\\&=\overline{\theta}^o \qquad \text{otherwise}\end{aligned}$$

Once again Monte-Carlo is an essential part of the optimization process, when we substitute stochastic constraints to deterministic constraints. A more easy problem is obtained as well as closed forms if we substitute (6) in (9), giving

$$Min_{\overline{\theta}}Prob\left[\left(\overline{a}-\langle\overline{a}\rangle\right)\left\langle f\left(P,\overline{\theta}\right),\overline{\nabla}_a\phi\left(P,\langle\overline{a}\rangle|\overline{\theta}\right)\right\rangle\alpha-\left\langle f\left(P,\overline{\theta}\right),\phi\left(P,\langle\overline{a}\rangle|\overline{\theta}\right)\right\rangle\right]$$

where again the knowledge of $<f(P,\overline{\theta}),\phi(P,<\overline{a}>|\overline{\theta})>$ and its derivatives is essential.

To conclude : the solution of optimization problems (often linked to inverse problems) with uncertain data can be treated by Monte-Carlo calculations imbedded in an iterative process.

6 Reformulation of problems

It is well known that incorporation of expected values or in general of a priori information will increase Monte-Carlo effectiveness.

Innovative Monte-Carlo methods stem sometimes from reinterpretations of the Fredholm equation (1) for physical problems where (1) is not a Boltzmann equation. For instance if we rewrite (1)

$$(I - K_o)\,\phi = (K - K_o)\,\phi + S$$

it may happen that a kernel K_o such that $(I - K_o)^{-1}$ can be obtained in closed form, i.e.

$$\phi = (I - K_o)^{-1}\,[(K - K_o)\,\phi + S]$$

with an improved convergence of the Neumann series development if $(I - K_o)^{-1} S$ is a good first approximation. This is the spirit of Macro Monte-Carlo types of simulation in radiotherapy where one wants to avoid the analog simulation of electron transport and use a kernel $(I - K_o)^{-1}$ where we have a good approximation of transport over distances large compared to m.f.p. The same is true for brownian movements which are subsumed in a diffusion process. Monte-Carlo treatment of radioactive waste transport is greatly helped by defining a proper kernel K_o.

Techniques based on numerical analytical continuation [4] and which amount to a reorganization of the Neuman series partake to the same spirit.

7 Distributions

The basic function sought in transport problems is $P(N, \overline{r}, dV, t|\overline{r}_o, \overline{v}_o)$, i.e. the probability of finding N particles at point $\overline{R} = (\overline{r}, \overline{v})$ in an infinitesimal volume dV at time t, if one particle is introduced at time $t = 0$ in $(\overline{r}_o, \overline{v}_o)$ [7]. The first moment

$$\left\langle N\left(\overline{R}, dV, t|\overline{r}_o, \overline{v}_o\right)\right\rangle = \sum_{N=0}^{\infty} NP\left(N, \overline{R}, dV, t|\overline{r}_o, \overline{v}_o\right)$$

leads to the particle density $n(\overline{r}, \overline{v}, t|\overline{r}_o, \overline{v}_o) = \lim_{dV\to 0} \frac{<N(\overline{R}, dV, t|\overline{r}_o, \overline{v}_o)>}{dV}$ obeys the usual (forward) linear Boltzmann equation and with a distributed source $S(\overline{r}_o, \overline{v}_o)$ to
$n(\overline{r}, \overline{v}, t) = \int n(\overline{r}, \overline{v}, t|\overline{r}_o, \overline{v}_o) S(\overline{r}_o, \overline{v}_o) d\overline{r}_o d\overline{v}_o$.

This is sometimes improperly characterized as a distribution of $\overline{r}, \overline{v}$, because if suitably normalized $n(\overline{r}, \overline{v}, t)$ is the probability density of finding a particle in $(\overline{r}, \overline{v})$ but in fact it is a first moment of distribution P.

Monte-Carlo calculations in transport theory are often concerned with the evaluation of linear functional (detector rates) like $\int \ell(\overline{r}, \overline{v}) n(\overline{r}, \overline{v}, t) d\overline{r} d\overline{v}$. Although it is meaningless to consider higher moments for an infinitesimal dV it is not so for

$$\left\langle N^m\left(\overline{R}, V, t|\overline{r}_o, \overline{v}_o\right)\right\rangle = \sum_{N=0}^{\infty} N^m P\left(N, \overline{R}, V, t|\overline{r}_o, \overline{v}_o\right) \;, m = 1, 2, \ldots$$

where as a function of $\overline{r}_o, \overline{v}_o$ the higher moments obey backwards or adjoint Boltzmann equations. Monte-Carlo can be used to solve them in the same spirit as forward equation, but now some information can be inferred on the distribution itself, for instance from the first and second moment. A

typical example is the distribution of the number of secondary electrons ejected from a target by an ion beam. The distribution yields interesting information over the cascade or branching process, like for instance the Fano factor.

The number of particle in V (or leaving V through a boundary) is an example of score, and it can be extended to more general concepts like consequence ("importance") or damage (like dose for waste transport or radiological consequence for dynamic reliability). Distribution problems are rarely treated, and generaly by straightforward analog simulation. However this is inefficient for rare events and therefore non analog Monte-Carlo solution of adjoint Boltzmann equation are certainly a valuable research topic.

REFERENCES

[1] P. KALL, Stein W. WALLACE, "Stochastic programming", J. Wiley (1994).

[2] A. KIBZUN, Y. KAN, "Stochastic programming problems", J. Wiley (1996).

[3] G.A. MIKHAILOV, "Minimization of computational costs of non analogue Monte-Carlo methods", World Scientific, Series on Soviet and East European Mathematics, Vol. 5 (1991).

[4] K.K. SABELFELD, "Monte-Carlo methods in boundary values problems", Springer (1991).

[5] C.T. KELLEY, "Iterative methods for linear and nonlinear equations", SIAM Frontiers in applied mathematics, Vol. 16 (1995).

[6] I. LUX, L. KOBLINGER, "Monte-Carlo particle transport methods : neutron and photon calculations", CRC Press, Boca Raton (1991).

[7] I. PASZIT, "Duality in transport theory", Ann. Nucl. Energy, Vol. 14, 25-41 (1986).

[8] G. POMRANING, "Linear kinetic theory and particle transport in stochastic mixtures", World Scientific, Vol. 7 (1991).

VI. Workshop Presentations

Monte Carlo Methods and Models for Applications in Energy and Technology

Workshop to be held at Forschungszentrum Karlsruhe, May 12-14, 1998

The double randomization technique in Monte Carlo simulations

Karl Sabelfeld

Weierstraß-Institut für Angewandte Analysis und Stochastik (WIAS)
Mohrenstrasse, 39, 10117, Berlin

Stochastic algorithms for solving integral equations with random parameters are constructed. As an important practical example, a linear radiative transfer equation can be considered. If the cross-sections are highly irregular, one describes them as random functions with given distributions. Then the problem is to calculate the average of the solution and its variance.

The method developed (the so-called double randomization technique) is based on a construction of a probability space which is a direct product of the space of trajectories (Markov chains) and the space generated by the random parameters. For practical implementations, a series of optimization problems should be solved. In particular, recommendations concerning the number of trajectories per one sample of the random parameter are given.

We present also a practically interesting example of nonlinear equation where the double randomization is also applicable. Namely, we construct a stochastic algorithm for solving a random Smoluchowski equation governing the coagulation of particles in a turbulent collision regime. Numerical calculations show that the intermittency of the turbulent flow affects much the growth rate of the particles.

Last modified: Thu Apr 23 15:23:12 1998

THE DOUBLE RANDOMIZATION TECHNIQUE IN MONTE CARLO SIMULATIONS

K. K. Sabelfeld

1. Introductory Remarks.
2. **Double Randomization.**
3. Integral equations.
4. Simulation of random fields.
5. Random Walk inside the domain
6. Random Walk on the Boundary
7. Eulerian and Lagrangian stochastic models of turbulent transport

6. **Some examples:**

1) Transport in a porous medium
2) Homogeneous nucleation
3) Heterogeneous nucleation
4) Saltation of particles
5) Coagulation in a turbulent flow

1. Introductory Remarks.

MC Methods

Deterministic Problems:

1) **Integrals,**
2) **Integral Equations,**
3) **BVP for PDE's,**

1) $I = \int f(x)\,\pi(dx)$

2) $\varphi = K\varphi + f$

$K\varphi = \int_G k(x,y)\,\pi(dy)$

3) $\begin{cases} Lu = f \\ Bu\big|_\Gamma = g \end{cases}$

$u(x) = E\,\Phi(\eta)$

$\eta : \Omega_\eta$

Simulation of Random events, variables, processes, fields:

$p(x) \to \xi_0, \xi_1 \ldots$

Random sensoring,
Markov chains,
$U(x,t)$ - random fields,
etc ...

$\xi : \Omega_\xi$

2. Double randomization.

(3)

$$\Omega = \Omega_\eta \otimes \Omega_\xi ,$$

1). $I_y = \int_G f_y(x)\,\pi(dx)$

y is a random parameter;

find expectation $E I_y =$

$$= \int dP_y \left\{ \int f_y(x)\, F(dx) \right\} =$$

$$= \left\langle f_\eta(\xi) \right\rangle_{\eta,\xi}$$

Algorithm. 1. Construct a sample of y; (say, η_1);

2. Choose a sample point $x \in G$ according $\pi(dx)$, (say, ξ_1)

3. $E I_y \cong \frac{1}{N} \sum_{i=1}^{N} f_{\eta_i}(\xi_i)$;

3. Integral Equations.

(4)

$$\varphi = K\varphi + f.$$

f random; k_{ij} are random

or BVP for PDE's:

$$\begin{cases} L u = f \\ B u|_\Gamma = g \end{cases} \quad \| \quad \begin{array}{l} f \text{ random; } L_{ij} \text{;} \\ \text{boundary random.} \end{array}$$

1) Construct an estimator for the deterministic equation (one sample).

2) Average over N independent ~~same~~ estimators.

$$\varphi(x) = \int_G k(x,x')\,\varphi(x')\,dx' + f(x).$$

$\rho(K) < 1$. (or $\|K\|_{L_2} < 1$).

$$\Rightarrow \quad \varphi(x) = \sum_{n=0}^{\infty} K^n f(x);$$

$$I_h = \int_G \varphi(x)\, h(x)\, dx$$

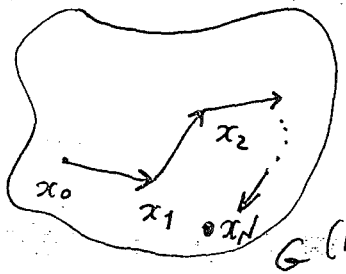

G (N random) transitions;

Define a Markov chain: $\{x_k\}_{k=0}^{\infty} \in G$:

$x_0 \sim \pi_0(x)$ (initial; quite arbitrary);

$x_{k-1} \to x_k$: $p(x_{k-1}, x_k) = z(x_{k-1}, x_k)(1 - \bar{q}(x_{k-1}$

where $z(x_{k-1}, x_k)$ (- pdf of x_k) / (x_{k-1} fixed).

$\bar{q}(x_{k-1})$ - termination probability in the transition $x_{k-1} \to x_k$.

Then: Let $\begin{cases} Q_0 = \dfrac{f(x_0)}{\pi_0(x_0)}; \\ Q_k = Q_{k-1} \dfrac{k(x_k, x_{k-1})}{p(x_{k-1}, x_k)}; \quad (k \geq 1 \end{cases}$

and

$$Q_0 = \frac{h(x_0)}{\pi_0(x_0)}; \qquad Q_k^* = Q_{k-1}^* \frac{k(x_{k-1}, x_k)}{p(x_{k-1}, x_k)} \quad (k \geq 1)$$

$$\xi_k = Q_k h(x_k); \quad \xi_k^* = Q_k^* f(x_k);$$

$$E\xi_k = E\xi_k^* = (K^k f, h) = (f, K^{*k} h),$$

$$\downarrow$$

$$\xi = \sum_{k=0}^{\tilde{N}} Q_k h(x_k); \quad \xi^* = \sum_{k=0}^{\tilde{N}} Q_k^* f(x_k),$$

$$\boxed{I_h = E\xi = E\xi^*.}$$

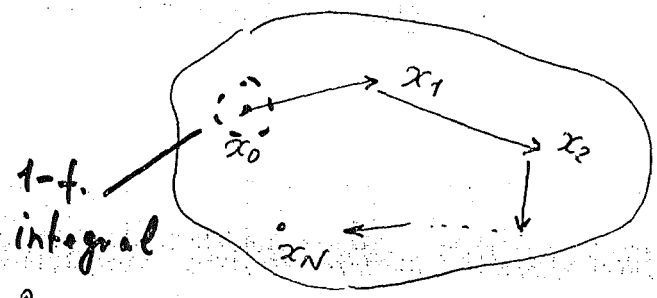

x_0;

$x_0 \to x_1$ (2-f integrals)

etc... $x_0 \to x_1 \to x_2 \ldots \to x_k$

k-fold: $\int_G \cdots \int_G k(x, x_1) k(x_1, x_2) \cdots k \times f(x_0)$

Direct estimator: ξ (x_0 is sampled from the source function) (k is a pdf w.r.t. ~~second~~ first argument (free argument))

Adjoint estimator: ξ^* (x_0 is sampled from the function h) (k is a pdf w.r.t. the second argument (integral. argument))

5. Random Walk inside the domain.

5.1. Very simple example.

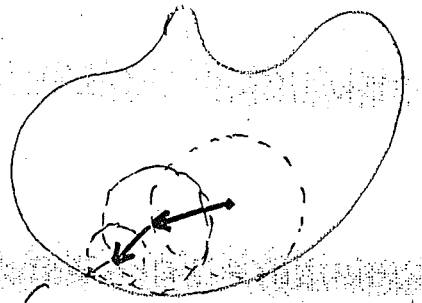

G. $\{x_k\} \to \Gamma = \partial G$;

$$\begin{cases} \Delta u(x) = 0 \\ u|_\Gamma = g \end{cases} \Downarrow$$

$$u(x) = \int_{S(x,R)} u(x + r\omega)\, d\sigma_\omega \;\Rightarrow$$

Adjoint estimator: $u(x) = \int u(y)\, \delta(x-y)\, dy$:

$$u(x) \cong \langle g(x_{N^*}) \rangle$$

$h = \delta(x-y)$;
$\pi = \delta(x-y)$;
k - uniform on $S(x,r)$;

5.2. The walk on Spheres algorithm can be generalized to

$$\begin{cases} \dfrac{\partial u}{\partial t} = Lu & L \text{ - elliptic;} \\ Bu|_\Gamma = g \end{cases}$$

$\{x_k\}$ – a diffusion process.

Random Walk on Boundary.

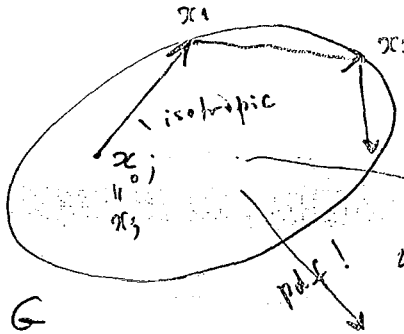

$$\Delta u = 0$$
$$u|_\Gamma = g$$

$$u(x) = \frac{1}{\gamma_0} \int_\Gamma \frac{\cos\varphi_{xy}}{|x-y|^2}\, \mu(y)\, dS_y$$

$$\boxed{\mu = \frac{1}{\gamma_0} \int_\Gamma \frac{\cos\varphi_{yy'}}{|y-y'|^2}\, \mu(y')\, dS_{y'} + g}$$

However, $\rho(K) = 1$ (Neumann series diverges!).

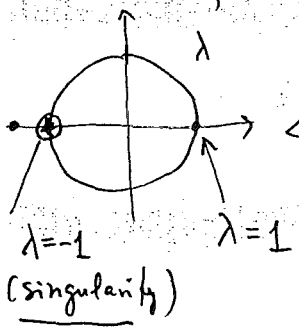

$\Leftrightarrow$ spectral transformation $\Rightarrow$

$$\mu = \sum_{k=1}^{\infty} l_k K^k g \;;$$

$\{x_k\}$; (isotropic on the boundary);

$$u(x) \cong \Big\langle 2\big[g(x_1) - g(x_2) + g(x_3) - g(x_4) + \dots + (-1)^{n+1} g(x_{n+1})\big] + (-1)^{n+1} g(x_{n+1}) \Big\rangle$$

n

4. Simulation of random fields

4.1. Scalar homogeneous random field (in R^n) with a given spectral density $F(\lambda)$:

$$F(\lambda) = \frac{1}{(2\pi)^n} \int_{R^n} B(\rho)\, e^{-i(\lambda,\rho)}\, d\rho ;$$

$$\langle u(x+\rho)\, u(x) \rangle = B(\rho) ; \quad x \in R^n ;$$

Let $u_*^2 = \int_{R^n} F(\lambda)\, d\lambda < \infty$.

$\lambda \sim p(\lambda) = F(\lambda) / u_*^2$ (pdf).

ξ, η : $\bar{\xi} = \bar{\eta} = 0$; $\overline{\xi^2} = \overline{\eta^2} = 1$; $\Rightarrow$

$$v(x) = u_* \left[\xi \cos(\lambda, x) + \eta \sin(\lambda, x) \right]$$

has the spectral density $F(\lambda)$.

R: If ξ, η are Gaussian $\Rightarrow$ $v(x)$ is also Gaussian !

$\Downarrow$ vector fields ?

Let $V(x) = (v_1(x), \dots, v_\ell(x))^T$, $x \in R^n$

$$F(\lambda) = \frac{1}{(2\pi)^n} \int_{R^n} B(\rho)\, e^{-i(\lambda,\rho)}\, d\rho$$

$B(\rho) = \langle V(x+\rho)\, V^*(x) \rangle$ is the correlation tensor.

Let $p(\lambda)$ be a p.d.f. in R^n.

Assume, $\lambda \sim p$;

$$V(x) = \frac{1}{\sqrt{p(\lambda)}}\, e^{i(\lambda,x)}\, \xi ,$$

ξ is a ℓ-dimensional random vector ;

$\bar{\xi} = 0$; $\langle \xi \xi^* \rangle = F(\lambda)$.

However, V is not Gaussian, even if ξ is Gaussian !

$\Longrightarrow$ Diride the spectral space.

Classical fully developed turbulence, with the Kolmogorov spectrum.

Assume, $v(x)$ is isotropic, Gaussian, incompressible, with the spectral density $E(k)$:

$$\Psi_{je}(\vec{k}) = \frac{E(k)}{4\pi k^2}\left(\delta_{je} - \frac{k_j k_e}{k^2}\right) \qquad j,e = 1,2,3$$

$k = |\vec{k}|$;

$$E(k) = \begin{cases} C_1 \bar{\varepsilon}^{2/3} k^{-5/3}, & k_0 \le k \le k_m \\ 0, & \text{otherwise} \end{cases}$$

$$\int_0^\infty E(k)\,dk = \frac{3}{2} v_0^2.$$

$\bar{\varepsilon}$ – mean rate of dissipation of kinetic energy,

$[k_0, k_m]$ – wave interval,

$\eta = 2\pi/k_m$ – inner scale of turbulence,

$L = 2\pi/k_0$ – external — " — . $\left(Re \sim \left(\frac{k_m}{k_0}\right)^{4/3}\right.$

$$v(x) = \sum_{j=1}^{n} \sqrt{E_j}\left\{(\xi_j \times \mathcal{R}_j)\cos\theta_j + (\eta_j \times \mathcal{R}_j)\sin\theta_j\right\}$$

where: $\theta_j = k_j(\mathcal{R}_j, x)$; $\mathcal{R}_j = (\mathcal{R}_j^{(1)}, \mathcal{R}_j^{(2)}, \mathcal{R}_j^{(3)})$

– independent 3D isotropic unit vectors;

$\xi_j = (\xi_j^{(1)}, \xi_j^{(2)}, \xi_j^{(3)})$, $\eta_j = (\eta_j^{(1)}, \eta_j^{(2)}, \eta_j^{(3)})$

are mutually independent standard (Gaussian) vectors; k_j $(j=1,\dots,n)$ are random variables with densities:

$$p_j(k) = \begin{cases} \frac{1}{E_j} E(k), & k \in \Delta_j \\ 0, & k \notin \Delta_j \end{cases}$$

$$E_j = \int_{\Delta_j} E(k)\,dk, \qquad j = 1,\dots,n,$$

Δ_j $(j=1,\dots,n)$ – are nonoverlapping intervals:

a partition of $\Delta = (k_0, k_m)$,

e.g. $\Delta_j = [\tilde{k}_j, \tilde{k}_{j+1})$; $j = 1,\dots,n$,

$\tilde{k}_1 = k_0$, $\tilde{k}_{n+1} = k_m$,

$$\int_{\Delta_j} E(k)\,dk = \frac{1}{n}\int_{\Delta} E(k)\,dk \Rightarrow$$

$$\tilde{k}_{j+1} = \left[k_0^{2/3}\left(1 - \frac{j}{n}\right) + \frac{j}{n} k_m^{-2/3}\right]^{-3/2} \Rightarrow$$

simulation:

$$k_j = \left[\tilde{k}_j^{-2/3} - \frac{v_0^2}{n C_1 \bar{\varepsilon}^{2/3}}\gamma_j\right]^{-3/2} \qquad (j = 1,\dots,n)$$

$\gamma_j \sim [0,1]$;

7. Eulerian and Lagrangian stochastic models of turbulent transport.

$$\begin{cases} \dfrac{\partial X(t,x_0)}{\partial t} = u(t, X(t,x_0)) \\ X(0, x_0) = x_0 \end{cases}$$

$X(t, x_0)$ is a random process, x_0 fixed.

↓ Described by a SDE. (Langevin-type models)

$$\begin{cases} \dfrac{d\hat{x}}{dt} = V(t) \\ \dfrac{dv}{dt} = a(\hat{x}, v) + b(x, v)\dfrac{dw}{dt} \quad \text{(Wiener / white noise)} \\ \hat{X}(0) = x_0; \\ V(0) - \xi \sim u(x_0) \end{cases}$$

Consistency between X and $\hat{X}$, $u(X(t),t)$ and $V(t)$

Let

$$p_{1L}(x,t;x_0) = \langle \delta(x - X(t,x_0)) \rangle,$$

$$p_{2L}(x,x',t;x_0,x_0') = \langle \delta(x - X(t,x_0))\,\delta(x' - X(t,x_0')) \rangle$$

$$\langle C(x,t) \rangle = \int p_{1L}(x,t;x_0)\, S(x_0)\, dx_0,$$

$$\langle c(x,t)c(x',t) \rangle = \int p_{2L}(x,x',t;x_0,x_0')\, S(x_0) S(x_0')\, dx_0\, dx_0'$$

Let

$$p_{nE}(v_1 \dots v_n; x_1, \dots, x_n) = \left\langle \prod_{i=1}^{n} \delta(v_i - u_E(x_i,t)) \right\rangle;$$

$$p_{nL}(x_1, v_1, \dots x_n, v_n, t; x_{01}, \dots, x_{0n}) =$$

$$\left\langle \prod_{i=1}^{n} \delta(x_i - X(t,x_{0i})) \cdot \prod_{j=1}^{n} \delta(v_j - V(t,x_{0j})) \right\rangle$$

⇒ Novikov's relation:

$$p_{nE}(v_1, \dots, v_n; x_1, \dots, x_n) = \int p_{nL}(x_1, v_1, \dots, x_n, v_n, t; x_{01}, \dots x_{0n})\, dx_{01} \dots dx_{0n}$$

⇒ constraints on the choice of $a(\hat{x}, v)$ and $b(x, v)$!

Examples.

1) Transport in a porous medium.

parameters of a porous medium is considered as a random function of a special statistical structure; e.g.,
the hydraulic conductivity ;

Let i be an integer characterizing an isotope, $\vec{r}$ its position, and $\vec{a}$ a vector describing the geological substrate. (density, porosity, diffusion tensor, temperature, ...).

The dynamics of isotope i :

$$\frac{d\vec{r}}{dt} = v_i$$

medium dynamics: $\frac{d\vec{a}}{dt} = g(\vec{a})$

Let $\pi(r, a, i, I, t)$ - p.d.f (r, a, i, I) — geological state (macroscopic)

Chapman-Kolmogorov:

$$\frac{\partial \pi}{\partial t} + \nabla_r(v_i \cdot \pi) + \nabla_a[g(\vec{a})\pi] + (\Lambda + \lambda_i)\pi - \sum p(j \to i)\pi - \sum_{J \neq I} p(J \to I)\pi = 0$$

transitions

$\Rightarrow$ internal system equation

2. Homogeneous nucleation

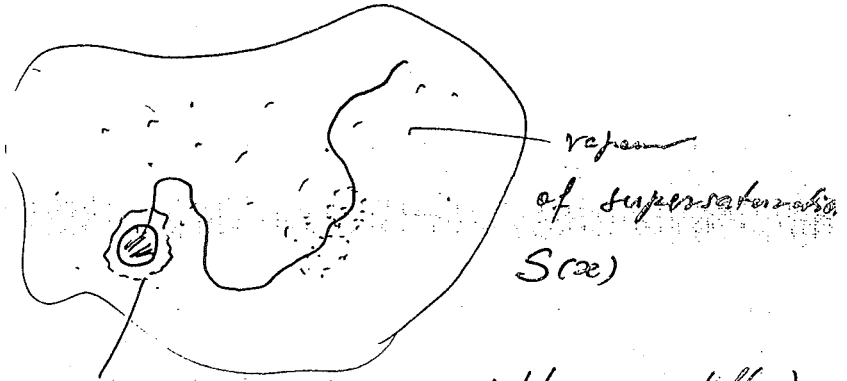

N number of particles $= \exp\{\Phi(S)\}$ — random field

$$\langle N \rangle = \langle \exp\{\Phi(S)\} \rangle \quad \text{average over all trajectories}$$

$$\neq \exp\{\Phi(\bar{S})\} ;$$

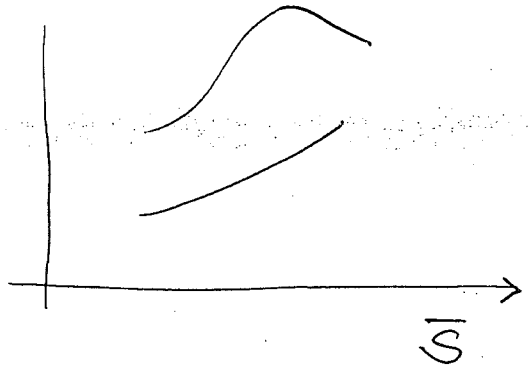

3. Heterogeneous nucleation. (18)

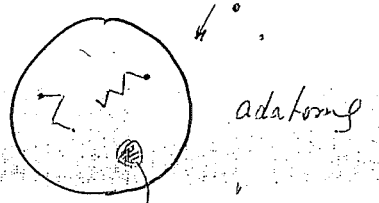

Tipical configurations: (too sensitive).

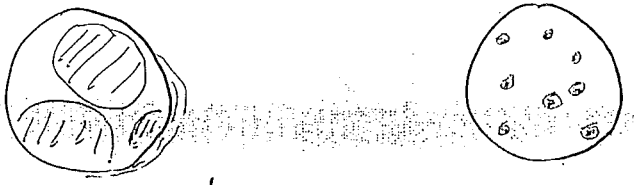

Double randomization: 1) Simulate a diffusion process on a sphere.

2). form a heterogeneous geometry.

3). jump of islands

4) etc.

4. Saltation of particles (19)

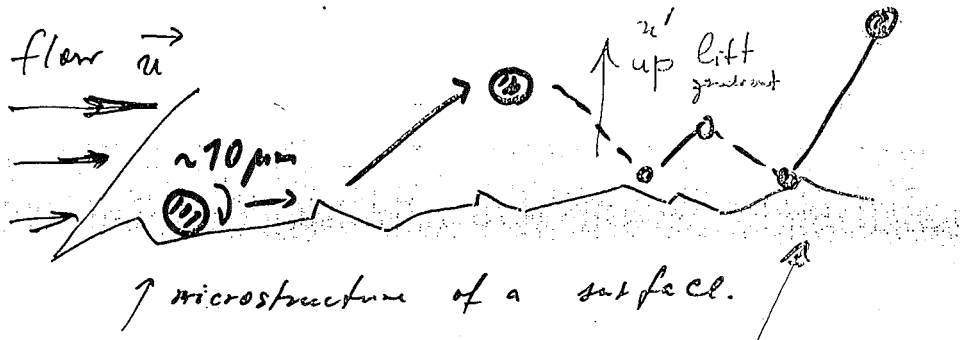

↑ microstructure of a surface.

double randomization: for each velocity and surface configuration construct the Lagrangian trajectory.

Calculate 1) Mean hight

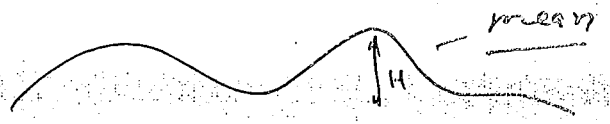

2) flux of particles in a direction ($\cos\alpha, \alpha$).

3) life time in a region G.

5. Coagulation of particles in a turbulent flow.

$$(1)\quad \frac{\partial n_\ell}{\partial t} + v\nabla n_\ell = \frac{1}{2}\sum_{i+j=\ell} K_{ij}\, n_i n_j - n_\ell \sum_{i=1}^{\infty} K_{\ell i} n_i + F_\ell(t)$$

$n_\ell(0) = n_0$, $\ell = 1, 2, \ldots$

(Smoluchowski equation). $\langle v \rangle = 0$

v - a turbulent velocity field,

K_{ij} - coagulation coefficients $\left(= \sqrt{\frac{\varepsilon}{\nu}} \cdot \left(i^{1/3} + j^{1/3}\right)^3\right)$.

Find $\overline{n_\ell}$; $\langle n_\ell \rangle$ $(v=0)$

1] Construct a random estimator for (1),

(Nanbu - estimator, Sabelfeld - estimator, etc.
Bird - estimator, ...).

$\hat{n} \xrightarrow{P} n_{disk.}(\Delta t_k)$ (in probability).

$\langle n_\ell \rangle \neq \overline{n_\ell}$!

References

1. K. K. Sabelfeld. Monte Carlo methods in Boundary value problems. Springer - Verlag, 1991.

2. O.A. Kurbanmuradov and K.K. Sabelfeld. Stochastic Lagrangian models of relative dispersion of a pair of fluid particles in turbulent flows. Monte Carlo methods and Applications. 1995, vol. 1, No. 2, 101 - 136.

3. Sabelfeld K.K., Pogasinsky S.V., Kolodko A.A. and Levykin A.I. Stochastic algorithms for solving Smoluchowski equation and applications to aerosol growth simulation. Monte Carlo methods and Applications. 1996, vol. 2, n 1, 41-87.

4. Williams M.M.R and Loyalka S.K. Aerosol Science. Theory and Practice. Pergamon, New York, 1991.

Monte Carlo Methods and Models for Applications in Energy and Technology

Workshop to be held at Forschungszentrum Karlsruhe, May 12-14, 1998

DSA: Past, Present and Future

Kenneth W. Burn

ENEA ERG-SIEC
Via M.M.Sole 4, 40129 Bologna, Italy

The objective of the DSA (Direct Statistical Approach) has been to provide a robust method to minimize the statistical error in fixed source Monte Carlo transport calculations under the most general of circumstances. It employs one of the least dangerous and simple variance reduction methods: population control through splitting and Russian roulette (RR). The DSA has been under development for some 16 years and for neutrons and photons in the fission/fusion energy range, this objective has been to a large extent reached around 5 years ago (Ref. 1).

In the meantime the following extensions have been implemented:

- improvement of the second moment by taking into account the contributions from bifurcations other than those due to splitting (Ref.2),
- treatment of non-analogue estimators (Ref.2),
- a weight-dependent splitting/RR capability designed for problems for which simple population control is not adequate and an independent biasing technique(s) is employed (Ref.3).

Recently a further extension to multi-response problems has been introduced (Ref.4). This has proved useful particularly in calculating flux spectra and as many as 84 responses have been treated simultaneously.

Currently the DSA is being extended to the higher energy domain and to other particle types: electrons, protons, pions, etc.

A possible spin-off from the inclusion of bifurcations other than those due to splitting (mentioned above), is the capacity to correctly estimate the second moment while simultaneously employing variance reduction. Immediate applications are the modelling of cosmic ray showers and of atomic collision cascades. In both these cases higher moments than the first are themselves quantities of interest. A future development might be to estimate the third and higher moments.

In the discussion, some of the following themes will be addressed:

Theoretical:

- The second moment is more difficult to estimate compared with the first, yet the DSA requires it. How can this possibly lead to a more efficient calculation? Relevant topics are:
  - the enhanced surface-point approximation. This approximation has proved to be excellent for neutral particle transport. How will it behave for charged particle transport?
  - iterative schemes for arriving near the optimum.
- It is well known that the second moment is separable only when splitting/RR is independent of the track weight. Any optimization method including the DSA requires separability. To get round this a further approximation is employed: the "non-integer approximation" (Ref.3). How good is

this approximation?

Practical Implementation and Programming:

- There can be an unacceptable slow-down when employing many energy and space cells and particle types, or many responses. Under exactly what circumstances does this occur? How can this be improved?
- The DSA currently employs some IMSL routines. How can these be substituted by public software?

DSA Performance:

- What are the advantages and disadvantages of the DSA over the most directly comparable variance reduction method of a general nature that employs Monte Carlo to generate the required information (viz. the weight-window generator).
    - how soon do you get to the optimum?
    - how do you know you have got to the optimum?
    - how good is the optimum?

Future:

- What problems can be expected to be encountered in multi-particle-type, high energy transport?
- Can the DSA be applied in other Monte Carlo applications apart from particle transport? Perhaps a question before this is: are population control and weight control useful variance reduction methods in other Monte Carlo applications?

P.S.:

- The diffusion or rather lack of it of the DSA may be due to its innate defects. Alternatively it may exemplify the total lack of any coordination in Europe between Monte Carlo development and use.

References:

1. K. W. Burn, "Complete Optimization of Space/Energy Cell Importances with the DSA Cell Importance Model," Ann. nucl. Energy 19-2 65 (1992)
2. K.W.Burn: "Extending the Direct Statistical Approach to include Particle Bifurcation between the Splitting Surfaces" Nucl. Sci. Eng. 119 44 (1995)
3. K.W.Burn: "A New Weight-Dependent Direct Statistical Approach Model"Nucl. Sci. Eng. 125 128 (1997)
4. K.W.Burn, E. Nava: "Use of an Innovative Monte Carlo Technique to calculate Neutron Spectra in BNCT P Application to the TAPIRO Reactor" Meeting on Boron Neutron Capture Therapy, Padua, Feb. 1998 (INFN report in press).

Last modified: Thu Apr 2 12:51:01 1998

DSA: PAST, PRESENT AND FUTURE

K. W. BURN
ENEA – ERG,
BOLOGNA, ITALY

(presented to the Workshop on Monte Carlo Methods and Models for Applications in Energy and Technology, Forschungszentrum Karlsruhe, May 12–14, 1998)

ABSTRACT

The objective of the DSA (Direct Statistical Approach) has been to provide a robust method to minimize the statistical error in fixed source Monte Carlo transport calculations under the most general of circumstances. It employs one of the least dangerous and simple variance reduction methods: population control through splitting and Russian roulette (RR). The DSA has been under development for some 16 years and for neutrons and photons in the fission/fusion energy range, this objective has been to a large extent reached some 5 years ago.

In the meantime the following extensions have been implemented:

- improvement of the second moment by taking into account the contributions from bifurcations other than those due to splitting. (A possible spin-off is the capacity to correctly estimate the second moment while simultaneously employing variance reduction. Immediate applications are the modelling of cosmic ray showers and of atomic collision cascades, in both cases higher moments than the first being themselves quantities of interest. A future development might be to estimate the third and higher moments.)
- treatment of non-analogue estimators.
- a weight-dependent splitting/RR capability designed for problems for which simple population control is not adequate and an independent biasing technique(s) is employed.

Recently a further extension to multi-response problems has been introduced. This has proved useful particularly in calculating flux spectra and as many as 84 responses have been treated simultaneously.

Currently the DSA is being extended to the higher energy domain and to other particle types: electrons, protons, pions, etc.

This paper highlights the important theoretical milestones in the development of the DSA, its current state and future developments.

I. PREAMBLE ON SPLITTING AND RUSSIAN ROULETTE

Splitting and Russian roulette (RR) rank among the oldest of variance reduction techniques. Unlike biasing, they do not involve altering the transport operator and are consequently easier to implement in a Monte Carlo code. As well as being easier to use compared with biasing, they are also generally considered safer. Above all splitting and Russian roulette are of totally general application. Their disadvantage lies in the fact that they may be relatively inefficient compared with a well biased calculation (an optimally biased calculation results in a zero variance whilst optimum splitting/RR does not). This is not usually in itself too great a disadvantage as it may be very difficult to bias a calculation well. However when the quantity of interest involves extremely rare events, splitting simply will not work as the events are not covered in the simulated random walk. (As an example consider particle streaming along very long, narrow ducts. The important particle tracks are those whose direction cosines are contained within an extremely small solid angle.) In this case biasing [or a technique such as DXTRAN (Ref. 1) that involves sampling from a non–analogue probability density function] must be employed.

Splitting and Russian roulette may be conveniently divided into two categories: weight–independent splitting/RR and weight–dependent splitting/RR. The former is also referred to as "geometrical" splitting/RR (although it is not necessarily executed only in space). The well–known "weight window" technique comes within the latter category. Weight–independent splitting/RR splits or Russian roulettes at a surface in phase space by the same amount independent of the weight of the progenitor striking the surface. Thus if weight variations are present (brought about by the use of some biasing technique), geometric splitting/RR will conserve them. Instead weight–dependent splitting/RR splits or Russian roulettes at a surface in phase space by an amount that depends on the weight of the progenitor. The objective is to smooth out weight variations by splitting high–weight tracks which, if they score, will damage the second moment, and Russian rouletting low weight tracks to avoid wasting too much time. Thus weight–dependent splitting/RR is employed when some other variance reduction method is being employed and controls the track weight. Weight–independent splitting/RR is appropriate when no other variance reduction method is being employed and controls the track population.

II. IMPORTANT MILESTONES IN THE DEVELOPMENT OF THE DSA

The Direct Statistical Approach (DSA) is a rigorous mathematical model for optimizing splitting and Russian roulette parameters in Monte Carlo particle transport calculations, originally developed by Dubi (Ref. 2). Dubi's general model of 1985 followed earlier more restrictive models of 1982 and 1983 (see for example Ref. 3). Earlier work by Juzaitis (Ref. 4) among others should also be mentioned. The impulse for this development derived from the recognition that there should exist some optimum amount of splitting/RR that gives a minimum error in a fixed time (splitting decreases the second moment and increases the time whilst Russian roulette increases the second moment and decreases the time). Splitting more than this optimum amount and the pay–off from the reduced second moment is more than compensated by the increased time. Splitting less than this optimum amount and the pay–off from the reduced time is more than compensated by the increased second moment. *Vice versa* for Russian roulette.

II.A. The Surface Parameter Model and the Cell Model

Dubi's 1985 model (Ref. 2) employs what has subsequently been named the "surface parameter model". A user–supplied parameter $\nu(i)$ is assigned to each surface i (the surface may be in normal space, in energy and in angle). In the direction of crossing that is towards the detector, the particle is split $\nu(i)$-to-1 with the weight of each progeny updated by the factor $1/\nu(i)$. In the other direction of crossing, the particle is Russian rouletted with survival probability $1/\nu(i)$. If

it survives, its weight is updated by the factor ν(i) (see Fig. 1). In the model described in Ref. 2, a general configuration of surfaces is allowed (Fig. 2). This model had the disadvantage that both the second moment and time functions had an open form (see for example Ref. 5). As both the coefficients and function form must be estimated, this lead to problems in estimating the functions that were particularly evident when there was a general diffusion of tracks between the surfaces. Another undesirable aspect was that tracks at the same phase space point could have different weights depending on the path they took to arrive at that point (this in the absence of any biasing). This tended to reduce the efficiency of the calculation. It should also be mentioned that the direction of splitting at a surface had to be chosen *a priori*.

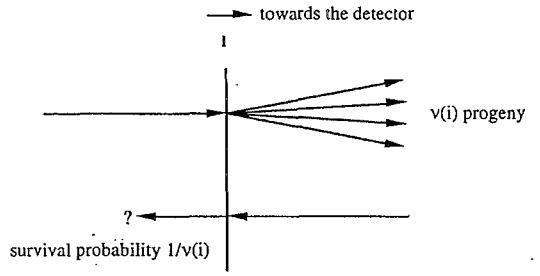

Fig. 1: Surface Splitting/RR

Fig. 2: General Surface Configuration in the DSA Surface Parameter Model

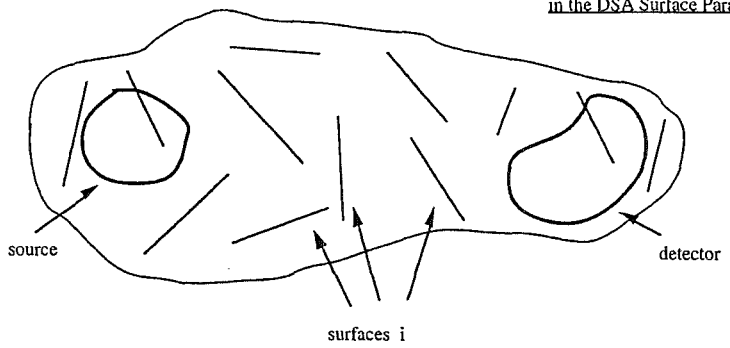

These disadvantages lead to the development of the "cell model". Firstly the parameter ν(i) was allowed to be non-integer (Ref. 6). This then permitted ν(i) to be defined as the ratio of parameters assigned to the volumes on either side of the surface i. If the particle is leaving volume J and entering volume K, with assigned parameters F(J) and F(K), splitting or Russian roulette is performed according to the ratio F(K)/F(J). If F(K)/F(J) > 1, splitting ensues. If F(K)/F(J) < 1, RR ensues (see Fig. 3).

The amount of splitting or RR is decided by the following algorithm: we put η(i) equal to F(K)/F(J). Then we define $\eta^*(i)$ as the integer part of η(i) and R(i) as the decimal part of η(i), i.e.

$$R(i) = \eta(i) - \eta^*(i)$$

When a track (the progenitor) of weight W impinges on the surface i, either with probability R(i) it is split into $[\eta^*(i) + 1]$ identical progeny each of weight $W/\eta(i)$, or (with probability [1 - R(i)]) it is split into $\eta^*(i)$ identical progeny each of weight $W/\eta(i)$. These two events are of course exclusive. When η(i) > 1, this model corresponds to what has been termed "expected value splitting" (Ref. 7). When η(i) < 1, it corresponds to Russian roulette.

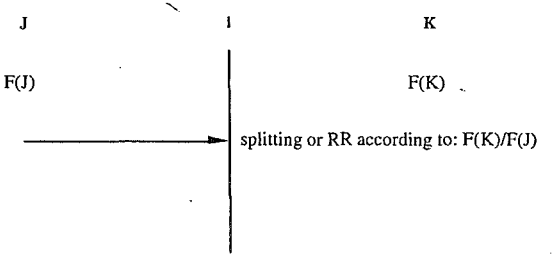

Fig. 3: Splitting/RR at Surfaces according to Cell Importances

Covering all space with volumes J and K produced the "cell model" (Refs. 8 and 5) (see Fig. 4). Note that the development from the "surface parameter model" through the "volume parameter model" to the "cell model" is described in logical and chronological order in Refs. 6, 8 and 5. The cell model, in contrast to the surface parameter model, has closed second moment and time functions. Thus only the coefficients of the functions need be estimated. Linked to this fact is the desirable feature that tracks at the same phase space point have the same weight, independent of the path they took to arrive at that point (this in the absence of any biasing). In fact the cell model is that employed in most codes, including MCNP, although with the DSA cells exist in a two-dimensional phase space consisting of normal space and energy (it has not been considered worthwhile to add the angular variable as this can be handled by the spatial variable).

Fig. 4: General Cell Configuration in the DSA Cell Model

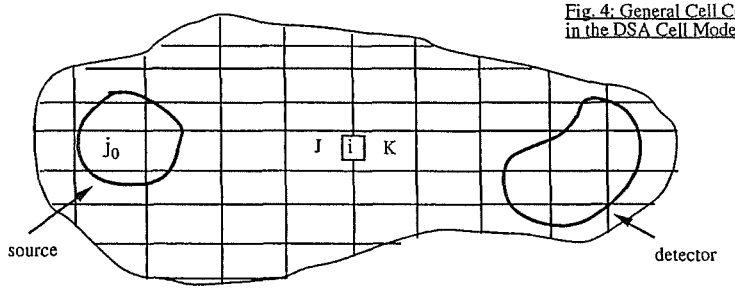

Concerning the form of the second moment and time functions in the cell model, we recopy expressions (27) and (43) of Ref. 9.

$$\Delta^o = \sum_{j_0} F(j_0) \sum_{I^i=1}^{L} \sum_{I^o=1}^{2N} \left\{ \text{Coef-d}(j_0, I^i/I^o) \cdot \frac{1}{F(K)} \cdot \frac{\text{Int}(G(J,K))}{G(J,K)} \cdot [2.G(J,K) - \text{Int}(G(J,K)) - 1] \right\} \quad (27)\ (\text{Ref. } 9)$$

where Δ^o represents the component of the second moment from surface splittings at a cell boundary, G(J,K) is F(K)/F(J), the sum over j_0 is over all source cells and the sum over I^o is over all cell boundaries (the sum over I^i plays no role here).

$$T = \sum_{j_0} \frac{1}{F(j_0)} \left\{ \text{Coef-t}(j_0) \cdot F(j_0) + \sum_{I^o=1}^{2N} \{\text{Coef-t}(j_0, I^o) \cdot F(K)\} \right\} \qquad (43)\ (\text{Ref. 9})$$

where T is the total CPU time (per source particle), the sum over j_0 is over all source cells and the second sum is again over all cell boundaries.

We have introduced these two expressions just to make the point that the second moment and time functions are closed – the number of source cells is finite and known, as is (in principle) the number of cell boundaries. Similar expressions are given in Sec. II.E where all components of the second moment function are shown. Instead with the surface parameter model, the equivalent second moment contribution is given by expression (10) in Ref. 9:

$$\delta(a_s^o, a_t^o - a_s^o, a_n^o - a_t^o, a'^o_k - a_t^o)$$

which must then be summed over all surface paths using one of the algorithms given in section V of Ref. 9. No closed form of the function exists. The time function with the surface parameter model is given by expression (38) in Ref. 9, $\tau(a_n^o)$, which again must be summed over all surface paths in an algorithmic fashion as discussed in VII.A of Ref. 9.

The closed nature of the function is the principal motive that the DSA cell model has been reasonably successful. A disadvantage of the cell model compared with the surface parameter model is that the form of the second moment function involves many cusps (local minima) that slow down the optimization routine (see Sec. III.B). Notwithstanding, the optimization remains feasible, and this disadvantage is far outweighed by the advantage in the facility of estimating the functions.

II.B. Estimating the square of the adjoint flux

The major obstacle has then been the necessity of estimating the square of the adjoint flux at a crossing point on a cell boundary. This appears in parts of the second moment function dealing with splittings at cell boundaries (in both the surface parameter and cell models). As an example we recopy expression (25) of Ref. 9:

$$\delta(a_s^o)(\text{cell}) = P(i^i_1) \cdot \underset{i^i_t}{<} <W^2(i^i_1; m^i_1)> \cdot \sum_{1^i_1=1}^{\lambda(i^i_1)} \Bigg[P(a^o_1; m^i_1, 1^i_1) \cdot \underset{i^o_1}{<} <W^2(a^o_1; b^o_1)> \cdot P(a^i_2; b^o_1) \cdot \underset{i^i_2}{<} <W^2(a^i_2; b^i_2)> \cdot$$

$$\sum_{1^i_2=1}^{\lambda(i^i_2)} \Bigg[P(a^o_2; b^i_2, 1^i_2) \cdot \underset{i^o_2}{<} <W^2(a^o_2; b^o_2)> \cdot P(a^i_3; b^o_2) \cdot \underset{i^i_3}{<} <W^2(a^i_3; b^i_3)> \cdot$$

$$\sum_{1^i_3=1}^{\lambda(i^i_3)} \Bigg[P(a^o_3; b^i_3, 1^i_3) \cdot \underset{i^o_3}{<} <W^2(a^o_3; b^o_3)> \cdot \ \ldots\ldots\ldots\ldots \ \cdot P(a^i_s; b^o_{s-1}) \cdot \underset{i^i_s}{<} <W^2(a^i_s; b^i_s)> \cdot$$

$$\sum_{1^i_s=1}^{\lambda(i^i_s)} \Bigg[P(a^o_s; b^i_s, 1^i_s) \cdot \underset{i^o_s}{<} <W^2(a^o_s; b^o_s)> \cdot \underset{i^o_s}{<} (\Phi^*(a^o_s; b^o_s))^2 > \Bigg] \underset{i^i_s}{>} \ \ldots\ldots\ldots\ldots \ \underset{i^o_3}{>} \Bigg] \underset{i^i_3}{>} \underset{i^o_2}{>} \Bigg] \underset{i^i_2}{>} \underset{i^o_1}{>} \Bigg] \underset{i^i_1}{>} \cdot$$

$$\frac{F(j_0)}{F(j_s)} \cdot \frac{\text{Int}(G(j_{s-1}, j_s))}{G(j_{s-1}, j_s)} \cdot [2.G(j_{s-1}, j_s) - \text{Int}(G(j_{s-1}, j_s)) - 1] \qquad (25)\ (\text{Ref. 9})$$

which is included within the coefficient in expression (27) from Ref. 9 above. We see in the penultimate line of expression (25) from Ref. 9 the appearance of the adjoint flux squared. As can be imagined, it turns out to be statistically difficult to estimate this quantity. The following expression (1) must be used to estimate the square of the adjoint flux at the particular phase space crossing point:

$$[\Phi^*(a^o_s; b^o_s)]^2 = [E(\bar{x})]^2 = \frac{1}{(N-1)} \cdot [N.E(\bar{x}^2) - E(\bar{x}^2)] \qquad (1)$$

where x is the detector contribution of a track at the phase space crossing point $(a^o_s; b^o_s)$ and N is the number of samples of x (see Ref. 10, Sec. IV.A). As discussed in Sec. IV.A of Ref. 10 and elsewhere, N must be greater than 1, so there must be a non–zero probability of splitting at all boundaries, implying a change of the previous cell model boundary crossing algorithm. Furthermore at least two tracks out of the N must give a non–zero detector contribution, to give a non–zero contribution to $(\Phi^*)^2$. This is extremely unlikely in any kind of deep penetration problem. It may help to consider a particular example of a particle crossing from one cell to another and suffering a 4–to–1 splitting (see Fig. 5).

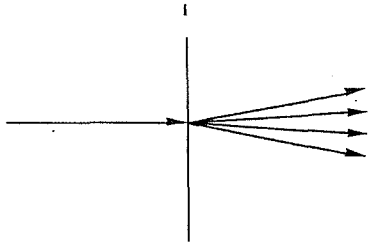

Fig. 5

At least two out of the four progeny should contribute to the detector to give a non–zero contribution to $(\Phi^*)^2$ at the crossing point. If zero or only one progeny give a detector contribution, a zero contribution to $(\Phi^*)^2$ ensues. Clearly unless there is a reasonably high probability of a progeny scoring, the error on $(\Phi^*)^2$ will be high. To increase the probability of one of the progeny scoring, we must increase the splitting between the boundary in question and the detector. But we remember that the same applies to every cell boundary crossing. It is clear that to estimate $(\Phi^*)^2$ with a reasonable error at all the boundary crossings, we would need to split by an ever–increasing amount going from the source to the detector. Such a calculation might sample very poorly the phase space near the source and consequently also phase space further from the source as the progenies further from the source come from the (few) nearer the source. Such a calculation might also be difficult to control, with the danger of creating an artificial supercriticality. Furthermore particles crossing the boundary towards the left in Fig. 5, which with the normal surface crossing algorithm would be Russian rouletted, would need also to be split, or at least to undergo splitting with some probability. Clearly problems exist with trying to estimate $(\Phi^*)^2$ correctly according to expression (1) at each boundary crossing.

An algorithm has been implemented that properly estimates the second moment function at all boundary crossings. Notwithstanding the problems mentioned above, the exact second moment function can be estimated and employed to determine the optimum phase space importances, but only in a restrictive class of problems. The objective has been to develop a method of general application. Therefore a series of approximation have been developed to deal with the problem of estimating $(\Phi^*)^2$. This development is described in Sec. IV.A of Ref. 10. Essentially it is necessary to group together progeny from different progenitors. As well as improving the statistics, this also solves the problem of what to do at a Russian roulette boundary so that the normal cell model boundary crossing algorithm may be employed. How do we group together progeny from different progenitors, given that the progenitors impinge at different phase space points on the boundary?

This question is addressed in Sec. IV.A of Ref. 10. To summarize that discussion, starting from a first approximation ("the standard point–surface approximation") improvements were made until an approximation ["the enhanced point–surface approximation (second version)"] was reached that gave extremely good results under the most general of circumstances. Whilst not repeating this discussion here, we may illustrate the operation of the standard point–surface approximation by considering Fig. 6 where we see four progenitors arriving at different points at a boundary at which 3–to–1 splitting is executed.

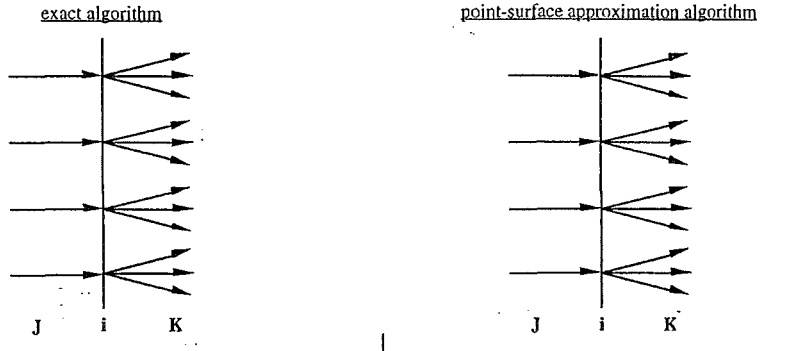

Fig. 6

Clearly the grouping together of the progenitors illustrated in Fig. 6 will lead to acceptable results only if the adjoint flux does not vary much between the points. If it does vary, then we will seriously underestimate $(\Phi^*)^2$ which leads to an overestimate in the splitting. Improving the standard point–surface approximation involved the introduction of a sub–binning of the progenitors. The angle variable proved to be the most difficult to treat (imagine just after crossing the boundary i that the particles enter a void streaming channel – the angle that the particle crosses the boundary i clearly then becomes critical). However as described in Sec. IV.A of Ref. 10, an acceptable solution was reached at least for neutron and photon transport at energies < 20 MeV.

More work could clearly be done on testing and improving the current version of the enhanced point–surface approximation. This is the central key to estimating a reasonable second moment function and therefore to the whole DSA. It is of interest to note that the next collision site is employed with the enhanced point–surface approximation. For neutral particle transport, this site serves to define an angular binning. Instead multiple scattering algorithms employed for charged particle transport alter the concept of a "collision". This problem is currently being faced for electron and positron transport. The current solution is to check whether the electron/positron has lost some fraction (currently 0.5) of its energy since the boundary crossing in question. If so, the electron/positron is considered to have suffered a "collision". This seems to be performing reasonably well so far but needs more testing. Some other solutions are also possible for charged particles.

II.C. Including all possible contributions to the second moment function

Up to this point in the DSA development, the only second moment contributions were:

– those mentioned above arising from surface splittings;

– those due to (the square of) the direct detector contributions. These are easier to calculate than the first kind of contributions and will not be discussed here. They are described in Ref. 9, Secs. IV.E and VI.D.

In fact there exist also contributions to the second moment from particle bifurcations, other than those due to splitting. These might be natural events such as (n,xn) or artificial events (such as DXTRAN). These have been named "volumetric bifurcations" in contradistinction to "surface bifurcations" i.e. splittings. There was a worry that not including such events might seriously underestimate the second moment, particularly for the case of DXTRAN spheres. In Ref. 9, the DSA theory was rewritten to include all such events. [At the same time a restraint was removed on the kind of estimator employed. Previous to Ref. 9 only an absorption or last event estimator was compatible with the DSA. In Ref. 9 all tally types (apart from pulse–height) were included. Tallies in which the particle survives were shown to be equivalent to volumetric bifurcations. This might be important in point detector applications.] It turned out that in most problems the contribution to the second moment from these volumetric bifurcations was relatively minor. It will be of interest if the same applies at high energies where there are more natural bifurcations.

In a similar fashion to surface splittings, an exact estimate of the second moment contribution from the volumetric bifurcations can be made, or alternatively an approximation bearing some resemblance to the point–surface approximation for surface splittings has been developed. Here the binning of the progeny is different because, whilst the progeny from a surface splitting event are identical, the progeny or "branches" from a volumetric bifurcation event are usually non–identical. This is discussed in Ref. 10, Sec. IV.B.

A spin–off from this development was the realization that it was possible to (correctly) estimate the second moment of a naturally bifurcating process whilst at the same time applying variance reduction in the form of the cell model and splitting/RR at cell boundaries. A first application seemed to be in the modelling of cosmic ray showers where moments higher than the first are of interest, and normally an analogue calculation is made to estimate them. Another application appeared in atomic collision cascades. It is important to note that in such calculations, whilst the exact algorithm for estimating the contribution to the second moment from the volumetric bifurcations must be employed, the exact algorithm would not need to be applied to the surface splitting contribution. This is because the function form of expressions such as (25) in Ref. 9, given here in Sec. II.B, force the latter contribution to be zero with analogue cell importances independently of the approximation attached to $(\Phi^*)^2$. An interesting related future theoretical development would be to estimate the third and higher moments.

II.D. Introducing a weight dependence

"Geometric" splitting/RR operates purely through population control and therefore conserves any weight variations that might be present due to the use of biasing or pseudo–biasing techniques. Thus the weight–independent splitting/RR in the DSA up to and including Ref. 9 may find an optimum in the presence of transport biasing but this optimum will be a poor one. This is because it is extremely important: a) to save time by Russian rouletting low weight particles and b) to reduce the weight of high weight particles by splitting thereby preventing a high weight particle scoring in the detector which would highly damage the error. Thus such problems require a weight control as well as a population control.

A word here on source biasing which is an exception to the above rule. If the source is biased in the same phase space structure as that used by the DSA, then it has been found that a reasonable optimum may be found with "geometric" splitting/RR. Furthermore it would actually be theoretically possible to include an optimization of the source biasing within the DSA under these conditions. However there is implemented at present a "pseudo–source biasing" (see Ref. 11, page 740) that within the DSA compensates for a poorly sampled source and that has proved satisfactory.

Returning to transport biasing, two examples that immediately spring to mind are:

1) gamma transport in a bulk medium where, as is well known, path length stretching (also known as the exponential transform) can greatly improve the efficiency of the calculation compared with simply controlling the gamma track population.

2) particle streaming in narrow ducts or particle leakage from a large space into a small exit hole. In such cases DXTRAN spheres (Ref. 1) are recommended. Their main role is to deterministically produce scattering into a predefined (and usually very small) solid angle, that in analogue transport might never be entered.

Both these techniques and especially the second produce large weight variations that must be dampened for the reasons given above. Usually this dampening was made with the weight window technique (Ref. 1).

To be able to optimize the quality function (the product of the second moment and time functions) the DSA requires the functions to be separable. For the case of weight–independent splitting/RR this is possible under most circumstances. Instead if the amount of splitting or Russian roulette depends on the weight of the progenitor arriving at the cell boundary, the second moment is no more simply separable (as discussed on page 142 of Ref. 10). This is a well–known result. The motive behind the work of Ref. 10 was to analyze this situation of non–separability and to attempt some approximations to try to overcome it. As it turned out, an approximation was found [named "the noninteger approximation" (Sec. III.D of Ref. 10)] which looked extremely promising, and a DSA version was developed to include weight–dependent splitting/RR using this approximation. This approximation tends to underestimate the second moment. In the case of gamma transport in a bulk medium with path length stretching (Sec. V.B of Ref. 10), this underestimate was very small. Instead for problems involving DXTRAN spheres the underestimate became noticeable but still acceptable (see Secs. V.C and V.D of Ref. 10). (The reason for the difference in the underestimate between the two kinds of problem is that the noninteger approximation calculates wrongly contributions to the second moment from Russian roulette events. With DXTRAN spheres there are many such events as there are many low weight tracks present.)

Concerning the weight–dependent DSA algorithm the following points may be mentioned:

– rather than using a window of acceptable weights, the method requires a single weight (a starting weight of all particles entering each phase space cell, per cell, see Fig. 7).

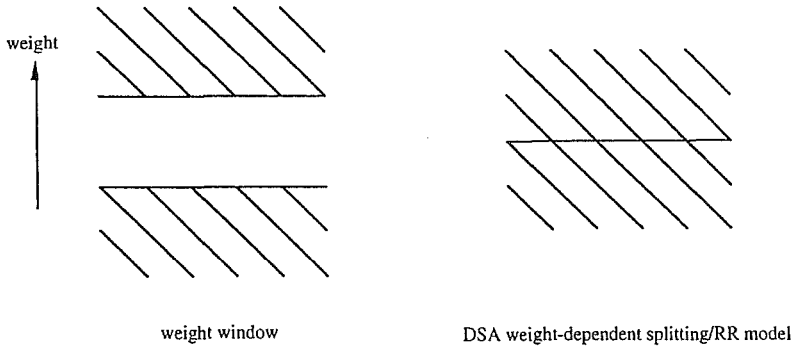

Fig. 7. Comparison of the DSA weight-dependent splitting/RR model with the weight window.

The weight line model was employed because it was believed that it would be more amenable to theoretical analysis, as proved the case. An analysis of the weight window model has not yet been attempted. When there are large weight variations present, then the behaviour of the two models should be similar. Instead if the weight variations are limited and the cells are relatively small, then the weight window could prove more efficient as the weight line imposes a splitting or Russian roulette sequence on every particle arriving at the cell boundary.

– compared with the weight–independent DSA algorithm, the weight–dependent algorithm may run into greater difficulties estimating the second moment coefficients as, with the noninteger approximation, a difference is made between two estimates [see expression (41) of Ref. 10 and Sec. II.E here]. In partial compensation, the form of the second moment function allows a much faster minimization compared with the weight–independent case.

– in general the weight–dependent DSA algorithm has been used and tested far less than the weight–independent algorithm, and conclusions on its utility are still tentative.

II.E. Summarizing the second moment and time functions in the DSA cell model.

It is convenient at this point to summarize the second moment and time functions in the DSA cell model, including all contributions to the second moment and with both weight–independent and weight–dependent splitting/RR. This section is taken from Sec. II of Ref. 12.

The DSA weight–independent cell importance model

The population second moment, S^2, consists of three kinds of terms: Δ^o, Δ^i, and Γ representing the contributions from splittings at cell boundaries, volumetric bifurcations and direct detector scores respectively. (See Figs. 3 and 4).

$$\Delta^o = \sum_{j_0} F(j_0) \sum_{I^i=1}^{L} \sum_{I^o=1}^{2N} \left\{ \text{coef–d}(j_0, I^i/I^o) \cdot \frac{1}{F(K)} \cdot \frac{\text{int}(G(J,K))}{G(J,K)} \cdot [2.G(J,K) - \text{int}(G(J,K)) - 1] \right\} \quad (1)\ \text{(Ref. 12)}$$

$$\Delta^i = \sum_{j_0} F(j_0) \sum_{I^i=1}^{L} \left\{ \text{coef–d}(j_0, I^i) \cdot \frac{1}{F(J)} \right\} \quad (2)\ \text{(Ref. 12)}$$

$$\Gamma = \sum_{j_0} F(j_0) \left\{ \text{coef–g}(j_0) \cdot \frac{1}{F(j_0)} + \sum_{I^o=1}^{2N} \left[\text{coef–g}(j_0, I^o) \cdot \frac{1}{F(K)} \right] \right\} \quad (3)\ \text{(Ref. 12)}$$

and

$$S^2 = \Delta^o + \Delta^i + \Gamma \quad (4)\ \text{(Ref. 12)}$$

In expression (1) (Ref. 12) each term within the summation brackets represents the contribution from splittings at the boundary between cells J and K with importances F(J) and F(K) respectively. [and G(J,K) = F(K)/F(J)]. The pair of variables: I^i/I^o represents the boundary between cells J and K, thus the double sum over I^i and I^o represents a sum over all cell boundaries.

In expression (2) (Ref. 12) each term within the summation brackets represents the contribution from bifurcations within each cell J. The variable I^i represents bifurcations of a certain type within cell J, thus the sum over I^i represents a sum over all bifurcation types and over all cells.

In expression (3) (Ref. 12) each term within the inner summation brackets represents the contribution from detector scores within each cell K. The sum over I^o represents a sum over all cells. The first term within the outer summation brackets represents the contribution from detector scores within each source cell j_0.

The coef–.... variables are problem–dependent coefficients whose values must be estimated:

– coef–$d(j_0,I^i/I^o)$ in expression (1) (Ref. 12) involves the product of the square of the track's weight as it crosses a cell boundary and the square of the adjoint flux at the crossing point.

– coef–$d(j_0,I^i)$ in expression (2) (Ref. 12) involves the product of the square of the track's weight as it experiences a bifurcation within a cell and the product of the adjoint fluxes of each pair of tracks at the bifurcation point.

– coef–$g(j_0)$ and coef–$g(j_0,I^o)$ in expression (3) (Ref. 12) involve the square of a track's detector score.

The estimates of these coefficients are all subject to greater statistical uncertainties compared with the estimate of a normal (linear) response as they include the squares of quantities. Estimating the square of the adjoint flux at a phase space point on a cell boundary, required in the coefficient: coef–$d(j_0,I^i/I^o)$, is particularly difficult and has been discussed in Sec. II.B.

The time per source particle is given as follows:

$$\bar{T} = \sum_{j_0} \frac{1}{F(j_0)} \left\{ \text{coef–t}(j_0) \cdot F(j_0) + \sum_{I^o=1}^{2N} [\text{coef–t}(j_0,I^o) \cdot F(K)] \right\} \qquad \text{(5) (Ref. 12)}$$

Each term within the inner summation brackets represents the CPU time spent by tracks within each cell K. The sum over I^o represents a sum over all cells. The first term within the outer summation brackets represents the CPU time spent by tracks within each source cell j_0. The problem–dependent coefficients: coef–t (j_0) and coef–t (j_0,I^o) are much easier to estimate compared with the second moment coefficients as they consist only of linear or first moment–like quantities.

The DSA weight–dependent weight line model

After applying the non–integer approximation, the three kinds of terms composing the population second moment, S^2, are given as follows:

$$\Delta_w^o = \sum_{j_0} \sum_{I^i=1}^{L} \sum_{I^o=1}^{2N} [\text{coef–}d_w(j_0,I^i/I^o)(1) \cdot \Omega(J) - \text{coef–}d_w(j_0,I^i/I^o)(2) \cdot \Omega(K)] \qquad \text{(6) (Ref. 12)}$$

$$\Delta_w^i = \sum_{j_0} \sum_{I^i=1}^{L} \text{coef–}d_w(j_0,I^i) \cdot \Omega(J) \qquad \text{(7) (Ref. 12)}$$

$$\Gamma_w = \sum_{j_0} \left\{ \text{coef–g}(j_0) + \sum_{I^o=1}^{2N} [\text{coef–}g_w(j_0,I^o) \cdot \Omega(K)] \right\} \qquad \text{(8) (Ref. 12)}$$

The time per source particle is given as follows:

$$T_w = \sum_{j_0} \left\{ \text{coef–t}(j_0) + \sum_{I^o=1}^{2N} \left[\text{coef–}t_w(j_0,I^o) \cdot \frac{1}{\Omega(K)} \right] \right\} \qquad \text{(9) (Ref. 12)}$$

As far as the function dependence is concerned, comparing the weight–dependent expressions with the weight–independent expressions, we see that the form is very different for the second moment contributions from the cell boundaries, Δ_w^o. [In particular we note the presence of negative terms in expression (6) (Ref. 12) which increase the statistical error on the estimates of this contribution.] Instead for the other second moment terms and the time, the form is similar once the cell starting weights $\Omega()$ are equated with the inverse of the cell importance F().

As far as the coefficients are concerned, the weight–dependent coefficients contain a different dependence on the surface–to–surface probabilities and accumulated weights compared with the weight–independent coefficients (see Ref. 10). However the coefficients dealing with track bifurcations in expressions (6) (Ref. 12) and (7) (Ref. 12) still contain the square of the adjoint flux at the cell boundary crossing point and the product of the adjoint fluxes of each pair of tracks at the bifurcation point, respectively.

II.F. Moving to multiple responses.

Although standard Monte Carlo methods may treat problems involving a high attenuation, they do so only by calculating a single response at a time. This is because each variance reduction method, including splitting/RR, requests a set of user–defined parameters. For a given response there exists an optimum set that provides a minimum statistical error in time T. (Here we have changed nomenclature. T will be now used for the total CPU time for all source particles in the run. The time per source particle is changed from T used previously to τ.) Parameters that are near optimum for one response may be far from optimum for another response.

The DSA provides a way to optimize a calculation to more than one response of interest. The development goes as follows (taken from Ref. 13):

The DSA searches for the set of variance reduction parameters that renders the quality factor q (the product of the second moment and the time) minimum, i.e.

$$q = S^2 \cdot \tau \qquad (2)$$

The justification for minimizing q is found in Ref. 3. Following Ref. 3, a reasonable measure of the inverse of the efficiency of a Monte Carlo calculation is:

$$q' = V_S \cdot T_S \qquad (3)$$

where V_S is the variance of a sample of N independent histories, and T_S is the computing time required for the sample. Then if V is the variance of the population and τ is as before, we have:

$$V_S = \frac{V}{N} \qquad (4)$$

and

$$T_S = \tau \cdot N \qquad (5)$$

Thus:

$$q' = V \cdot \tau \qquad (6)$$

where in expression (6) we have quantities that are independent of the size of our sample N. Finally:

$$V = S^2 - D^2 \qquad (7)$$

where D is the first moment. In problems that require a non–analogue treatment, $S^2 >> D^2$. Thus q' in expression (6) can be approximated by q in expression (2).

So far we have been assuming a single response of interest. We rewrite expression (2) for response i as:

$$q_i = S_i^2 \cdot \tau \quad (8)$$

or:

$$\frac{q_i}{D_i^2} = \frac{S_i^2}{D_i^2} \cdot \tau \quad (9)$$

and for the case of M responses, we have:

$$q_{fc} = \sum_{i=1}^{M} \frac{q_i}{D_i^2} = \sum_{i=1}^{M} \frac{S_i^2}{D_i^2} \cdot \tau \quad (10)$$

where the subscript "fc" stands for "fractional and compound".

The well–known quantity the "figure of merit" (fom) used in such codes as MCNP to give a measure of the quality of a calculation on a given machine is defined as:

$$fom = (fsd^2 \cdot T_S)^{-1} \quad (11)$$

where fsd is the fractional standard deviation and T_S is the computing time for the sample N. If we define a "compound figure of merit" (fom_c) for a number of responses i, i=1,M as:

$$fom_c = \left(\sum_{i=1}^{M} (fsd_i)^2 \cdot T_S \right)^{-1} \quad (12)$$

then $(q_{fc})^{-1}$ and fom_c are equivalent with the approximation of employing the second moment instead of the variance. Thus our objective is to maximize fom_c, through the estimation using the DSA model of S_i^2 and τ (and of D_i).

An immediate doubt that springs to mind is whether it is actually useful to optimize variance reduction parameters to more than one response. Even if we could find the optimum, perhaps it would be a very poor one – imagine a deep penetration problem and the calculation of doses at different spatial locations, for example around an accelerator experiment. It may be that the sets of optimum variance reduction parameters related to each individual response are so different from one another, that it would be more efficient to run a calculation for each response in turn. However if the spatial locations are near each other, or if we wish to calculate different responses at the same spatial location, then there will be a correlation between tracks that contribute to one response and tracks that contribute to another. Under this circumstance a multi–response optimization can be more efficient than a number of single response optimizations.

In Ref. 13 the problem under consideration was an epithermal column attached to a research reactor for use in BNCT. Here a number of responses need to be calculated at the same location: the neutron flux in a sufficient number of energy groups to give a reasonable spectrum, the fast neutron dose and the gamma dose. Under these circumstances the multi–response optimization was more efficient compared with single response optimizations, both in terms of CPU time and, more importantly as is emphasized in Ref. 13, in terms of human time and effort (see also Ref. 14).

Recently a multi–response optimization has successfully been made with 84 responses on a thermal neutron facility for calibration of dosimetric instruments (Ref. 15). The 84 responses were all point detectors and were made up of 6 neutron energy groups at 14 spatial points, with the objective of calculating a finer neutron spectrum (29 energy groups) at all 14 spatial positions. This is an unusually high number of responses and normally such a number would not be treatable. It was only possible because of the relatively small number of spatial cells (13) and energy groups used in the transport to define the phase space cells (8) (see Sec. III.B).

The multi–response facility has not yet been tested with the weight–dependent DSA.

III. THE CURRENT SITUATION

We now have the following situation: a method that finds the optimum population control (within the constraints of the cell model), that can work with any estimator (apart of course from pulse–height), that takes into account all contributions to the second moment and that can handle any number of responses (with *caveats* given below). The DSA is attached to the code MCNP, currently version 4B (Ref. 1). Until recently the DSA could handle neutron and photon transport only. Under these conditions and in the energy range covered by MCNP4B, the approximation employed in the estimation of the second moment [the second version of the enhanced point–surface approximation used in the estimation of $(\Phi^*)^2$] has proved generally excellent. An extension has recently been made to electron transport in MCNP4B (any combination of the 3 species – neutron, photon and electron – may be treated), and this is currently being tested.

As far as the weight–dependent DSA algorithm is concerned, this functions under exactly the same circumstances as the weight–independent algorithm above, with the provisos already mentioned in Sec.II.D. It has in general been far less tested compared with the weight–independent algorithm.

III.A. Comparison with other methods available

A basic choice was to use Monte Carlo to generate the information required by the DSA. Therefore comparisons have not been made with approaches that employ adjoint deterministic calculations to generate importances. Such approaches can be very powerful under certain circumstances. They are not of general application. Thus the method that has been used as a yardstick for the DSA has been the weight–window generator, and in particular its form in MCNP.

We need to ask the following questions:

1) How long does it take to reach the optimum?
2) How do we know we have reached the optimum?
3) How good is the optimum?

The third question will be taken first as it allows a more definitive reply. In Ref. 11 some comparisons were made between an early version of the cell model weight–independent DSA and the "quasi–deterministic weight–window generator" which, as its name implies, is a development of the standard weight–window generator with added deterministic features. The comparisons concerned problems which had no transport biasing. In Ref. 11 it was found that for bulk penetration problems, the DSA and weight–window optima were quite similar. Instead for streaming problems the DSA produced a better optimum than the weight–window. Such problems are characterized by a very large change in the expected response contribution (importance) of a track after a single sampling (see Ref. 11, page 762). In the case of streaming, this sampling is of the angle that a particle exits from a collision that takes place at one end of the duct. In general the conclusions of Ref. 11 have been confirmed by other unpublished comparisons. A factor of roughly 2 between the quality of the calculations was noted in Ref. 11. Instead in Ref. 12 a factor of approximately 8 for a deep penetration problem ("activation rate in wire in reactor core") was found between the DSA and the standard weight–window generator of MCNP. Again this problem had the characteristic of a very large change in the expected response contribution of a track after a single sampling. In Ref. 10 some comparisons were made between the weight–dependent DSA and the weight–window generator. The conclusions were tentative but similar to those above for weight–independent splitting/RR, although it is to be noted that there was little difference in the quality of the streaming calculations in Ref. 10 when DXTRAN spheres were used. Unpublished comparisons between weight–dependent DSA and the weight–window generator for the "activation rate in wire in reactor core" problem of Ref. 12 have been made, the difference with the problem in Ref. 12 being the inclusion of a rather strong path length stretching towards the

central wire, creating thus a strong weight variation. Again the DSA gave a calculational quality 8 to 10 times that of the weight–window generator.

The first two questions are linked – if we are not sure when we have reached the optimum, then we might spend longer before we are sure we have reached it. Furthermore the first question depends to some extent on user experience and also on luck. In a rather informal discussion here we hope to show certain advantages that may be perceived in the DSA as far as the second question is concerned.

We wish to adopt some kind of iterative technique to arrive at the optimum so that we can gauge how near we are getting. With a method that employs Monte Carlo to generate the required information, we must first start off with some guessed variance reduction parameters at the zero'th iteration. The run that employs these parameters will provide a response, an error, a figure–of–merit (measuring the calculational quality) and a set of generated variance reduction parameters. This set of parameters is employed in the first iteration run that provides again a response, an error, a figure–of–merit and a set of generated variance reduction parameters. This set of parameters is employed in the second iteration run, etc. With the weight–window generator in MCNP, the set of parameters consists of the weight–window lower bounds in each space/energy cell.

The information we have available at each iteration is the response, error, figure–of–merit and set of generated parameters. It is the author's experience that changes in the generated variance reduction parameters from iteration to iteration offer no enlightenment on the approach to the optimum. (Exceptions are gross or absurd parameter values.) This is because we do not know if an appreciable change in one of the variance reduction parameters (e.g. the weight–window lower bound in some cell and in some energy group in MCNP) is important or not to our response of interest. Our postulate is that the only information we have is the response, error and figure–of–merit at each iteration.

Now let us consider the situation with the DSA. As an example we take a real problem that had a single response of interest and employed the weight–independent DSA. The first point to note is that the DSA allows all information pertaining to the second moment and time functions to be accumulated between iterations. (This is not a basic characteristic of the method and the weight–window generator could be reprogrammed to do this.) Variance weighting is employed for all the quantities that are accumulated. Secondly as with the weight–window generator, the actual variance reduction parameters, in this case the phase space cell importances, are not examined, apart from a check for parameters that are clearly grossly in error.

Table I shows the iteration procedure for this problem. Most of the quantities have already been defined in Sec. II.F. CPU is the computer time for the run, MCT is the computer time for the Monte Carlo tracking – the difference between the two is time spent on book–keeping in generating the second moment and time functions. "stat fail" is the number of statistical failures (from 0 to 10) forming part of the statistical checks in MCNP4B. As has been seen, D^2/q is similar to the figure–of–merit. In Table I all quantities under the heading "Generation of second moment and time functions" are direct estimates from the modified version of MCNP. All quantities under the heading "Minimization of quality function" are from the functions summarized in Sec. II.E. (apart from D, the detector response) and are accumulated. The quantities under the heading "Generation of second moment and time functions" are also available with other methods based on Monte Carlo generation of information, such as the weight–window generator. Instead the quantities under the heading "Minimization of quality function" are peculiar to the DSA. We have a single integral quantity, D^2/q, which the DSA is maximizing. We see at iteration numbers 2 and 3 that the DSA is unable to increase this quantity appreciably. Therefore we conclude we have reached the optimum.

We may also compare the direct estimate of D^2/q with the function value: D^2/q (init) at the same iteration, and the best function value: D^2/q (opt) with the direct estimate at the next iteration. (Actually rather than compare the D^2/q values in this fashion, it is of greater significance to compare the S^2 values which are more uncertain compared with the time values.)

With the weight–dependent splitting/RR algorithm discussed in Sec. II.D, we have already noted that the non–integer approximation underestimates the second moment. Therefore when we make a table such as Table I with the weight–dependent algorithm, we expect the function value of S^2 to be lower than the direct estimate. Examples of such tables with weight–dependent splitting/RR can be found in Refs. 10 and 12. We reproduce here (as Table II) Table V from Ref. 10 in which we see quite clearly the (small) underestimate in the functional value of S^2 and the consequent overestimate in D^2/q. [Note that in Table II the "S^2 (opt)" and "τ (opt)" are not written, neither is the Monte Carlo tracking time (which was very near the CPU time for this problem), but the "q" values are written.] Thus in general with the weight–dependent splitting/RR algorithm we may employ the same "handles" as with the weight–independent splitting/RR algorithm in deciding when we have reached the optimum but with a small decrease in the amount of freedom in the sense that the direct estimate and function values of S^2 differ because of the non–integer approximation. However the difference in the problems treated so far has not been large (< 40% in Ref. 10).

It is worthwhile here noting that the difference between the direct estimate and the function values of S^2 can be large, even with the weight–independent splitting/RR algorithm, when the point–surface approximation breaks down, as happened in the problem "activation rate in wire in reactor core" in Ref. 12. However for the kind of problem in which this happens, the DSA is usually giving far superior results to other methods, even when the point–surface approximation begins to break down.

In the case of more than one response, there still exist the integral parameters S^2_{fc} [defined as the sum of the normalized second moments as in expression (10)] and q_{fc} [in expression (10)] and the same criteria may be used to approach the optimum, using these single integral parameters. An example of the optimization procedure for 4 responses is given in Table III (where the percentage error and number of statistical failures – "sf" – are under their respective responses). This was actually a BNCT problem; the first 3 responses were neutron fluxes and the 4th response was the gamma ray dose. The method was unable to bring the error on the gamma ray dose down to the errors on the neutron fluxes because of a high correlation between the two quantities, with the neutrons producing the contributing gammas after the neutrons had already scored.

Thus to summarize, as discussed in Sec. II.B the DSA would certainly have much more difficulty in generating information compared with conventional methods based simply on the importance estimate if the exact second moment function were estimated (involving an estimate of a second order quantity). Instead employment of the point–surface approximation involves a square of a first order estimate and eases the statistics considerably. Then the availability of more information with the DSA compared with conventional methods allows tables such as Tables I, II and III to be composed which permits the process of data generation to be controlled. It may also be that the second moment function form shown in Sec. II.E allows some relaxation on the precision of the coefficient estimates, referring particularly to the weight–independent algorithm. (This point has yet to be properly examined.)

III.B. The main current problems

1) Once reasonable coefficients of the second moment and time functions have been estimated, a multi–dimensional minimization must be carried out to find the cell importances, F(J) and F(K) with the weight–independent algorithm or the cell starting weights, Ω(J) and Ω(K) with the weight–dependent algorithm. The code that carries out this minimization is built around an IMSL routine called UMING. This routine carries out an unconstrained minimization. As we have the constraint of requiring +ve quantities, a transformation $y=x^2$ is made. This actually further slows down the minimization which is already difficult due to the presence of many local minima ["cusps", because of the integer operator in expression (25) of Ref. 9 reproduced in Sec. II.B] in the weight–independent splitting/RR second moment function. In fact the choice of an unconstrained minimization routine was probably a mistake, as a constrained routine might be faster. However the main problem is that IMSL is a commercial library

which is not available everywhere. Thus the DSA cell model codes are not 100% transportable and the minimization code should be rewritten using only open software.

2) When we have a large number of phase space cells, species or responses, or a combination of these, the book–keeping time in the modified form of MCNP that generates the second moment and time functions becomes an appreciable fraction of the total CPU time. We can see already in Table III that the Monte Carlo tracking time, MCT, is about 60 – 70% of the total CPU time. In this problem there were 4 responses, 28 spatial cells and 2 species (neutron and gamma) with 5 neutron energy groups and 5 gamma energy groups. For this problem, the useful tracking time is still a reasonable percentage of the total. Instead for other problems the useful tracking time has fallen to only 20% of the total. Why? The problem seems to lie in the way the coefficients of the second moment function are tallied, with by far the worst culprit being the component accounting for splitting at cell boundaries.

As noted in Sec. II.B, the enhanced point–surface approximation requires the boundaries between the cells to be subdivided both using the progenitors' characteristics at the boundary crossing point as well as the progenies' characteristics at the next collision point or detector score. When we consider all boundaries between pairs of cells in energy and space (and species), we realize that we are dealing with a large amount of data. The problem is that this data is not formatted in a simple fashion. *A priori* we do not have the information on which spatial cells are adjacent to each other, other than by observing the geometry. (This is a markedly different situation from the weight–window generator where instead of looking at cell boundaries, we are interested in cells.) Because of this, a variable multi–level format has been used, with pointers in one level defining data locations in the next level down. As an example we take the component of the second moment function accounting for splitting at cell boundaries:

The first level is for cells of type K in Fig. 3. The second level is for source cells (j_0 in Fig. 4). The third level is for cells of type J in Fig. 3. The fourth level is for the response number and the coefficient for cells j_0, J and K [as in expression (1) of Ref. 12 shown in Sec. II.E]. The fifth level is for the sub–cell in which the progenitor is binned, the sixth level is for sub–cell in which the progeny are binned and the seventh level is again for the response number and the tallying of the intermediary coefficients through which the coefficients at the fourth level are constructed with the enhanced point–surface approximation.

Now it is clear that when the amount of data becomes significant, non–negligible time is spent in searching for the correct location through the seven levels at all boundary crossing events. Furthermore when an item of data must be inserted for a new cell/sub–cell combination, the data from that point onwards must be shifted to leave space for the new item. These two appear to be the main factors for the large book–keeping times in some problems. It is possible that a different programming structure might strongly reduce this "dead time".

IV. THE FUTURE

The main line of current development is the extension of the DSA to the higher energy domain and to other particle types: electrons, protons, pions, etc. As a step along this road, the DSA has recently been extended to electron and positron transport in MCNP4B. As noted in Sec. II.B, the multiple scattering feature for charged particles has an influence on the enhanced point–surface algorithm. This problem seems to have been solved but requires further testing.

With more particle species and a greater energy range, problems will certainly be encountered with both the time wasted in book–keeping as well as possibly with the minimization time (at least for weight–independent splitting/RR), both problems mentioned in Sec. III.B. This is because the number of variables will be greatly increased. The current idea is to include only the important species within the DSA treatment and to ignore the other species. This is similar in some ways to how voids are treated – the option exists of excluding a void from the DSA: when a track enters a void, it suffers neither splitting nor Russian roulette; when a track leaves a void, splitting or RR is carried out using the importance of the cell to be entered and the importance of the last non–void cell. Applying the same idea to particle species, if a species A creates a species B which in turn creates a species C, and if A and C are DSA species, but not B, it is clearly important to know *a priori* that species B does not travel far compared with A or C. A number of automatic warning devices will need to be inserted to verify such hypotheses.

Another possibile way of getting round the explosion in the number of variabes will be to group together particle species. Again warning devices will need to be included to verify that the grouped species transport in a similar fashion.

REFERENCES

1. "MCNP – A General Monte Carlo N–Particle Transport Code" LA–12625–M, J.F. BRIESMEISTER, Ed., Group XTM, Los Alamos National Laboratory (1993).

2. A. DUBI: "General Statistical Model for Geometrical Splitting in Monte Carlo - parts I and II" *Trans. Theory and Stat. Phys.* **14–2** 167 and 195 (1985)

3. A. DUBI, T. ELPERIN and D. J. DUDZIAK: "Geometrical Splitting in Monte Carlo" *Nucl. Sci. Eng.* **80** 139 (1982)

4. R. J. JUZAITIS: "Minimizing the Cost of Splitting in Monte Carlo Radiation Transport Simulation" LA–8546–T, Los Alamos National Laboratory (1980)

5. K. W. BURN: "Complete Optimization of Space/Energy Cell Importances with the DSA Cell Importance Model" *Ann. nucl. Energy* **19–2** 65 (1992)

6. K. W. BURN: "Extension of the Direct Statistical Approach to a Volume Parameter Model (Non–Integer Splitting)" *Ann. nucl. Energy* **17–6** 293 (1990)

7. T. E. BOOTH: "Monte Carlo Variance Comparison for Expected–Value Versus Sampled Splitting" *Nucl. Sci. Eng.*, **89**, 305 (1984).

8. K. W. BURN: "Optimizing Cell Importances using an Extension of the DSA – Theory, Implementation, Preliminary Results" *Progress in Nuclear Energy* **24**, 39 (1990).

9. K. W. BURN: "Extending the Direct Statistical Approach to include Particle Bifurcation between the Splitting Surfaces" *Nucl. Sci. Eng.*, **119**, 44 (1995).

10. K. W. BURN: "A New Weight–Dependent Direct Statistical Approach Model" *Nucl. Sci. Eng.*, **125**, 128 (1997).

11. T. E. BOOTH and K. W. BURN: "Some Sample Problem Comparisons Between the DSA Cell Model and the Quasi–Deterministic Method" *Ann. nucl. Energy* **20–11** 733 (1993)

12. K. W. BURN: "Learning Aspects of the Direct Statistical Approach to the Optimization of Monte Carlo Radiation Transport Calculations" Workshop on Adaptive Monte Carlo Methods, Los Alamos, Aug. 1996 (see web site: http://www-xdiv.lanl.gov/XTM/projects/mc21/abs/pdf/burn.pdf)

13. K. W. BURN, E. NAVA: "Optimization of Variance Reduction Parameters in Monte Carlo Radiation Transport Calculations to a Number of Responses of Interest" Proc. Int. Conf. Nuclear Data for Science and Technology, Trieste, Italy, May 1997 (p. 260) (Italian Physical Society) (also web site:

http://www-xdiv.lanl.gov/XTM/projects/mc21/docs/pdfs/brn970616.pdf)

14. K. W. BURN, E. NAVA: "Use of an Innovative Monte Carlo Technique to calculate Neutron Spectra in BNCT – Application to the TAPIRO Reactor" Meeting on BNCT, University of Padua, Feb. 1998 (INFN report, in press)

15. K. W. BURN, G. F. GUALDRINI, F. MONTEVENTI, B. MORELLI, E. VILELA: "Experimental and Monte Carlo Evaluation of the Dosimetric Characteristics of a Thermal Neutron Calibration Assembly" Int. Conf. on Solid State Dosimetry, Burgos, Spain, July 1998.

TABLE I

Weight–independent DSA test problem

#	Generation of second moment and time functions								Minimization of quality function						
	CPU (min)	MCT (min)	D	fsd (%)	stat fail	S^2	τ	D^2/q	D	S^2 (init)	τ (init)	D^2/q (init)	S^2 (opt)	τ (opt)	D^2/q (opt)
0	21.4	19.4	5.31+10	13.9	2	1.06+1	3.89–2	2.42	5.31+10	8.91+0	3.85-2	2.92	2.39+1	9.69–4	43.2
1	21.0	17.9	4.56+10	5.0	1	3.17+1	1.46–3	21.6	4.64+10	3.55+1	1.42-3	19.8	5.08+1	5.30–4	37.1
2	16.0	13.8	4.82+10	4.4	0	5.05+1	5.44–4	36.4	4.74+10	5.25+1	5.35-4	35.6	5.63+1	4.89–4	36.4
3	21.0	18.4	4.71+10	3.8	0	5.42+1	4.97–4	37.1	4.73+10	5.77+1	4.91-4	35.3	5.51+1	5.08–4	35.7

TABLE II

Weight–dependent DSA test problem

#	Generation of second moment and time functions								Minimization of quality function					
	CPU (min)	D	fsd (%)	stat fail	S^2	τ	q	D^2/q	D	S^2	τ	q	D^2/q (init)	D^2/q (opt)
0	4.0	4.00–5	4.86	2	1.13–6	1.09–5	1.23–11	130.0	4.00–5	1.09–6	1.09–5	1.19–11	134.4	435.2
1	4.0	4.16–5	3.22	1	3.16–7	1.83–5	5.80–12	298.4	4.06–5	2.18–7	1.75–5	3.81–12	432.9	438.0
2	4.0	4.39–5	3.51	4	3.94–7	2.01–5	7.92–12	243.2	4.14–5	2.29–7	1.92–5	4.40–12	390.7	444.6
3	4.0	4.27–5	2.95	2	2.68–7	1.98–5	5.32–12	343.0	4.17–5	1.95–7	1.94–5	3.77–12	461.1	443.8
4	4.0	4.26–5	2.91	0	2.59–7	2.00–5	5.18–12	350.4	4.19–5	2.01–7	1.96–5	3.95–12	444.1	450.3
5	8.0	4.35–5	1.97	0	2.41–7	2.10–5	5.05–12	375.6	4.23–5	1.93–7	2.00–5	3.87–12	462.3	466.4

TABLE III

4–response weight–independent DSA test problem

#	Generation of second moment and time functions									Minimization of quality function									
	CPU (min)	MCT (min)	D_1 (%/sf)	D_2 (%/sf)	D_3 (%/sf)	D_4 (%/sf)	S^2_{fc}	τ	$1/q_{fc}$	D_1	D_2	D_3	D_4	S^2_{fc} (init)	τ (init)	$1/q_{fc}$ (init)	S^2_{fc} (opt)	τ (opt)	$1/q_{fc}$ (opt)
0	33.5	28.3	5.75+10 11.2 /2	1.99+11 10.5 /2	1.26+10 17.4 /3	1.26+8 18.8 /3	6.12+1	4.39–2	0.37	5.75+10	1.99+11	1.26+10	1.26+8	5.55+1	4.15-2	0.43	1.76+2	1.21–3	4.69
1	125.0	69.9	4.76+10 3.0 /0	1.75+11 2.4 /0	8.45+9 3.5 /0	8.02+7 8.8 /3	6.20+2	1.19–3	1.35	4.83+10	1.76+11	8.61+9	8.86+7	4.33+2	1.06-3	2.18	2.46+2	1.50–3	2.71
2	120.0	78.0	4.57+10 3.0 /0	1.68+11 2.3 /1	8.40+9 2.8 /0	8.11+7 5.6 /0	2.79+2	1.52–3	2.36	4.70+10	1.72+11	8.48+9	8.35+7	2.80+2	1.48-3	2.42	2.59+2	1.60–3	2.42
3	300.0	189.4	4.53+10 1.9 /0	1.68+11 1.5 /0	8.34+9 1.9 /0	8.68+7 5.0 /1	3.99+2	1.62–3	1.54	4.61+10	1.70+11	8.40+9	8.50+7	3.68+2	1.58-3	1.72	3.05+2	1.48–3	2.22
4	90.1	58.3	4.53+10 3.4 /0	1.65+11 2.7 /0	8.28+9 3.4 /0	8.47+7 7.1 /0	3.17+2	1.50–3	2.11										

Monte Carlo Methods and Models for Applications in Energy and Technology

Workshop to be held at Forschungszentrum Karlsruhe, May 12-14, 1998

On Geometry Generation for Monte Carlo Particle Transport Using CAD Systems

H. Tsige-Tamirat

Forschungszentrum Karlsruhe GmbH
Institut für Neutronenphysik und Reaktortechnik
Postfach 3640, D-76021 Karlsruhe, Germany

One of the strengths of Monte Carlo (MC) method for particle transport lies in its ability to handle the problem geometry in arbitrary detail. However, describing and verifying the problem geometry and the geometrical tracking of particles in the resulting geometry are the most complex and time consuming tasks of a MC particle transport problem setup and calculation, respectively. The geometry description for MC calculation is typically provided by manually collecting coordinates and vectors from an engineering drawing which is a tedious and error-prone process.

It seems, therefore, that an efficient and reliable geometry describing procedure is due. In 1997, a project was launched at FZK with the goal to build an interface between a Computer Aided Design (CAD) system and a MC particle transport code, in order to access the geometric and topological data of manifold solids in CAD systems and construct from it a geometry model for a MC code. The advantage of such an interface compared to an ad hoc graphical user interface for a particular MC code lies in the fact that it allows to access the full features of a modern CAD system facilitating the geometric modeling and enhancing the exchange of data with engineering codes.

Besides several implementation issues, the main problem that arises in building such an interface is embedded in the intrinsic different description and representation of the modeling space in CAD systems and MC codes. The geometry needed for a MC calculation is a cellular decomposition of the problem space into finite collection of disjoint regions whose union is the problem space. (Such regions are not necessarily compact and regular.) CAD systems describe a shape of a rigid solid physical object as a compact and regular point set in 3-space either by defining its oriented boundary (boundary representation (B-rep)) or by its interior and closure (constructive solid geometry (CSG)). In both CAD systems and MC geometry, the mathematical modeling space encompasses the class of semi-algebraic sets.

The theoretical problem which has to be solved prior to the building of the interface is to find an equivalence relationship between cellular decomposition of space and a manifold solid represented as a compact and regular point set. Ultimately, the problem can be formulated as a conversion between different geometric representation schemes. This paper will further elaborate the problem and in particular discuss following points:

- Formal description of a MC geometry as a semi-algebraic set
- Representation schemes of manifold solids in a CAD systems, and
- Conversion from representation schemes in CAD systems to a MC geometry as used for particle transport.

On Geometry Generation for Monte Carlo Particle Transport using CAD Systems

H. Tsige-Tamirat

Institut für Neutronenphysik und Reaktortechnik
Forschungszentrum Karlsruhe GmbH [1]

Contents

[1]This work has been performed in the framework of the Nuclear Fusion Project of the Forschungszentrum Karlsruhe.

1 Introduction

▶ One of the strengths of the Monte Carlo (MC) method for particle transport lies in its ability to handle the problem geometry in arbitrary detail.

- Describing the problem geometry is a complex task.
- Typically, it is provided by manually collecting coordinates and vectors from an engineering drawing.

▶ The objective of our project is to build an interface between a Computer Aided Design (CAD) system and an MC particle transport code.

- Advantages of such an interface are:
  - Access to the full features of a modern CAD system, and
  - Ability to exchange data with engineering codes.
- Following problems have to be solved:
  - Practical implementation issues, like how to access data of CAD systems, GUI, etc., are not discussed here.
  - Theoretical problems stemming from the intrinsic different description and representation of the modeling space.

▶ We proceed as follows:

- A description of the geometrical particle tracking algorithm is given.
- The geometry needed for MC particle transport is formalized as a semi-algebraic cellular decomposition of the problem space.
- The representation of a rigid solid in CAD systems as a compact and regular semi-algebraic set is then described.
- A conversion problem between the involved representation schemes is formulated.
- Sketches of algorithms for conversion problems are given.

2 Geometrical Particle Tracking

▶ We consider the transport of neutral particles in matter:

- The flight path of a particle after traveling a distance u is given by the ray equation

$$r = r_0 + \Omega u \tag{1}$$

  where r_0 is the emission position, and Ω is the direction of flight.
- u can be sampled by

$$u = -\ln \xi = \int_0^u \Sigma_t(u')du'. \tag{2}$$

- By decomposing the Problem space into piecewise homogeneous regions, Eq.2 is solved by evaluating the path lengths in each region.

▶ The tracking algorithm solves instances of the so called point location problem in $\mathbf{R}^d$ which can be stated as follows.
Let the set $\mathbf{X} \subset \mathbf{R}^d$ be the problem space which is decomposed into finite disjoint d-dimensional regions $S_i, \ldots, S_n$, i.e., $\mathbf{X} = \cup_{i=1}^n S_i$ with $S_i \cap S_j = \emptyset$ for $i \neq j$, and let r be a ray segment starting at r_0 and ending at r_q. The goal is to solve following problems:

- Determine all regions $S_i, \ldots, S_m$ in $\mathbf{X}$ that contain r, and
- Given a region $S_i \subset \mathbf{X}$ and a point $r_q = r - r_0 \in \mathbf{X}$, decide whether $r_q \in S_i$.

▶ Main computational steps are:

- Find all intersection points of a ray with the boundary of a region.
- Determine which boundary element is intersected first.
- Classify a ray segment with respect to a region.
- $\Rightarrow$ If a ray segment is classified outside, proceed to the next region.

▶ Required data:

- Geometric representation of the decomposition of the problem space.
- Topological adjacency of regions in the decomposition.

3 Geometry Representation for MC Particle Transport

Basic requirements

▶ The geometric representation needed for MC particle transport should:

- have sufficient descriptive power to model physical objects,
- allow unambiguous representation of the mathematical model, i.e., interiors and boundaries of sets should be well defined.
- support efficient particle path tracking,
- be easy to construct, and
- allow the detection of an invalid geometry description.

▶ The problem space is, in general, inhomogeneous, i.e., it is composed of materials with different ray attenuation coefficients.

▶ By decomposing the problem space into piecewise homogeneous regions, the line integral of Eq.2 is transformed to a summation over segment pieces.

▶ A useful class of sets, which partially fulfill the above requirements are semi-algebraic sets.

▶ Hence, the problem space for MC particle transport is well represented by decomposing it into disjoint regions (cells) and representing each region as a *semi-algebraic* cell.

Geometry for MC particle transport

▶ Let $\mathbf{R}^d$ denotes the d-dimensional Euclidean space. A region refers to a non-empty connected [2] subset of $\mathbf{R}^d$.

Definition 3.1. *Given a set $\mathbf{X} \subset \mathbf{R}^d$ representing the problem space, a* decomposition *of $\mathbf{X}$ is a finite collection of disjoint regions whose union is $\mathbf{X}$.*

Definition 3.2. *For $0 \leq i \leq d$, an i-dimensional cell in $\mathbf{R}^d$ is a subset of $\mathbf{R}^d$ which is homeomorphic [3] to $\mathbf{R}^i$. A decomposition of $\mathbf{X} \subset \mathbf{R}^d$ is cellular if each of its regions is a cell.*

Definition 3.3. *If each cell in a decomposition is semi-algebraic, then the decomposition is called a semi-algebraic cell decomposition.*

Definition 3.4. *A subset of $\mathbf{R}^d$ is said to be semi-algebraic if and only if it can be described in $\mathbf{R}^d$ by a set of polynomials.*

▶ Typically, a semi-algebraic set $\mathbf{X} \subset \mathbf{R}^d$ is derived from sets

$$\begin{aligned} h_i &= \{(x_1, \ldots, x_d) \in \mathbf{R}^d \mid f_i(x_1, \ldots, x_d) > 0\} \\ &\vdots \\ h_m &= \{(x_1, \ldots, x_d) \in \mathbf{R}^d \mid f_m(x_1, \ldots, x_d) > 0\} \end{aligned} \tag{3}$$

defined by polynomials $f_i, \ldots, f_m$ by finite union, intersection, and complementation. $h_i, \cdots, h_m$ are algebraic half-spaces.

▶ Any semi-algebraic set $\mathbf{X} \subset \mathbf{R}^d$ can be represented as

$$\mathbf{X} = \bigcup_i^n \bigcap_j^{m_i} \{(x_1, \ldots, x_d) \in \mathbf{R}^d \mid f_{i,j}(x_1, \ldots, x_d) \geq 0\}, \tag{4}$$

as $\{f_{i,j} \geq 0\} = \{-f_{i,j} \leq 0\}$ and $\{f_{i,j} \geq 0\} = \{f_{i,j} = 0\} \cup \{f_{i,j} > 0\}$.

[2] A set is called connected if it can not be written as a union of disjoint non-empty sets.

[3] Two topological spaces $\mathbf{X}$ and $\mathbf{Y}$ are said to homeomorphic (or of the same topology) if there exists a continuous bijective mapping $f : \mathbf{X} \to \mathbf{Y}$ which has a continuous inverse. Such mapping is called homeomorphism.

▶ The representation of a semi-algebraic set is far from being canonical.
▶ The representation lacks any geometric information.
▶ Semi-algebraic sets are more descriptive than algebraic sets [4].
▶ *Following properties of semi-algebraic cells are evident:*

- A cellular decomposition is a generalization of triangulation, hence it is non-unique.
- A cellular decomposition is unambiguous.
- Cells have a finite number of faces, but are not necessarily compact.
- Cells touch each other at common faces.

▶ *Some elementary Properties of semi-algebraic sets* [5].
Let $\mathbf{X} \subset \mathbf{R}^d$ and $\mathbf{Y} \subset \mathbf{R}^d$ be semi-algebraic sets.

- The sets $\mathbf{X} \times \mathbf{Y} \subset \mathbf{R}^d \times \mathbf{R}^d$, $\mathbf{X}', \mathbf{X} \cap \mathbf{Y}$, and $\mathbf{X} - \mathbf{Y}$ are semi-algebraic.
- If $\mathbf{X} \subseteq \mathbf{Y}$ then $dim\mathbf{X} \leq dim\mathbf{Y}$, $dim(\mathbf{X} \cup \mathbf{Y}) = max(dim\mathbf{X}, dim\mathbf{Y})$, and if $\mathbf{X} \neq \emptyset$, then $dim(\mathbf{X}' - \mathbf{X}) < dim\mathbf{X}$ [6].
- Every semi-algebraic set is locally connected if it is not the disjoint union of two non-empty closed semi-algebraic sets.
- The number of the connected components of a semi-algebraic set is finite, and each connected component is semi-algebraic. *The number of connected components of a semi-algebraic set is a measure of its complexity.*
- Connected components have the same sign sequence generated by the polynomials $f_i, \ldots, f_n$ in the defining formula. If points $x^1 = (x_1^1, \ldots, x_d^1)$ and $x^2 = (x_1^2, \ldots, x_d^2)$ are in the same connected components, then the sign sequence of $f_i(x^1), \ldots, f_n(x^1)$ is the same as $f_i(x^2), \ldots, f_n(x^2)$, the sign sequence being 1, 0, or -1.

[4] A subset $\mathbf{X}$ of $\mathbf{R}^d$ is called an algebraic set if it is zeros of a polynomial system.
[5] R. Benedetti and J.J. Risler, Real algebraic and semi-algebraic sets, Hermann, 1990.
G. Brumfiel, Partially ordered rings and semi-algebraic geometry, Cambridge UP 1979.
M. Shiota, Geometry of Subanalytic and semi-algebraic set, Progress in Mathematics, Birkhäuser, Boston, 1997.
[6] For convenience, we assume $dim\emptyset = -1$.

4 Representation of Solids in CAD Systems

Theory [7]
▶ Within the field of computer aided-design, solid modeling deals with an unambiguous representation of rigid solids.
▶ An abstract solid with following properties is assumed: rigid, homogeneously three dimensional, of bounded volume, and boundary.
▶ A suitable mathematical modeling space for such solids are subsets of $\mathbf{R}^d$ that are bounded, closed, regular, and semi-algebraic. Such sets are called regular sets (to be denoted by r-sets).
Basic notions. Let $\mathbf{X} \subset \mathbf{R}^d$ and let $\mathbf{X}'$ denotes its complement.

- The closure $\overline{\mathbf{X}}$ of $\mathbf{X}$ is the set $\mathbf{X}$ augmented by its accumulation points.
- A set $\mathbf{X}$ is closed if $\mathbf{X} = \overline{\mathbf{X}}$.
- The boundary $\partial\mathbf{X}$ of a set $\mathbf{X}$ is the set $\partial\mathbf{X} = \overline{\mathbf{X}} \cap \mathbf{X}'$.
- The interior $int(\mathbf{X})$ of $\mathbf{X}$ is the set $int(\mathbf{X}) = \mathbf{X} - \partial\mathbf{X}$.

Definition 4.1. *A set $\mathbf{X}$ is closed and regular (r-set) if it is equal to the closure of its interior, i.e.,* $\mathbf{X} = \overline{int(\mathbf{X})}$.
▶ Under the standard set operations, r-sets are not algebraically closed, but with the so called regularized set operations they form an algebraically closed system.
▶ A relation that maps elements of the mathematical modeling space M into a representation space R, i.e., $s : M \rightarrow R$, is called a representation scheme.
▶ s is said to be an unambiguous or complete if the inverse s^{-1} is a function. It is unique if it is an injection (one-to-one).
▶ At least six families of complete representation schemes are currently known: the most widely used are *Constructive Solid Geometry representation (CSG-rep)* and *Boundary representation (B-rep).* [8]

[7] A. A. G. Requicha, Representations for Rigid Solids: Theory and Systems, Comp. Surveys, 12(4), 437-464, 1980.
[8] B-rep is de facto industry standard because of its ability to naturally model solids with arbitrary surfaces.

Constructive Solid Geometry Representation

▶ A CSG representation of a rigid solid S, which is a compact regular semi-algebraic set in some real space, is a Boolean form Φ, i.e., an expression composed from literals and symbols, where literals refer to primitives and symbols refer to regularized set operations (union, intersection, difference, and complementation).
▶ We say that the solid S is defined by its CSG representation Φ, and that the CSG representation Φ is a defining formula for S:

$$S = \Phi. \tag{5}$$

S is then the set of points in some $\mathbf{R}^d$ that satisfy Φ.
▶ CSG representations are unambiguous, but not unique.
▶ A CSG representation does not contain explicit information about the boundary of the represented solid.
▶ Thus, it is expensive to determine whether a CSG representation defines a non-empty set or two representations define the same solid.
▶ The data structure used to implement CSG-reps are directed acyclic binary trees. Interior nodes represent either regularized set operations or rigid motions. Leaf nodes are either primitives or defining arguments of rigid motions.

Boundary Representation

▶ A solid can be represented unambiguously by its boundary and its topological orientation, i.e., the side of its interior. It is assumed that the boundary of a solid in 3-space is a closed oriented 2-manifold [9].
▶ A B-rep of a solid S is a representation of its boundary in the following form

$$\partial S = \bigcup_{i=1}^{n} (S \bigcap h_i) \tag{6}$$

where $h_i, \ldots, h_n$ are the half-spaces bounding the solid S . The sets $(S \cap h_i)$ are called the faces of S.
▶ $\partial S, int(S)$, and S' are unions of connected sets.
▶ ∂S is an algebraic set, hence semi-algebraic, and its unique up to the reordering of the half-spaces.
▶ Faces in ∂S are either disjoint or intersect at common edges. Three faces intersect at isolated vertices. Edges intersect at vertices. An edge may have two vertices or none.
▶ The data structure for a B-rep of a solid has two parts:

- a topological description of the connectivity and orientation of boundary elements (vertices, edges, and faces), and
- a geometric description of faces, i.e., algebraic equations for the functions defining the half-spaces.

▶ There are many implementation variants for the data structure of B-reps. The oldest appears to be the so called winged-edge representation for polyhedral solids: it is essentially a table recording the topological connectivity and orientation of vertices, edges, and faces.

[9] An i-manifold M in $\mathbf{R}^d$ with $i < d$ is a set that is locally homeomorphic to $\mathbf{R}^i$, i.e., for every point of the manifold, there exists a neighborhood that is homeomorphic to $\mathbf{R}^i$. A manifold is orientable if it has two different sides.

Assemblies of Solids

▶ Our intended application -MC particle transport- operates on systems, like detectors, nuclear reactors, shielding systems, etc., which are generally assemblies of different parts made up of different materials.
▶ Moreover, the geometry representation needed for MC particle transport has to describe the whole problem space, including interior voids of individual parts, which is not explicitly covered by the representation of the part, and the space between the parts.
▶ In general, CAD systems provide no operations on assemblies other than rigid motions. Typically, a representation of an assembly is then a logical hierarchy which reflects the spatial relationship between disconnected single parts.
▶ For our purpose, an assembly should be converted to a single connected piece which corresponds to the cellular decomposition of the problem space. Thereby, the following issues should be considered:

- internal voids in individual part,
- voids between parts, and
- shared boundaries.

▶ The last point means that if two parts touch each other in an assembly, then their spatial relationship is encoded so that the parts are zero distance apart, but in the context of our intended application, the two parts would share a common boundary.

5 Conversion between Representation Schemes

Basic considerations

▶ The representation of geometry of solid objects in CAD systems is different from the geometry representation used in MC particle transport.
▶ Assume that an assembly of solids is given, and let it corresponds to the cellular decomposition of the problem space for MC particle transport. Then, a single solid in an assembly corresponds to some cells in a decomposition.
▶ *Our goal is to solve the following problem:*
Given a solid by its CSG- or B-representation, find a semi-algebraic representation for each cell defining the interior and exterior of the solid. We refer to this problem as a CSG to cell conversion, or as a B-rep to cell conversion.
▶ Conversion between different representation schemes is a well known problem in solid modeling:

- Methods for CSG to B-rep conversion are well established. They are known as boundary evaluation algorithms [10].
- The problem of conversion from B-rep to CSG is yet unsolved. In fact, there exists solutions for simple polygons in the plane. In case of non-simple polygons, curved solids, and in 3-space, many questions remain unanswered and are topics of current research.

▶ In what follows, we deal with the conversion problem. The CSG to cell conversion is straight forward and less interesting, as most commercial CAD systems use B-reps. Therefore, we are primarily concerned with the B-rep to cell conversion problem and treat this case in detail.

[10] A. A. G. Requicha and H. B. Voelcker, Boolean Operations in Solid Modeling: Boundary Evaluation and Merging Algorithms, Proceedings of the IEEE, 73(1), pp. 30-44, January 1985.

CSG to Cell conversion

▶ The CSG to cell conversion problem is tractable in a straight forward way, since both representations describe a point set in some $\mathbf{R}^d$ in the same way, namely as a semi-algebraic set.
▶ The following differences are obvious:

- In a CSG representation the primitives are bounded half-spaces, while they may be unbounded in a cell decomposition.
- A CSG representation uses regularized Boolean operations, in contrast, for a cell decomposition, standard Boolean operations are sufficient.
- A CSG representation describes only the bounded interior of a solid, where as a cell decomposition has to include also the unbounded exterior of the solid.

▶ A sketch for a CSG to cell conversion algorithm:

- A CSG to cell conversion is achieved for a Boolean form of a solid by simply dropping the demand for the boundedness of the half-spaces and the regularity of the Boolean operations.
- The exterior of a solid is given by the complementation of the Boolean form describing the solid, although this not the most concise form in the sense of the present application.

B-rep to Cell conversion

▶ An instance of the B-rep to cell conversion problem is the B-rep to CSG conversion problem which is being studied currently in the solid modeling research.
▶ Most known methods for B-rep to CSG conversion problem consider simple polygons in the plane. They can be can be divided into two groups:

- **Convex hull methods:** produce monotone Boolean formulae for the CSG of a simple polygon by recursively splitting its boundary into simpler chains using the vertices of the convex hull of the chains. These methods seem to be inefficient for non-polygonal objects and in higher dimensions.
- **Decomposition methods:** represent polygons by decomposing them into simple convex pieces. The Boolean form for the CSG is then the union of the intersection terms defining the convex pieces. Depending on the type of decomposition, convex pieces may or may not overlap.

▶ The decomposition method seems to lend itself for the B-rep to cell conversion problem. Moreover, it has been recently applied to the B-rep to CSG conversion problem in 3-space including restricted classes of curved solids.
▶ In the following we deal with an algorithm for the B-rep to Cell conversion problem. Our approach is based on that of Shapiro and Vossler [11].

[11] V. Shapiro and D. L. Vossler, Separation for Boundary to CSG Conversion, ACM Transactions on Graphics, 12(1), pp. 35-55, January 1993.

Preliminaries

▶ Let S be a solid and let its B-rep be given by

$$\partial S = \bigcup_{i=1}^{n} (S \bigcap h_i) \tag{7}$$

where $h_i, \ldots, h_n$ are the half-spaces bounding the solid. We say a half-space h_i and its complement h_i' constitute a partition of the space $\mathrm{E} = \mathbf{R}^d$ [12].

▶ The space $E = \mathbf{R}^d$ can be decomposed into disjoint regions using the half-spaces $h_i, \ldots, h_n$ bounding the solid S and their complements $h_i', \ldots, h_n'$ as follows:

$$E = \bigcup_{k=1}^{N} \bigcap_{i=1}^{n} h_i^{\alpha_i} \qquad (\alpha_i = \{\ \} \text{ or } \alpha_i = \{'\}, \quad \text{for} \quad i = 1, \ldots, n). \tag{8}$$

▶ The product terms $C_k = \cap_{i=1}^{n} h_i^{\alpha_i}$ are called constituents. The total number of distinct constituents is at most $N \leq 2^n$, and they are always disjoint.

▶ If non-planar half-spaces are present among $h_i, \ldots, h_n$, then constituents may be composed of some connected components thus

$$C_k = \bigcup_{m=1}^{M_k} CC_{m,k} \tag{9}$$

where $CC_{m,k}$ is the m-th component of C_k, and M_k is the total number of components in C_k.

▶ Note that $N \leq M = \sum_{k=1}^{N} M_k$. If all half-spaces are planar, then $N = M$, which means each constituent has only one component.

[12]

Definition 5.1. *A* partition *of a set* E *is a collection of disjoint subsets of* E *whose union is* E. *Two sets* $\mathrm{X} \neq \emptyset \subset \mathrm{E}$ *and* $\mathrm{Y} \neq \emptyset \subset \mathrm{E}$ *are said to constitute a partition of* E *provided that* $\mathrm{X} \cap \mathrm{Y} = \mathrm{E}$, $\mathrm{X} \cup \mathrm{Y} = \emptyset$, $\mathrm{X}' \cup \mathrm{Y} = \emptyset$, *and* $\mathrm{X} \cup \mathrm{Y}' = \emptyset$.

Theorem 5.1. [13] *Each non-empty set obtained from the sets* $h_i, \ldots, h_n$ *by applying the operations of union, intersection, and subtraction is a union of a certain number of constituents.*

▶ By the above theorem we have the following:

Given a set of half-spaces $h_i, \ldots, h_n$ deduced from a B-rep of a solid S, and if they are sufficient for a CSG representation of S, then the Boolean form for S is a union of a certain number of constituents.

▶ The CSG representation achieved so is canonical, i.e., it contains all half-spaces and their complements, and therefore is inefficient.

▶ The sufficiency of a given set of half-spaces $h_i, \ldots, h_n$ for a CSG representation of S is established by the following theorem:

Theorem 5.2. [11] *Given a set of half-spaces* $h_i, \ldots, h_n$ *and a solid* S, *there exists a CSG representation for* S *using* $h_i, \ldots, h_n$ *if and only if all connected components of every constituent have the same classification with respect to* S.

▶ Conversely, if one of the connected components of a given constituent has different classification with respect to S, then the half-spaces $h_i, \ldots, h_n$ are insufficient for a CSG representation of S.

[13] K. Kuratowski and A. Mostowski, Set theory, North-Holland Publishing Company, Amsterdam, 1968.

A Sketch for an Algorithm. ▶ Based on the above, an algorithm for the solution of the B-rep to cell conversion problem includes following steps:

- Decompose the space using $h_i, \ldots, h_n$ from the B-rep of the solid S. This step produces constituents C_ks, which may be composed of connected components $CC_{m,k}$s.
- Find characteristic points in each $CC_{m,k}$ and classify each $CC_{m,k}$ with respect to all constituents and with respect to the solid.
- If every $CC_{m,k}$ of a given C_k have the same classification and this is true for all C_ks, then the union of the constituents classified inside is a canonical CSG representation of S and we terminate.
- But if $CC_{m,k}$s of a given C_k have different classification with respect to S, then $h_i, \ldots, h_n$ are insufficient for a CSG representation of S.
- In the latter case, a set of additional so called separation half-spaces are introduced into the available half-spaces in such a way that $CC_{m,k}$s of that particular C_k are separated.
- Return to the first step.

Comments. ▶ The algorithm is not yet implemented, and we are currently dealing with the following problems:

- Finding characteristic points in the connected components is difficult; this is a known problem in algebraic geometry.
- The classification of the connected components with respect to constituents and with respect to the solid require exhaustive searches, therefore, it is computationally expensive.
- Constructing separation half-spaces is hard, this is also a known problem in algebraic geometry.
- CSG representations achieved by this algorithm are verbose and have to be optimized. Optimization of Boolean forms is a problem known in switching theory and it is difficult to cope with.
- etc.

6 Summary

- The objective of our project is to build an interface between a CAD system and an MC particle transport code.
- Besides practical implementation issues, we are faced with a conversion problem between representation schemes.
- To solve this problem, we have formalized the geometry needed for MC particle transport as a semi-algebraic cellular decomposition of the problem space.
- Thus, a correspondence with the representation of a rigid solid in CAD systems has been established.
- A conversion problem between representation schemes has been formulated.
- Sketches of algorithms have been given.

Monte Carlo Methods and Models for Applications in Energy and Technology

Workshop to be held at Forschungszentrum Karlsruhe, May 12-14, 1998

Monte Carlo Calculation of Point-Detector Sensitivities to Material Parameters

R. L. Perel, J.J. Wagschal and Y. Yeivin

Racah Institute of Physics
The Hebrew University of Jerusalem
91904 Jerusalem, Israel

Abstract

The Monte Carlo Method for neutron transport calculations has been developed about half a century ago. It is now extensively applied in reactor physics analyses. Yet Monte Carlo methods for the calculation of sensitivities were developed only much later. Since any meaningful scientific or technical calculation is likely to be followed by an estimate of the relevant sensitivities, and since the Monte Carlo methods for calculation of sensitivities are elegant, straightforward and well established, one might expect that these calculations should also be widely applied. However, their actual use is much less frequent than that of conventional Monte Carlo calculations. The reason for this might well be the fact that relevant publications on Monte Carlo calculations of sensitivities mainly dealt with specific types of responses (such as the average reaction rate in a cell), while no explicit formulations of the algorithms for other kinds of calculations were given. Another reason, of course, is the fact that until recently the public versions of many of the popular Monte Carlo codes did not incorporate a standard option to calculate sensitivities: the latest version of MCNP (4B) has already some sensitivity capabilities, although not for point detectors.

In this work we present the explicit prescriptions for the Monte Carlo calculation of sensitivities of a point detector (or ring detector) to material parameters: cross sections, average number of fission neutrons, and number densities of isotopes. This algorithm, which is an extension of Hall?s differential operator method, has been incorporated in our local version of the MCNP code. As an illustration, the sensitivities of a few experiments to material parameters are discussed.

Last modified: Thu Apr 2 13:53:37 1998

Monte Carlo Calculation of Point-Detector Sensitivities to Material Parameters

Reuven L. Perel
Jehudah J. Wagschal
Yehuda Yeivin

Racah Institute of Physics
The Hebrew University of Jerusalem
91904 Jerusalem
Israel

Sensitivities

Calculation of Sensitivities by

- "Brute Force"
- Use of adjoint fluxes (deterministic)
- Correlated Sampling (Monte Carlo)
- Differential Operator (Monte Carlo)

Sensitivities

Calculation of Sensitivities by

- Brute Force
- Use of adjoint fluxes (S_n)
- Differential Operator (Monte Carlo)
- Correlated Sampling (Monte Carlo)

Brute Force:

For each change of p recalculate $\bar{r}(p+\delta p)$.

$\partial\bar{r}/\partial p \approx (\bar{r}(p+\delta p) - \bar{r}(p))/\delta p$.

(Problems: Time consuming.

Are the changes δp small enough?)

Adjoint Fluxes:

Example:

$D = D(\mathbf{x},\mathbf{v})$ = detector's response to a neutron

$\bar{r} = (D\psi)$, where $(...)\equiv\int...d^3x d^3v$

ψ = solution of the transport equation $H\psi=S$

ψ^*= solution of the adjoint tr. eq. $H^*\psi^*=D$

if $H' = H+\delta H$

then $\delta\bar{r} = \bar{r}'-\bar{r} \approx -(\psi^* \delta H \psi)$

(Solve transport equation for each response.

With resulting ψ and ψ^* calculate any sensitivity needed)

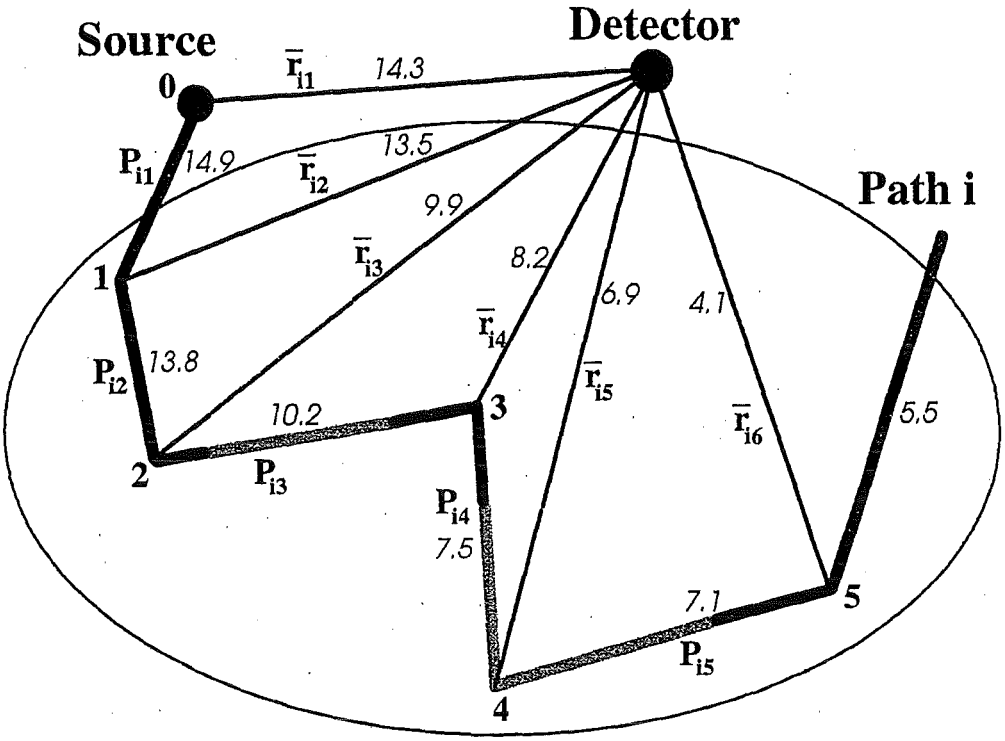

Contributions of Path i to Flux at Point Detector

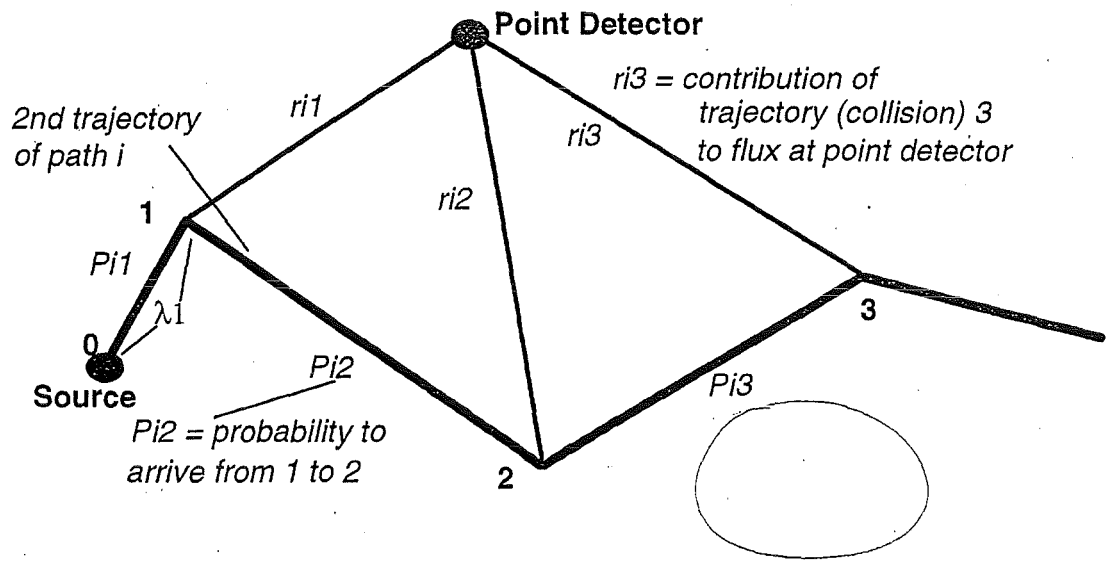

Special case: Detector response independent of cross sections in yellow region

Contributions of Path i to Flux at Point Detector

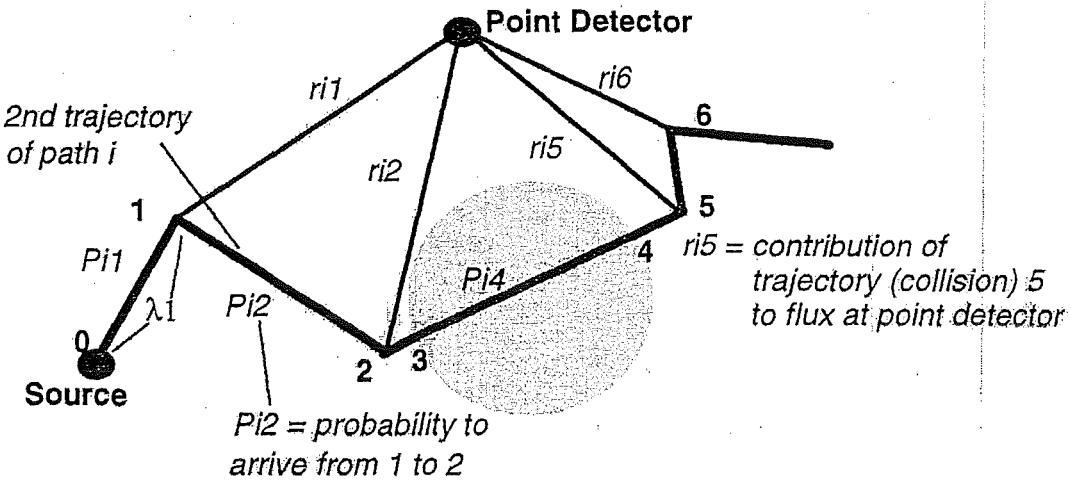

Special case: Only flux terms *Pij*
are affected by changes in cross sections in yellow region.

Contributions of Path i to Flux at Point Detector

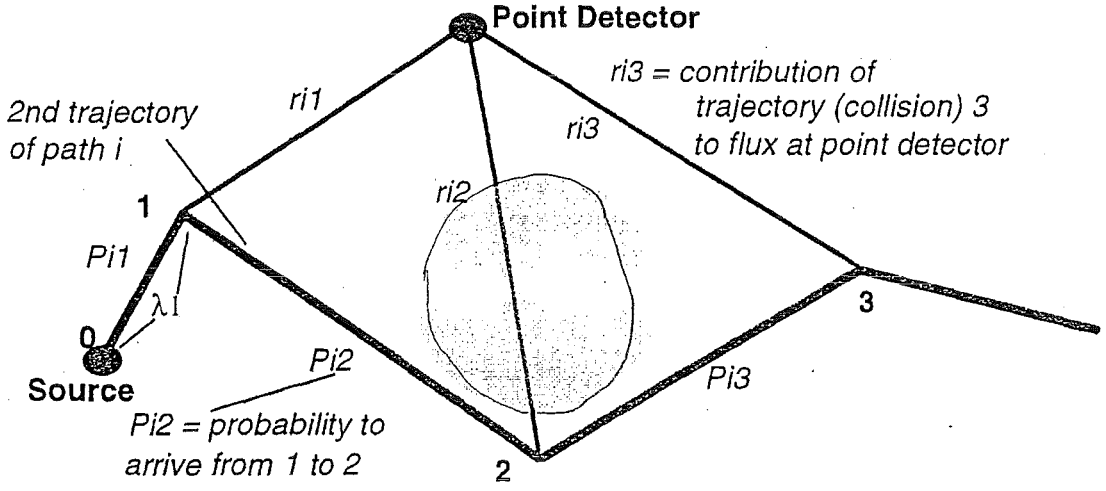

Special case: Only response terms *rij*

are affected by changes in cross sections in yellow region.

Contributions of Path i to Flux at Point Detector

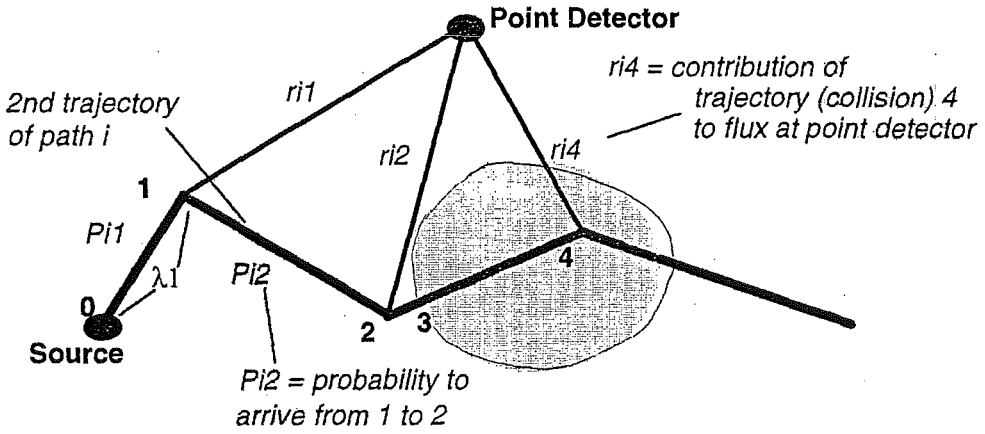

$\langle r \rangle = \Sigma_i r_i P_i$ (Σ_i : all paths i (=histories))

$P_i = \Pi_k P_{ik}$ (Π_k : all trajectories k of path i)

$r_i P_i = \Sigma_j r_{ij} \prod_{k=1}^{j} P_{ik}$ (Σ_j : all trajectories j of path i). In MC codes r_{ij} are actually summed along the path.

$$r_i P_i = \Sigma_j r_{ij} \prod_{k=1}^{j} P_{ik}$$

$$\sigma_\alpha(E) \frac{\partial}{\partial \sigma_\alpha(E)} r_i P_i = \Sigma_j \{.....\} r_{ij} \prod_{k=1}^{j} P_{ik}$$

$$P_{ik} = S_{x_{k-1}}(E_k \leftarrow E_{k-1}, \Omega_k \leftarrow \Omega_{k-1}) \times e^{\left[-\sum\Sigma_{tot,z}(E_k)\lambda_{k,z}\right]} \times \Sigma_{x_k}(E_k)\, dE_k\, d\Omega_k\, d\lambda_k$$

$$r_{ij} = S_{x_j}(E_d \leftarrow E_j, \Omega_d \leftarrow \Omega_j) \times e^{\left[-\sum\Sigma_{tot,z}(E_d)\lambda_{d,z}\right]} / \lambda_d^2\, dE_d$$

$$S\alpha i = \sigma_\alpha(E)\frac{\partial(r_i P_i)}{\partial\sigma_\alpha(E)}$$

$$= \sigma_\alpha(E) \sum_{j=1}^{J_i} \left\{ \frac{\partial r_{ij}}{\partial\sigma_\alpha(E)} \prod_{k=1}^{j} P_{ik} + r_{ij} \frac{\partial}{\partial\sigma_\alpha(E)} \left(\prod_{k=1}^{j} P_{ik} \right) \right\}$$

$$= \ldots$$

$$= \sum_{j=1}^{J_i} \sigma_\alpha(E) \frac{\partial}{\partial\sigma_\alpha(E)} \left(\ell n r_{ij} + \sum_{k=1}^{j} \ell n P_{ik} \right) r_{ij} \prod_{k=1}^{j} P_{ik}$$

The logarithmic derivative of the response term r_{ij} is

$$\sigma_\alpha \frac{\partial}{\partial\sigma_\alpha}\left(\ell n r_{ij}\right) = \frac{\sigma_\alpha(E)}{r_{ij}} \frac{\partial r_{ij}}{\partial\sigma_\alpha(E)}$$

$$= -\delta(E - E_d) \sum_z \Sigma_{\alpha,z}(E_d)\lambda_{d,z}$$

The logarithmic derivative of the flux term P_{ik} is

$$\sigma_\alpha \frac{\partial}{\partial\sigma_\alpha}\left(\ell n P_{ik}\right) = \frac{\sigma_\alpha(E)}{P_{ik}} \frac{\partial P_{ik}}{\partial\sigma_\alpha(E)}$$

$$= \delta(E - E_k)[\delta_{\alpha,x_k} - \sum_z \Sigma_{\alpha,z}(E_k)\lambda_{k,z}]$$

The logarithmic derivatives of the response- and flux terms to ρ are

$$\rho_\alpha \frac{\partial}{\partial \rho_\alpha}\left(\ell n r_{ij}\right) = \sum_z \Sigma_{tot,\alpha,z}(E_d)\lambda_{d,z}$$

and

$$\rho_\alpha \frac{\partial}{\partial \rho_\alpha}\left(\ell n P_{ik}\right) = \delta_{\alpha,x_k} - \sum_z \Sigma_{tot,\alpha,z}(E_k)\lambda_{k,z}$$

The logarithmic derivatives of the response- and flux terms to $\bar{\nu}$ are

$$\bar{\nu}_\alpha \frac{\partial}{\partial \bar{\nu}_\alpha}\left(\ell n r_{ij}\right) = 0$$

and

$$\bar{\nu}_\alpha \frac{\partial}{\partial \bar{\nu}_\alpha}\left(\ell n P_{ik}\right) = \frac{\bar{\nu}_\alpha(E)}{P_{ik}} \frac{\partial P_{ik}}{\partial \bar{\nu}_\alpha(E)} = \delta_{\alpha,x_k}\delta(E - E_k)$$

$\Rightarrow$ Collecting r_{ij} at each collision we simultaneously also collect:

$r_{ij} \{ \partial(\ln r_{ij})/\partial p_n + \Sigma_k (\partial(\ln P_{ik})/\partial p_n) \}$

The expressions multiplying r_{ij} are evaluated analytically. They are simple to calculate and many of them are zero.

OTHER RESPONSES

(a) r_{ij} not explicitly dependent on a cross section, e.g. flux in cell

$$\sigma_\alpha \frac{\partial}{\partial \sigma_\alpha}\left(\ell n r_{ij}\right) = 0$$

(b) $r_{ij} = c_{ij}\, \Sigma_{\alpha 0}(E_j)$ (linear in a given cross section).

e.g. track length estimator of k_{eff} : $c_{ij} = \bar{\nu}(E_j)\ \lambda_j$

$\Sigma_{\alpha 0}(E_j)$ = fission cross section of a given isotope

$$\sigma_\alpha \frac{\partial}{\partial \sigma_\alpha}\left(\ell n r_{ij}\right) = \frac{\sigma_\alpha(E)}{r_{ij}} \frac{\partial r_{ij}\left(E_j\right)}{\partial \sigma_\alpha(E)} = \delta_{\alpha,\alpha_0}\delta\left(E - E_j\right)$$

```
      subroutine schematic_sensitivity_monte_carlo
      common/sencom/count(ntime),dcount_dsig(nerg,nsig,ntime),bj(nerg,nsig)
      count = 0   ; dcount_dsig = 0 ; ,....
      ================================================================
      loop on paths
      do ipath=1,npath
          bj = 0
          itraj=0
          repeat
          ================================================================
          loop on trajectories
              itraj=itraj+1
!             ---------------------------------------------------------
              CALCULATE THE COUNT_NOW IN TIME(ITIME)
              count(itime)=count(itime)+count_now
!             ---------------------------------------------------------
              UPDATE BJ (FLUX TERM MULTIPLIER)
              do isig=1,nsig
                  if(arriving_traj not in sensivity cell) goto 500
                  ierg=index_of_colliding_energy
                  if(isig.eq.i_current_reaction)then
                      bjk=1
                  else
                      bjk=0
                  endif
                  bjk=bjk-arriving_distance*sigmacro(ierg,isig)
                  bj(ierg,isig)=bj(ierg,isig)+bjk
              enddo
!             ---------------------------------------------------------
!             RESPONSE TERM
 500          continue
              if(distance_to_detector_in_senscell.eq.0)goto 600
              do isig=1,nsig
                  ierg=index_of_detector_energy
                  count_del=-count_now
     x                 *distance_to_detector_in_senscell*sigmacro(ierg,isig)
                  dcount_dsig(ierg,isig,itime)=
     x                 dcount_dsig(ierg,isig,itime)+count_del
              enddo
!             ---------------------------------------------------------
!             FLUX TERM
 600          continue
              do isig=1,nsig
                  do ierg=1,nerg
                      count_del=count_now*bj(ierg,isig)
                      dcount_dsig(ierg,isig,itime)=
     x                    dcount_dsig(ierg,isig,itime)+count_del
                  enddo
              enddo
!             ---------------------------------------------------------
          until last trajectory
          loop on trajectories of the current path finished
          ================================================================
      enddo
      loop on paths finished
      ================================================================
      stop
      end
```

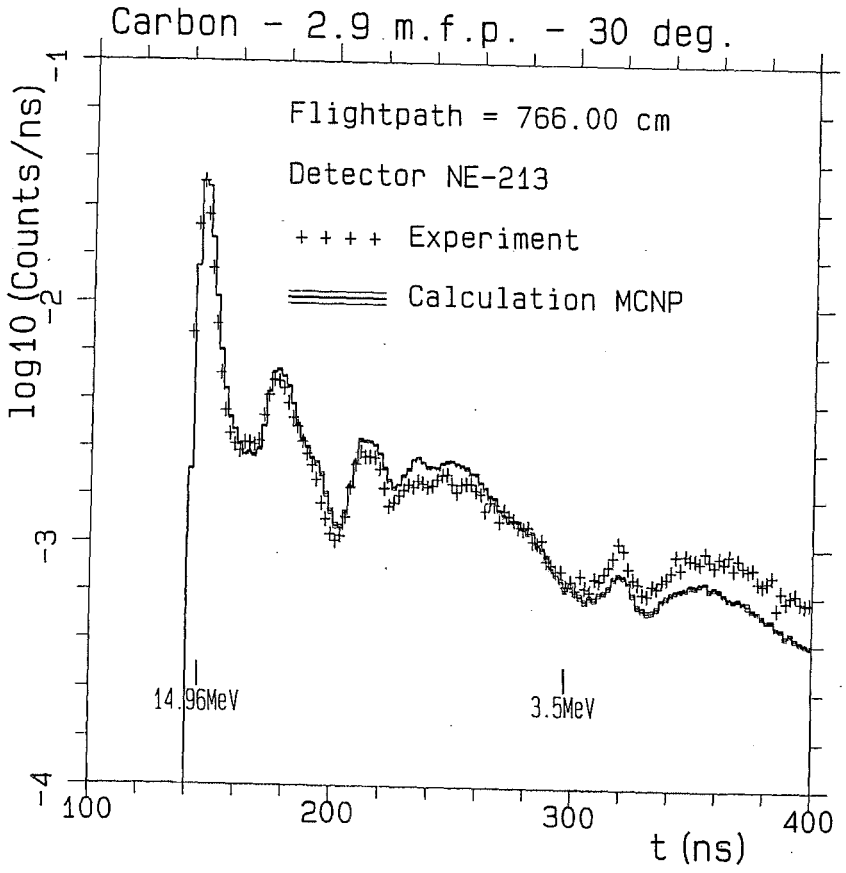
Carbon - 2.9 m.f.p. - 30 deg.
Flightpath = 766.00 cm
Detector NE-213
++++ Experiment
Calculation MCNP
14.96MeV
3.5MeV
log10 (Counts/ns)
t (ns)

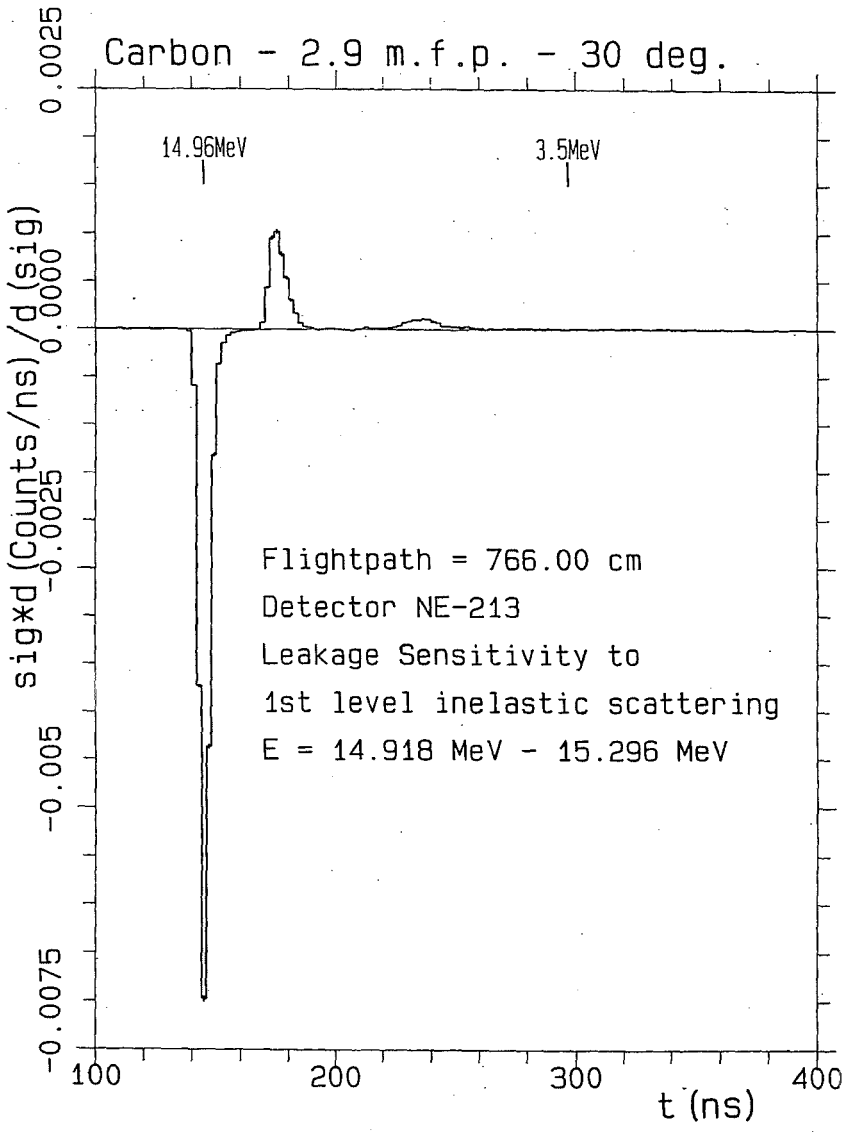
Carbon - 2.9 m.f.p. - 30 deg.
14.96MeV
3.5MeV
Flightpath = 766.00 cm
Detector NE-213
Leakage Sensitivity to
1st level inelastic scattering
E = 14.918 MeV - 15.296 MeV
sig*d (Counts/ns) /d (sig)
t (ns)

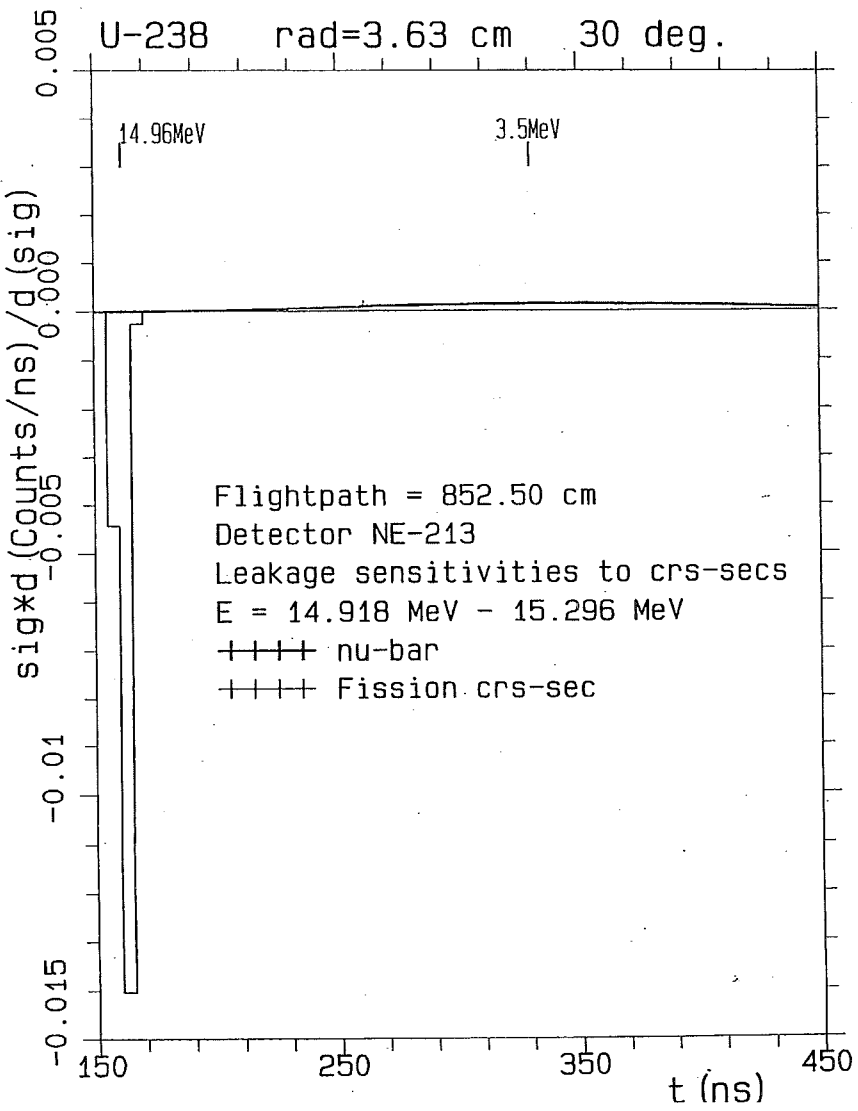
U-238 rad=3.63 cm 30 deg.
14.96MeV
3.5MeV
sig*d(Counts/ns)/d(sig)
0.005
0.000
-0.005
-0.01
-0.015
150
250
350
450
t (ns)
Flightpath = 852.50 cm
Detector NE-213
Leakage sensitivities to crs-secs
E = 14.918 MeV - 15.296 MeV
nu-bar
Fission crs-sec

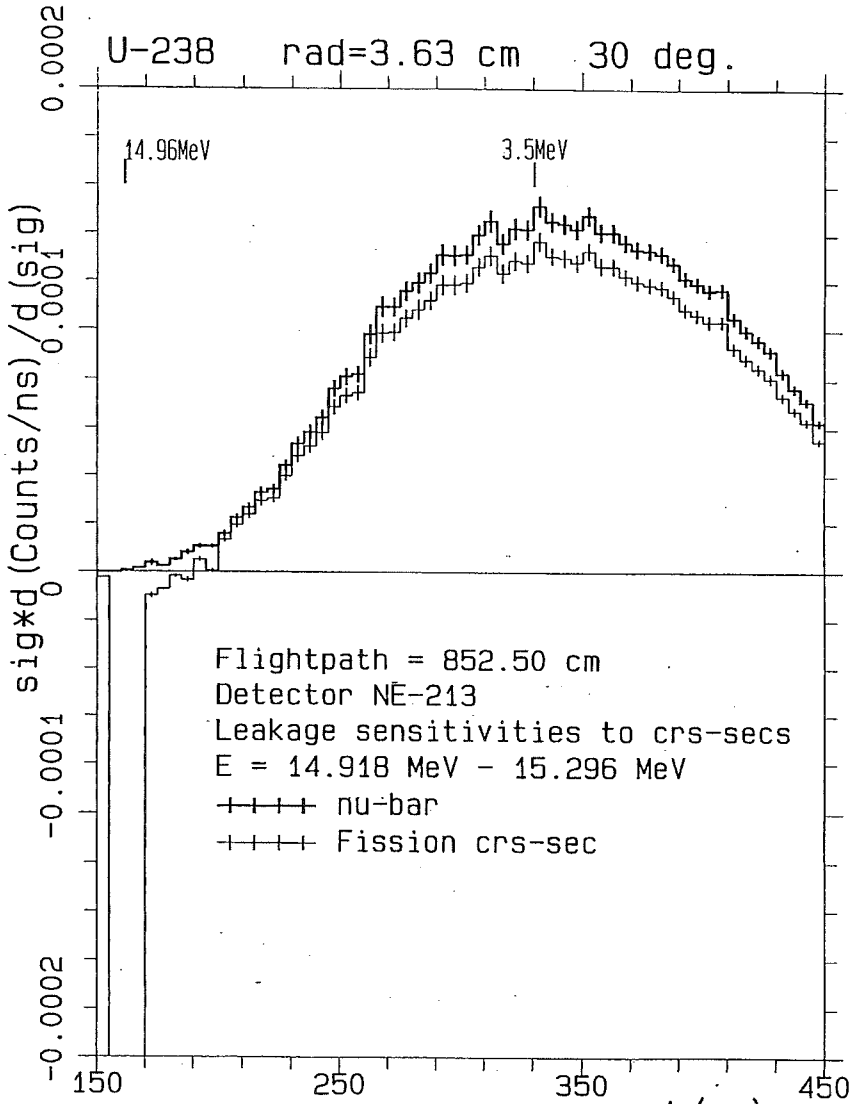
U-238 rad=3.63 cm 30 deg.
14.96MeV
3.5MeV
sig*d(Counts/ns)/d(sig)
0.0002
0.0001
0
-0.0001
-0.0002
150
250
350
450
Flightpath = 852.50 cm
Detector NE-213
Leakage sensitivities to crs-secs
E = 14.918 MeV - 15.296 MeV
nu-bar
Fission crs-sec

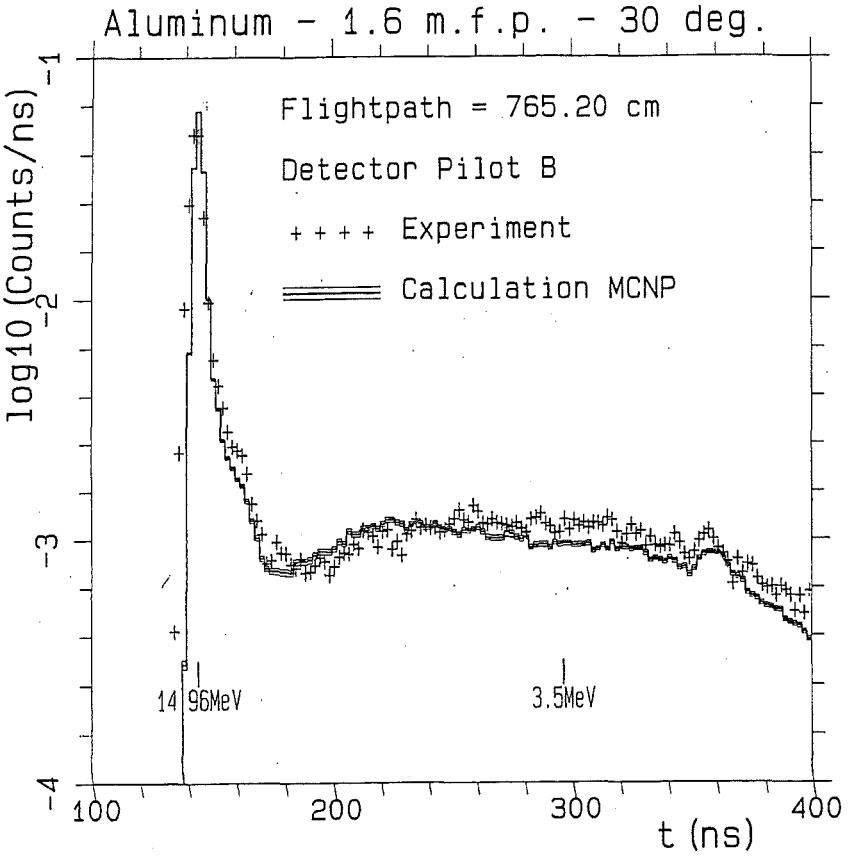

Perel, Magschal, Yeivin: Monte Carlo Calculation of Point Detector Sensitivities - Fig.6

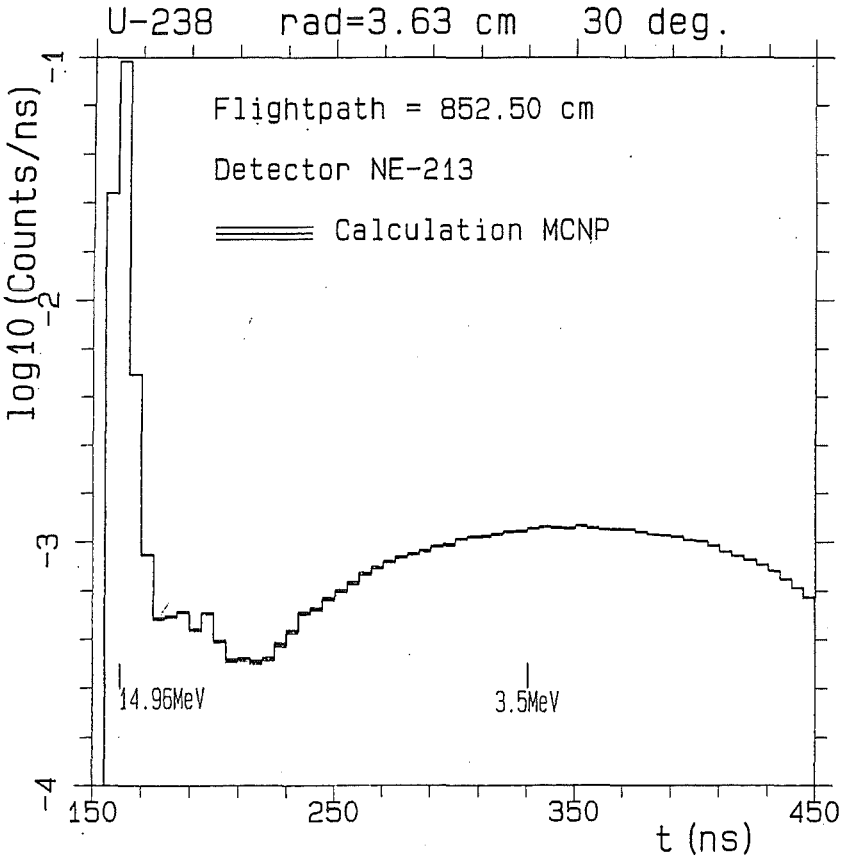

Perel, Magschal, Yeivin: Monte Carlo Calculation of Point Detector Sensitivities - Fig.4

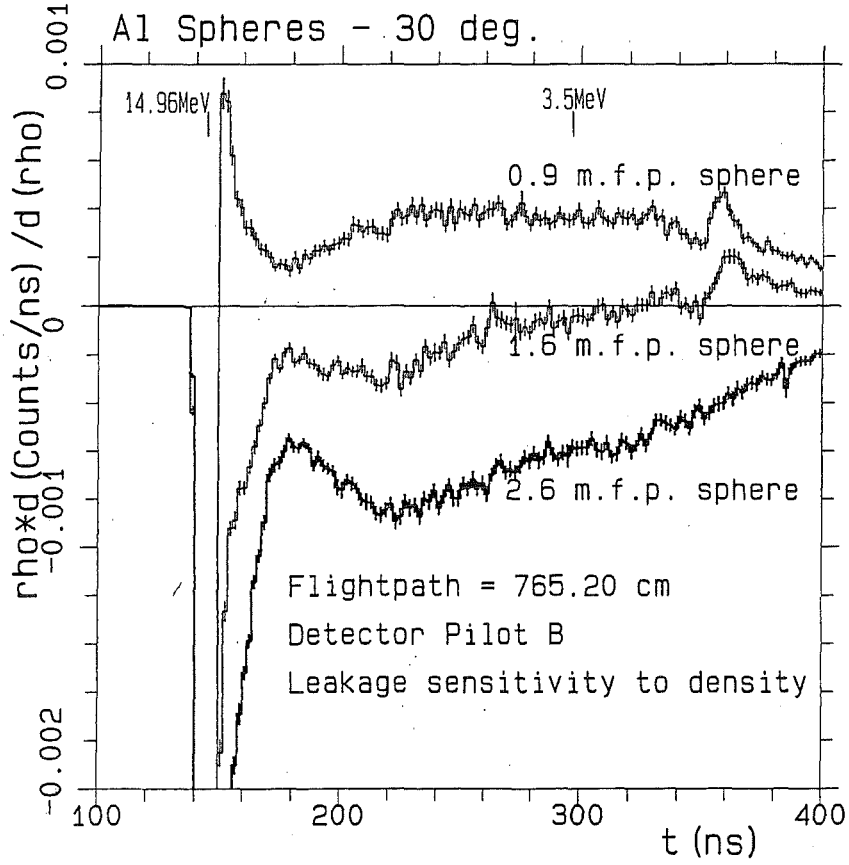

Perel, Nagschal, Yeivin: Monte Carlo Calculation of Point Detector Sensitivities - Fig.7b

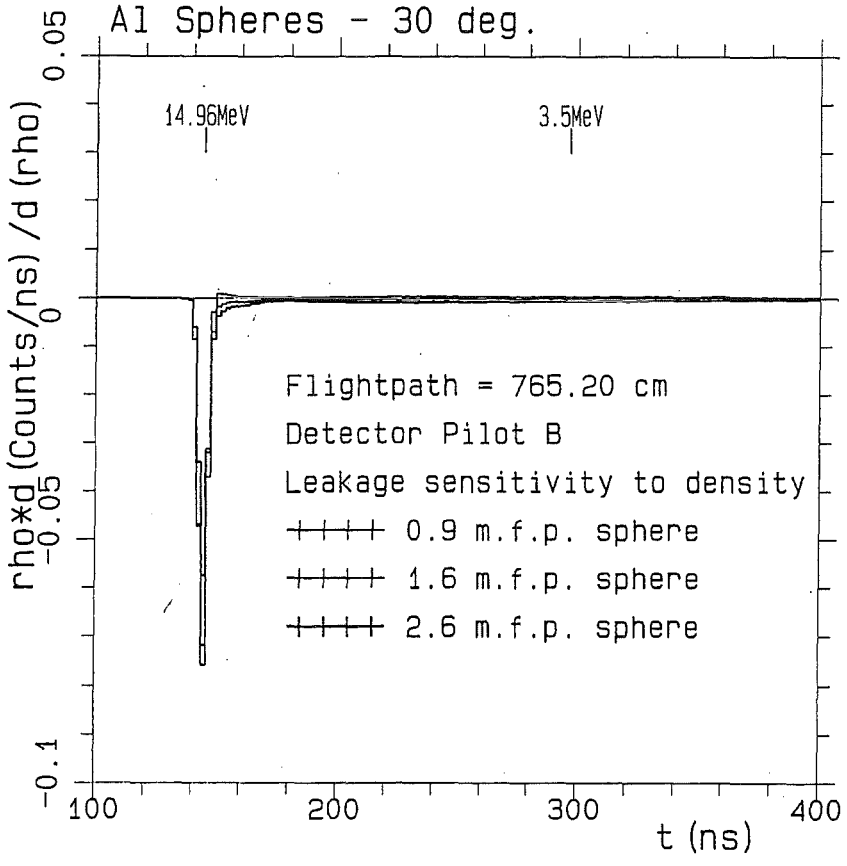

Perel, Nagschal, Yeivin: Monte Carlo Calculation of Point Detector Sensitivities - Fig.7a

NUCLEAR SCIENCE AND ENGINEERING: 124, 197–209 (1996)

Monte Carlo Calculation of Point-Detector Sensitivities to Material Parameters

R. L. Perel, J. J. Wagschal, and Y. Yeivin

The Hebrew University of Jerusalem, Racah Institute of Physics, 91904 Jerusalem, Israel

Received October 13, 1995
Accepted February 16, 1996

Abstract – *Hall's differential operator method for the Monte Carlo calculation of sensitivities was extended so as to apply to point-detector-type problems. By this method, the evaluation of the sensitivities of the detector response (or, equivalently, those of the neutron flux at the detector) to material parameters of interest (cross sections, average number of fission neutrons, number densities) is concurrent with that of the very response. In such a Monte Carlo game, the neutron histories, or paths, are sampled, collision by collision, and the calculated contributions of each collision to the response and to its partial derivatives with respect to the parameters of interest are accumulated. For each path, these sums are the estimates for the response and its respective sensitivities. The Monte Carlo evaluations are then the respective averages of the individual path estimates. This procedure was applied to the analysis of the time-of-flight spectra of the leakage from several of the Livermore pulsed spheres.*

Monte Carlo Methods and Models for Applications in Energy and Technology

Workshop to be held at Forschungszentrum Karlsruhe, May 12-14, 1998

Assessment of Uncertainties in Monte Carlo Particle Transport Calculations

Bernd R.L. Siebert

Physikalisch-Technische Bundesanstal Q.102
Bundesallee 100, D 38116 Braunschweig

Abstract

In many applications of Monte Carlo methods to particle transport problems it is desirable or even necessary to estimate the uncertainties associated with the computed results. This is especially true for applications in metrology or if the results are used in sensitivity studies, e.g. the work by Hall(2). The uncertainties associated with the computed results arise mainly from three sources:

- the affordable sampling statistics
- the estimators and the variance reduction employed and
- the uncertainties associated with the input data, e.g. geometry, material composition and cross section data.

There are several methods available to estimate the uncertainties. The newest version of MCNP(3) uses the differential operator technique for perturbation studies. This method (PERT- card in MCNP) is closely related to the method developed by Hall. There are also other methods available which either substitute or complement the differential operator technique. In this presentation an attempt will be made to discuss some of these methods with special emphasis laid on their implementation in home made Monte Carlo codes. The methods will be demonstrated using the integration of functions depending on one or two parameters as a simple example. Furthermore, the calculation of the response of a recoil proton telescope(4) will serve as a more practical example.

The author is just about to begin the study mentioned above. The main aim of this contribution is therefore to provoke discussions and potentially find collaborators on these topics.

1. Hall, M.C.: Cross Section Adjustment with Monte Carlo: Application to the Winfrith Iron Benchmark. Nucl. Sci. Eng. 81 (1982) p 423-431
2. Briesmeister, J., (Editor): MCNP - A General Monte Carlo Code N-Particle Transport -Version 4B Report: LA 12625-M, 1997, Los Alamos, USA).
3. Used for the determination of neutron fluence for incident neutron energies ranging from 10 to 100 MeV.

Last modified: Thu Apr 2 12:55:08 1998

Discussion of Methods for the Assessment of Uncertainties in Monte Carlo Particle Transport Calculations.

Bernd R.L. Siebert
Physikalisch-Technische Bundesanstalt Q.102
Bundesallee 100, D 38116 Braunschweig

Revised and Extended Version

Presented in part at the Workshop on
Monte Carlo Methods and Models for Applications in Energy and Technology,
Forschungszentrum Karlsruhe, May 12-14,1998

Abstract:

In many applications of the Monte Carlo method to particle transport problems it is desirable or even necessary to estimate the uncertainties associated with the computed results. This is especially true for applications in metrology or if the results are used in sensitivity studies.

Apart from systematic uncertainties inherently associated with the use of an incomplete model the uncertainties associated with the computed results arise in Monte Carlo calculations from mainly three sources:

- **the affordable sampling statistics**
- **the estimators and the variance reduction employed and, last not least**
- **the uncertainties associated with the input data, *e.g.* geometry, material composition and cross section data.**

First, the term model will be defined and the various sources of uncertainties encountered in the comparison of experimental and calculated results will be briefly discussed. Then some methods available to estimate the propagation of the uncertainties associated with the input data will be briefly discussed. These methods are brute force, randomisation of input data, correlated sampling and the differential operator technique. Emphasis is given to the estimation of the sensitivity of the results with respect to the variances associated with input data. The perturbation of input data is seen as a possible method to achieve such an estimation.

Finally, it will be concluded that all but the brute force method are in part suitable for the assessment of uncertainties in Monte Carlo transport calculation and that an increased effort in code development is still needed in order to fully utilise the potential of these methods. In the appendix the calculation of the response of a proton recoil telescope is discussed as an example for the need to estimate the sensitivity of the results with respect to the variances associated with the input data.

The main aim of this contribution is to provoke discussions and potentially find collaborators on these topics.

INTRODUCTION

Systematic uncertainties associated with the model used are often a major contribution to the total uncertainties in Monte Carlo calculations. A model is in general approximate and only a theory may be believed to be exact. A theory is a formulation of apparent relationships or underlying principles of certain observed phenomena which has been verified to some degree. A theory therefore serves two purposes: it 'explains' observed data and, by the process of induction, predicts the outcome of potential experiments. Models possess some features of a theory but are usually or perhaps even in general limited in scope. They attempt to describe known data rather than to predict new information: models are not founded on first principles but are merely descriptive. For instance, target theory[1] as applied to the photographic action of X-rays is indeed a theory, however, its numerous offspring applied to biological cells are better termed models. In this paper the term model is used for the computational image of an experiment, *i.e.,* as a general term for all input data and the algorithms used for simulating an experiment[2]. Such an image is always an approximation to reality. Apart from technical restrictions such as finite computing resources there are limitations in describing the experimental situation.

Indeed, modelling is therefore often an iterative process which is promoted by a careful comparison of calculated and experimentally measured results and an analysis of the deviations seen. A basic requirement for a meaningful comparison is the analysis of the variances which are not associated with the experiment and the model itself. The affordable sampling statistics is for both, experiment and computation, a source of uncertainty. The experimental method is as well a source of variance as the estimation scheme and the variance reduction methods employed in calculations. The geometry and material composition may be viewed as being part of the model. Here, however, they are treated as input data which influence the interactions of the transported particle and we are interested in the contribution of the uncertainties associated with them to the uncertainties associated with the computed results. Finally, the uncertainties associated with the input data which describe the interactions of the transported particle, *i.e.* first of all cross sections, are in some applications of special interest.

The reduction of variances associated with experimentally measured results will not be discussed in detail here. The sampling statistics in calculations can in most applications be improved by the use of appropriate variance reduction methods. However, caution is needed, as these techniques -apart from point estimators- merely redistribute the variances. For a given problem the estimation of particle fluences may be quite sensitive to the use of either a surface crossing (cut-off angle) or track length estimator and furthermore to the size of the area or volume, respectively. The uncertainties of the input data can not be reduced below certain values as measured values are associated with finite uncertainties, *e.g.* values for lengths, material composition and densities, isotope ratios and last not least cross sections or quantities derived from cross sections (W-values, stopping power, kerma or heating numbers). In addition, especially with neutron cross sections there are often strong covariances encountered, which stem from the use of reference cross sections, *e.g.* H(n,p) and the methods used in their determination.

The *perturbation* of input data is a method which allows to estimate the *sensitivity* of the results with respect to the input data. The total uncertainty may then be obtained by multiplying the *sensitivity matrix* from the left and from the right with the specified standard deviations the input data. The determination of a sensitivity matrix may be quite cumbersome in practice and it may be necessary to resort to approximate estimates of the total uncertainty. However, any such approximation should be consistent with the ISO guide to the expression of uncertainty in measurement[3].

BRUTE FORCE METHOD

The most simple approach to analyse the propagation of uncertainties associated with input data in Monte Carlo transport calculations would be to simply make a serious of calculations with changed input data. Obviously, this method can only be applied to cases where the calculated results differ significantly as the variance for the difference -assuming statistically uncorrelated runs and Poisson statistics- is proportional to $(2\cdot \langle a\rangle + \langle\Delta\rangle)/(N\cdot\Delta)$, where $\langle a\rangle$ is the unperturbed expectation value, $\langle a\rangle + \langle\Delta\rangle$ is the perturbed expectation value and N is the number of histories. With other words, small differences tend to be masked by random noise unless expensive long runs are made. Furthermore, if the sensitivity with respect to several potentially correlated input data is to be examined one needs many runs and a complex book keeping.

It is interesting to note, that this brute force method would work perfectly with deterministic algorithms such as the finite element method (FEM). A perturbation of input data would lead to results which by definition are not masked by random noise. Even in problems which are on account of their complex geometry and/or significant contributions from high order multiple scattering best solved with the Monto Carlo method it could be an interesting approach to create a simplified model for FEM calculations and use FEM for an approximate sensitivity study.

RANDOMIZATION OF INPUT DATA

A straightforward possibility to study the propagation of uncertainties associated with input data in Monte Carlo transport calculations is to sample from a Gaussian probability[4] density, and to use different tallies to sort the results with respect to the sampled input data. For instance, sample a total cross section from:

$$p(t) = \left(2\cdot p\cdot s\right)^{1/2}\cdot exp\left[\left(t - s_{tot}(E)\right)^2 / \left(2s^2\right)\right] \qquad (1)$$

where s is a measure of the uncertainty of the total cross section and use n tallies for $P^{-1}(t) \equiv \rho \in [0,1/n),...[(n-1)/n,1.0]$. The problem of random noise would still be serious, if a sensitivity analysis is tried and the expectation values of the n tallies do not differ sufficiently. However, if s is a correct measure of the uncertainty of this total cross section, then its global influence could easily bee seen by appropriate estimators.

In principle, an arbitrary number m of input data can be randomised as shown in Eq.(1). However, it would be already cumbersome to compute m·n tallies with sufficient statistics and simply not feasible if the correlation of the input data is to be seen also.

On the other hand, it is possible to compute only one mean value but list for each contribution to the mean value the value, its weight and the values of all randomly selected input data use in the calculation of this value. This list file could then be used to determine the sensitivities of the mean value with respect to the randomly sampled input data. To that purpose one determines the mean values of estimand, y, as seen in N histories and the m input data x_μ:

$$\overline{y} = \sum_{\nu=1}^{N} w_\nu\cdot y_\nu \Big/ \sum_{\nu=1}^{N} w_\nu \quad \text{and} \quad \overline{x_\mu} = \sum_{\nu=1}^{N} w_\nu\cdot x_{\mu,\nu} \Big/ \sum_{\nu=1}^{N} w_\nu \qquad (2)$$

and creates the following over determined linear system of N equations for the elements of the sensitivity matrix:

$$(\bar{y} - y_\nu)^2 = \Delta \vec{x}_\nu \cdot \vec{s} \qquad (3)$$

where the components of $\vec{s}$ are given by (s_{11}, s_{12},...s_{1m}, s_{22}, s_{23}...s_{2m}, ...s_{mm}) and the ones of $\Delta \vec{x}_\nu$ are then correspondingly given by $((\overline{x_1} - x_{1,\nu})\cdot(\overline{x_1} - x_{1,\nu}), (\overline{x_1} - x_{1,\nu})\cdot 2\cdot(\overline{x_2} - x_{2,\nu})....)$. The standard least squares solution of Eq. (3) yields an estimate of the sensitivity matrix. It is to be noted, that the sampling of the value, its weight and the values of all randomly selected input data use in the calculation of this value are partially correlated. A possible gain is seen with a strictly correlated sampling of the input data[1]. Here, however, extreme caution is needed in order to avoid an undue biasing.

CORRELATED SAMPLING

Correlated sampling is a well established tool to directly compute small differences. The masking by random noise is avoided by sampling the unperturbed and the perturbed values with the same chain of random numbers[5] or simultaneously. The latter approach, simultaneous correlated sampling[6] is closely related to the differential operator technique which will be discussed below. The use of the same chain of random numbers works fine with simple integration problems. However, if in a transport calculation slight changes of an input datum lead to large differences for subsequent multiple scattering then this method can not maintain the needed correlation.

DIFFERENTIAL OPERATOR TECHNIQUE

The newest version of MCNP[7] uses the differential operator technique for perturbation studies which is closely related to the method developed by Hall[8] and in detail demonstrated by McKinney and Iverson[9].

The *differential operator technique* is based on the use of a Taylor series in up to second order to express the dependence of the Monte Carlo estimand on changes in the input parameter. However, the existing implementation of the method (PERT-card in MCNP) is still limited in scope. A very strong restriction is that the PERT-card does not work with point estimators and is not yet applicable to electron transport. Another restriction with the present implementation is the restriction, that only the *statistical weight* but not the *physical state* of the transported particle may depend on the perturbation. For instance, if an angular cross section distribution density is perturbed, then with a given random number and a given perturbation one would not only change the statistical weight of the produced or scattered particle, but also its energy.

It should be mentioned that also the *commercially* distributed neutron transport code MCBEND[2] allows for an uncertainty assessment based on the differential operator technique by Hall[8].

[1] Instead of a Gaussian one could of course use an actually given probability density. In order to facilitate the correlated sampling of the randomised input data also a discrete distribution density could be advantageous, *e.g.* at -2σ, -σ, 0, σ, 2 σ.

[2] Available from AEA Technology, Winfrith Technology Centre, Dorchester, Dorset DT2 8DH, UK

SUMMARY AND CONCLUSION

The assessment of uncertainties in Monte Carlo particle transport calculations has been shown to be a complex problem. The uncertainties associated with the model itself, the schemes used for the estimation and the variance reduction methods applied are in praxis of importance. However, the discussion in this contribution concentrated on methods to estimate the sensitivity of the calculated results with respect to the uncertainties associated with the input data. All methods discussed but the brute force method are seen as suitable for the assessment of uncertainties in Monte Carlo transport calculation. However, an increased effort in code development seems to be still needed in order to fully utilise the potential of these methods as meaningful and efficient approaches to estimate the sensitivity of the calculated results with respect to the variances of the input data. In any case, correlated sampling is needed to avoid the masking by random noise. The greatest potential is seen with the differential operator technique. However, the method of correlated randomised sampling of the input data is also seen as an interesting powerful method.

The appendix describes the *Monte Carlo Simulation of a Proton Recoil Telescope.* This problem seem to be well suited to try and to improve both, the differential operator technique and the correlated sampling from randomised input data.

REFERENCES

1. Blau, M. and Altenburger, K.: *Über einige Wirkungen von Strahlen, II* Z.Physik, **12**, pp. 315-329 (1922).
2. Siebert, B.R.L and Thomas, R.H.: *Computational Dosimetry*
   Rad. Protect. Dosimetry, **70**, pp. 371-378 (1997).
3. International Organization for Standardization: *Guide to the Expression of Uncertainty in Measurement*
   ISO, Case postale 56, 1211 Genève 20, Switzerland, ISBN 92-67-10188-9 (1993)
4. Private communication from Bernd Großwendt, PTB
5. Weise, K. and Zhang, H.: *Uncertainty treatment in MonteCarlo simulation*
   J.Phys.A:Math. Gen **30** (1997) pp. 5971-5980
6. Rief, H.: *Generalized Monte Carlo Perturbation Algorithms for Correlated Sampling and a Second-Order Taylor Series Approach* Ann. nucl. Energy. Vol II No 9 (1984) p 455-476
7. Briesmeister, J. (Editor): *MCNP - A General Monte Carlo Code N-Particle Transport -Version 4B*
   Report: LA 12625-M, 1997, Los Alamos, USA).
8. Hall, M.C.: *Cross Section Adjustment with Monte Carlo: Application to the Winfrith Iron Benchmark.*
   Nucl. Sci. Eng. **81** (1982) p 423-431
9. McKinney, G.W. and Iverson J.L.: *Verification of the Monter Carlo Differential Operator Technique for MCNP^{TM}* Report: LA 13098, 1996, Los Alamos, USA).
10. Siebert, B.R.L.; Brede, H.J.; Lesiecki, H.: *Corrections and Uncertainties for Neutron Fluence Measurements with Proton Recoil Telescopes in Anisotropic Fields.* Nucl. Instr. & Meth. **A 235** (1985) S. 542-552.
11. Schuhmacher, H.; Siebert, B.R.L.; Brede, H.J.: *Measurement of Neutron Fluence for Energies between 20 and 60 MeV Using a Proton Recoil Telescope.* In: Proceedings of a Specialist's Meeting on Neutron Cross Section Standards for the Energy Region above 20 MeV, Uppsala (Schweden), Mai 1991. Paris: OECD, 1991 (NEANDC-305 Report), S. 123-134.

APPENDIX: Monte Carlo Simulation of a Proton Recoil Telescope

The calculation of the response of a recoil proton telescope (RPT) is a practical example for the need to assess the uncertainties of the results. The RPT considered here is designed for the determination of neutron fluence for incident neutron energies ranging from 10 to 100 MeV. Its essential parts are a hydrogen containing radiator in which neutrons produce recoil protons via the reaction H(n,p), slits to determine the spatial angle for the proton emission, and a thin and a thick silicon sensor to determine the energy loss (thin $\Rightarrow \Delta E$) and the total energy (thick $\Rightarrow E$) of the proton. The result of a measurement are the spectrum (energy distribution densities) of the detected protons and a matrix, ΔE versus E. The peak in the spectrum allows to determine the incident neutron energy and their fluence directly, if mono-energetic neutrons are used or via an unfolding procedure the determination of the incident neutron spectrum. The matrix is used to discriminate protons against ^{2}H, ^{4}He and other "unwanted" ions. The code for the simulation of this RPT and the sensitivity analysis are in part based on previous work[10,11].

The main sources of uncertainties are associated with the H(n,p)-cross section and its angular distribution density, the number density of H-atoms in the radiator layer, the size and geometry of the radiator, the position, thickness and diameter of the slit and the stopping power and straggling data used in transporting the proton from its origin in the radiator to the and inside the silicon sensors.

The variance of the elastic H(n,p)-cross section are very small, but *correlated* with respect to the incident neutron energy. The variances of the angular distribution density of the elastic H(n,p)-cross section are not very well known and must be estimated by comparing different evaluations. A possible but not yet formulated approach could be to describe this cross section by a Legendre expansion and to specify a *covariance matrix* for the Legendre coefficients. Here, a perturbation implies via the kinematics a *change in the proton energy* ! As the radiator is thin one may can assume that the uncertainty of the number density of H-atoms in the radiator layer is propagated linearly to the results, however, an additional source of uncertainty is a possible inhomogeneity of the hydrogen density. The size and geometry of the radiator are quite well known, nevertheless it is of interest to study the influence of possible deviations from the assumed values. The same comment applies to the position, thickness and diameter of the slit. Due to the high energies considered stopping power data are only taken from the Bethe region far above the Bragg peak and it is sufficient assume merely an uncertainty of the values without changing the dependence on energy. But again, a perturbation implies via the energy loss a *change in the proton energy* ! Straggling in energy, range and direction leads to fairly small changes. However, their perturbation influences both, the proton energy and its direction of flight. The range straggling influence those protons which lose almost all of their energy in the edges of a slit.

In summary, the calculation or the response function of a RPT is for two reasons an almost perfect example to test and develop methods to estimate the sensitivity of the response function with respect to the variance of the input data. First, the model of the underlying physics is quite simple and second, the propagation of the variances of the input data is sufficiently complex as to require improvements of the above discussed methods.

Suggestions and or collaboration on the implementation of both, the differential operator technique and the correlated sampling from randomised input data, would be appreciated.
EMAIL: ***Bernd.Siebert@PTB.DE***

Monte Carlo Methods and Models for Applications in Energy and Technology

Workshop to be held at Forschungszentrum Karlsruhe, May 12-14, 1998

Monte Carlo Methods in Dynamic Reliability (ULB)

P. E. Labeau

Service de Métrologie
Université Libre de Bruxelles
1050 Bruxelles - BELGIUM

Dynamic reliability presents a fully integrated dynamic approach to system reliability, able to account for all aspects of the problem : changes in the hardware status, dynamic evolution of the system, operating procedures, scenario history ... In this framework, the interaction between the dynamic evolution of the process variables describing the system behaviour and the stochastic or deterministic transitions between component states is modeled :

- depending on the system configuration, the evolution equations of the variables can differ;
- the values taken by these variables influence the transitions, either by defining a threshold at which a control device is triggered, or by affecting the value of some transition rates.

A coupling thereby appears between the deterministic dynamic modelling and the stochastic process between states. A trajectory of the system in the process variables space is thus a piecewise deterministic curve with random or deterministic bifurcations between its parts. Some of these evolutions could bring the system out of a safety domain defined in the variables space. This situation corresponds to a system failure. All the information on this process is contained in the probability density to find the system in a given state, with given values of the variables, as a function of time. Reliability characteristics are then expressed as functionals of this pdf. But the computation of such a high-dimensional pdf is a very demanding numerical task for realistic installations. MC simulation appears as a good candidate to tackle this dimensionality problem. However, an analog algorithm is inefficient for the estimation of the very small risk probabilities of engineered systems. Various ways of improving the simulation efficiency have been propounded and will be reviewed during the talk :

- First, a formal analogy has been established between dynamic reliability and neutron transport. This provides a framework for developing biased algorithms (e.g. approximate zero-variance schemes) or for defining efficient estimators.

- The concept of most probable evolutions (MPEs) was introduced. When an initiating event occurs, a transient is induced; the system has then a large probability to evolve up to a first control threshold without undergoing any stochastic transition; the corresponding control device is also very likely to work as expected, and so on ... until a safe situation is reached. These MPEs will be often followed in an analog game. Therefore, they can be played and memorized before the simulation itself. Different efficient algorithms were deduced from this memorization approach.

- Hybrid techniques appear very efficient. They are based on a further development of the MPE concept : the complete deterministic tree based only on transitions on demand (when thresholds

are reached) can be computed beforehands; MC trials are then used to estimate the perturbation due to scenarios (not included in this tree) consecutive to a first stochastic transition.

- Many parameters in dynamic reliability are not always precisely known, and can thereby be distributed : transition rates and probabilities, response times of the control and protection means, parameters of the dynamics ... A MC simulation can give allowance to them, but much larger numbers of histories are required for a given efficiency. To avoid this situation, different techniques are considered : double randomization, correlated sampling, or estimators embodying the mean effect of uncertain parameters.

Last modified: Thu Apr 2 13:40:38 1998

Monte Carlo methods in dynamic reliability

Pierre-Etienne Labeau
Université Libre de Bruxelles
Belgium

Classical reliability techniques.

Dynamic reliability.

Monte Carlo simulation in dynamic reliability.

Application : a PWR pressurizer.

Handling uncertainties.

Conclusions.

Classical reliability techniques

Fault tree (FT)

Logical decomposition of a complex situation (*top event*) in basic events

+ boolean algebra

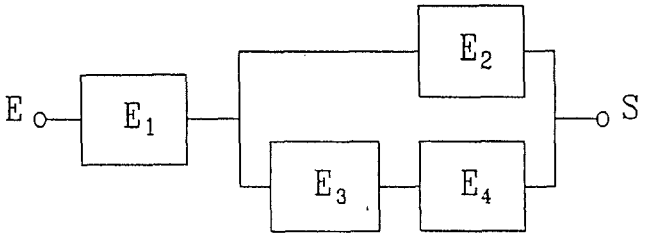

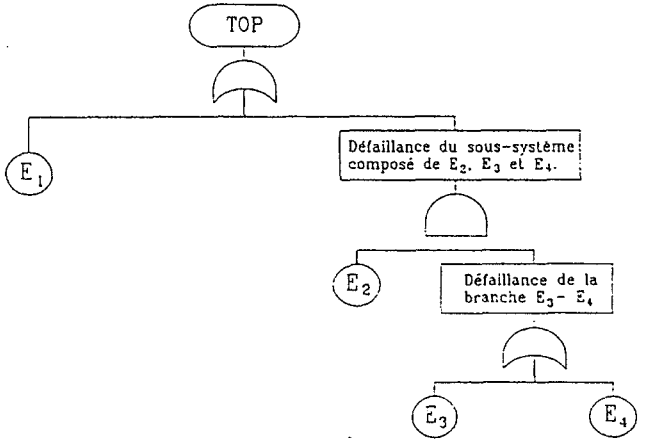

Event tree (ET)

Branching process after an *initiating event* : all combinations of top events considered.

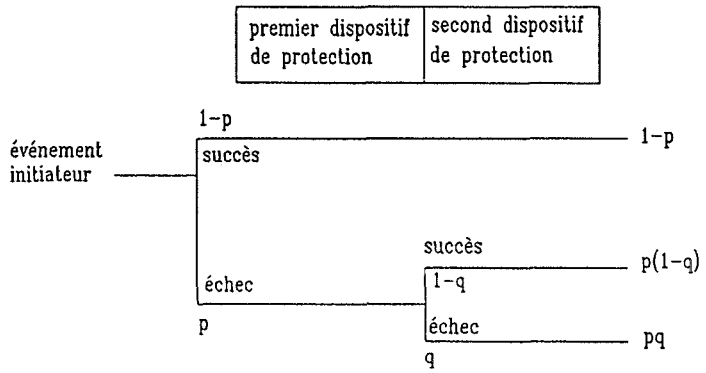

ET/FT :

Accidental scenario ≡ set of successes and failures of top events

⟶ static and logical approach to risk, based on assumptions :

- possible variations in the ordering of the success and failure events?
  ⟶ no influence on the final outcome and its likelihood
- variation in the timing of events?
  ⟶ no effect on scenario outcomes and frequencies
- effect of process variables and operator behaviour on scenario development?
  ⟶ ⊂ definition of success criteria

Always realistic ??

Dynamic reliability

Event trees

timing and ordering of events?

⟶ **Theory of continuous event trees**

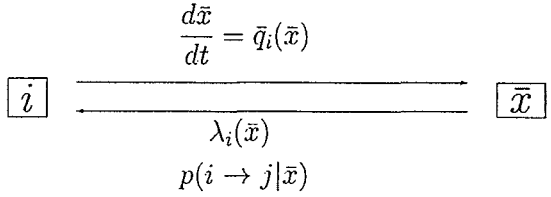

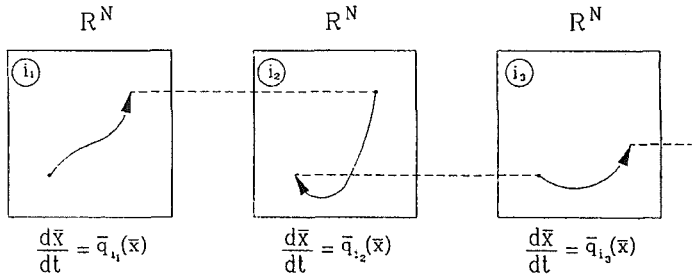

Failure = exit of a safety domain defined in $\mathcal{R}^N$

$\pi(i, \bar{x}, t)$ = probability that the system is at time t in state i in $d\bar{x}$ about $\bar{x}$

$\longrightarrow$ **Chapman-Kolmogorov equation** (Markovian assumption)

$$\frac{\partial \pi(i, \bar{x}, t)}{\partial t} + div(\bar{q}_i(\bar{x})\pi(i, \bar{x}, t)) + \lambda_i(\bar{x})\pi(i, \bar{x}, t) = \sum_{j \neq i} p(j \longrightarrow i|\bar{x})\pi(j, \bar{x}, t)$$

Characteristics

- number of states!
- $N >$ ($\gg$)10 for realistic applications

$\longrightarrow$ specific solution schemes :

- discrete event trees
- Monte Carlo simulation
- other approaches

Integral form :

$$\begin{aligned}\pi(i, \bar{x}, t) = & \int_{\mathcal{R}^n} \pi(i, \bar{u}, 0)\delta(\bar{x} - \bar{g}_i(t, \bar{u}))e^{-\int_0^t \lambda_i(\bar{g}_i(s,\bar{u}))ds} d\bar{u} \\ & + \sum_{j \neq i} \int_{\mathcal{R}^n} p(j \rightarrow i \mid \bar{u}) d\bar{u} \int_0^t \delta(\bar{x} - \bar{g}_i(t - \tau, \bar{u}))e^{-\int_0^{t-\tau} \lambda_i(\bar{g}_i(s,\bar{u}))ds} \\ & \times \pi(j, \bar{u}, \tau) d\tau\end{aligned}$$

Generalized unreliability

Two failure modes :

- transition from state $j \in X$ to failed state $\ell \in Y$
- escape of a safety domain D in phase space

$$\begin{aligned}1 - R(t) = & \int_0^t \int_{\mathcal{R}^n} \sum_{j \in X} \pi(j, \bar{x}', t') \cdot [\sum_{\ell \in Y} p(j \rightarrow \ell | \bar{x}') H_D(\bar{x}') \\ & + \delta(t - t')\,(1 - H_D(\bar{x}'))]\; d\bar{x}'\, dt'\end{aligned}$$

Monte Carlo simulation in dynamic reliability

Advantages

- Monte Carlo almost insensitive to dimensionality problems
- Direct estimation of functionals of $\pi(i, \bar{x}, t)$
- Still applicable in the presence of uncertainties
- Representative sample of histories ($\longrightarrow$ no combinatorial explosion)
- ...

An analog algorithm

a. Sampling of i and $\bar{x}$ at $t = 0$

b. Sampling of the next transition time

c. Computation of $\bar{x}(t)$ in state i

t_{lim} reached? safety border crossed? $\longrightarrow$ stop

d. Sampling of new state j : $j \in Y$? $\longrightarrow$ stop

$i \longleftarrow j$; go to b.

Last-event estimator : $f(t) = H(t - t_f)$

Monte Carlo estimation of unreliability :

$$1 - \tilde{R}(t) = \frac{1}{N} \sum_{i=1}^{N} H(t - t_{fi})$$

Drawbacks :

- failures = rare events
  - $\longrightarrow$ most histories wasted
  - $\longrightarrow$ poor statistical quality of the estimation
  - $\longrightarrow$ very large number of histories mandatory
  - $\longrightarrow$ inacceptable computer times
- Is the sample of trajectores representative?

Figure of merit :

$$FOM = \frac{1}{\sigma^2 \overline{T}}$$

σ^2 : variance of the game
$\overline{T}$: mean time per history

Towards MC games with higher FOMs

Analogy with neutron transport theory

Estimation of a reaction rate

Free-flight estimator

Most probable evolutions

Perturbation of a deterministic event tree

Variance-reduction techniques

Analogy with neutron transport theory

Conceptual analogy

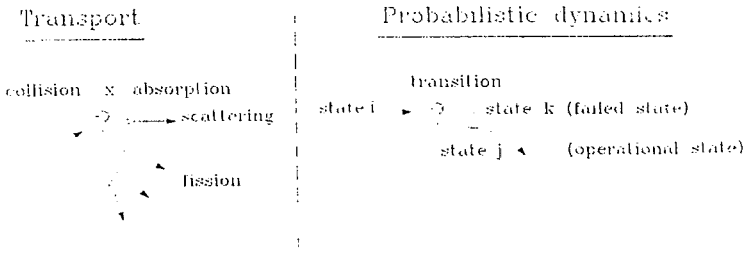

Formal analogy

Integral form of transport equation :

$$\rightarrow \Psi(P) = \int T(P', P) Q(P')\, dP' + \int\int C(P'', P') T(P', P) \Psi(P'')\, dP''$$

with
$$\begin{aligned} P &= (\bar{r}, v, \bar{\omega}) \\ \Psi(P) &= \text{collision density} \\ Q(P) &= \text{source density} \\ T(P', P) &= \text{trnaistion kernel} \\ C(P'', P') &= \text{collision kernel} \end{aligned}$$

Integral form of C-K equation :

$$\begin{aligned} \pi(i, \bar{x}, t) &= \int_{\mathcal{R}^n} \pi(i, \bar{u}, 0) \delta(\bar{x} - \bar{g}_i(t, \bar{u})) e^{-\int_0^t \lambda_i(\bar{g}_i(s,\bar{u}))ds} d\bar{u} \\ &+ \sum_{j \neq i} \int_{\mathcal{R}^n} p(j \rightarrow i \mid \bar{u}) d\bar{u} \int_0^t \delta(\bar{x} - \bar{g}_i(t-\tau, \bar{u})) e^{-\int_0^{t-\tau} \lambda_i(\bar{g}_i(s,\bar{u}))ds} \\ &\quad \times \pi(j, \bar{u}, \tau) d\tau \end{aligned}$$

Definitions :

$$\begin{aligned} P &= (i, \bar{x}, t) \\ P' &= (j, \bar{x}', t') \\ P'' &= (k, \bar{x}'', t'') \\ \psi(P) &= \Psi(i, \bar{x}, t) = \lambda_i(\bar{x}) \pi(i, \bar{x}, t) \\ Q(P') &= Q(j, \bar{x}', t') = \pi(j, \bar{x}', t') \delta(t') \\ T(P', P) &= T(j, \bar{x}', t'; i, \bar{x}, t) = \lambda_i(\bar{x}) \delta(\bar{x} - \bar{g}_i(t - t', \bar{x}')) \\ &\quad \times e^{-\int_0^{t-t'} \lambda_i[\bar{g}_i(s,\bar{x}')]ds} \delta^i_j H(t - t') \\ C(P'', P') &= C(k, \bar{x}'', t''; j, \bar{x}', t') = \frac{p(k \rightarrow j \mid \bar{x}'')}{\lambda_k(\bar{x}'')} \delta(\bar{x}' - \bar{x}'') \delta(t' - t'') \\ &= c_a(P') \delta(P'' - \bar{P}) + c_s(P')\, C_s(P', P'') \end{aligned}$$

Since $\int \ldots dP = \sum_i \int_0^\infty \ldots dt \int_{\mathcal{R}^n} \ldots d\bar{x}$:

$$\begin{aligned} \int T(P', P) dP &= 1 \\ \int C(P'', P') dP' &= 1 \qquad \text{(cf. no fission)} \\ \int Q(P) dP &= 1 \end{aligned}$$

Devising efficient games

- Set of partially unbiased estimators

$$\begin{cases} f(P,P') & : \text{free-flight between } P \text{ and } P' \\ f_a(P') & : \text{absorption in } P' \\ f_s(P',P'') & : \text{scattering from } P' \text{ to } P'' \end{cases}$$

unbiased estimation $\longrightarrow$ conservation of $M_1(P)$, expected score from P

- Biased games
  - $\longrightarrow$ biased kernels $\tilde{T}$ and $\tilde{C}$
  - $\longrightarrow$ interesting rare events more often sampled

unbiasedness? Scores multiplied by statistical weights :

$$w_T = \frac{T}{\tilde{T}} \quad \text{and} \quad w_C = \frac{C}{\tilde{C}}$$

Free-flight estimator :

During the *free flight* PP', we score :

- from P' : the probability of escaping D in state i before t_{lim};
- from P : the probability of a transition to a failure state.

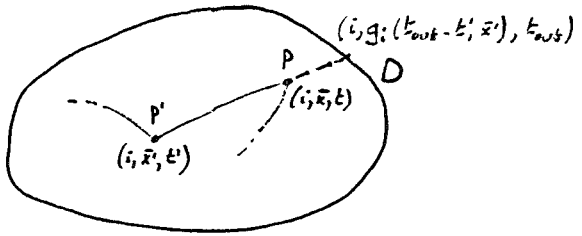

$$f(T;i,\bar{x}',t',\bar{x},t) = \sum_{j\in\Gamma} \frac{p(j\to i|\bar{x})}{\lambda_i(\bar{x})} H_D(\bar{x}) H(T-t)$$
$$+e^{-\int_{t'}^{t_{out}} \lambda_i(\bar{g}_i(s-t',\bar{x}'))dt'} .(1-H_D(\bar{g}_i(t_{out}-t',\bar{x}'))) H(T-t_{out})$$

$\longrightarrow$ multiple contributions to the score in each history

(scores even if no failure occurs : *expected values*)

$\longrightarrow$ much better statistical accuracy

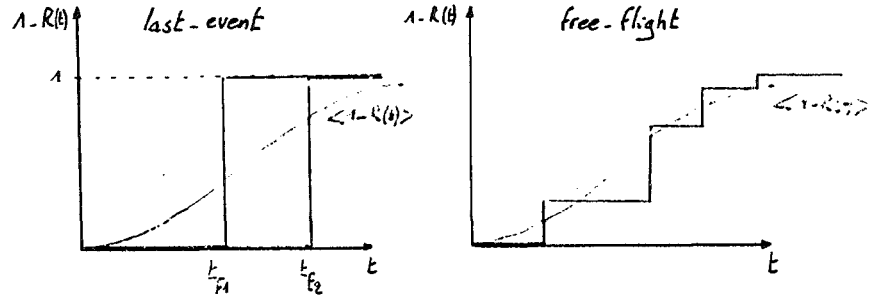

Most probable evolutions (MPEs) :

Well-protected systems

$\longrightarrow$ accidental transients mitigated with a large probability

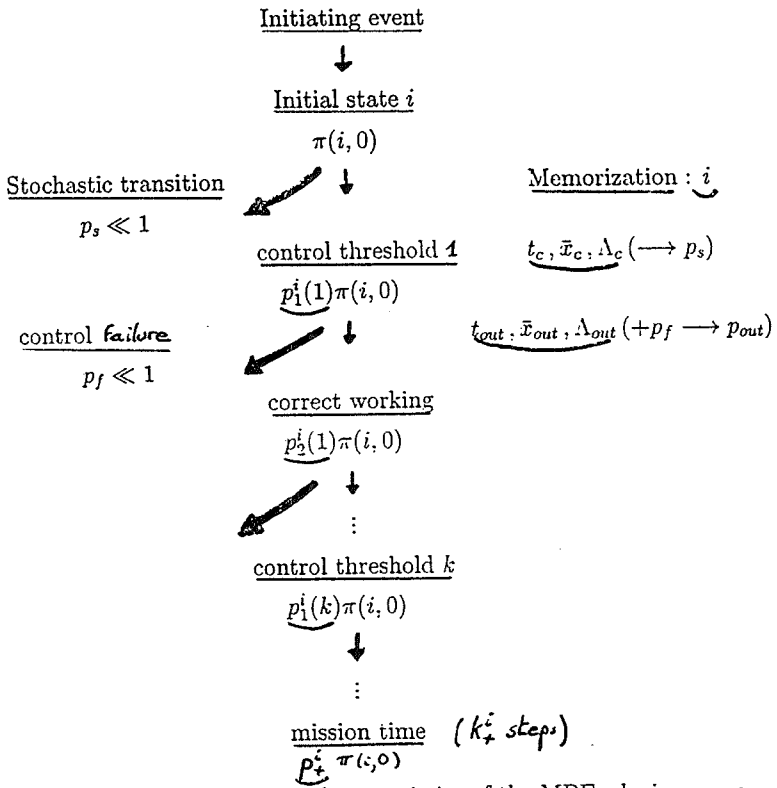

$\longrightarrow$ memorization of the main characteristics of the MPEs during a pre-simulation stage

$\longrightarrow$ use of memorized information to speed up the simulation

Important memorized features :

- probabilities to follow a MPE up to a given stage
- partial scores collected up to the different stages

Improved games

1.a. Analog simulation with bypass of most dynamic calculations

1.b. Sampling of the stage of a MPE where an unexpected event occurs

$\longrightarrow$ [acceleration
statistical accuracy $\sim$ analog simulation

2. Unexpected event forced to occur before the mission time in each history + correction of results

$\longrightarrow$ [slower
much more accurate estimations
(large effective number of runs)

3. Independent estimations of unreliabilities conditional to a kind of unexpected event along a MPE

$\longrightarrow$ [computer time $\sim$ game 2
systematic investigation of rare events

Memorization

acceleration of an analog game $\longrightarrow$ definition of histories worth to be played (in an analog way)

$\longrightarrow$ **Variance reduction techniques**

- stratified sampling
- survival biasing ($\longleftarrow$ free-flight estimator)

Perturbation of a deterministic discrete event tree

Extension of the MPEs

Assumption : all control/protection systems have constant response times

⟶ Deterministic event tree : built while considering solely transitions on demand

⟶ to be calculated before the simulation

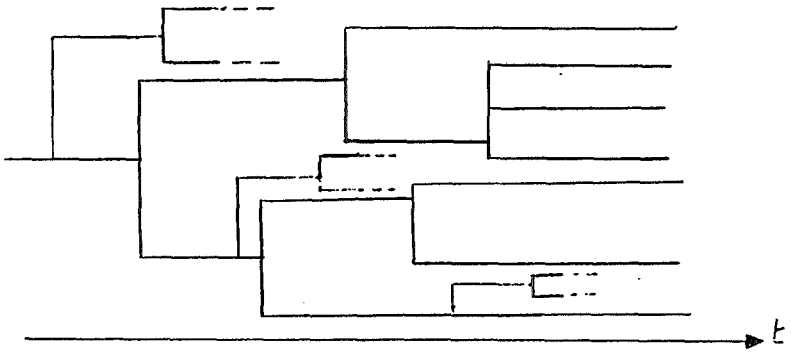

Sequences induced by a stochastic transition = perturbation

⟶ systematic MC investigation of such scenarios from each section of the deterministic tree

⟶ hybrid approach between discrete event trees and MC simulation

Variance-reduction techniques

Efficient MC games

⟶ simulation restricted to possibly interesting scenarios

But : histories played in an analog fashion

⟶ variance-reduction techniques

Survival biasing

Free-flight estimator

⟶ no new information if the failure actually occurs

⟶ failure forbidden at each sampling + introduction of statistical weights

- new state sampled from the set of operational states
- next transition time sampled before exiting D

Stratified sampling

Monte Carlo MPE-based estimation of unreliability

$\longrightarrow$ estimation of a linear combination of random variables with known coefficients

$$S = \sum_\ell \beta_\ell S_\ell$$

$\longrightarrow$ independent batches of N_ℓ histories

Problem :

What are the optimal N_ℓ 's minimizing

$$D^2(E(S)) = \sum_\ell \beta_\ell^2 \frac{V_\ell}{N_\ell}$$

for a given computer time $T = \sum_\ell N_\ell T_\ell$?

Solution :

$$\frac{N_\ell}{N} = \frac{\beta_\ell \sqrt{\frac{V_\ell}{T_\ell}}}{\sum_m \beta_m \sqrt{\frac{V_m}{T_m}}}$$

approximated in the simulation

Probability threshold

$\exists$ unexpected events along MPEs with insignificant probabilities

$\longrightarrow$ probability threshold to cut off branches of the continuous ET

$\longrightarrow$ meaningless histories not played and computer resources saved

Application : a PWR pressurizer

- 6 components $\longrightarrow$ 900 component states
- 12 process variables
- initiating event : fast decrease of the average primary temperature, return to its setpoint
- safety domain : limits of p and ℓ triggering the scram
- inacceptable states : multiple failures of protection systems

game	number of histories	computation time
analogue	10000	2h14'40"
memorization	10000	14"3
biased game	10000	12'22"4
stratified sampling ($\alpha = 0.1$)	10801	21'36"
stratified sampling ($\alpha = 0.2$)	10839	21'37"
stratified sampling ($\alpha = 0.5$)	12074	25'55"

Comments :

- expected values compulsory for large reliable systems
- stepwise behaviour = way to validate the estimations
- coherent estimations for all methods with free-flight estimator
- important acceleration due to memorization
- better statistical accuracy when forcing transitions
- biased game and VRTs : estimation of small contributions to risk
- VRTs : very high efficiency

Summary of MC games :

Analog game :

Analog sampling of events + free-flight estimator

Memorization :

Analog sampling of the stage of a MPE up to which dynamic calculations are bypassed

Biased game :

Unexpected event forced to occur before the mission time

Stratified :

Estimations of the unreliabilities conditional to the various failures likely to occur along a MPE

+ stratified sampling and variance-reduction techniques

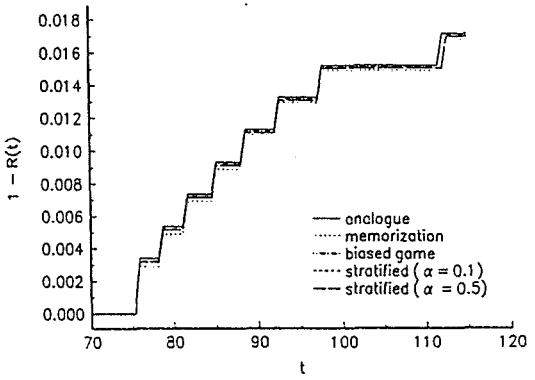

Figure 1: Estimation of unreliability

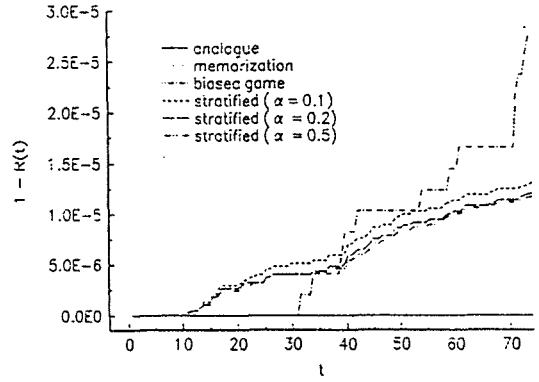

Figure 2: Estimation of unreliability

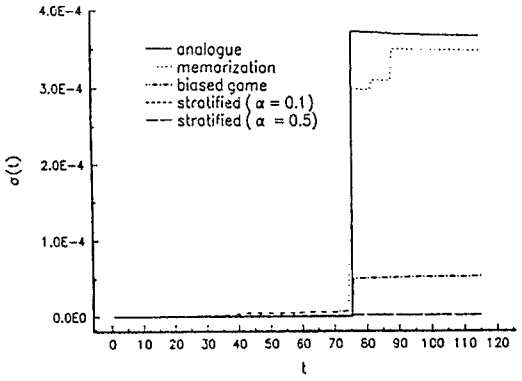

Figure 3: Standard deviation

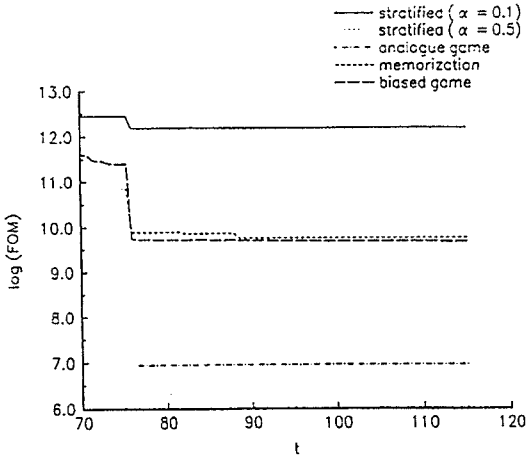

Figure 4: Figures of merit

Handling uncertainties

Uncertainty sources :

- initial distribution of $\vec{x}$
- distributed parameters in the dynamics
- distributed transition rates and probabilities
- distributed control systems or human operator response times
- ...

Uncertainties in an analogue simulation

- sampling of parameter distributions
  - + at the beginning of an history
  - + whenever necessary
- random walk with sampled data

More random parameters → more histories to be played

Efficient MC simulation with data uncertainties?

- free-flight estimator
- memorization-based techniques? MPEs function of :
  - * initial value of $\vec{x}$
  - * values of transition rates and probabilities
  - * fixed response times

Double randomization (batching)

Sampling of uncertain data before playing a batch of histories

→ memorization before each batch

Computation time

Without uncertainties :

$$T_1 = t_m + Nt_h$$

Batching ($m \times n$ histories) :

$$T_2 = mt_m + Nt_h$$

Variance

σ^2_{rw} : random walk
σ^2_{dd} : distributed data

$$\sigma^2_{\bar{s}} = \frac{1}{m}\left(\frac{\sigma^2_{rw}}{n} + \sigma^2_{dd}\right)$$

Efficiency

Minimize $\sigma^2_{\bar{s}}\frac{T_2}{N}$ with $mn = N$

$$\rightarrow \begin{cases} n = \sqrt{\dfrac{\sigma^2_{rw} t_m}{\sigma^2_{dd} t_h}} \\ m = N.\sqrt{\dfrac{\sigma^2_{dd} t_h}{\sigma^2_{rw} t_m}} \end{cases}$$

Conclusions

- Dynamic reliability = framework for a global treatment of reliability
- Numerical challenge ⟶ Monte Carlo simulation
- Analog algorithm inefficient
  - ⟶ free-flight estimator
  - ⟶ memorization
  - ⟶ systematic investigation of possibly dangerous sequences
- Efficient games applicable to large-scale installations
- Possible efficient tretament of parametric uncertainties
- Applicability to level-2 PSA studies?

References

[1] Siu N. Risk assessment for dynamic systems : an overview. Rel Eng Syst Safety 1994; 43(1):43-73.

[2] Devooght J. Dynamic reliability. Ad Nucl Sci Tech 1997; 25:215-278.

[3] Devooght J, Smidts C. Probabilistic dynamics as a tool for dynamic PSA. Rel Eng Syst Safety 1996; 52:185-196.

[4] Marseguerra M, Zio E, Devooght J, Labeau PE. A concept paper on dynamic reliability via Monte Carlo simulation. Mathematics and Computers in Simulation 1998; 1557.

[5] Marseguerra M, Zio E. Monte Carlo approach to PSA for dynamic process systems. Rel Eng Syst Safety 1996; 52:227-241.

[6] Lux I, Koblinger L. Monte Carlo particle transport methods : neutron and photon calculations. CRC Press. Boca Raton, 1991.

[7] Labeau PE. Probabilistic dynamics : estimation of generalized unreliability through efficient Monte Carlo simulation. Ann Nucl En 1996; 23(17):1355-1369.

[8] Labeau PE. Monte Carlo estimation of generalized unreliability in probabilistic dynamics. I.Application to a PWR pressurizer. Nuclear Science and Engineering 1997; 126(2):131-145.

[9] Labeau PE. Variance reduction techniques in Monte Carlo simulation applied to dynamic reliability. In : Guedes Soares C (ed) Advances in Safety and Reliability. Pergamon, Oxford, 1997, pp 2129-2137.

[10] Labeau PE. A survey on Monte Carlo estimation of small failure risks in dynamic reliability. Int J Electron Commun 1998; 52(3):205-211.

Monte Carlo Methods and Models for Applications in Energy and Technology

Workshop to be held at Forschungszentrum Karlsruhe, May 12-14, 1998

Weight Updating in Forced Monte Carlo Approach to Dynamic PSA

M. Marseguerra, E. Zio

Dept. of Nuclear Engineering
Polytechnic of Milan-Italy
Via Ponzio 34/3, 20133 Milano, Italy

ABSTRACT

In dynamic PSA (Probabilistic Safety Analysis), in addition to the stochastic failures, which are normally accounted for in the classic, event tree/fault tree--based approach, one has to consider the physical evolution of the process variables. Correspondingly, the control/protection system needs to be simulated, its intervention being demanded when anyone of the process variables crosses pre--established thresholds.

The Monte Carlo methodology lends itself to an efficient estimate of the reliability of systems with dynamic features. In this respect, the high reliability of current components and control/protection systems renders prohibitive the use of analog Monte Carlo, thus making the use of variance reduction techniques almost mandatory.

In the present paper we tackle a new problem arising in this context. More specifically, once the next failure time is forced and the weight of the representative point is correspondingly updated, we have to follow the system dynamics up to that time, e.g. by numerical integration of the equations pertaining to that hardware configuration. During this time, some process variables may reach the pre--established thresholds, thus requiring the intervention of the control/protection system. Each intervention modifies the system hardware configuration, thus invalidating the choice of the forced failure time and the accompanying Monte Carlo weight of the representative point.

This issue is here analyzed in details and suitable expressions for a proper weight updating are provided.

Last modified: Thu Apr 2 13:49:26 1998

Workshop on
Monte Carlo Methods and Models for Applications
in Energy and Technology

Forschungszentrum Karlsruhe, May 12 – 14, 1998

WEIGHT UPDATING IN FORCED MONTE CARLO APPROACH TO DYNAMIC PSA

M. Marseguerra, Enrico Zio

Department of Nuclear Engineering
Polytechnic of Milan

STATEMENT OF THE PROBLEM

- Dynamic Probabilistic Safety Analysis (PSA) = PSA + physical time-evolution.

- Issues to be accounted for:
  - ordering and timing of events;
  - dependence of failure rates and criteria on the process variables;
  - human operator actions;
  - control/protection devices.

- Need to follow the dynamics ⇒ computational burden enormously increased.

OBJECTIVE

- Monte Carlo is an efficient tool for dynamic PSA but computationally demanding

⇓

Biased Monte Carlo

HOW TO BIAS IN MONTE CARLO DYNAMIC PSA?

A DEFINITION: ACCIDENT DURATION

Accident Duration = the time required to drive the system towards a safe state or for the accident to reach an unrecoverable state.

- Accident duration << *Mission Time*

- Dynamic PSA ∈ Accident duration

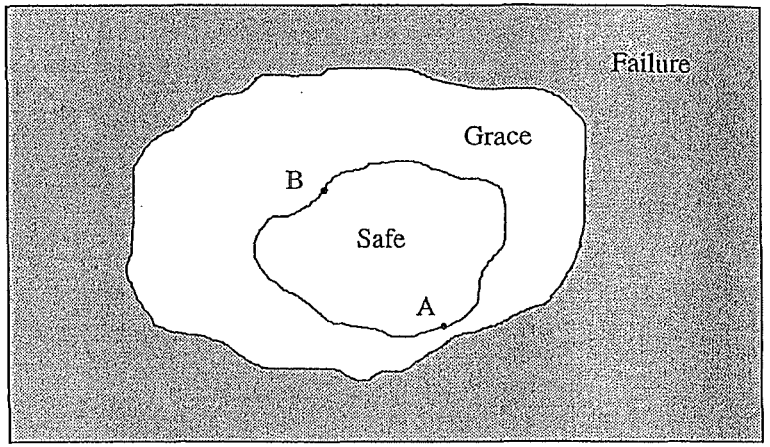

Figure 1
Marseguerra & Zio

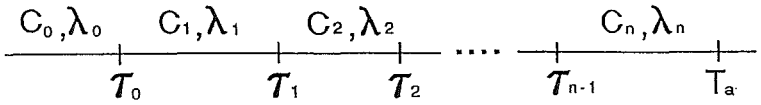

Figure 2
Marseguerra & Zio

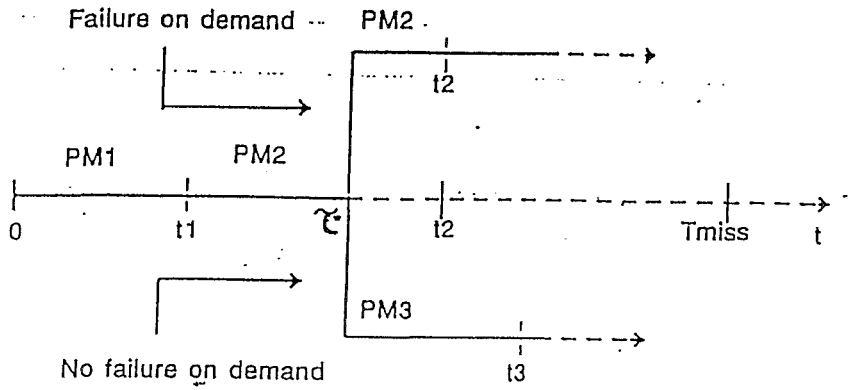

- Deterministic τ's of control intervention are not known 'a priori' $\Rightarrow$ *zero–story* with only dynamics.

- **Failure time cdf of the mixed–type**

– $\underline{t \in \Delta_k}$

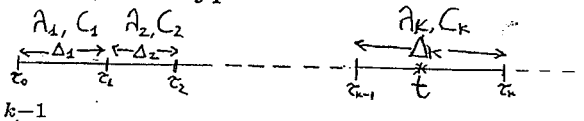

$$F_k(t|\lambda,\mathbf{q}) = 1 - [\prod_{l=1}^{k-1}(q_l e^{-\lambda_l \Delta_l})] \cdot e^{-\lambda_k (t-\tau_{k-1})} \qquad t \in \Delta_k$$

– $\underline{t = \tau_k}$ (discontinuity)

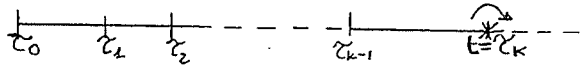

$$F_k(\tau_k^-|\lambda,\mathbf{q}) = 1 - [\prod_{l=1}^{k-1}(q_l e^{-\lambda_l \Delta_l})] \cdot e^{-\lambda_k \Delta_k}$$

$$F_{k+1}(\tau_k^+|\lambda,\mathbf{q}) = 1 - [\prod_{l=1}^{k}(q_l e^{-\lambda_l \Delta_l})]$$

- **Failure time pdf**

– $\underline{t \in \Delta_k}$

$$f_k(t|\lambda,\mathbf{q}) = \lambda_k[1 - F_k(t|\lambda,\mathbf{q})] \qquad t \in \Delta_k$$

– $\underline{t = \tau_k}$

$$\begin{aligned} f_k(\tau_k|\lambda,\mathbf{q}) &= F_{k+1}(\tau_k^+|\lambda,\mathbf{q})] - F_k(\tau_k^-|\lambda,\mathbf{q})] \\ &= [\prod_{l=1}^{k-1}(q_l e^{-\lambda_l \Delta_l})] \cdot e^{-\lambda_k \Delta_k} p_k \end{aligned}$$

$\tau_k^- = F_k(\tau_k^- | \lambda, q)$

$\tau_k^+ = F_{k+1}(\tau_k^+ | \lambda, q)$

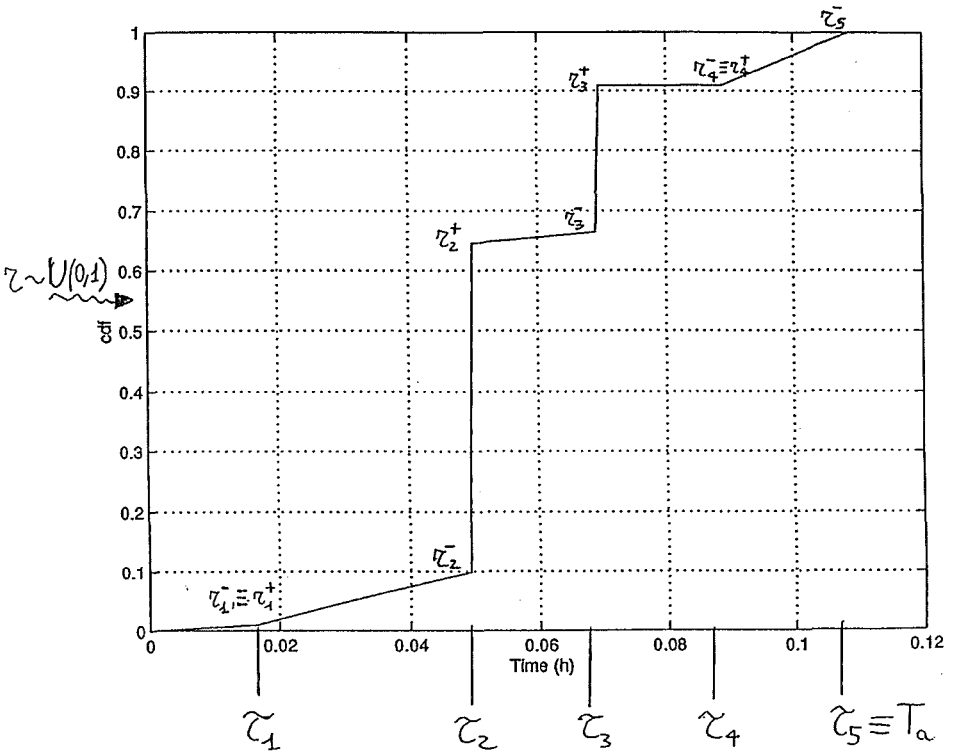

- $r_k^- = F_k(\tau_k^- | \lambda, \mathbf{q})$
  $r_k^+ = F_{k+1}(\tau_k^+ | \lambda, \mathbf{q})$

- $r \sim U(0,1)$

a. $r > r_n^-$; then the failure occurs at a time $t > \tau_n \rightarrow$ no failure within T_a;

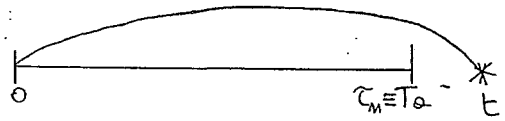

b. $r < r_n^-$; at what time $t < \tau_n$ does the failure occur?

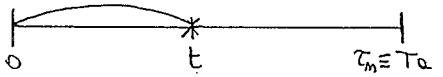

b1. $r_k^+ \leq r < r_{k+1}^-$; then, the failure occurs at

$$t = \tau_{k-1} - \frac{1}{\lambda_k} \cdot ln\left(\frac{1-r}{[\prod_{l=1}^{k-1}(q_l e^{-\lambda_l \Delta_l})]}\right)$$

b2. $r_k^- \leq r < r_k^+$; then, the failure occurs at

$$t = \tau_{k-1}$$

BIASED MONTE CARLO

- Force transitions to occur within T_a.

- Favour those failures which are more critical, i.e. for which the successive *grace time* is shorter (point A).

$$\lambda, \mathbf{q} \Rightarrow \lambda^*, \mathbf{q}^*$$

- Only first failure after initiating event is forced because:

  - if after first forced failure the system is still in the safe region λ's would still be very small $\rightarrow$ further weight reduction would make the weight negligible;

  - if the first failure is of a CP device then the system enters the grace region where the λ's reach large values $\rightarrow$ analog.

- **Failure time cdf**

  - $t \in \Delta_k$

$$F_k^*(t|\lambda^*, \mathbf{q}^*) = \frac{F_k(t|\lambda^*, \mathbf{q}^*)}{F_n(\tau_n^-|\lambda^*, \mathbf{q}^*)} \qquad t \in \Delta_k$$

  - $t = \tau_k$

$$F_{k+1}^*(\tau_k^+|\lambda^*, \mathbf{q}^*) = \frac{F_{k+1}(\tau_k^+|\lambda^*, \mathbf{q}^*)}{F_n(\tau_n^-|\lambda^*, \mathbf{q}^*)}$$

$$F_k^*(\tau_k^-|\lambda^*, \mathbf{q}^*) = \frac{F_k(\tau_k^-|\lambda^*, \mathbf{q}^*)}{F_n(\tau_n^-|\lambda^*, \mathbf{q}^*)}$$

- **Failure time pdf**

  - $t \in \Delta_k$

$$f_k^*(t|\lambda^*, \mathbf{q}^*) = \frac{f_k(t|\lambda^*, \mathbf{q}^*)}{F_n(\tau_n^-|\lambda^*, \mathbf{q}^*)}$$

  - $t = \tau_k$

$$f_k^*(\tau_k|\lambda^*, \mathbf{q}^*) = \frac{f_k(\tau_k|\lambda^*, \mathbf{q}^*)}{F_n(\tau_n^-|\lambda^*, \mathbf{q}^*)}$$

- **Unbiased result $\Rightarrow$ weight updating**

  - $t \in \Delta_k$

$$\frac{f_k(t|\lambda, \mathbf{q})}{f_k^*(t|\lambda^*, \mathbf{q}^*)} = \frac{\lambda_k}{\lambda_k^*} \cdot \frac{1 - F_k(t|\lambda, \mathbf{q})}{1 - F_k^*(t|\lambda^*, \mathbf{q}^*)} \cdot F_n^*(\tau_n^-|\lambda^*, \mathbf{q}^*) \qquad t \in \Delta_k$$

  - $t = \tau_k$

$$\frac{f_k(\tau_k|\lambda, \mathbf{q})}{f_k^*(\tau_k|\lambda^*, \mathbf{q}^*)} = \frac{[\prod_{l=1}^{k-1}(q_l e^{-\lambda_l \Delta_l})] \cdot e^{-\lambda_k \Delta_k} p_k}{[\prod_{l=1}^{k-1}(q_l^* e^{-\lambda_l^* \Delta_l})] \cdot e^{-\lambda_k^* \Delta_k} p_k^*} \cdot F_n^*(\tau_n^-|\lambda^*, \mathbf{q}^*)$$

i	τ_i	λ_i	λ_i^*	p_i	p_i^*
1	$1.667 \cdot 10^{-2}$	$1 \cdot 10^{-4}$	$1 \cdot 10^{-1}$	0.	0.
2	$5 \cdot 10^{-2}$	$5 \cdot 10^{-4}$	$5 \cdot 10^{-1}$	$1 \cdot 10^{-5}$	$1 \cdot 10^{-1}$
3	$7 \cdot 10^{-2}$	$2 \cdot 10^{-4}$	$2 \cdot 10^{-1}$	$5 \cdot 10^{-5}$	$5 \cdot 10^{-2}$
4	$9 \cdot 10^{-2}$	$1 \cdot 10^{-5}$	$1 \cdot 10^{-2}$	$1 \cdot 10^{-5}$	$1 \cdot 10^{-3}$
5	$11 \cdot 10^{-2}$	$1 \cdot 10^{-3}$	1.	—	—

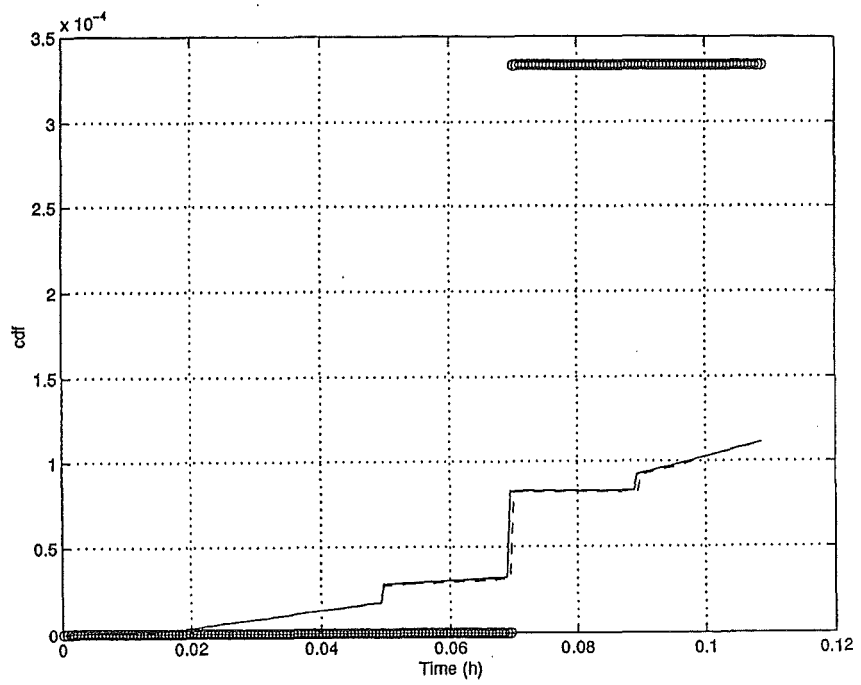

3,000 Trials

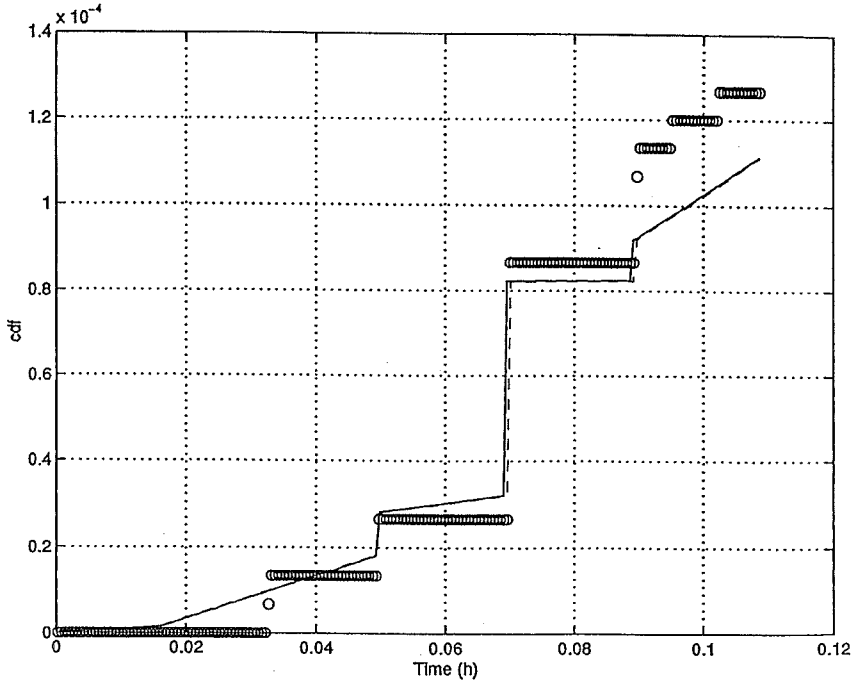

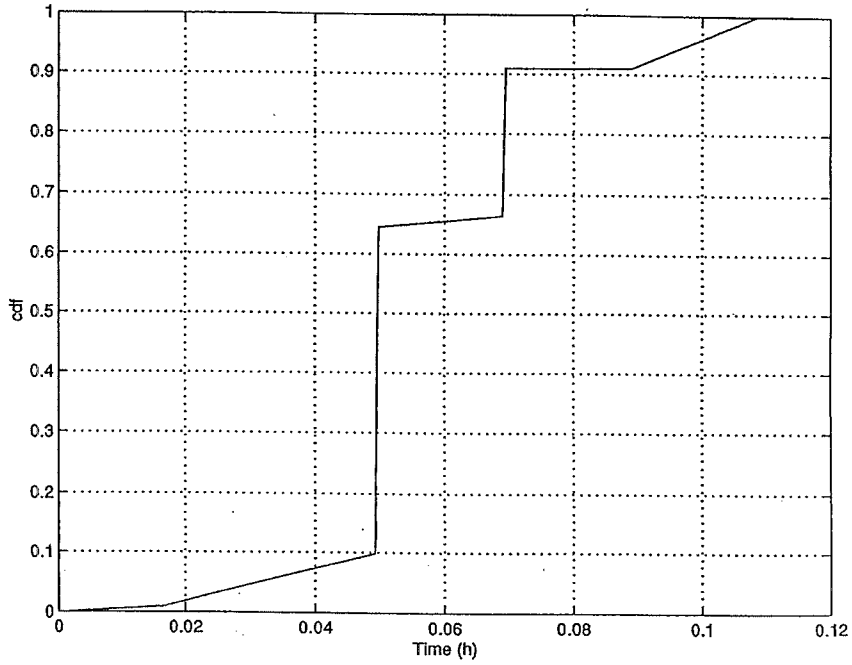

150,000 TRIALS

$\eta = \frac{1}{\sigma^2_L}$ ~ 4 orders of magnitude

CONCLUSIONS

- Monte Carlo dynamic PSA requires biasing.
- Coupling of deterministic and stochastic times makes it non–trivial.
- Practical approach is proposed based on the pre–simulation of the dynamics in a *zero–story* to determine deterministic times of intervention.
- Biasing renders the simulation more efficient (numerical examples).
- Appropriate choice of the biased parameters allows to zoom in on failures which are considered critical as they lead the system to portions of the grace region which are characterized by short grace times.

References

Aldemir T., Siu N., Mosleh A., Cacciabue P.C., Göktepe B.G. (1994), Eds.: Reliability and Safety Assessment of Dynamic Process System NATO–ASI Series F, Vol. 120 Springer–Verlag, Berlin.

Cacciabue P.C., Amendola A., Cojazzi G. (1986), Dynamic Logical Analytical Methodology Versus Fault Tree: The Case Study for the Auxiliary Feedwater System of a Nuclear Power Plant, Nucl. Tech., 74, pp. 195–208.

Devooght J., Smidts C.(1992), Probabilistic Reactor Dynamics I. The Theory of Continuous Event Trees, Nucl. Sci. and Eng. 111, 3, pp. 229–240

Devooght J., Smidts C. (1998), Dynamic Reliability Workshop: Future Directions White Paper, 1998.

Labeau P.E. and Zio E. (1998), The cell–to–boundary method in the frame of memorization–based Monte Carlo algorithms. A new computational improvement in dynamic reliability, Mathematics and Computers in Simulation, 1557, pp. 1–14 .

Lewis, E.E. and Bohm, F. (1984), Monte Carlo simulation of Markov unreliability models, Nuclear Engineering and Design, 77, pp. 49–62.

Marseguerra M., Zio E. (1993), Nonlinear Monte Carlo reliability analysis with biasing towards top event Reliab. Eng. & System Safety, vol. 40, pp. 31–42.

Marseguerra M., Zio E. (1996), Monte Carlo approach to PSA for dynamic process systems. Reliab. Eng. & System Safety, vol. 52, pp. 227–241.

Marseguerra M., Zio E., Devooght J. and Labeau P.E. (1998), A concept paper on dynamic reliability via Monte Carlo simulation, Mathematics and Computers in Simulation,1557.

Siu N. (1994), Risk Assessment for Dynamic Systems: An Overview, Reliab. Eng. & System Safety, vol. 43, pp. 43–74.

Monte Carlo Methods and Models for Applications
in Energy and Technology

Workshop to be held at Forschungszentrum Karlsruhe, May 12-14, 1998

Influence of the Photoneutrons on the Kinetics of Beryllium Reflected Core of the Budapest Research Reactor

G. Hordosy, A. Kereszturi, Cs. Hegedus, P. Vertes

KFKI Atomic Energy Research Institute
Reactor Analysis Department
Budapest, Hungary

Some important reactor materials such as deuterium and beryllium have non-negligible photon-neutron cross-section in the energy range of fission product's gamma radiation. Although the influence of this effect is negligibly small for stationary state of a rector core, the delayed photons from short-living fission products can result kinetic effects analogous to that of the delayed neutrons.

The Budapest Research Reactor has a beryllium reflector and the control rod worth measurements are based on the doubling time method. In this paper the calculation of the parameters necessary for the evaluation of these measurements taking into account of the photoneutrons is described. For this purpose a number of Monte Carlo calculations were performed with different photon energy spectra because the spectrum of the delayed photons depends strongly on the time elapsed after the fission event. Due to the large number of necessary calculations and to the low cross-section of the photoneutron creation process the variance reduction methods have high importance in these calculations. It is shown that the neglection of the photoneutrons leads to an underestimation of the control rod worth.

Last modified: Thu Apr 2 13:33:31 1998

Influence of the Photoneutrons on the Interpretation of the Control Rod Worth Measurements at the Budapest Research Reactor

G. Hordósy, A. Keresztúri, Cs. Hegedûs, P. Vértes
KFKI Atomic Energy Research Institute
H-2525 Budapest 114, POB 49
Hungary
e-mail: hordosy@sunserv.kfki.hu

Motivation, possibility, history

Budapest Research Reactor : beryllium reflector

Kinetic effects

Necessary : a code for photoneutron treatment

and a code for calculation of spectrum of delayed photons from fission products

photoneutron production inclusion into MCNP4A by F.X. Gallmeier in

OAK RIDGE [2]

delayed γ : TIBSO by Péter Vértes in KFKI AEKI [1]

December 1996 : question to MCNP forum

reply from F.X. Gallmeier

start: this year

result at present : the effect is not negligible

future plan: inclusion into the 3D kinetic code KIKO3D [3]

Budapest Research Reactor

water cooled water moderated

atmospheric pressure

Russian made VVR-SM type fuel

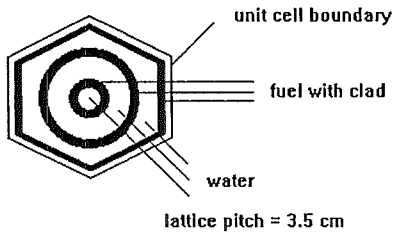

"meat" : uranium-aluminium eutectic

clad : aluminium

1 mm thickness

36 % enrichment

active length : 58 cm

220 - 230 fuel elements in the core

Technical data :

thermal power : 10 MW

max. thermal flux : 1.4×10^{14} n/cm**2 s

max. fast flux : 1.0×10^{14} n/cm**2 s

cooling water temperature : 54 - 60 Celsius

Use of the reactor : isotope production, solid state physics, reactor pressure vessel , neutron activation analysis, neutron radiography

Differences between VVR-SM and VVER reactors : fuel geometry, enrichment 36 %, atmospheric pressure, *beryllium reflector*

Delayed neutron groups

Total number of neutron from a fission : ν
Number of prompt neutron from a fission : $(1-\beta)\,\nu$
Number of delayed neutron from a fission : $\beta\,\nu$

Delayed neutrons : from fission products with delay time from less then a second to about a minute

All precursors are divided into 6 groups with decay constants λ_i

$$\beta = \sum_{i=1}^{6} \beta_i$$

+ delayed photons

Point kinetic equations [5]

frequently used approximation : space dependence neglected

$$\frac{dn(t)}{dt} = \frac{\rho - \beta}{\Lambda} n(t) + \sum_{i=1}^{N} \lambda_i c_i(t)$$

$$\frac{dc_i(t)}{dt} = \frac{\beta_i}{\Lambda} n(t) - \lambda_i c_i(t)$$

n : **number of neutrons in the system;** $\rho = \dfrac{k_{eff} - 1}{k_{eff}}$ **reactivity**

Λ : **prompt neutron lifetime;** c_i : **density of the precursor in group i,** β_i **and** c_i **averaged over the system. Averaging is performed with neutron flux from a static, space dependent calculations**

Inhour equation : rod worth from flux increase

$$\rho = \alpha \left(\Lambda + \sum_{j=1}^{N} \frac{\beta_j}{\lambda_j + \alpha} \right),$$

$$\alpha = \ln 2 / T_{1/2}$$

photoneutrons : considered as emitted from fictitious precursors with density c_i^*, decay constant λ_i^* and abundance β_i^*

Calculational steps :

- Delayed gamma particles due to the decay of fission products are born in the fuel region.
- Gamma radiation is attenuated by the fuel and reflector regions.
- Gamma particles reaching the reflector region induce photoneutrons.
- The photoneutrons reaching the fuel region result fissions
- The time-dependence of this fission rate caused by the photoneutrons are fitted by a sum of exponential functions. Determining the coefficients and decay constants of these functions the additional delayed neutron groups are identified.

γ source rate in the fuel : proportional to fission density distribution from a kcode MCNP calculation

Influence of prompt photons on k_{eff} is negligable

Energy spectrum of delayed photons from fission products as a function of time : calculated by TIBSO taking into account 1265 isotopes.

Production rates and decay constants from the servers of NEA Data Bank, the Los Alamos National Library, the IAEA Nuclear Data Section and from the Brookhaven National Laboratory.

Eight photon energy groups with boundaries in MeV : 1.67 (threshold energy in beryllium for photoneutron production), 2.0, 2.4, 3.0, 3.5, 4.0, 4.5, 5.0, ∞.

Photons below the (γ,n) threshold of Be are omitted. About 12% of photon has energy over threshold at any time. Total number of photons in the first 100 sec is 6.84 and in the next 900 sec is 4.0 .

Angular dependence : isotropic

Photon transport : the secondary photons produced by electrons neglected, the simple physics options of the MCNP4A [4] used. This means that

- at photoelectric events the fluorescent photons are neglected and the event is treated as pure absorption by implicit capture (the photon weight is reduced and the history of the photon with reduced weight is followed)
- at Compton scattering the Klein-Nishina formula is used (free electron approximation) because the threshold energy for photons of interest is 1.67 MeV
- at pair production, the original photon disappears, the created positron is assumed to be annihilated immediately and thus two photons created with energy 0.511 MeV and with opposite directions.

It was checked in a fully detailed photon-electron calculations that the number of photons going from the fuel into the reflector region and having energy higher then 1.67 MeV is influenced less than the statistical uncertainty with these approximation.

Photoneutron production in the reflector : MCNP4A modified by Gallmeier

Using a fixed gamma source due to a particular time after a fission event and normalised to unity : the number of fissions caused by the photoneutrons and the incoming neutron current at the core surface per source photon

Multiplying with the photon intensity from one fission: the same quantities per fission

Performing these steps with several spectra due to different times : number of fissions and the current as function of time after a fission event.

A number of calculations, low cross-sections: variance reduction

Weight-window generator : FOM increased from 4-6 to about 1200

Calculations with 400.000 source photons on ORIGIN 2000 Silicon

Graphics under IRIX 6.4 : 10 - 15 minutes, rel. error 0.008 - 0.01

Calculation of the point kinetic parameters

Approximations :

- The shape of the fission source is fixed (not depending on time).
- The worth of the neutrons originating from the fission caused by the photoneutrons is the same as the worth of neutrons originating from normal fission.

The derivation of the additional point kinetic parameters is based on the curve of the fission rate due to photoneutrons from one fission. The integral of this curve - denoted by β^* - gives the total number of fission caused by the delayed photoneutrons originated from one fission. This value is equal to the total fraction of the additional delayed neutron groups because the number of neutrons resulting from the photoneutron effect due to one fission is $\nu\beta^*(1-\beta) \cong \nu\beta^*$ if we suppose that ν is the same for the fission from the photoneutrons as for the normal fission

The partial fractions (β^*_j) and decay constants (λ^*_j) can be determined by fitting the expression

$$H(t) = \sum_{j=1}^{N} \lambda_j^* C_j^*(t) = \sum_{j=1}^{N} \lambda_j^* \beta_j^* e^{-\lambda_j^* t}$$

to the curve of fission rate obtained from the Monte-Carlo calculations

Condition for β^* is satisfied: $\int_0^\infty H(t)dt = \sum_{j=1}^{N} \beta_j^* = \beta^*$.

The best fit : by N=4

Fitted parameters of the additional delayed neutron groups :

β^*= 1.132E-04

j	1	2	3	4
β_j^*	2.94534E-06	4.08960E-05	3.24097E-05	3.69290E-05
λ_j^*	1.83795E+00	1.28757E-01	1.41045E-02	1.83498E-03

Table 1. The fitted additional delayed neutron group parameters

Influence on the evaluation of the control rod measurements

A control rod was withdrawn from the core step by step. The reactivity was evaluated by using the in-hour equation with and without the new delayed neutron group.

The obtained reactivity values in units of cent (i.e. in units of β) are shown

control rod position h1 [cm]	control rod position h2 [cm]	Δh [cm]	Measured doubling time $T_{1/2}$ [s]	Evaluated reactivity without additional groups [cent]	Evaluated reactivity with additional groups [cent]
3.0	13.0	10.0	229.0	3.49	3.81
13.0	20.0	7.0	141.0	5.37	5.75
20.0	27.0	7.0	109.0	6.69	7.10
27.0	35.0	8.0	79.0	8.71	9.15
35.0	42.0	7.0	113.0	6.49	6.90
42.0	52.0	10.0	104.0	6.96	7.37
52.0	70.0	18.0	300.0	2.73	3.01

Reactivity change measurements using the doubling time

Evaluated total reactivity without additional delayed neutron groups [cent]	Evaluated total reactivity with additional delayed neutron groups [cent]
40.44	43.09

Total reactivity of the measured control rod

The results show that the evaluation not taking into account the photoneutron leads to a 6.6 % underestimation of the control rod worth.

Reason : longer "life time"

Future plans :

Investigate the space dependence of this kinetic effect in a more accurate manner. A series of modifications in the KIKO3D three-dimensional nodal kinetic code are planned. (KIKO3D is a code with coupled neutronics and thermohydraulics developed in KFKI AERI. It is widely used for safety analysis of WWER-440 power plants.)
The additional response matrices required for this modifications are planed to be derived from the Monte-Carlo calculations. The use of the three-dimensional coupled kinetic calculations seems to be important because of the strong space dependence of the static and the photoneutron-induced fission density.

References:

[1] P. Vértes, TIBSO: A Computer Code for Calculating the Production, Decay and Spreading of Radioactive Isotopes, submitted to Nuclear Technology

[2] F.X. Gallmeier : General Purpose Photoneutron Production in MCNP4A, ORNL/TM-13073, 1995

[3] A. Keresztúri: KIKO3D - A 3D Kinetics Code for VVER-440, TRANSACTIONS of the American Nuclear Society, 1994 Winter Meeting, Washington DC, 1994.

[4] J.F. Breismeister, Ed., MCNP - A General Monte Carlo N-Particle Transpor Code, Ver. 4A, LA-12625-M

[5] G.I. Bell, S. Glasstone: Nuclear Reactor Theory, Van Nostrand Reinhold Company, 1970

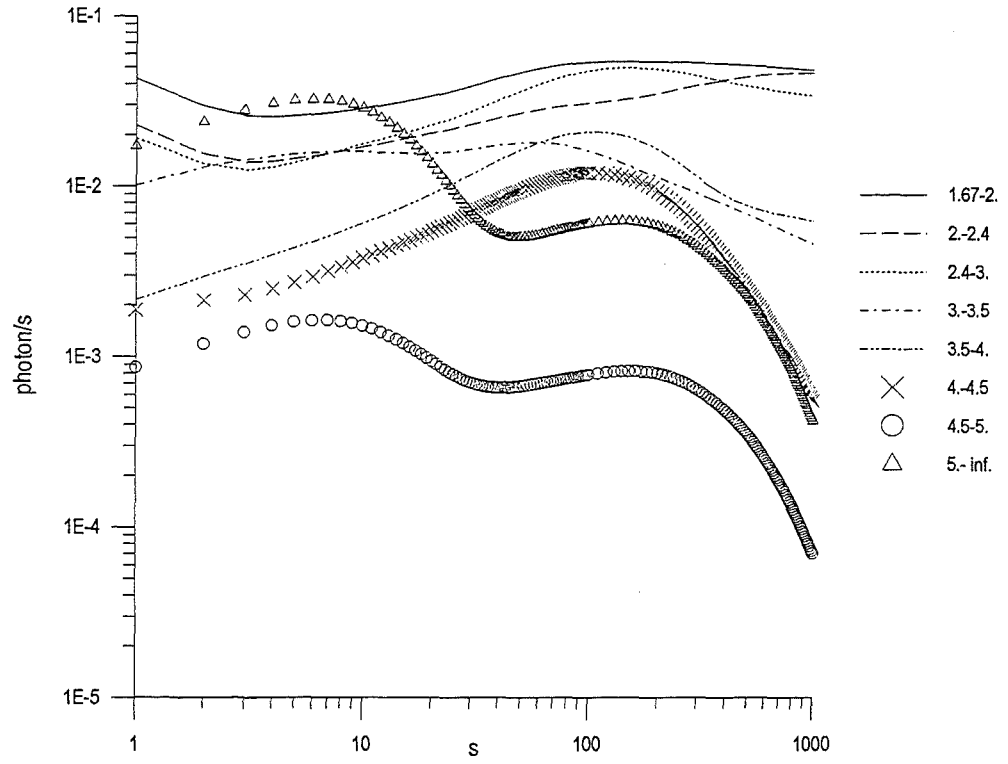

Fig.1 Photon intensity for gamma groups over (gamma,n) threshold of Be

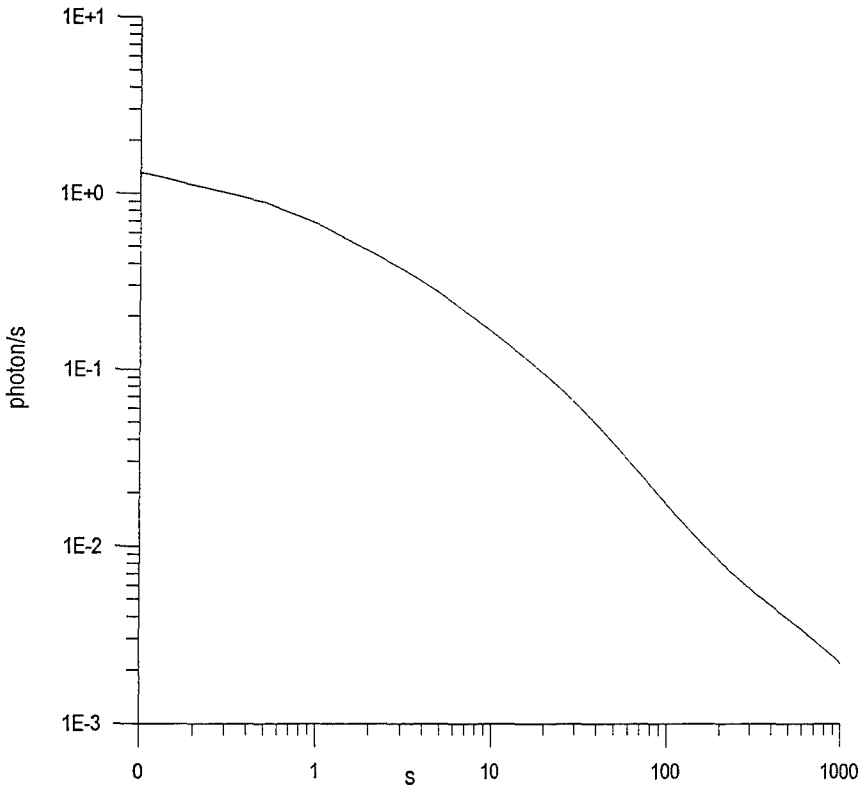

Fig.2 Photon intensity of fission products from one fission event

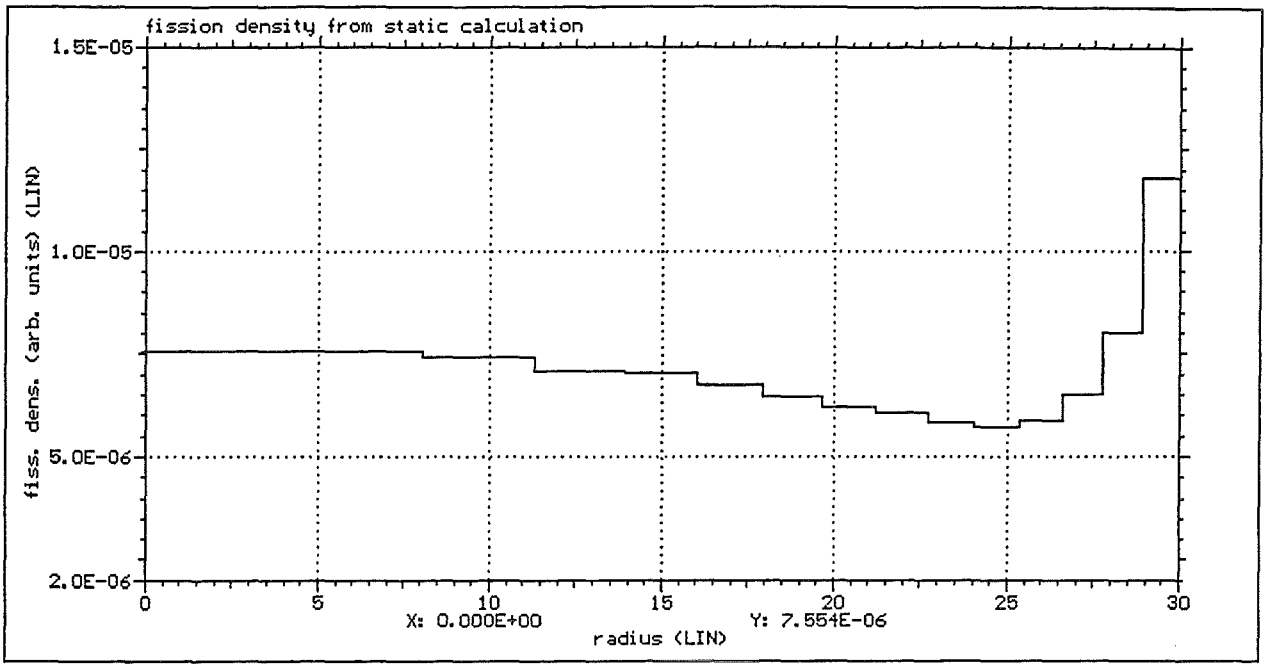

Fig. 3. Radial dependence of fission density in the core from a criticality calculation

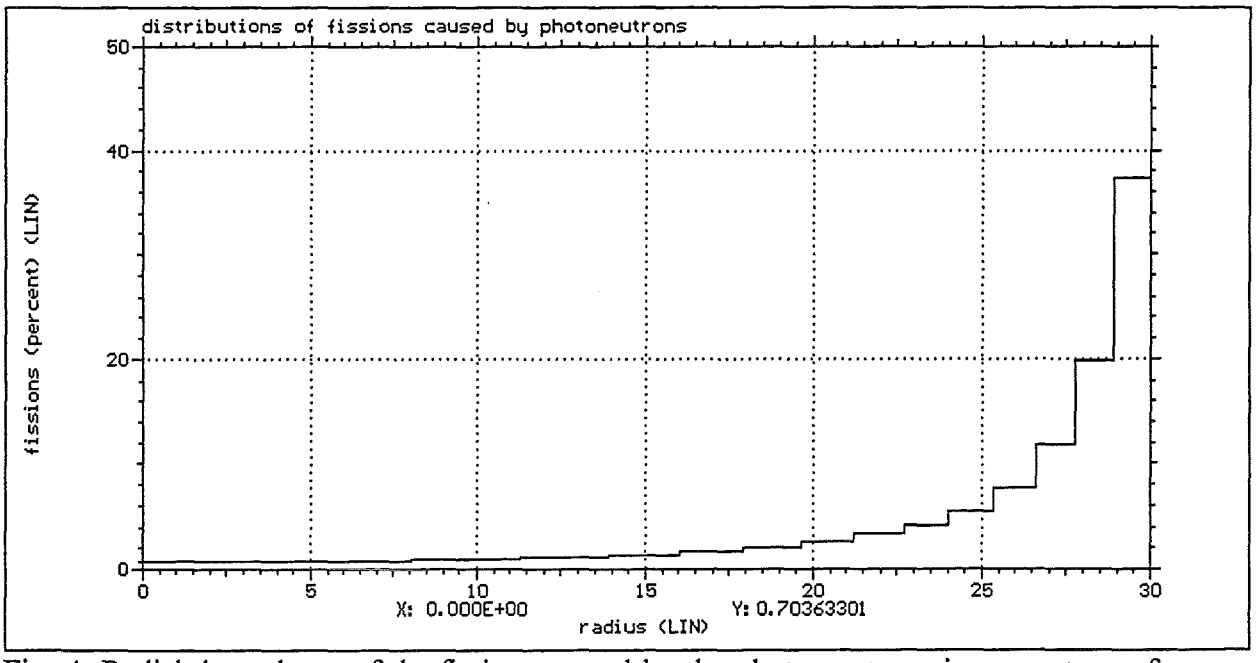

Fig. 4. Radial dependence of the fissions caused by the photo-neutrons in percentage of their full sum

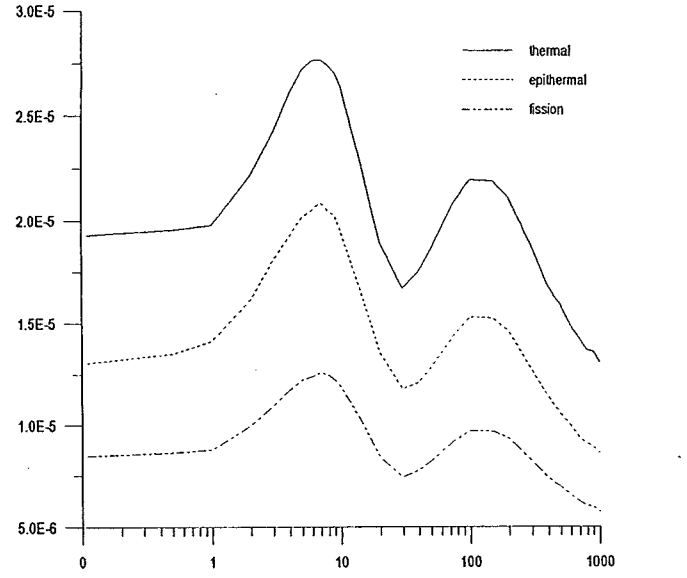

Fig. 5 Number of photoneutrons directed from reflector to core and number fissions caused by them depending on the time variation of gamma spectra

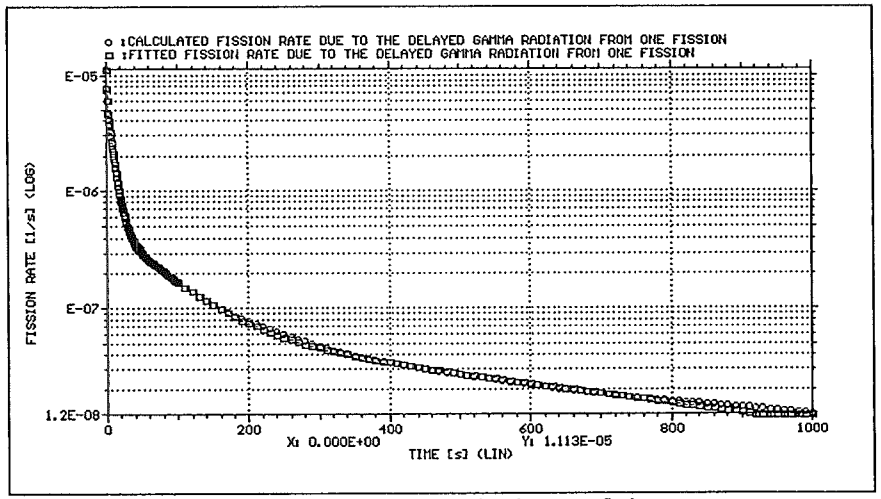

Fig. 6. Fission rate due to the delayed gamma radiation from one fission

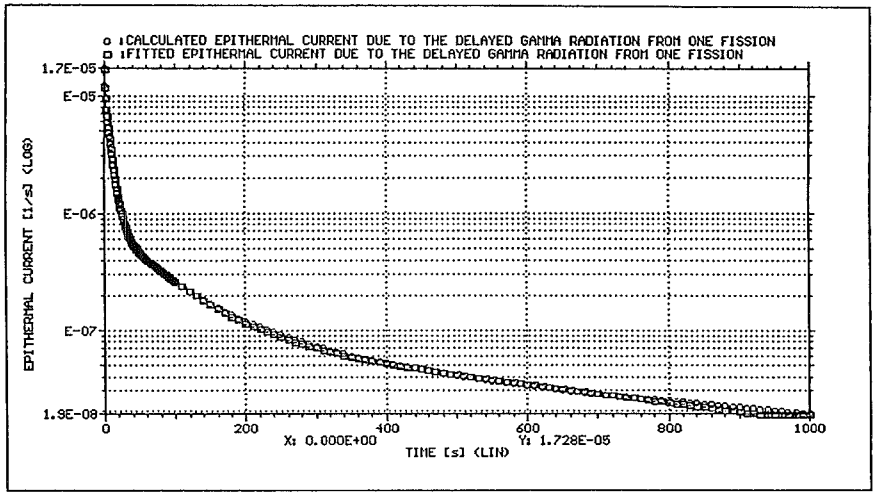

Fig. 7. Epithermal current due to the delayed gamma radiation from one fission

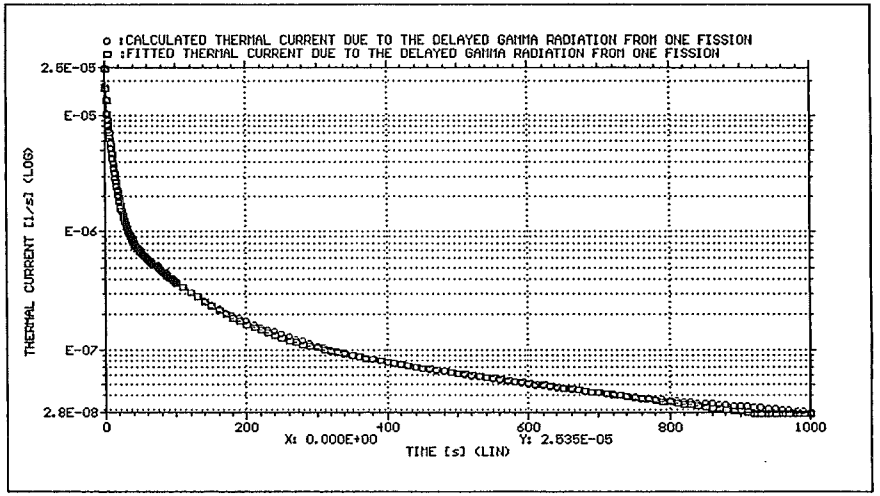

Fig. 8. Thermal current due to the delayed gamma radiation from one fission

Monte Carlo Methods and Models for Applications in Energy and Technology

Workshop to be held at Forschungszentrum Karlsruhe, May 12-14, 1998

Application of MCNP to Accelerator Shielding

J. Ródenas, G. Verdú

Department of Nuclear Engineering
Polytechnic University
P. O. Box 22012, E-46071 Valencia, Spain

The shielding thickness in a linear electron accelerator is directly proportional to tenth-value thickness, which depends on the shielding material and the energy of the incident radiation. It can be obtained from curves recommended by DIN-6847, the most suitable standard to estimate shielding requirements in medical radiotherapy installations using linear electron accelerators. On the other hand, the tenth-value thickness can be estimated in terms of dose rates calculated for two different values of shielding thickness and related distances.

MCNP code has been used to determine doses at distances considered, for various energy values up to 50 MeV and the following materials: concrete, barytic concrete, aluminium, iron, copper and lead. Shielding thickness values have been taken in such a way that for each energy the obtained doses differ by a magnitude order at least. The photon source was point isotropic and monoenergetic, with all particles being emitted inside a small solid angle.

Results from MCNP have been compared with values recommended by DIN-6847. They match reasonably well except for lead, in which the behaviour is very different. Concordance for the other materials would have been better if we had considered a continuous actual spectrum rather than a monoenergetic source.

As to lead discrepancies, it can be said that the MCNP version used did not include the transport of photoelectrons, Compton electrons nor electron-positron pairs. At higher energies these electrons collide with hard atomic nuclei producing electromagnetic radiation (Bremsstrahlung). These phenomena become more evident in lead. Therefore, calculations should be repeated using the latest version of the code in order to find out if a better behaviour of lead can be predicted.

Another line of development would be the estimation of the actual X-ray spectrum for the accelerator. For a continuous actual spectrum, the maximal value of z within the spectrum energy range should be used. If the spectrum is well known, the tenth-value thickness can be obtained by decomposition.

Moreover, for higher values of energy the interaction of photons in the shielding material can produce neutrons. This should be taken into account in order to estimate the right shielding requirements. Hence, it is necessary to develop a routine to estimate those photoneutrons.

An additional line of work could be to obtain the method used by DIN-6847 to elaborate the recommended curves and then both methods and models can be compared.

Last modified: Thu Apr 2 14:03:26 1998

Monte Carlo Methods and Models for Applications in Energy and Technology

Workshop held at Karlsruhe (Germany), May 12-14, 1998

APPLICATION OF MCNP TO ACCELERATOR SHIELDING ANALYSIS

José Ródenas, Gumersindo Verdú

Department of Nuclear Engineering

Polytechnic University of Valencia (Spain)

CONTENTS

INTRODUCTION

- *Importance of accurate estimation of doses produced in particle accelerators used for radiotherapy.*
- *ICRP 60 ➡ recalculation of shielding.*
- *Two standards, NCRP-51 and DIN-6847, have been comparatively analysed.*
- *DIN-6847 is based on various semiempirical approaches, which should be adequately verified.*
- *Accelerator shielding calculation methodology.*
- *Estimation of the tenth-value thickness for X-rays produced in medical electron accelerators.*
- *MCNP - Monte Carlo method has been applied.*

SHIELDING ANALYSIS

$$s_i = z_i \log_{10}\left(\frac{W_A\ U\ T\ K_i\ q_i}{H_w}\right)$$

- *Calculation scheme:*
  - *Establish the geometrical features of the reference point;*
  - *Identify all types of radiation involved in the calculation;*
  - *Obtain the shielding thickness s_i, from equation (1) for each type of radiation.*
- *tenth-value thickness, $z_i = z_r$, depends on the shielding material and energy (curves recommended by DIN-6847).*

DIN CURVES

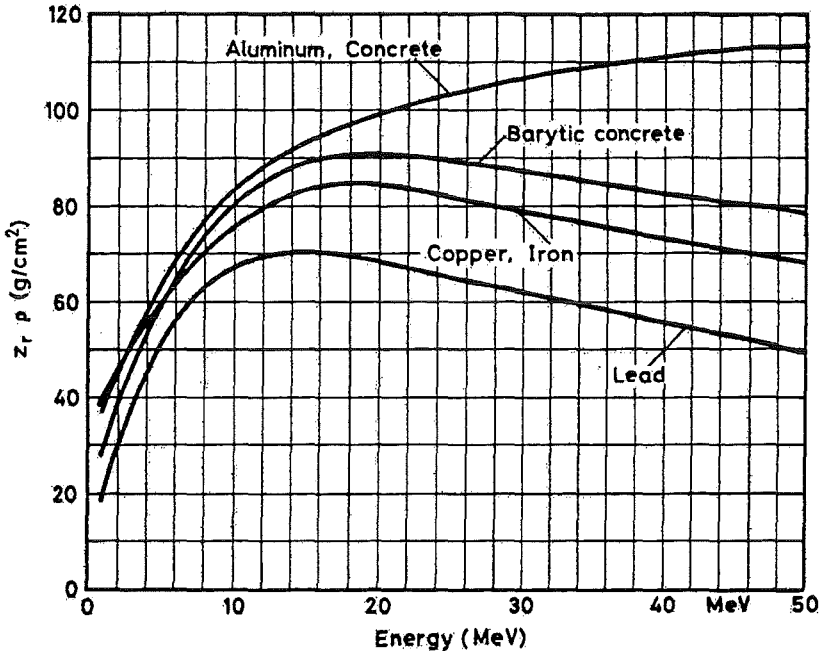

Monte Carlo Workshop

TENTH-VALUE THICKNESS ESTIMATION

$$H_W = \frac{C}{a_n^2}\left(\frac{1}{10}\right)^{\frac{s}{z}}$$

$$z = -\frac{s_2 - s_1}{\log_{10}\dfrac{H_{2W}\,a_2^2}{H_{1W}\,a_1^2}}$$

- *MCNP code has been used to determine doses at distances considered, for various energy values up to 50 MeV and materials of interest.*
- *Shielding thickness values (s_1, s_2) have been taken in such a way that for each energy the doses obtained differ by a magnitude order at least.*

DIRECT RADIATION

Results MCNP 3.2

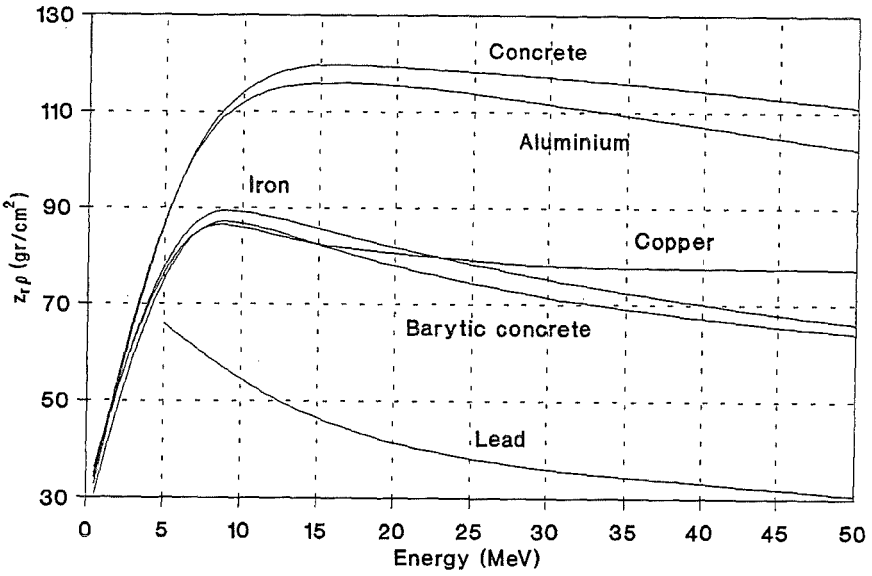

Monte Carlo Workshop

SCATTERED RADIATION

Mass Tenth-value Thickness for Secondary X-rays (DIN)

Material	Concrete	Barytic concrete	Iron	Lead
$z_r \rho$	37	29	38	17

MCNP 3.2

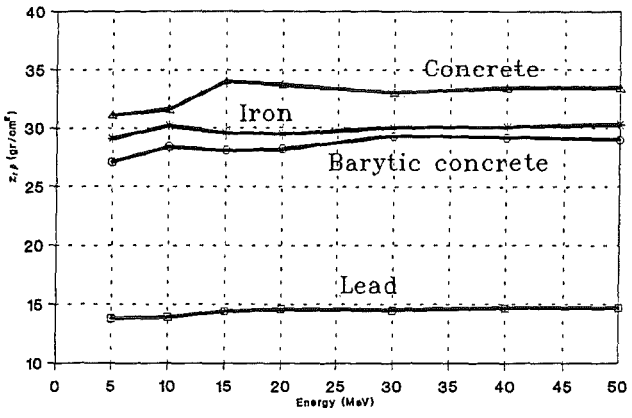

Comparison for Al

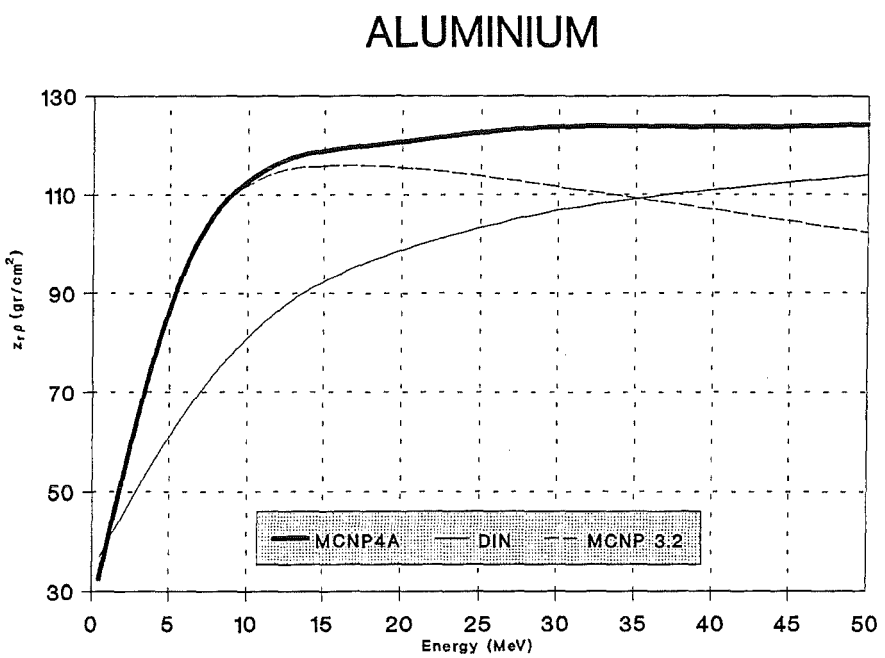

Comparison for Concrete

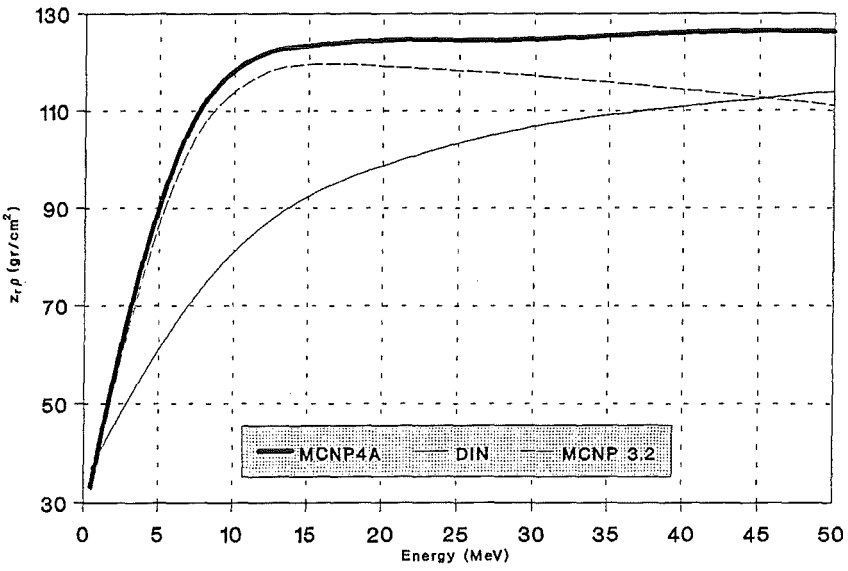

Comparison for Barytic Concrete

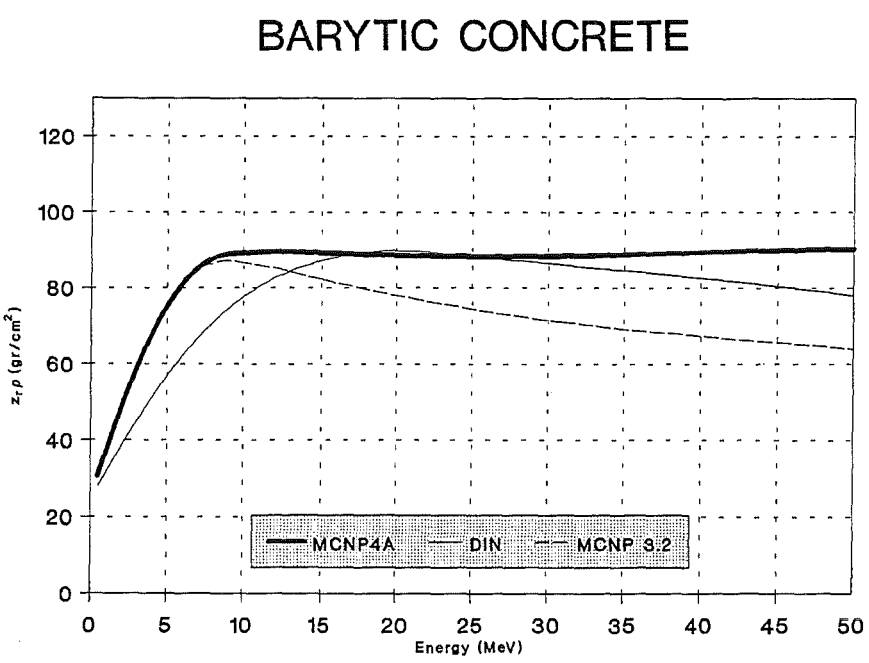

Comparison for Fe

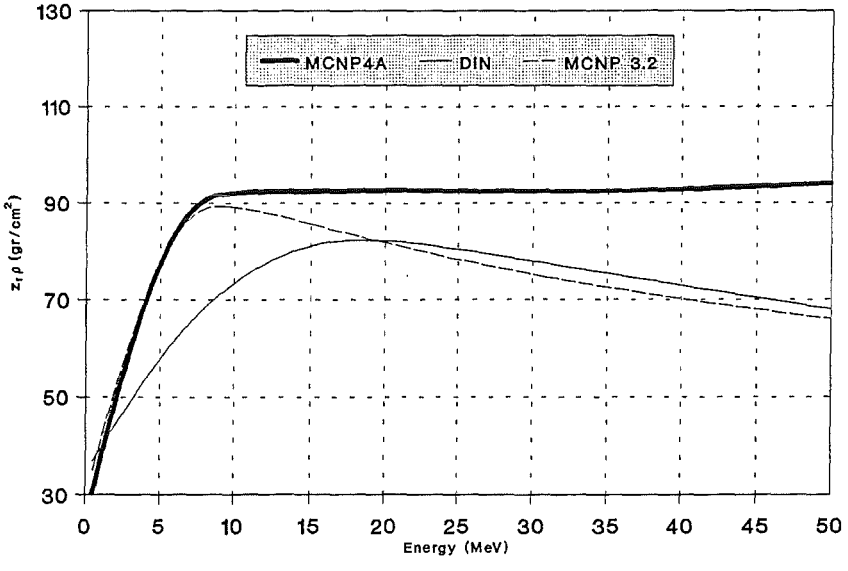

Comparison for Cu

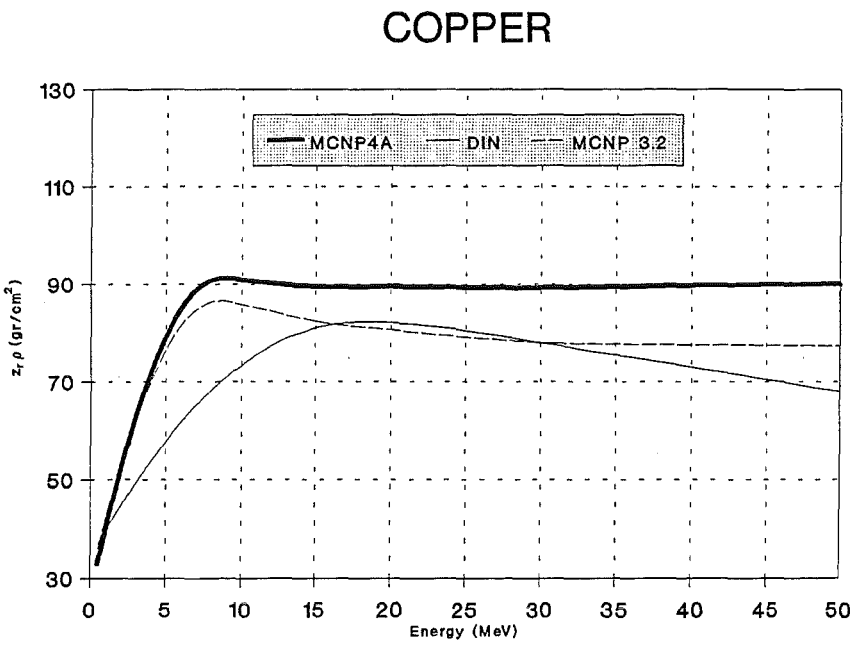

Monte Carlo Workshop

Comparison for Pb

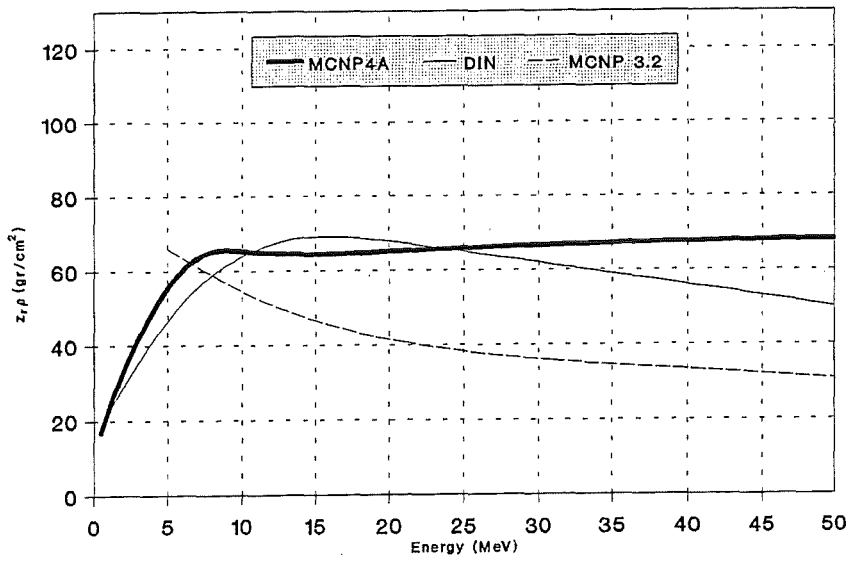

DIRECT RADIATION

Monte Carlo Workshop

Results MCNP 4A

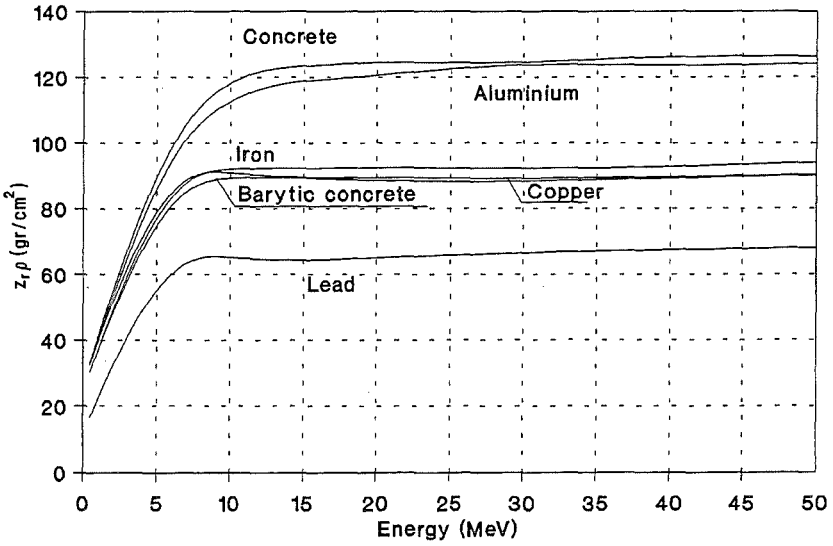

REMARKS

Monte Carlo Workshop

- *For primary radiation, the same curve may be used (without significant errors) for different materials:*
  - *concrete and aluminium,*
  - *iron and copper, even barytic concrete.*
- *For secondary radiation, results proved that the single table given by the guide is sufficient to obtain tenth-value thickness independently of incident beam energy.*
- *Electron transport has been incorporated to MCNP 4A, so all phenomena formerly omitted are now taken into account*
  - ➡ *results are quite improved not only for lead but also for the rest of materials, especially at higher energies.*
- *It would be convenient to dispose of more appropriate dose conversion factors.*

CONCLUSIONS

- *Two versions of MCNP (3.2 and 4A) have been used to estimate tenth-value thickness for X-ray direct and scattered beams in medical electron accelerators. Results have been compared between them and with values recommended by the DIN-6847 standard.*
- *It is not easy to perform experimental dose measurements, in particular in a linear accelerator, so it turns out the importance of simulation methods.*
- *Since the primary beam spectrum in an accelerator is generally unknown, a monoenergetic source has been considered. For a continuous actual spectrum there should be used the maximal value of z within the spectrum energy range. If the spectrum is well known, the tenth-value thickness can be obtained by decomposition.*

FUTURE DEVELOPMENTS

- *Estimation of the actual X-ray spectrum for the accelerator*
- *At higher energies, the interaction of photons in the shielding material can produce neutrons. This should be taken into account in order to estimate the right shielding requirements.*
  - ➡ *It is necessary to develop a routine to estimate those photoneutrons.*
- *An additional line of work could be to obtain the method used by DIN-6847 to elaborate the recommended curves and then compare both methods and models.*

REFERENCES

[1] *ICRP Publication 60, "New Recommendations of the Commission", approved on 9 November 1990.*

[2] *G. Verdú, J. Ródenas, J. M. Campayo, "Radiation Protection for Particle Accelerators", I International Conference on Implications of the new ICRP Recommendations, Salamanca (Spain), 26-29 November 1991.*

[3] *NCRP Report 51, !Radiation Protection Design Guidelines for 0.1-100 MeV Particle Accelerator Facilities", National Council on Radiation Protection and Measurements, 1977.*

[4] *DIN-6847, "Medizinische Elektronenbeschleuniger-Anlagen; Teil 2: Strahlenschutzregeln für die Errichtung", (Medical electron accelerators; Part 2: Radiation protection rules for installation), DIN Deutsches Institut für Normung e. V., 1977.*

Monte Carlo Workshop

REFERENCES

[5] *J. Ródenas, G. Verdú, "Análisis de la normativa aplicable al cálculo de blindajes en aceleradores lineales", PROTECCIÓN RADIOLÓGICA, Revista de la Sociedad Española, núm. 2, Mayo 1992.*

[6] *W. L. Thompson, (Monte Carlo Group Leader), "MCNP - A General Monte Carlo Code for Neutron and Photon Transport", Version 3, Los Alamos Monte Carlo Group, Los Alamos National Laboratory, Los Alamos, New Mexico, 1983.*

[7] *J. F. Briesmeister (Editor), "MCNP - A General Monte Carlo N-Particle Transport Code, Version 4A", LA-12625, Los Alamos National Laboratory, Los Alamos, New Mexico, November 1993.*

[8] *A. B. Chilton, J. K. Shultis, R. E. Faw, "Principles of Radiation Shielding", Prentice Hall, 1984.*

Monte Carlo Workshop

REFERENCES

[9] *J. Ródenas, G. Verdú, "Application of the Monte Carlo Method to Estimate the Tenth-value Thickness for X-rays in Medical Electron Accelerators", PAC'93, IEEE, 1993 Particle Accelerator Conference, Washington, D. C., 17-20 May 1993.*

[10] *J. Ródenas, G. Verdú, J. I. Villaescusa, J. M. Campayo, "Cálculo de dosis y estudio de blindajes en un acelerador lineal", MEDICAL PHYSICS 93, IX Congreso Nacional de Física Médica, Puerto de la Cruz, Tenerife, 22-24 Septiembre 1993.*

[11] *J. Ródenas, G. Verdú, R. Máiquez, "Aplicación del método de Monte Carlo al cálculo de blindajes en un acelerador lineal", XVIII Reunión Anual de la Sociedad Nuclear Española, Jerez de la Frontera — Puerto de Santa María (Spain), 28-30 October 1992.*

REFERENCES

[12] *NCRP Report 49, "Structural Shielding Design and Evaluation for Medical Use of X-Rays and Gamma Rays of Energies up to 10 MeV", National Council on Radiation Protection and Measurements, 1976.*

[13] *R. G. Jaeger (Ed.), "Engineering Compendium on Radiation Shielding", Volume I: Shielding Fundamentals and Methods, Springer-Verlag, 1968.*

[14] *J. Ródenas, G. Verdú, A. Nieto, "La simulación del transporte de partículas mediante el método de Monte Carlo: el código MCNP 4A", XX Reunión Anual de la Sociedad Nuclear Española (SNE), Córdoba (Spain), October 1994.*

Monte Carlo Workshop

Monte Carlo Methods and Models for Applications
in Energy and Technology

Workshop to be held at Forschungszentrum Karlsruhe, May 12-14, 1998

Monte Carlo Simulation of Groundwater Contaminant Transport

M. Marseguerra, E. Zio

Dept. of Nuclear Engineering
Polytechnic of Milan-Italy
Via Ponzio 34/3, 20133 Milano, Italy

ABSTRACT

One of the most vulnerable spots of nuclear power systems is the hazard posed by the radioactive wastes at the end of the fuel cycle. Currently, the most widely pursued end solution consists of disposing the radioactive wastes in repositories buried in deep geologic formations of presumed high stability. Licensing of such repositories is conditioned on the assessment of the reliability of such confinement for quite extensive periods of time ranging from 10,000 to 1 million years.

Over such long time scales the repositories may leak, thus releasing contaminants to the surrounding medium. The released contaminant may reach the groundwater and be transported for substantial distances, eventually returning to the biosphere where it poses a hazard for the human health and the environment.

In the present paper, we propose a phenomenological model based on the Kolmogorov--Dmitriev theory of branching stochastic processes in which a distributed source releases contaminant which is transported over a bidimensional medium whose physical properties are stochastic in space.

The proposed model is implemented within a Monte Carlo scheme which exploits variance reduction techniques.

Last modified: Thu Apr 2 13:49:18 1998

121

Workshop on
Monte Carlo Methods and Models for Applications
in Energy and Technology

Forshungszentrum, Karlsruhe, May 12-14, 1998

MONTE CARLO SIMULATION OF GROUNDWATER CONTAMINANT TRANSPORT

M. Marseguerra, Enrico Zio

Department of Nuclear Engineering
Polytechnic of Milan, Italy

STATEMENT OF THE PROBLEM

- Performance assessment of high–level radioactive waste repositories relies on predictive models
- Burial in geologic formations ⇒ contaminant transport in groundwater (main vector for return to biosphere)

MODELS OF CONTAMINANT TRANSPORT

Advection–dispersion

- deterministic
- equilibrium adsortpion/desorption phenomena
- scale effect

Kolmogorov–Dmitriev

- elementary particles and phenomena followed singularly

  ⇒ *flexibility*
- adsortpion/desorption reactions described explicitly

  ⇒ *non–equilibrium*
- pgf domain

  ⇒ *higher moments*

SYSTEM DESCRIPTION

- N_Z spatial zones, $z = 1, 2, \ldots, N_z$
  (1D, 2D, 3D)

- Particle kinds:
  solutons: s_z = N. solutons in zone z
  trappons: t_z = N. trappons in zone z

- System state:

$$\mathbf{s} = (s_1, s_2, \ldots, s_{N_z})$$

$$\mathbf{t} = (t_1^1, t_2^1, \ldots, t_{N_z}^1; t_2^2, \ldots, t_{N_z}^2; t_1^{N_t}, t_2^{N_t}, \ldots, t_{N_z}^{N_t})$$

EQUATIONS FOR EXPECTED VALUES

$$\frac{\partial S(z,t)}{\partial t} = -\Big[f + b + a\Big]\, S(z,t) + fS(z-1,t) + bS(z+1,t) + dT(z,t)$$

$$\frac{\partial T(z,t)}{\partial t} = -dT(z,t) + aS(z,t)$$

STOCHASTIC BIDIMENSIONAL TRANSPORT

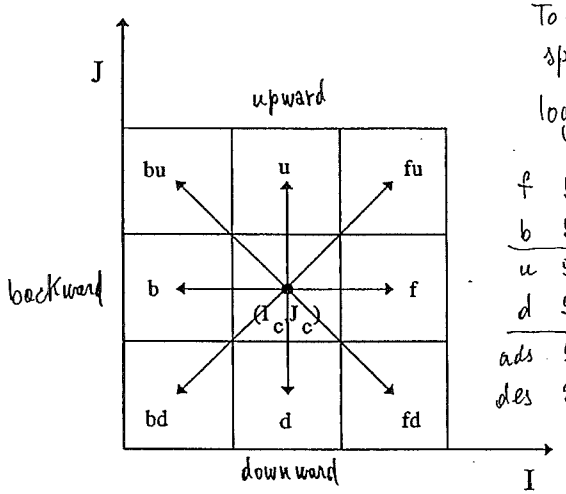

To account for spatial heterogeneity: log-normally distributed.

	P_5	P_{95}
f	$5 \cdot 10^{-3}$	$8\ 10^{-3}$
b	$5 \cdot 10^{-4}$	$8 \cdot 10^{-4}$
u	$5 \cdot 10^{-5}$	$8 \cdot 10^{-5}$
d	$5.5\ 10^{-3}$	$8.5\ 10^{-3}$
ads	$5 \cdot 10^{-3}$	$8 \cdot 10^{-3}$
des	$2 \cdot 10^{-4}$	$3 \cdot 10^{-4}$

Possible moves of the contaminant

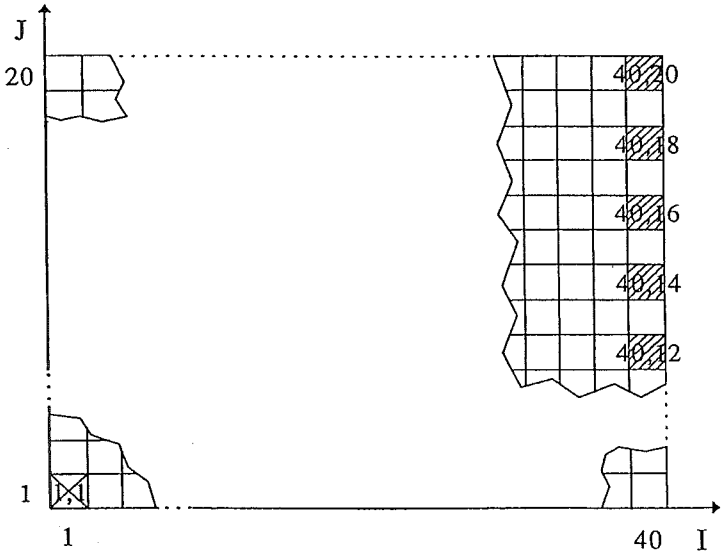

The stochastic region in which contaminant transport occurs
(1,1) = source ; ▨ *= wells for human consumption*

BIASING

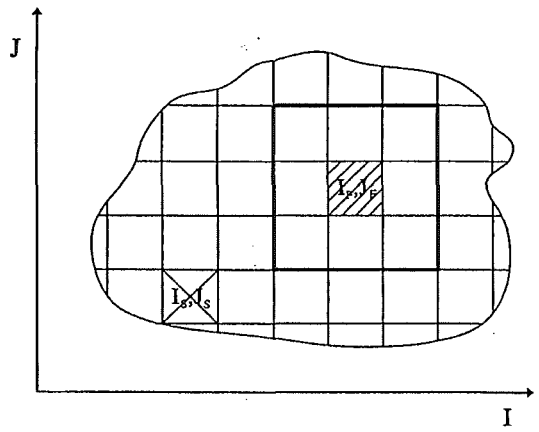

Domain of influence for biasing

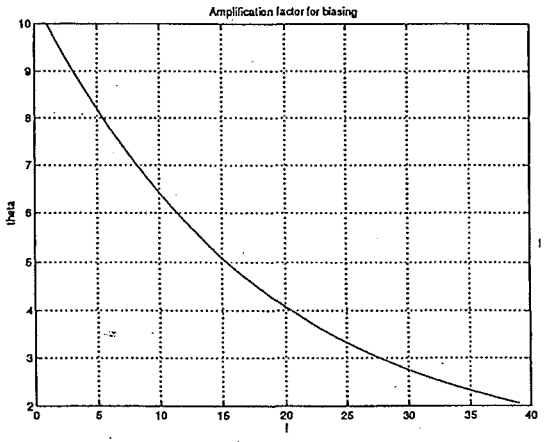

Amplification factor θ vs. distance from target pixel

- The shape of the amplification factor θ should be chosen coherently with that of the domain of influence.
  Inappropriate choices may lead to:
  - excessively small weights at the collection points;
  - excessively large weights to unfavoured trajectories.

RESULTS

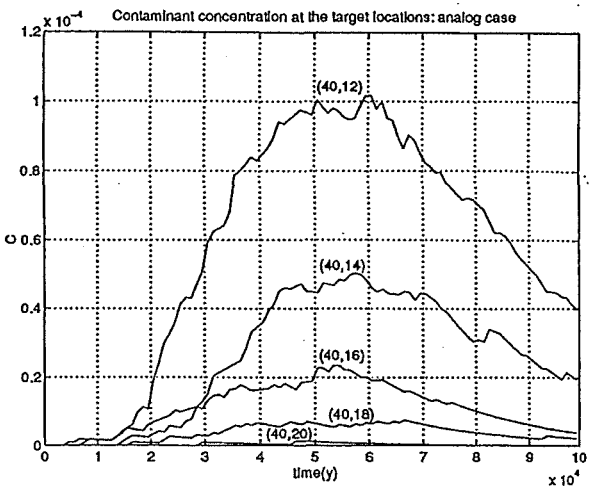

Time evolution of the contaminant concentration at the target locations: analog simulation

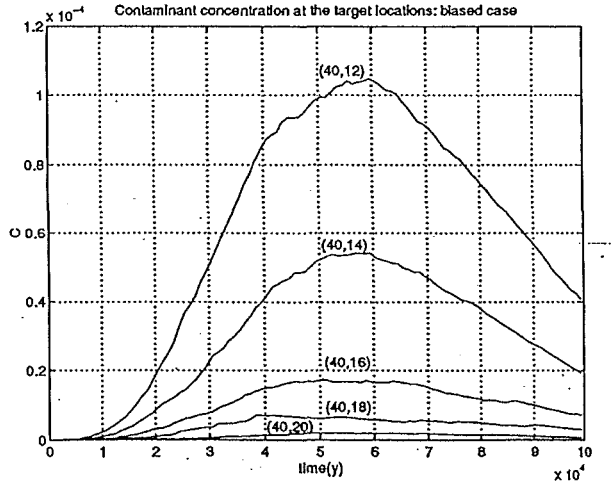

Time evolution of the contaminant concentration at the target locations: biased simulation

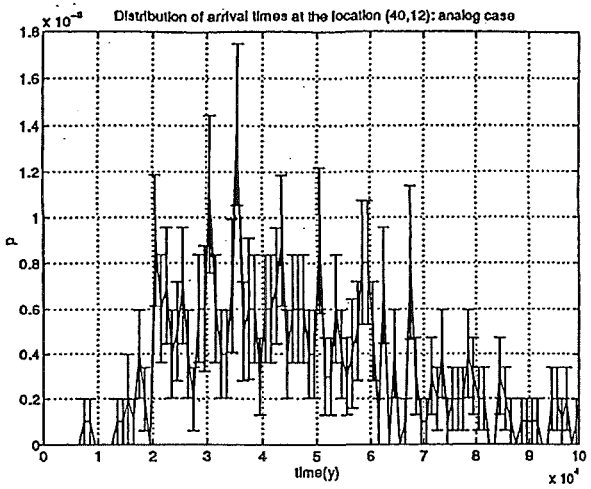

Distribution of arrival times at location (40,12): analog simulation

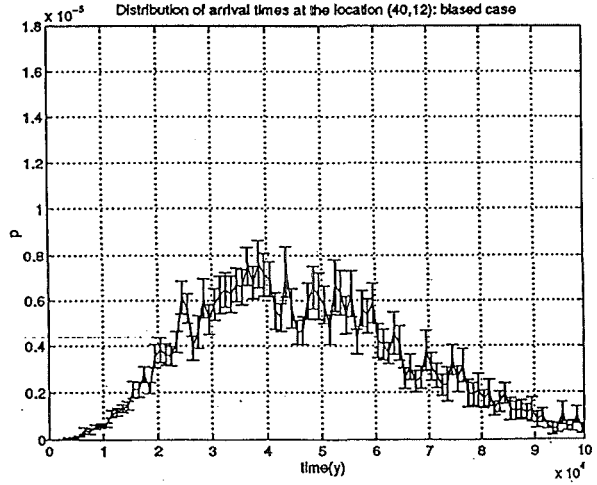

Distribution of arrival times at location (40,12): biased simulation

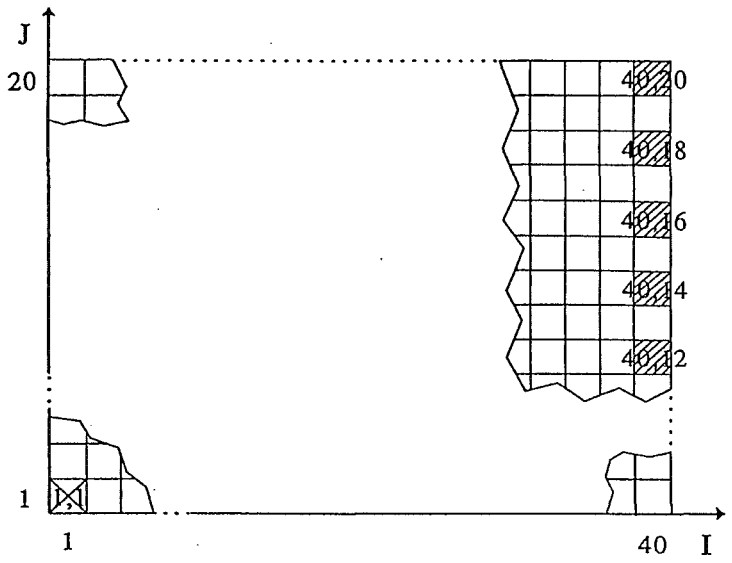

The stochastic region in which contaminant transport occurs
(1,1) = source ; ▨ *= wells for human consumption*

target (I_F, J_F)	σ_C *analog* $(t_c = 2.51min)$	σ_C *biased* $(t_c = 21.6min)$	ϕ *analog* $(t_c = 2.51min)$	ϕ *biased* $(t_c = 21.6min)$
$(40,12)$	$3.03 \cdot 10^{-6}$	$9.92 \cdot 10^{-7}$	$4.34 \cdot 10^{10}$	$5.45 \cdot 10^{10}$
$(40,14)$	$2.13 \cdot 10^{-6}$	$5.96 \cdot 10^{-7}$	$8.78 \cdot 10^{10}$	$1.43 \cdot 10^{11}$
$(40,16)$	$1.40 \cdot 10^{-6}$	$3.39 \cdot 10^{-7}$	$2.03 \cdot 10^{11}$	$4.03 \cdot 10^{11}$
$(40,18)$	$8.56 \cdot 10^{-7}$	$1.04 \cdot 10^{-7}$	$5.44 \cdot 10^{11}$	$4.30 \cdot 10^{12}$
$(40,20)$	∞	$5.62 \cdot 10^{-8}$	0	$1.26 \cdot 10^{14}$

Table 3. Figures of merit for the estimates of concentration in the various pixels at $t^* = 2 \cdot 10^4$ *y.*

t_c = *computer time (min)*

σ_C = *standard deviation of the concentration in* (I_F, J_F) *at* t^*

$\phi = \frac{1}{\sigma_C^2 t_c}$

CONCLUSIONS

- Kolmogorov–Dmitriev model offers a flexible structure to describe the many phenomena occurring in contaminant trasnsport, even under non–equilibrium conditions.

- High–order systems of equations ⇒ Monte Carlo

- Possible introduction of stochastic models of spatial heterogeneity

- *Rare events* ⇒ efficient biasing techniques can be formulated.

REFERENCES

Antonopoulos–Domis, M., Clouvas, A. and Marseguerra, M. (1995) On the compartmental modeling of cesium migration in soils. *Nucl. Sci. & Eng.* **121**, 461.

Gelhar, L. W., Welty, C. and Rehfeldt, K. R. (1992) A critical review of data on field–scale dispersion in aquifers. *Water Resour. Res.* **28**(7), 1955.

Hughes, D. J., Sanders, J. E. and Horowitz, J. (1958) Physics and mathematics. *Progress in Nuclear Energy* **2**, 315–368.

Kolmogorov, A. N. and Dmitriev, N. A. (1947) *C. r. Acad. Sci., USSR* **56**, 1.

Lee, Y. and Lee, K. J. (1995) Nuclide transport of decay chain in the fractured rock medium: a model using continuous time Markov process. *Ann. Nucl. Energy* **22**(2), 71.

Marseguerra, M. and Zio, E. (1997) Modelling the transport of contaminants in groundwater as a branching stochastic process. *Ann. Nucl. Energy* **24**(8), 625–644.

Marsily, G. de (1986) *Quantitative Hydrogeology*. Academic Press, San Diego, California

Prickett, T. A., Naymik, T. G. and Lonnguist, C. G. (1981) A 'random–walk' solute transport model for selected groundwater quality evaluations. ISWS/BUL–65/81, Bulletin 65, State of Illinois, Illinois Department of Energy and Natural Resources, Champaign.

Williams, M. M. R. (1992) A new model for describing the transport of radionuclides through fractured rock. *Ann. Nucl. Energy* **19**(10), 791.

Monte Carlo Methods and Models for Applications
in Energy and Technology

Workshop to be held at Forschungszentrum Karlsruhe, May 12-14, 1998

Point and Surface Activities of Radionuclide Chains in Porous Media by a Non Analog Monte Carlo Simulation

O.F. Smidts and J. Devooght

Service de Métrologie
Université Libre de Bruxelles
1050 Bruxelles - BELGIUM

In the risk assesment of highly radioactive waste in deep geological repositories, the migration of radionuclide chains in porous media by advection and dispersion processes are of main concern. The computation of activities (or cumulated activities over time) in confined zones of the medium are required in most of the contamination scenarios (e.g.: radionuclides extracted from wells, discharged to rivers or accumulated on the upper surface of the geological medium). In this context, we address here the problem of computing doses by Monte Carlo at specific points or on specific surfaces with low statistical uncertainties.

The random walks of the Monte Carlo simulation are constructed from an integral equation applied recently to the migration of a radionuclide chain [1]. The simulation uses the solution of an adjoint reference problem to improve the efficiency of the calculations [2].

During a pre-processing step, transition probabilities from any location of the domain to specific points or surfaces are computed and memorized. These additional transitions are taken into account in a re-organized simulation with new banches in the walks. This method allows to force, at each step, transitions of random walkers to specific zones where their presence is expected with a very low probability.

The organization of the simulations will be described and the computation of point and surface scores will be illustrated by numerical results.

1. Smidts, O.F. and Devooght, J. "Analysis of the transport of radionuclide chains in a stochastic geological medium by a biased Monte Carlo simulation, Nuclear Science and Engineering, in press (1998).
2. Smidts, O.F. and Devooght, J. "A non analog Monte Carlo simulation of transport of radionuclides in a porous medium", Mathematics and Computers in Simulation, in press (1998).

Last modified: Thu Apr 2 14:05:17 1998

Point and surface activities of radionuclide chains in porous media by a non analog Monte Carlo simulation

O. F. Smidts and J. Devooght

Service de Métrologie Nucléaire
Université Libre de Bruxelles
osmidts@metronu.ulb.ac.be

1. Introduction
2. Integral equation
3. Transport of one radionuclide
4. Transport of a radionuclide chain
5. Simulation with a random field
6. Cumulated and instantaneous activities on surfaces and at points
7. Numerical results
8. Conclusions

1. Introduction

Risk assessment of radioactive waste repositories

→ transport of radionuclide chains

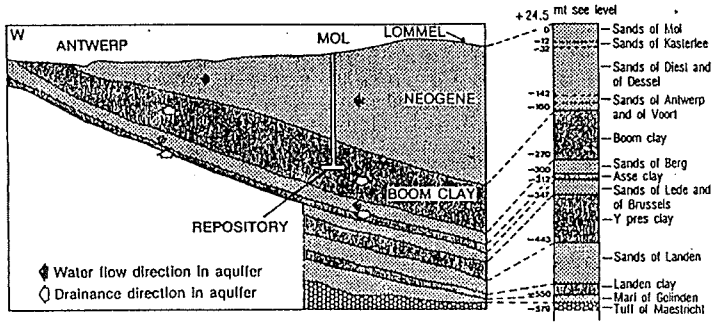

Geological Cross-Section and Conceptual Hydrological Regime at the Mol Site.

PRA studies → (cumulated) activities:

- on upper surface of the geological medium
- in local regions
- at extraction wells

→ difficulties encountered in analog simulations:

- long and unlikely pathways
- scores on surfaces and at points

⇒ application of non analog Monte Carlo:

integral equation

$$c(\bar{r},t) \;=\; Q(\bar{r},t) + \int dt' \int d\bar{r}'\; K\left(\bar{r}',t'|\bar{r},t\right)\; c\left(\bar{r}',t'\right)$$

$$\mu = \int dt \int d\bar{r} \;\; \underbrace{f\left(\bar{r},t\right)}_{\substack{\text{pay-off}\\ \text{function}}} \;\; c\left(\bar{r},t\right) \equiv \text{score by M.C.}$$

⇒ construction of random walks

$(n^0$, photons, aerosols, $\ldots)$

$$c \;=\; Q + \kappa c \quad \Rightarrow \quad c \;=\; (I-\kappa)^{-1} Q$$

→ expansion in Neumann series

$$c \;=\; Q \;+\; \kappa Q \;+\; \kappa^2 Q \;+\; \kappa^3 Q \;+\; \ldots$$

$$\mu \;=\; \mu_0 \;+\; \mu_1 \;+\; \mu_2 \;+\; \mu_3 \;+\; \ldots$$

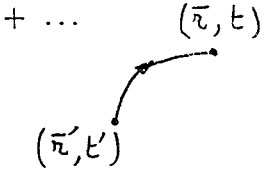

2. Integral equation

advection-dispersion-retention PDE in a porous medium $\mathcal{D} \cup \mathcal{S}$:

$$\left\{ \frac{\partial [\omega(\bar{r}').]}{\partial t'} + \overline{\nabla}_{r'} \left[\bar{q}(\bar{r}'). \right] - \overline{\nabla}_{r'} \left[\overline{\overline{D}}(\bar{r}') \overline{\nabla}_{r'} . \right] \right.$$

$$\left. + \lambda \omega (\bar{r}') \right\} c(\bar{r}', t') = S(\bar{r}', t')$$

where $\omega = \theta R$

+ boundary conditions on $\mathcal{S}$:

$$\bar{n} \left\{ -\overline{\overline{D}}(\bar{r}') \overline{\nabla}_{r'} c(\bar{r}', t') + \bar{q}(\bar{r}') c(\bar{r}', t') \right\} = \beta(\bar{r}')$$

$\rightarrow$ integral formulation not unique

definition of an auxiliary problem:

$$\left\{ -\omega_0 \frac{\partial .}{\partial t'} - \bar{q}_0 \overline{\nabla}_{r'} . - \overline{\nabla}_{r'} \left[\overline{\overline{D_0}} \overline{\nabla}_{r'} . \right] + \lambda \omega_0 \right\} c_0^* = \delta(\bar{r}' - \bar{r}) \, \delta(t' - t)$$

adjoint reference problem
$c_0^* \equiv c_0^*(\bar{r}', t' | \bar{r}, t)$

1/2
1

$$u_S(\bar{r}) \, c(\bar{r}, t) = \frac{1}{T_0} \int_{t-T_0}^{t} dt' \int_{\mathcal{D}} d\bar{r}' \left[T_0 - (t - t') \right] c_0^*(\bar{r}', t' | \bar{r}, t) \, S(\bar{r}', t')$$

$$+ \frac{1}{T_0} \int_{t-T_0}^{t} dt' \oint_{\mathcal{S}} d\bar{r}' \left[T_0 - (t - t') \right] \bar{n} \left[-\beta(\bar{r}') c_0^* - \overline{\overline{D}}(\bar{r}') \overline{\nabla}_{r'} c_0^* \right] c(\bar{r}', t')$$

$$+ \frac{1}{T_0} \int_{t-T_0}^{t} dt' \int_{\mathcal{D}} d\bar{r}' \left\{ \omega(\bar{r}') \, c_0^* + \left[T_0 - (t - t') \right] \right.$$

$$\left. \left[\Delta\omega \frac{\partial c_0^*}{\partial t'} + \Delta \bar{q} \overline{\nabla}_{r'} c_0^* + \overline{\nabla}_{r'} \left(\Delta \overline{\overline{D}} \, \overline{\nabla}_{r'} c_0^* \right) - \lambda \Delta\omega \, c_0^* \right] \right\} c(\bar{r}', t')$$

$$\rightarrow \; u_S \, c = Q + \int_{t-T_0}^{t} dt' \int_{\overline{\mathcal{D}}} d\bar{r}' \left[K_{\mathcal{D}}(\bar{r}', t' | \bar{r}, t) + \delta_2(\bar{r}' - \bar{r}'_S) K_S(\bar{r}', t' | \bar{r}, t) \right] u_S(\bar{r}') c(\bar{r}', t')$$

with $\begin{cases} \Delta\omega = \omega(\bar{r}') - \omega_0 \; ; \; \Delta \bar{q} = \bar{q}(\bar{r}') - \bar{q}_0 \\ \Delta \overline{\overline{D}} = \overline{\overline{D}}(\bar{r}') - \overline{\overline{D}}_0 \end{cases}$

role of c_0^* ?
$\rightarrow$ influence on the efficiency of the M.C. simulation

$\rightarrow$ c_0^* "guides" the simulations (like the importance function in neutron transport)

$\Rightarrow$ may also be applied to 1D problems

3. Transport of one radionuclide

form of integral kernel: $K = K_{\mathcal{D}} + \delta_2(\bar{r}' - \bar{r}'_{\mathcal{S}})\, K_{\mathcal{S}}$

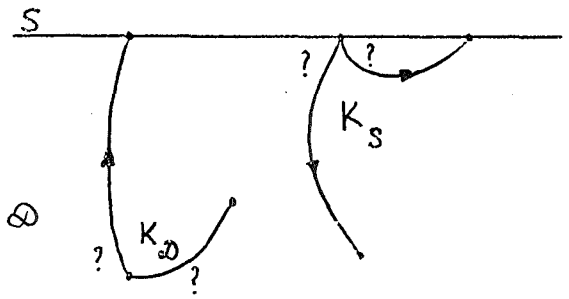

$Q(\bar{r}, t) \quad \Rightarrow \quad p_{Q\to\mathcal{D}}, p_{Q\to\mathcal{S}}$ and $f_{Q\to\mathcal{D}}, f_{Q\to\mathcal{S}}$

$K_{\mathcal{D}}(\bar{r}', t'|\bar{r}, t) \quad \Rightarrow \quad p_{\mathcal{D}\to\mathcal{D}}, p_{\mathcal{D}\to\mathcal{S}}$ and $f_{\mathcal{D}\to\mathcal{D}}, f_{\mathcal{D}\to\mathcal{S}}$

$K_{\mathcal{S}}(\bar{r}', t'|\bar{r}, t) \quad \Rightarrow \quad p_{\mathcal{S}\to\mathcal{D}}, p_{\mathcal{S}\to\mathcal{S}}$ and $f_{\mathcal{S}\to\mathcal{D}}, f_{\mathcal{S}\to\mathcal{S}}$

in practice:

- simplified kernels $\widetilde{K}_{\mathcal{D}}$ and $\widetilde{K}_{\mathcal{S}}$ and source term $\widetilde{Q}$
- pre-processing of $p_{Q\to\mathcal{D}}$, $p_{\mathcal{D}\to\mathcal{S}}$, ...
- computation of $\frac{Q}{\widetilde{Q}}$, $\frac{K_{\mathcal{D}}}{\widetilde{K}_{\mathcal{D}}}$, $\frac{K_{\mathcal{S}}}{\widetilde{K}_{\mathcal{S}}}$ in statistical weights during the simulation

4. Transport of a radionuclide chain

N_r-member chain:

$$i \xrightarrow{\lambda_i} j \xrightarrow{\lambda_j} k \xrightarrow{\lambda_k} \ldots$$

$i, j, k \ldots \equiv$ states of a particle

$\rightarrow$ generalized integral equation:

$$\begin{aligned} u_{\mathcal{S}}(\bar{r})\, A(\bar{r}, t; i) \;=\; & Q(\bar{r}, t; i) \\ & + \sum_{j=1}^{N_r} \int_{t-T_0}^{t} dt' \int_{\mathcal{D}} d\bar{r}' \Big[K^{j\to j}(\bar{r}', t'; j|\bar{r}, t; i)\; \delta_{j,i} \\ & + \; K^{j\to i}(\bar{r}', t'; j|\bar{r}, t; i)\; (1 - \delta_{j,i}) \Big]\, u_{\mathcal{S}}(\bar{r}')\, A(\bar{r}', t'; j) \end{aligned}$$

where $A(\bar{r}, t; i) = \lambda_i\, c(\bar{r}, t; i)$

$\rightarrow$ *one* integral equation in $(\bar{r}, t; i)$

no need to solve a system of coupled PDE's !

Simulation:

- j (source)
- $Q(\vec{r}, t; j)$
- branch $j \rightarrow i$ or $j \rightarrow j$?
  if $j \rightarrow j$: $K^{j \rightarrow j}$
  if $j \rightarrow i$: $K^{j \rightarrow i}$

in practice:

- simplified kernels $\widetilde{K}^{j \rightarrow j}$ and $\widetilde{K}^{j \rightarrow i}$ and source term $\widetilde{Q}$
- pre-processing of $p^{j \rightarrow i}$ $(= 1 - p^{j \rightarrow j})$
- computation of $\frac{Q}{\widetilde{Q}}$, $\frac{K^{j \rightarrow i}}{\widetilde{K}^{j \rightarrow i}}$, $\frac{K^{j \rightarrow j}}{\widetilde{K}^{j \rightarrow j}}$ in statistical weights during the simulation

5. Simulation with a random field

random parameters in the transport equation :

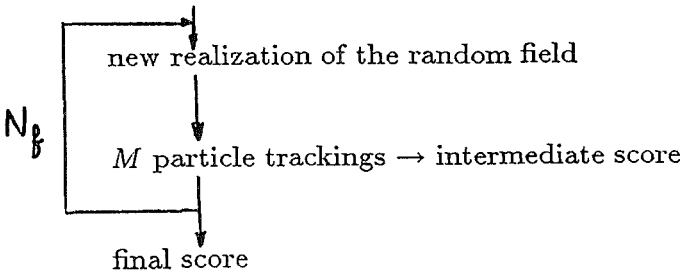

How many particle trackings (M) for 1 realization of the random field ?

→ double randomization theory:

$$\sigma^2_{\text{simulation}} = \frac{\sigma^2_{\text{particle tracking}}}{M} + \sigma^2_{\text{random parameters}}$$

$M \equiv$ batch size $=$?

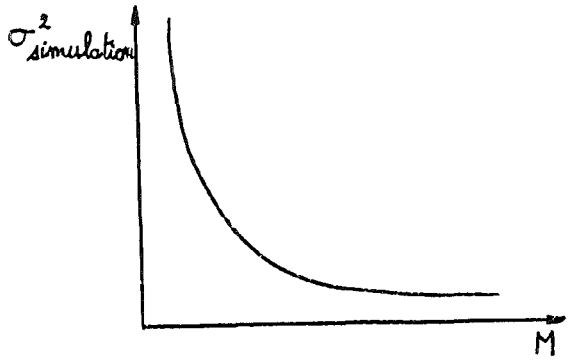

6. Cumulated and instantaneous activities on surfaces and at points

Cumulated activities

$$\bullet \int_0^{T_0} dt \int_{S_\ell} d\bar{r}\, A_i(\bar{r},t)$$

→ during the pre-processing step:

$$p_{\mathcal{D}\to S_\ell} = \frac{\displaystyle\int_{t'}^{T_0} dt \int_{S_\ell} d\bar{r}\ \widetilde{K}_{\mathcal{D}}}{\displaystyle\int_{t'}^{T_0} dt \int_{\mathcal{D}} d\bar{r}\ \widetilde{K}_{\mathcal{D}} + \int_{t'}^{T_0} dt \int_{\mathcal{S}} d\bar{r}\ \widetilde{K}_{\mathcal{D}} + \sum_{j=1}^{N_S} \int_{t'}^{T_0} dt \int_{S_j} d\bar{r}\ \widetilde{K}_{\mathcal{D}}}$$

$$\bullet \int_0^{T_0} dt\, A_l(\bar{r}_k,t)$$

→ idem

$$p_{\mathcal{D}\to\bar{r}_k} = \frac{\displaystyle\int_{t'}^{T_0} dt\ \widetilde{K}_{\mathcal{D}}(\bar{r}',t'|\bar{r}_k,t)}{\displaystyle\int_{t'}^{T_0} dt \int_{\mathcal{D}} d\bar{r}\ \widetilde{K}_{\mathcal{D}} + \int_{t'}^{T_0} dt \int_{\mathcal{S}} d\bar{r}\ \widetilde{K}_{\mathcal{D}} + \sum_{m=1}^{N_P} \int_{t'}^{T_0} dt\ \widetilde{K}_{\mathcal{D}}(\bar{r}',t'|\bar{r}_m,t)}$$

→ new organization of the simulation (1 Radionuclide)

branches: $\mathcal{D}, \mathcal{S}, S_\ell(\ell = 1,\ldots,N_S), \bar{r}_k(k = 1,\ldots,N_P)$

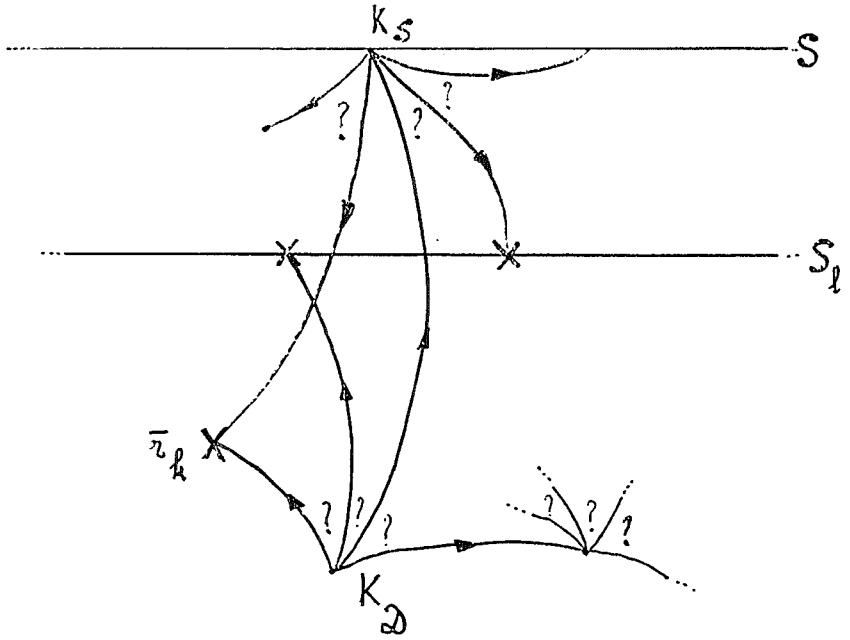

X ≡ dead-end for the random walker

? ≡ random sampling between different branches

Instantaneous activities

$$\bullet A_i(\bar{r}_k, T_0) \qquad \bar{r}_k \in \mathcal{D}$$

$\Rightarrow$ integral equation

$$\begin{aligned} A(\bar{r}_k, T_0; i) \;=\; & Q(\bar{r}_k, T_0; i) \\ & + \sum_{j=1}^{N_r} \int_0^{T_0} dt' \int_{\mathcal{D}} d\bar{r}' \Big[K^{j\to j}(\bar{r}', t'; j|\bar{r}_k, T_0; i)\ \delta_{j,i} \\ & + \; K^{j\to i}(\bar{r}', t'; j|\bar{r}_k, T_0; i)\ (1-\delta_{j,i}) \Big]\ u_{\mathcal{S}}(\bar{r}')\ A(\bar{r}', t'; j) \end{aligned}$$

simulation with the pay-off function:

$$f \;=\; K^{j\to j}\delta_{j,i} + K^{j\to i}(1-\delta_{j,i})$$

- in neutron transport: $f \div \frac{1}{|\bar{r}-\bar{r}_k|^2}$
- in this context: $f \div \frac{1}{|t-t'|^{3/2}}$ (sharp Gaussian function when $\sigma \div |t-t'|^{1/2} << 1$)

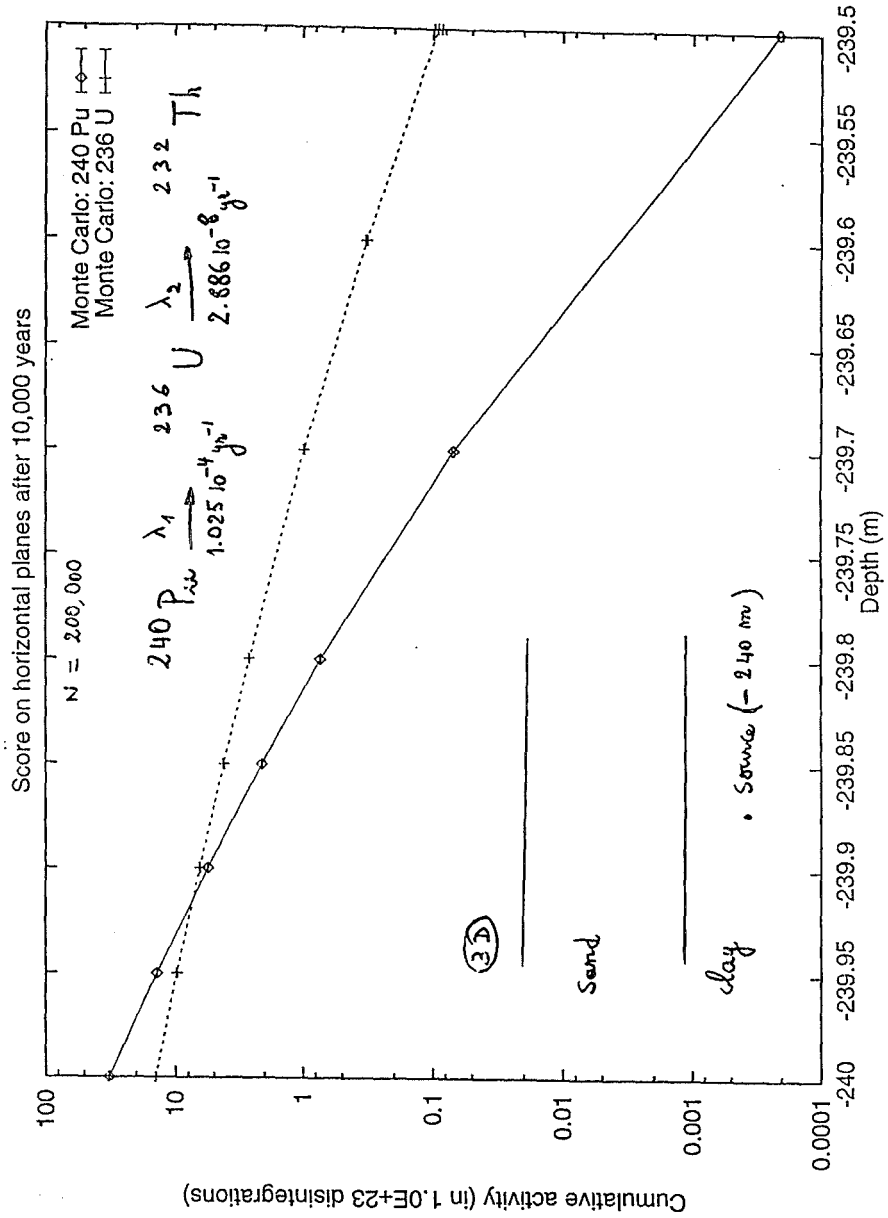

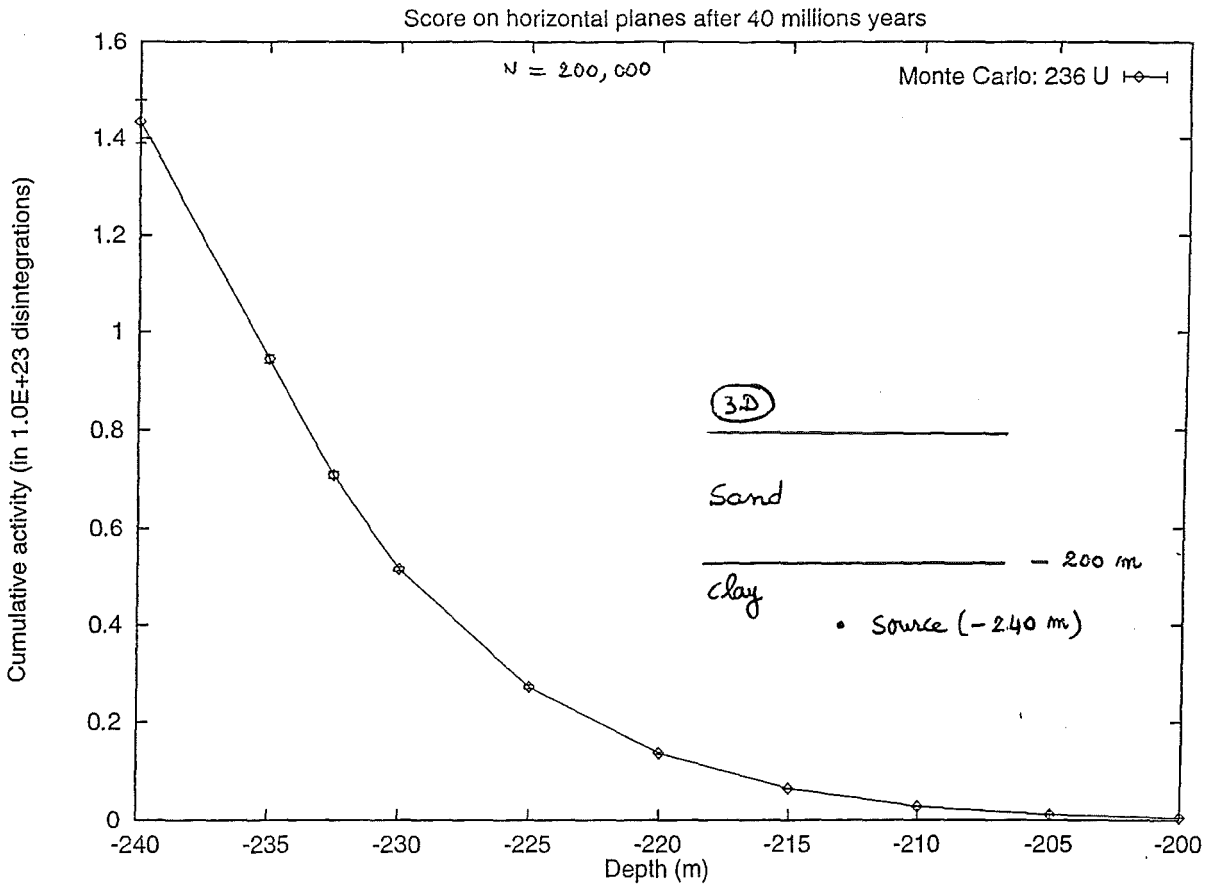
Score on horizontal planes after 40 millions years
N = 200,000
Monte Carlo: 236 U
Cumulative activity (in 1.0E+23 disintegrations)
1.6
1.4
1.2
1
0.8
0.6
0.4
0.2
0
-240
-235
-230
-225
-220
-215
-210
-205
-200
Depth (m)
3D
Sand
- 200 m
Clay
Source (-240 m)

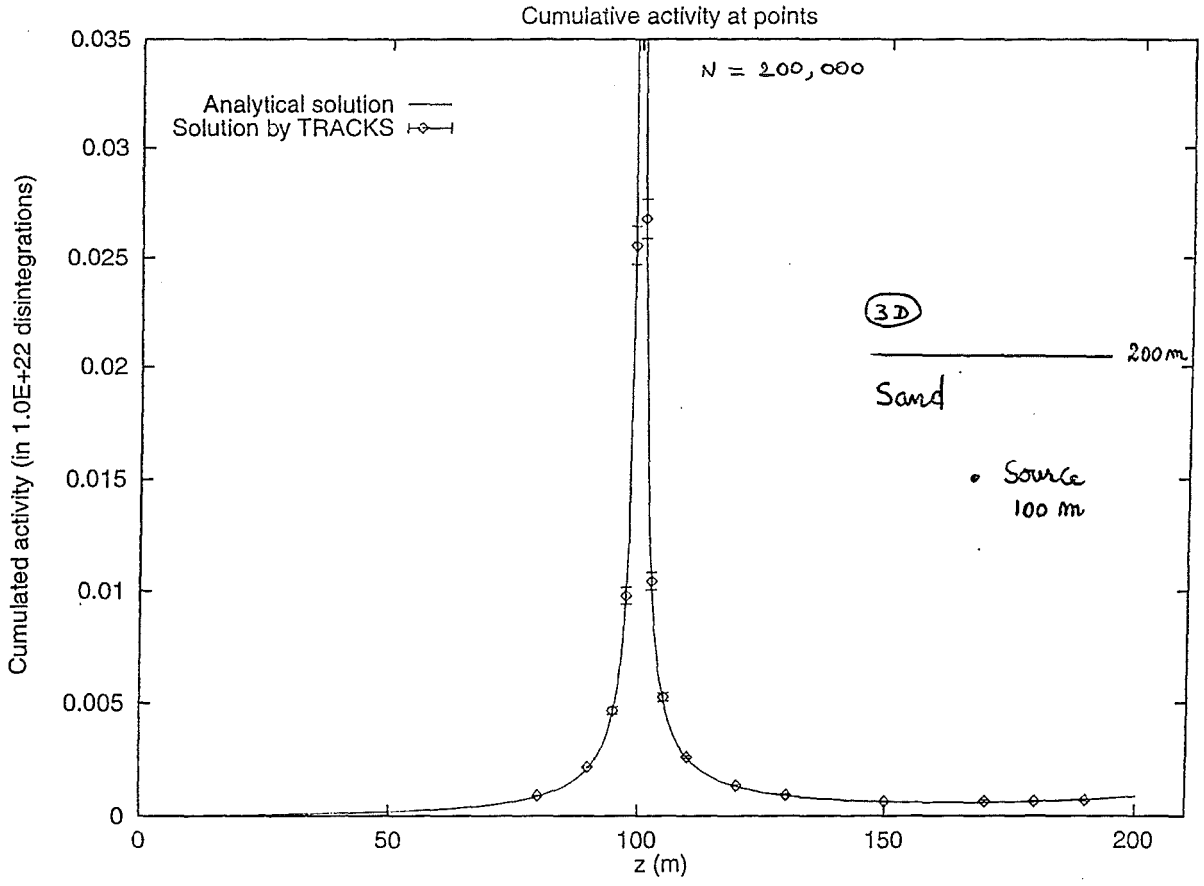
Cumulative activity at points
N = 200,000
Analytical solution
Solution by TRACKS
Cumulated activity (in 1.0E+22 disintegrations)
0.035
0.03
0.025
0.02
0.015
0.01
0.005
0
0
50
100
150
200
z (m)
3D
200m
Sand
Source
100 m

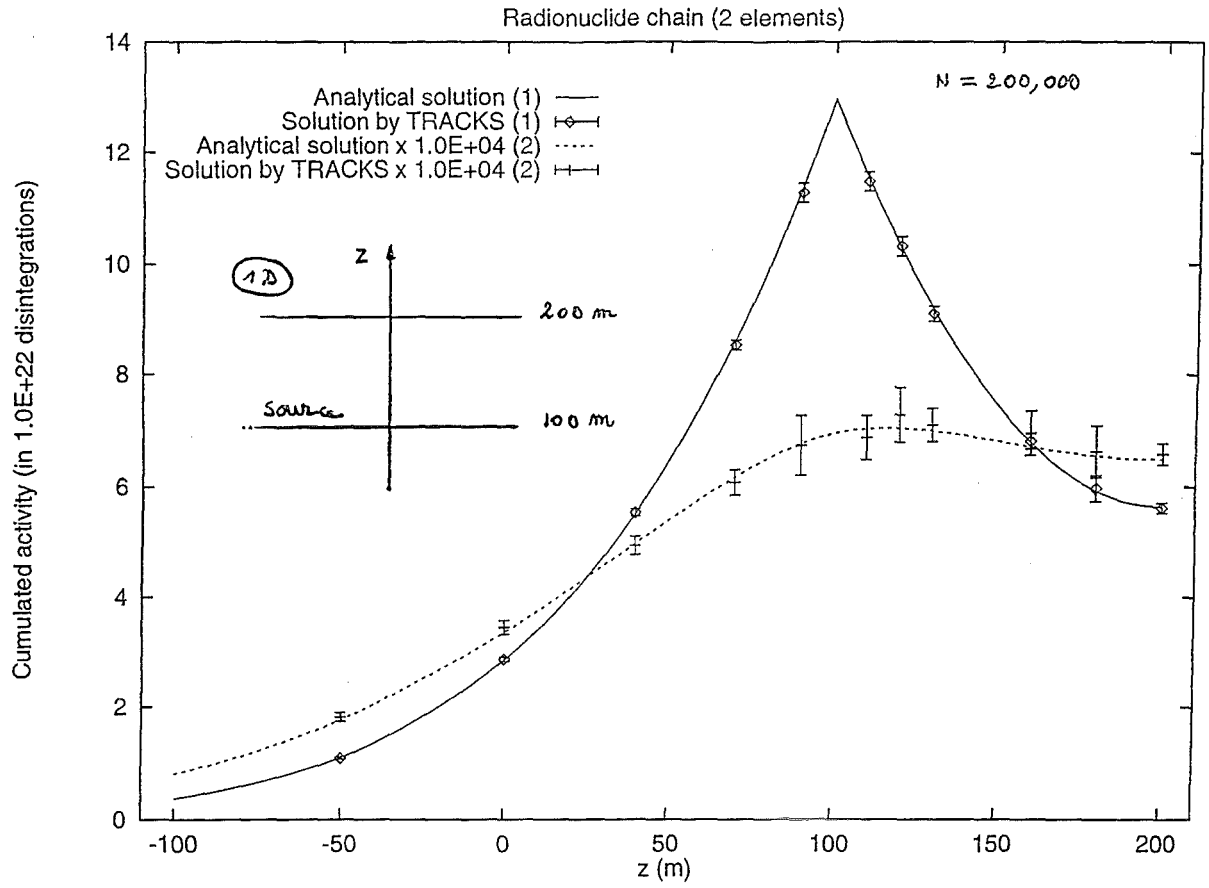
Radionuclide chain (2 elements)
N = 200,000
Analytical solution (1)
Solution by TRACKS (1)
Analytical solution x 1.0E+04 (2)
Solution by TRACKS x 1.0E+04 (2)
1D
z
200 m
Source
100 m
Cumulated activity (in 1.0E+22 disintegrations)
z (m)
0
2
4
6
8
10
12
14
-100
-50
0
50
100
150
200

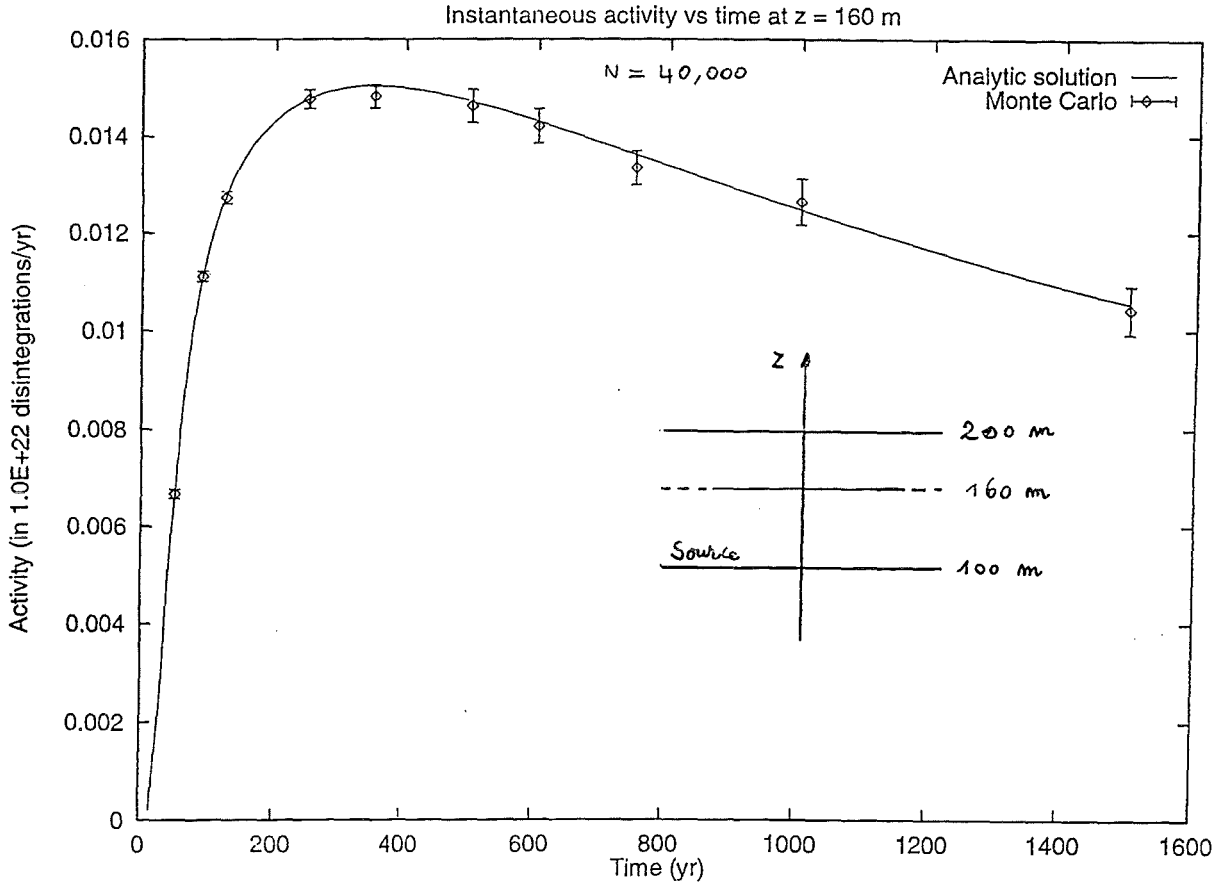
Instantaneous activity vs time at z = 160 m
N = 40,000
Analytic solution
Monte Carlo
z
200 m
160 m
Source
100 m
Activity (in 1.0E+22 disintegrations/yr)
Time (yr)
0
0.002
0.004
0.006
0.008
0.01
0.012
0.014
0.016
0
200
400
600
800
1000
1200
1400
1600

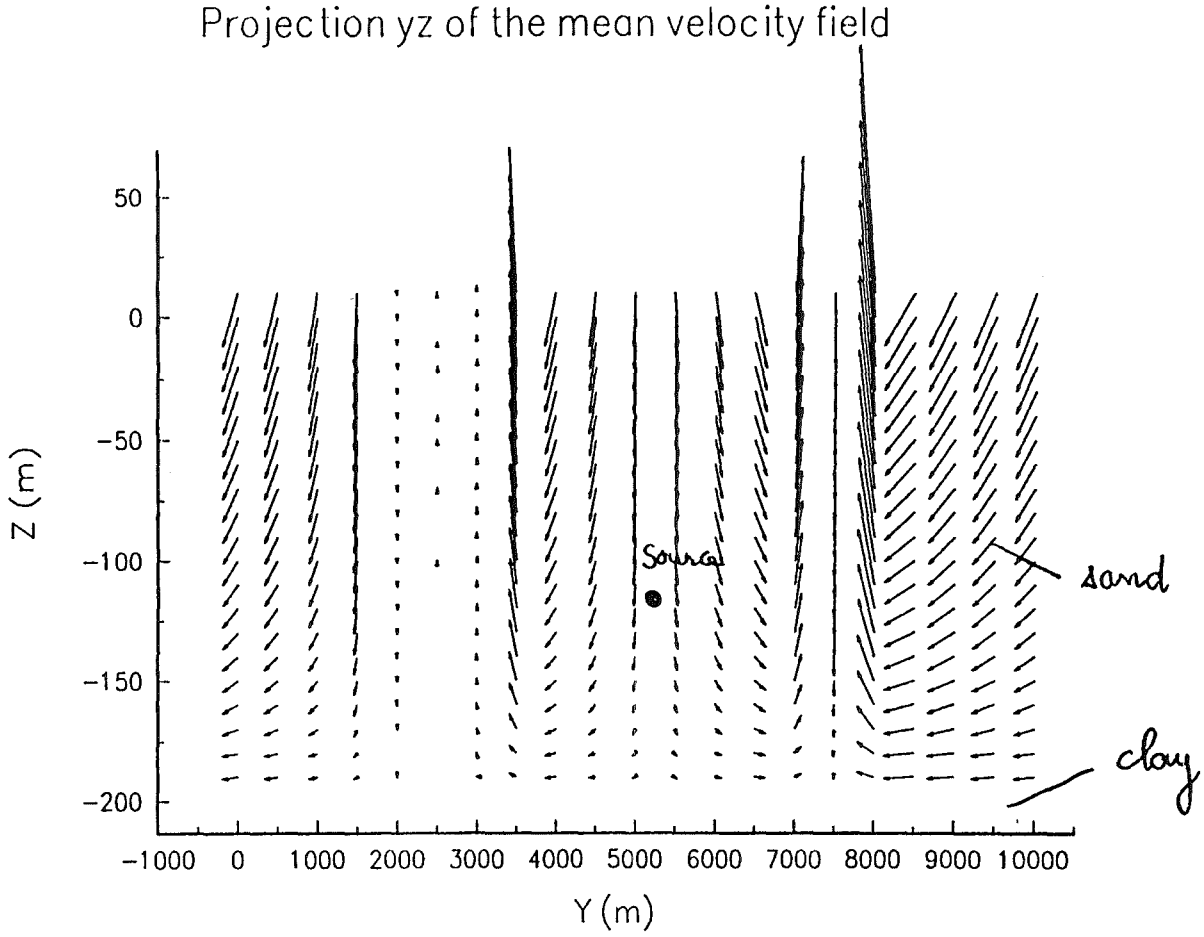
Projection yz of the mean velocity field
50
0
−50
−100
−150
−200
Z (m)
−1000
0
1000
2000
3000
4000
5000
6000
7000
8000
9000
10000
Y (m)
Source
sand
clay

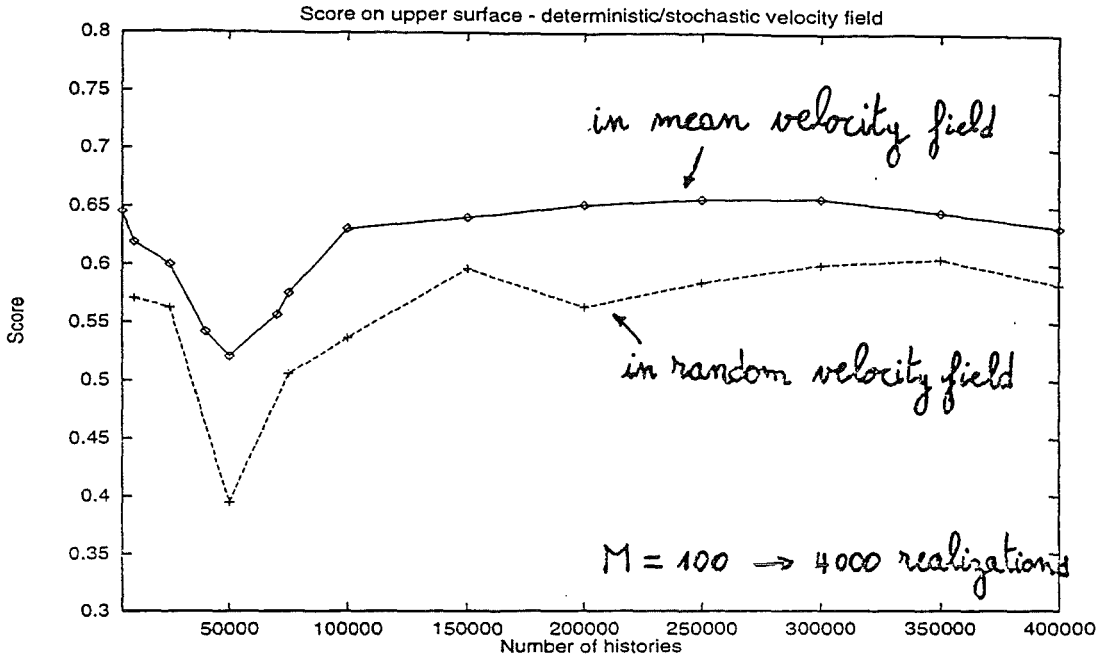
Score on upper surface - deterministic/stochastic velocity field
Score
Number of histories
in mean velocity field
in random velocity field
M = 100 → 4000 realizations
0.8
0.75
0.7
0.65
0.6
0.55
0.5
0.45
0.4
0.35
0.3
50000
100000
150000
200000
250000
300000
350000
400000

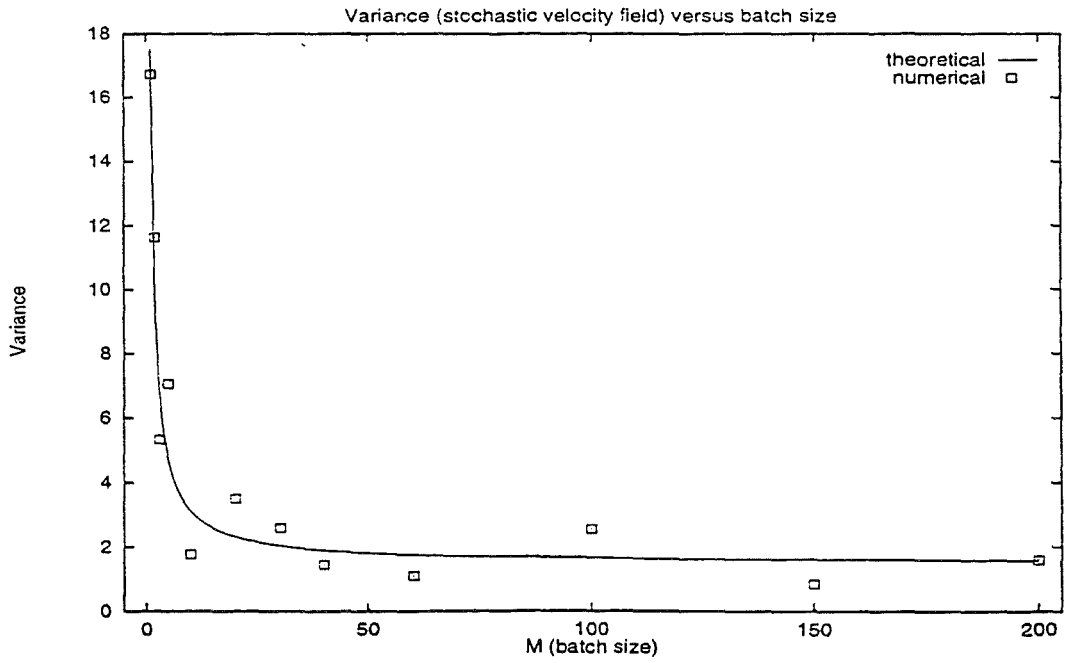
Variance (stochastic velocity field) versus batch size
Variance
M (batch size)
theoretical
numerical
18
16
14
12
10
8
6
4
2
0
0
50
100
150
200

8. Conclusions

- application of non-analog Monte Carlo to transport of R.N. chains in porous media using an adjoint reference problem
- needs a pre-processing (transition probabilities)
- not too time-consuming (simple non negative kernels and source term)
- efficient for a radionuclide chain (state of a particle)
- double randomization technique → minimization of computational costs (application in PRA for uncertain parameters)
- computation of activities on surfaces and at points with good accuracy (biased transitions)
- needs an additional pre-processing but of moderate cost (no new pre-processing when $\bar{r}_k$ is moved in the same geological layer)
- "singularity" in the pay-off function for instantaneous activity: limited consequences in practice

Some references

1. O.F. Smidts and J. Devooght, "A non-analog Monte Carlo simulation of transport of radionuclides in a porous medium", *Mathematics and Computers in Simulation*, in press 1998.

2. O.F. Smidts and J.Devooght, "Analysis of the transport of radionuclide chains in a stochastic geological medium by a biased Monte Carlo simulation", *Nuclear Science and Engineering*, in press 1998.

3. K.K. Sabelfeld, *Monte Carlo Methods in Boundary Value Problems*, Springer Series in Computational Physics, Springer-Verlag, Berlin 1991.

4. I. Lux and L. Koblinger, *Monte Carlo Particle Transport Methods: Neutron and Photon Calculations*, CRC Press, 1991.

5. E.E. Lewis and F. Böhm, "Monte Carlo Simulation of Markov Unreliability models", Nuclear Engineering and Design, 77:49-62, 1984.

6. J. Spanier and E.M. Gelbard, *Monte Carlo Principles and Neutron Transport Problems*, Addislon-Wesley, 1969.

Monte Carlo Methods and Models for Applications in Energy and Technology

Workshop to be held at Forschungszentrum Karlsruhe, May 12-14, 1998

Monte Carlo Applications in Fusion Neutronics

U. Fischer

Forschungszentrum Karlsruhe GmbH
Institut für Neutronenphysik und Reaktortechnik
Postfach 3640, D-76021 Karlsruhe, Germany

Fusion neutronics is devoted to problems dealing with neutron and photon radiation transport in fusion reactor systems where 14 MeV source neutrons are generated through (d,t) fusion reactions in the plasma chamber and subsequently are transported through the surrounding matter. The Monte Carlo method is a suitable computational technique to simulate the truly random path of a neutron in matter based on stochastic nuclear interactions with the nuclei.

With regard to fusion reactor applications, there are, in addition, further major advantages of the Monte Carlo method over the deterministic approaches: the ease and flexibility in representing even a complex problem geometry as is typical for tokamak fusion reactors, the possibility of using continuous energy cross-section data thus not being subjected to approximations and limitations when generating and applying group averaged data and, finally, the absence of any numerical convergence problems.

At Forschungszentrum Karlsruhe, the Los Alamos National Laboratory Monte Carlo code MCNP is the main computational tools for applications to fusion neutronics problems. In the paper, an overview is given of different task areas with specific examples for blanket and shield design related issues currently being performed in the framework of the European Fusion Technology Programme for ITER, the International Thermonuclear Experimental Reactor, as well as for a Demo-type European tokamak reactor. The focus is on typical design-related neutronic issues such as blanket and shielding performance in terms of tritium breeding, nuclear power generation, radiation penetration through the bulk blanket/shield system, radiation streaming through void gaps, as well as the resulting loads to the superconducting toroidal field coils. For addressing these problems, suitable three- dimensional torus sector models of the different reactors have been developed with the help of the MCNP code. In addition, examples are given of applications to analyses of fusion benchmark experiments which are mainly being performed to validate both the Monte Carlo code and the underlying nuclear cross-section data against fusion relevant integral experiments.

The paper finally aims at identifying issues which, in the author's view, require future development work to allow the successful application of the Monte Carlo technique in this and possibly other areas such as advanced means for sensitivity/uncertainty calculations, integration of burn-up calculations and use of CAD generated geometry models in the Monte Carlo calculation.

Last modified: Thu Apr 2 13:30:31 1998

Monte Carlo Applications in Fusion Neutronics

U. Fischer

Forschungszentrum Karlsruhe - Technik und Umwelt
Institut für Neutronenphysik u. Reaktortechnik

Overview

I. Introduction

II. Fusion Neutronics: Tasks, Methods, Tools & Data

III. Application Areas: Demo, ITER, NS & Experiments

IV. Development Goals

Fusion reaction

$$d + t \longrightarrow \underset{3.5}{\alpha} + \underset{14.1\ MeV}{n}$$

⇒ Nuclear interaction processes

- ♦ first wall & blanket
- ♦ vacuum vessel / shield
- ♦ magnetic field coils
- ♦ divertor & other reactor components

⇒ Fusion Neutronics

- ♦ Simulation of neutron & gamma - transport
  - * 14 MeV source neutrons
  - * Secondary neutrons & photons

Computational Methods & Tools

♦ Macroscopic description

deterministic, numerical approximations

⇒ Boltzmann transport equation

e. g. S_N - procedure (discrete ordinates)

- Codes: ANISN, ONEDANT (1d)
  DORT, TWODANT (2d)

♦ Microscopic description

probabilistic, individual particle histories

⇒ Monte Carlo simulation of random pathways

- Codes: MCNP, TRIPOLI, MORSE

⇒ **Monte Carlo preference in fusion neutronics**

- Continuous energy cross-section data
- Flexible geometrical modelling
- Accuracy limited by statistical and data uncertainties only

⇒ **LANL Monte Carlo code MCNP**

Nuclear data needs

♦ Neutron transport (14 MeV)

σ_a (E), σ_{tot}(E) *E: neutron energy*

σ_{nem} (E, E', μ) *μ=cos (θ), θ=scattering angle*

Energy-angle distributions for neutron emitting reactions: elastic scattering, (n,n'γ), (n,2n),...

♦ Gamma transport

γ - production cross-section, - spectra,

γ - interaction cross-section data

♦ Nuclear response data

- Tritium production $\sigma_{n,t}$(E)
- Power production: k_n(E), k_γ (E)
- Gas production $\sigma_{n,H}$(E),$\sigma_{n,He}$(E)
- Radiation damage: σ_d(E)
- Activation and transmutation $\sigma_{n,x}$(E)

Fusion reactor materials

- Breeder materials: Li, Pb-17Li, Li_4SiO_4, $LiAlO_2$, Li_2ZrO_3, Li_2O, Li_2TiO_3
- Neutron multipliers: Be, Pb
- Structural materials: SS-316, MANET, V-5Ti, SiC
  ⇒ Fe, Cr, Mn, Ni, Mo, Cu, Co, Nb, V, Si, C, ...
- Cooling materials: He, H_2O, Pb-17Li, Li
- Other materials: B_4C, Nb_3Sn, W, Al_2O_3, MgO

⇒ **Nuclear data libraries for fusion applications**

- ♦ FENDL-1,-2 (IAEA, ITER-project)
- ♦ EFF-1,-2 (European Fusion File Project)
- ♦ JENDL-FF (Japanese Fusion File)
- ♦ ENDF/B-VI (US nuclear data file)

⇒ *Available as working libraries for use with MCNP (continuous energy representation)*

Tasks and Objectives

Nuclear design analyses for fusion reactors & related systems

FZK Nuclear Fusion Project ⇔ EU Fusion Technology Programme

♦ **Blanket Development**

Nuclear design & optimisation (Demo & ITER)

- ♦ Tritium breeding & nuclear heating
- ♦ Radiation shielding
- ♦ Activation & afterheat, radiation damage

♦ **Nuclear Data Base**

Benchmark data testing & validation

(EFF-, FENDL-projects; ITER)

- ♦ Analyses of integral experiments
- ♦ C/E-data, uncertainties

♦ **Neutron Sources for Material Testing**

Design analyses, code & data development

- ♦ IFMIF - International Fusion Material Irradiation Facility *(IEA-activity)*
- ♦ Gas Dynamic Trap (GDT) Mirror *(Novosibirsk)*

Computational tools

- **Monte Carlo code MCNP (Versions 4A, 4B)**

  J. Briesmeister (ed.): MCNP - A General Monte Carlo N-Particle Transport Code, Version 4B, Los Alamos National Laboratory, Report LA-12625-M, March 1997

  - IBM RISC/6000-595
  - IBM SP/2-256 Parallel Computer

    (running under PVM „Parallel Virtual Machine")

Nuclear Data

- **Fusion Nuclear Data Libraries**
  - EFF-1, -2 -3 (European Fusion File)
  - FENDL-1, -2 (Fusion Evaluated Nuclear Data)
  - JENDL-FF (JAERI)
- **Intermediate Energy (IE) Data Evaluations**
  - FZK-INP Obninsk (RF) (up to 50 MeV)
  - LANL IE Data Files (up to 150 MeV)

Computational models

Three-dimensional geometry models developed (manually) with MCNP

Application Area I: Demo Blanket Development

(EU Fusion Technology Long-term Programme)

Objective: Development of an Engineering Design for a Demo-relevant Breeder Blanket

Nuclear design & optimisation of blanket using appropriate 3d torus sector model of EU Demo tokamak reactor („DEMONET")

- **EU Helium-cooled pebble bed (HCPB) blanket** with Li_4SiO_4 pebbles as breeder and Beryllium pebbles as neutron multiplier
  - Tritium self-sufficiency

    Global tritium breeding ratio (TBR) ≥ 1.05
  - Thermal-hydraulic & mechanical layout

    Nuclear heating, radiation shielding
  - Safety analyses

    Activation & afterheat calculation

Critical issues:

- Maximum temperature in Li_4SiO_4 pebble bed

  ⇒ *uncertainty in nuclear heating*
- TBR-uncertainty

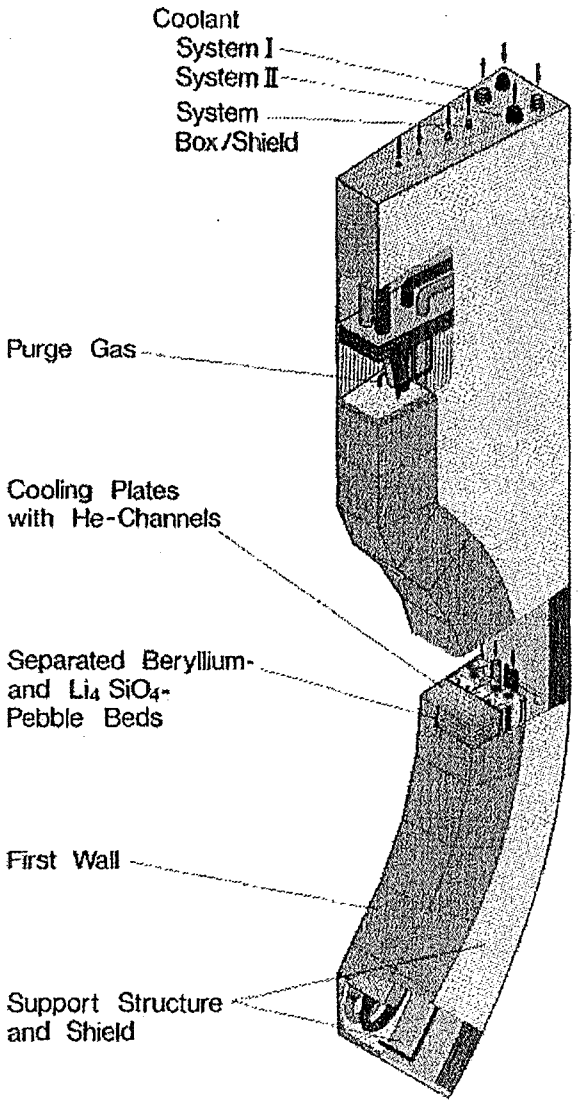
Coolant
System I
System II
System
Box/Shield
Purge Gas
Cooling Plates
with He-Channels
Separated Beryllium-
and Li_4SiO_4-
Pebble Beds
First Wall
Support Structure
and Shield

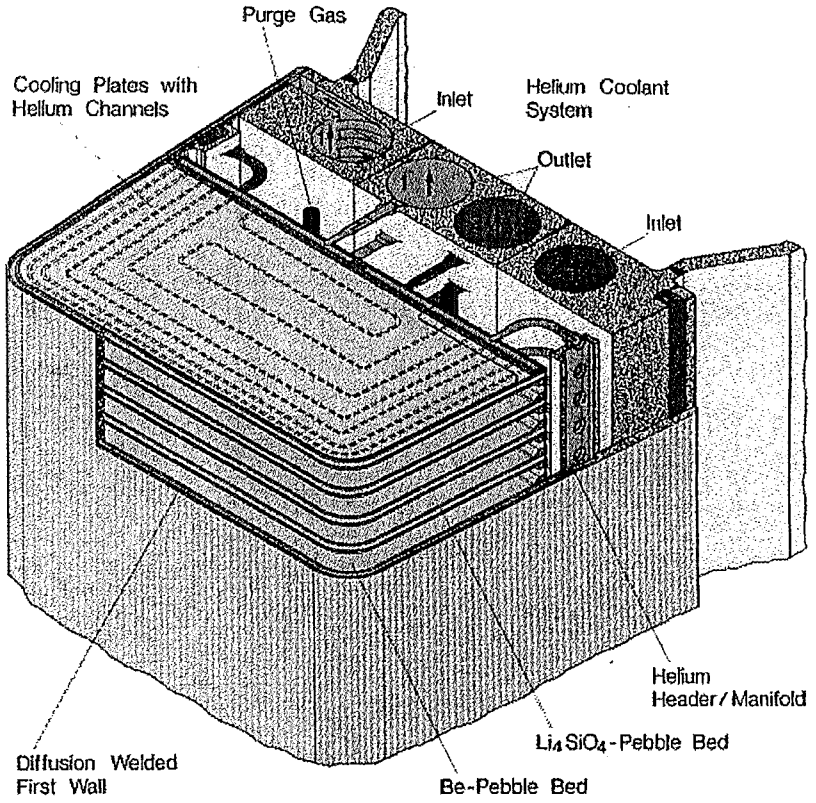
Purge Gas
Cooling Plates with
Helium Channels
Inlet
Helium Coolant
System
Outlet
Inlet
Helium
Header / Manifold
Li_4SiO_4-Pebble Bed
Be-Pebble Bed
Diffusion Welded
First Wall

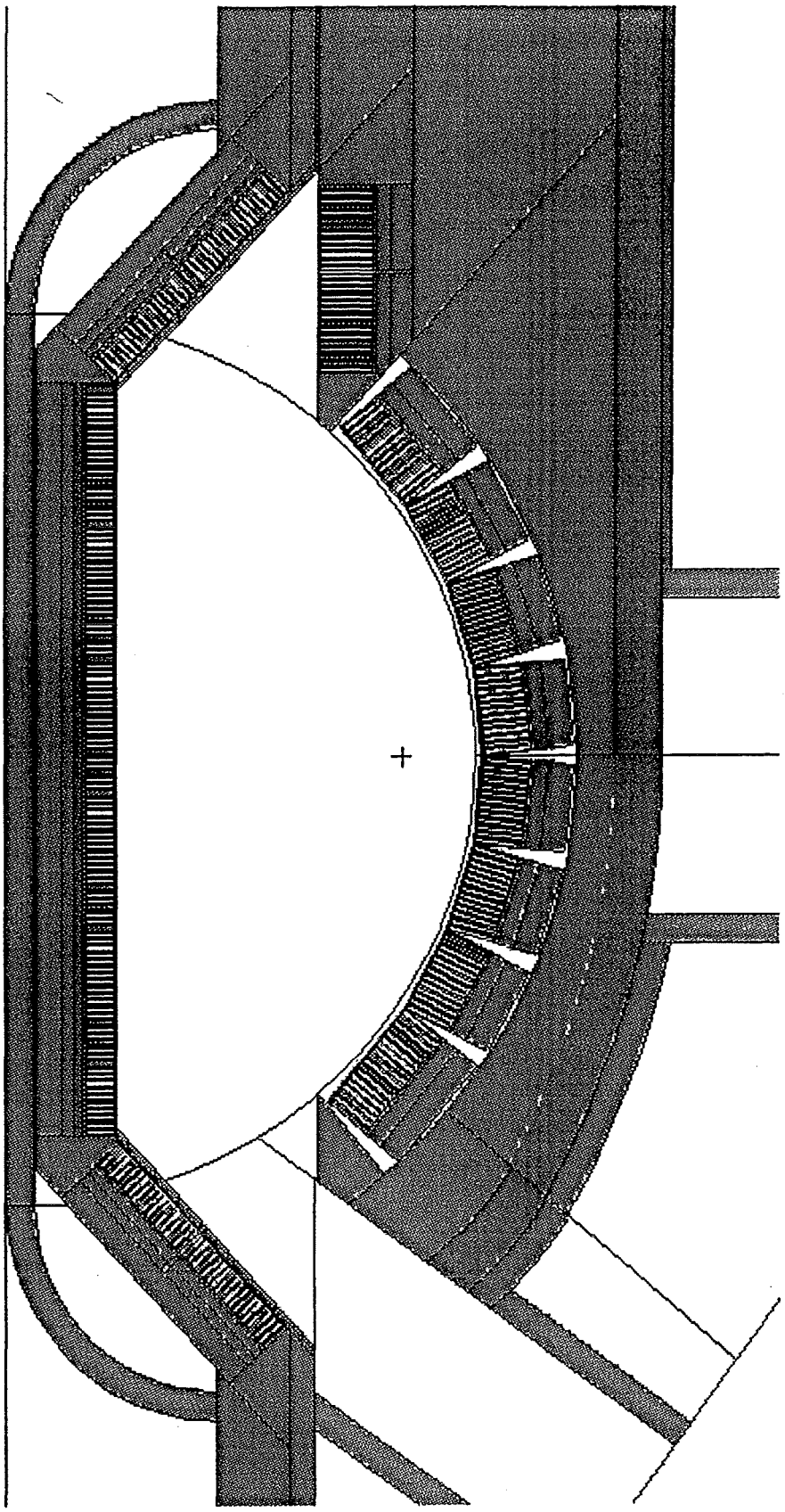

TBR-comparison for HCPB DEMO blanket
(MANET as structural material)

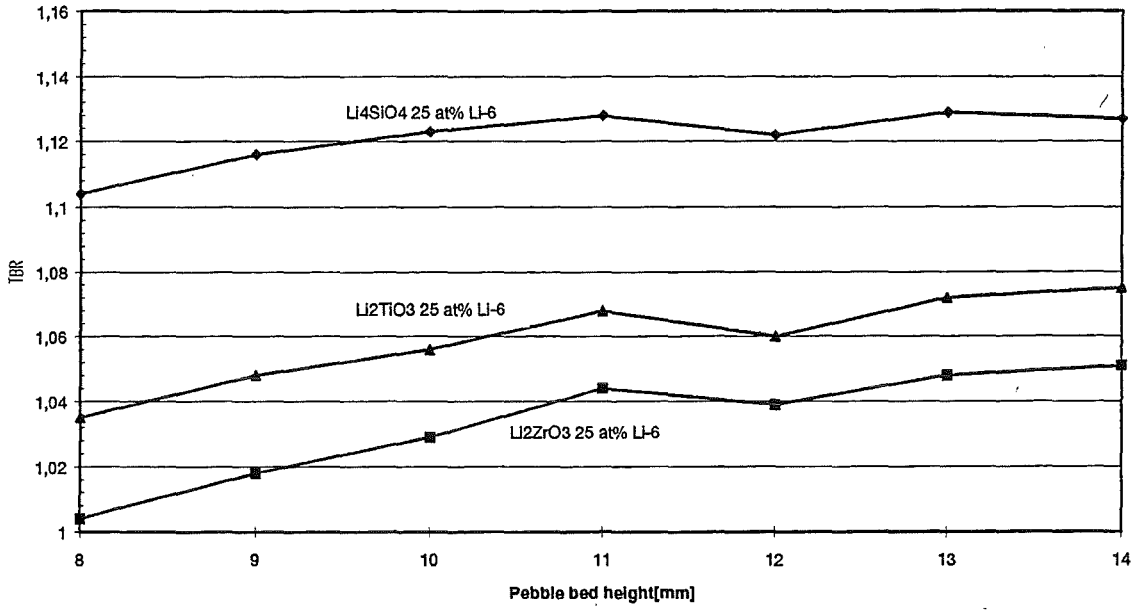

Power density in central outboard segment of HCPB Demo blanket
- Li4SiO4, 25 at% Li6, 9 mm pebble bed height, MANET -

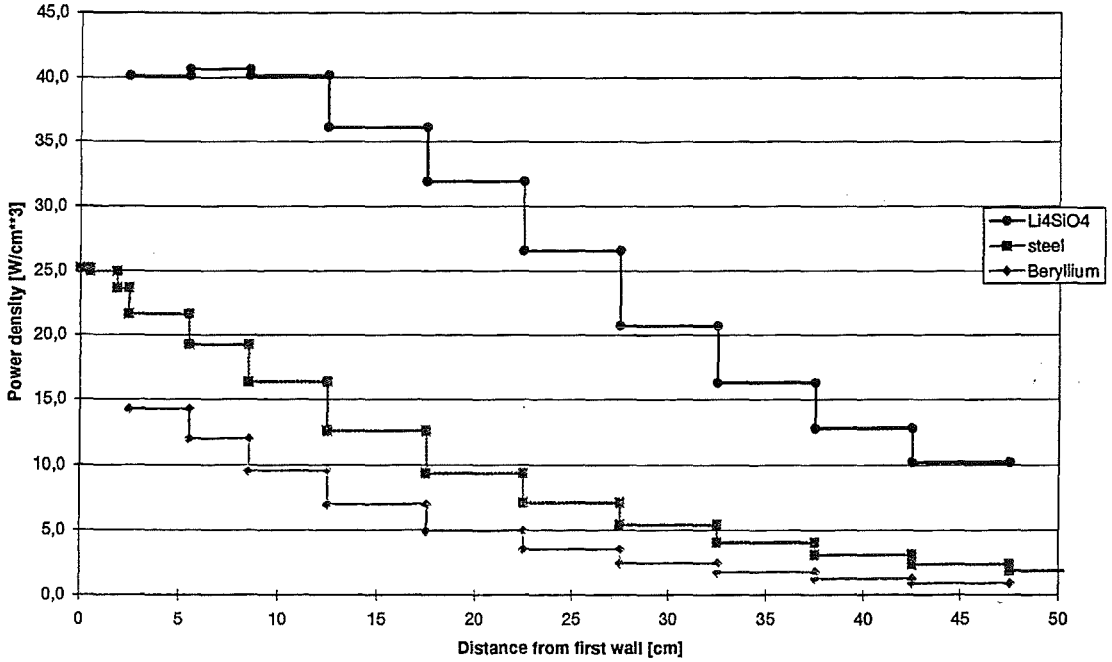

U. Fischer, 19.01.98

Application Area II: ITER Test Blanket Design

(ITER project, Test Blanket Programme)

Objective: Test and Validation in ITER of a Blanket Concept Relevant to Demo

Design & evaluation of a module using 3d ITER torus sector model including test blanket port and modules.

- **EU HCPB Test Blanket Module**
  - Tritium generation in module
    Online tritium recovery + post-irradiation release
  - Thermal-hydraulic & mechanical layout
    Heat removal, attachment, maintenance
  - Shielding analysis for port section
    Deep penetration + streaming through gap

Specific issue:

- Possibility of Validation of Code & Data in Complex Configuration (tokamak + small size blanket module)
  $\Rightarrow$ *uncertainty in calculation (spectra & responses)*
  $\Rightarrow$ *uncertainty in experiment*
  $\Rightarrow C \pm \delta C$ *vs.* $E \pm \delta E$

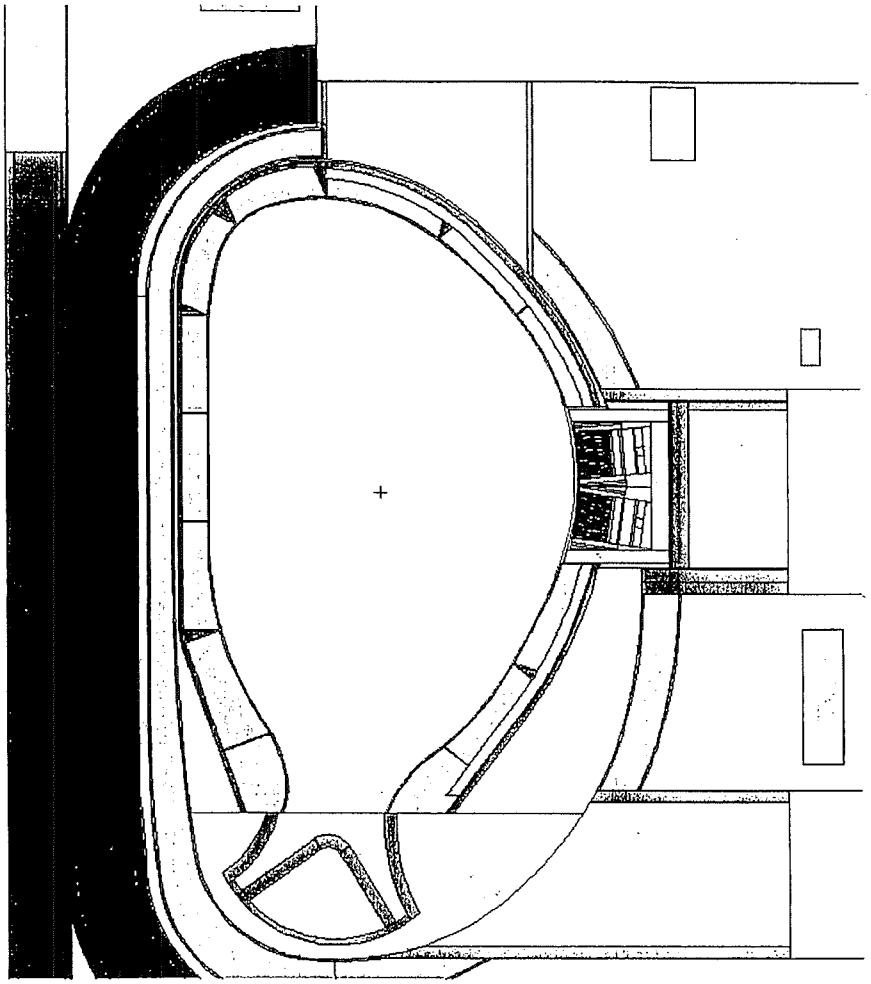

Shielding efficiency

Radiation loads to the TF-coil and the vacuum vessel at BTM first wall fluence of 1 MWa/m²

	HCPB BTM 3d -calculation	Radiation load limits
Vacuum vessel		
Helium production [appm]	0.09	1.0
TF-coil		
Peak dose to electrical insulator (Epoxy) [rad]	$9.4 \cdot 10^{7}$	$3 \cdot 10^{8}$
Peak displacement damage to copper stabiliser [dpa]	$2.2 \cdot 10^{-5}$	$6 \cdot 10^{-3}$
Peak fast neutron fluence (E>0.1 MeV) to the NB_3Sn superconductor [cm^{-2}]	$6.2 \cdot 10^{16}$	$1 \cdot 10^{19}$
Peak nuclear heating in winding pack [$mWcm^{-3}$]	0.03	1.0

H. Tsige-Tamirat, FZK-INR

Activation and afterheat calculations (TBM-I)

- **Code system for 3d activation calculations**
  - * **MCNP/FENDL-1**
    - ⇒ neutron transport calculations
  - * **FISPACT/EAF-4.1**
    - ⇒ activation inventory calculations
    - ⇒ EAF-4.1 (European Activation File) activation data
- **Irradiation conditions**
  - * continuous irradiation at full power (1500 MW) over 0.3 years
  - ⇒ 0.36 Mwa/m² first wall fluence
  - * structural material: EUROFER LA steel
  - * material compositions with minor elemental constituents & impurities

Volumes and masses of materials of TBM-I

	Volume [cm^3]	Mass[kg]
First wall protection layer (Be)	4.48E+03	8.31E+00
Neutron multiplier (Be)	2.95E+05	4.31E+02
Breeder (Li_4SiO_4)	5.18E+04	7.93E+01
EUROFER blanket structure (FW, cooling plates, side walls)	2.00E+05	1.56E+03
Top/bottom walls (EUROFER)	2.85E+05	2.22E+03
Support frame (SS- 316)	2.25E+06	1.79E+04
Back shield (EUROFER)	9.71E+05	7.57E+03

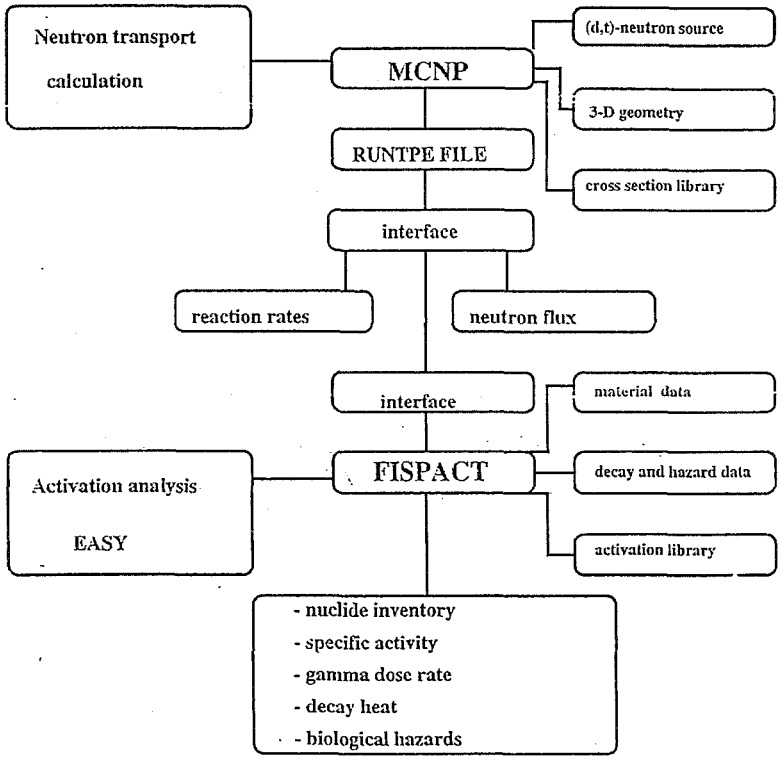

Application Area III: Nuclear Data Testing & Integral Experiments

(EFF/FENDL, ITER project)

Objectives:

- ***(1) Benchmark Testing and Qualification of Fusion Nuclear Data***
- ***(2) Validation of the Nuclear Performance of Engineering Design Systems***

Computational analyses of integral 14-MeV neutron experiments to arrive at C/E data for relevant nuclear responses.

(1) TU Dresden Iron Benchmark Experiment

EFF-project, Fusion Technology Programme

- 30 cm thick iron slab irradiated by 14-MeV neutrons
- Measurement of neutron & photon leakage spectra at 300 cm distance from slab
- C/E-comparison (full 3d model)
- Sensitivity/uncertainty analysis using MC Point Detector Sensitivities *(R. Perel, et al.)*

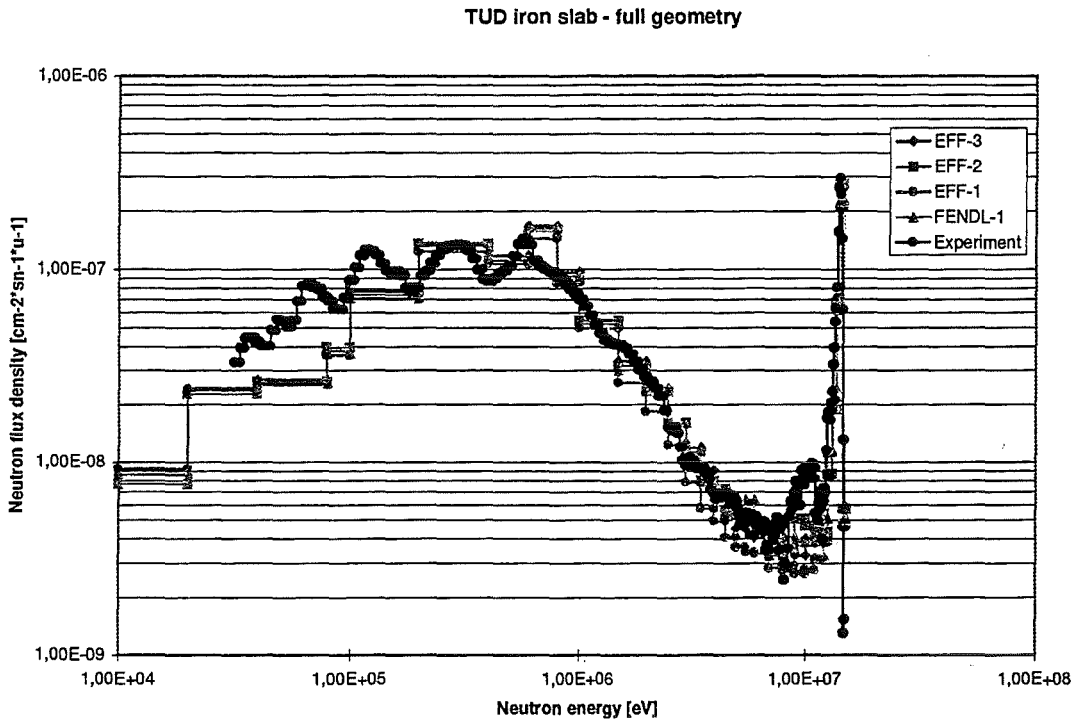

U. Fischer, 16.06.1997

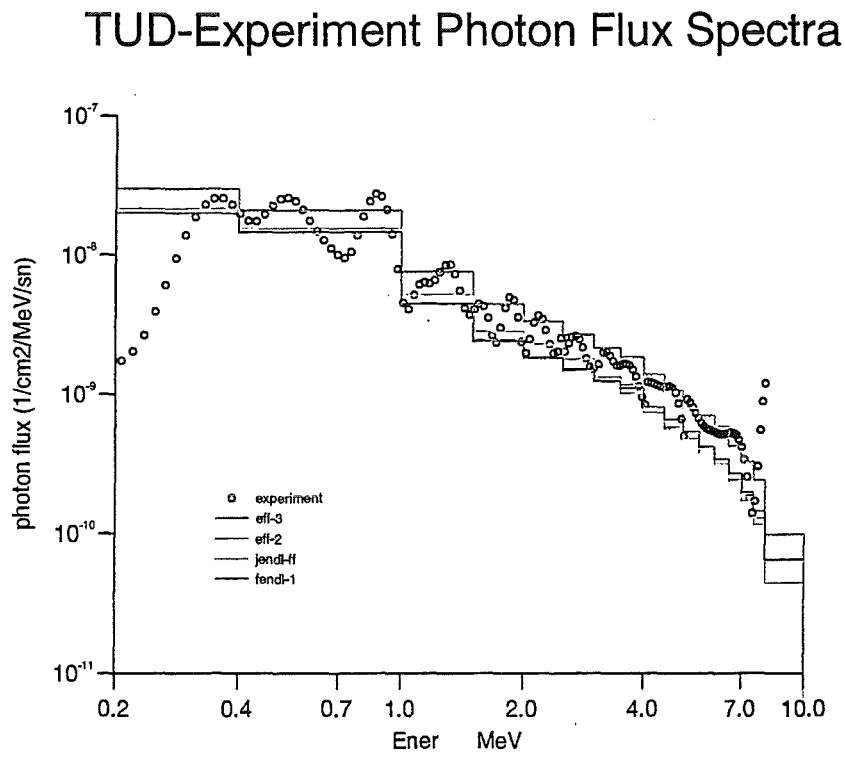

TUD iron slab experiment: C/E data for integrated neutron spectra
- Results based on MCNP4A calculations for full 3d geometry

Energy range [MeV]	TUD experiment	C/E				
		EFF-3	EFF-2	EFF-1	FENDL-1	JENDL-FF
0.1 - 1.0	$(2.56 \pm 0.28)\cdot10^{-7}$	1.037	1.015	0.944	0.990	1.028
1.0 - 5.0	$(4.51 \pm 0.21)\cdot10^{-8}$	0.993	0.975	0.826	0.944	0.920
5.0 - 10.0	$(3.42 \pm 0.19)\cdot10^{-9}$	0.739	0.899	0.637	0.953	0.877
E > 10.0	$(1.59 \pm 0.07)\cdot10^{-8}$	0.870	0.909	0.720	0.825	0.786
E > 0.1	$(3.2 \pm 0.31)\cdot10^{-7}$	1.021	0.980	0.913	0.980	1.00

TUD iron slab experiment: uncertainties in calculated neutron fluxes due to uncertainties in ^{56}Fe cross-section data and comparison to experimental data.

Results of 3d MC sensitivity calculations for point detector responses.

Energy interval [MeV]	EFF-2.4 MC calculation ideal geometry	EFF-3.0 MC calculation ideal geometry	EFF-3.0 MC calculation real geometry	TUD experiment Experimental uncertainty	TUD experiment EFF-3 C/E
<0.1	9	9	3	-	-
0.1-1	4	3	3	11	1.04
1-5	20	1.6	1.5	2.2	0.99
5-10	27	8	6	2.9	0.74
>10	19	4	4	1.9	0.87
total	4	3	2.5	-	-

Application Area III: Nuclear Data Testing & Integral Experiments (cont'd))

(2) ITER Bulk Shield Experiment at the Frascati Neutron Generator (FNG)

ITER project, Task T-218: Co-operation ENEA Frascati, TU Dresden, CEA Cadarache, FZK-Karlsruhe

- Mock-up of ITER inboard shield system (blanket, vacuum vessel+TF-coil)
- Irradiated by 14-MeV neutrons („point source")
- Various measurements: activation rates, fission rates, nuclear heating

  $\Rightarrow$ neutron + γ - spectra inside Mock-up
- C/E data for spectra & design relevant responses

  $\Rightarrow$ how well can we predict responses in design calculations ?

Specific issues:

$\Rightarrow$ *sensitivity to specific cross-section data*

$\Rightarrow$ *uncertainty in experiment & calculation*

$\Rightarrow$ *$C \pm \delta C$ vs. $E \pm \delta C$ $\Leftrightarrow$ design applications*

```
  03/22/96 17:31:42
fng neutron generator -
 shielding mock-up configuration
    uf. march 1996
probid =   03/22/96 17:26:45
basis:
( 1.000000,  .000000,  .000000)
(  .000000, 1.000000,  .000000)
origin:
(      .00,    60.00,      .00)
extent = (   100.00,   100.00)
```

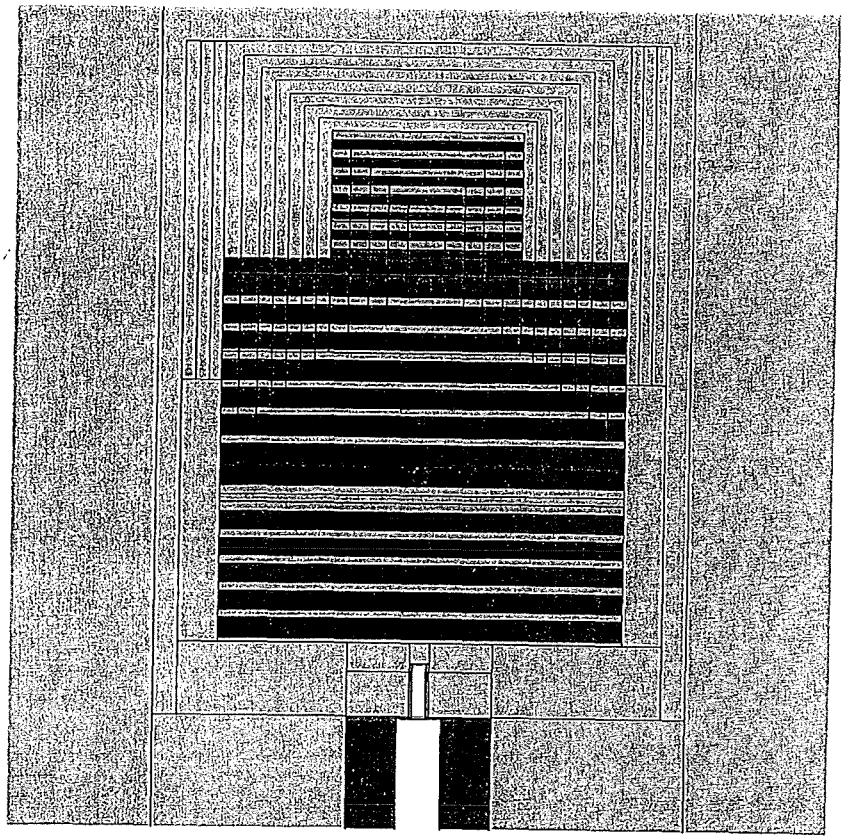

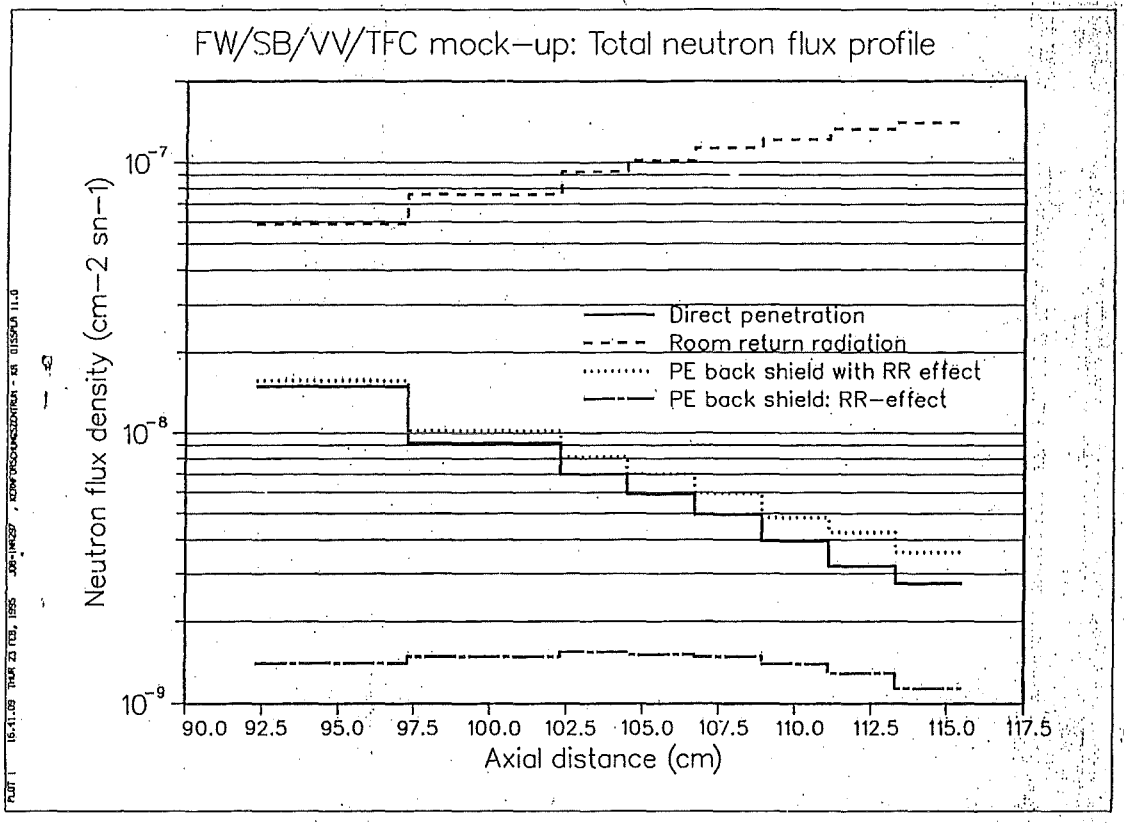

Central channel

FNG Gamma Flux Spectra (Position A)

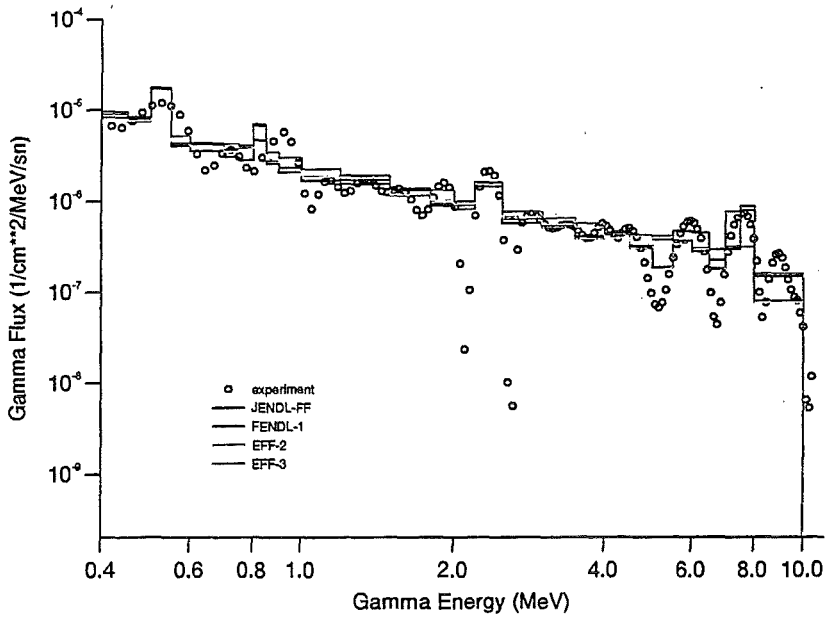

FNG Gamma Flux Spectra (Position B)

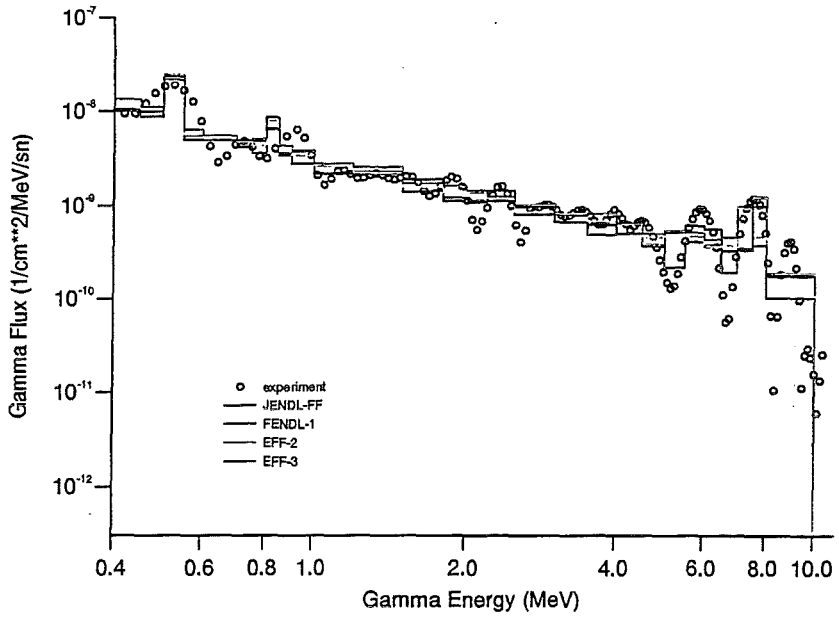

Position A: C/E data for integrated neutron spectra

Energy interval [MeV]	TUD experiment	C/E				Statistical error [%]
		EFF-3	EFF-2	FENDL-1	JENDL-FF	
0.1 - 1	$(2.76\pm0.28)\cdot10^{-6}$	0.90	0.91	0.86	0.89	0.06
1 - 5	$(1.43\pm0.08)\cdot10^{-6}$	0.95	0.99	0.91	0.89	0.08
5- 10	$(2.47\pm0.13)\cdot10^{-7}$	1.02	1.02	1.04	0.97	1.0
E > 10 MeV	$(5.42\pm0.14)\cdot10^{-7}$	0.99	0.98	0.99	1.00	0.9
E > 0.1 MeV	$5.74\cdot10^{-6}\pm6.1\%$	0.94	0.94	0.88	0.91	0.4

Position B: C/E data for integrated neutron spectra

Energy interval [MeV]	TUD experiment	C/E				Statistical error [%]
		EFF-3	EFF-2	FENDL-1	JENDL-FF	
0.1 - 1	$(8.78\pm0.89)\cdot10^{-9}$	0.73	0.74	0.68	0.73	0.08
1 - 5	$(2.37\pm0.13)\cdot10^{-9}$	0.84	0.86	0.77	0.78	0.09
5- 10	$(2.69\pm0.14)\cdot10^{-10}$	1.07	1.07	0.99	0.97	1.5
E > 10 MeV	$(5.79\pm0.15)\cdot10^{-10}$	0.87	0.87	0.81	0.83	1.5
E > 0.1 MeV	$1.20\cdot10^{-8}\pm7.5\%$	0.77	0.77	0.72	0.77	0.7

Application Area IV: Neutron Sources for Fusion Material Irradiations

Objective: Design & Development Qualification of Fusion Nuclear Data

Design analyses & optimisation with regard to the needs of fusion material research (neutron fluences, radiation damage & gas production)

(1) International Fusion Material Irradiation Facility (IFMIF)

IEA-activity, EU Fusion Technology Programme

- Accelerator-based d-Li neutron source
- d(Li,xn) source function ⇒ neutron yield
- Irradiation characteristics: dpa & gas production
- Data base development $E \geq 20$ MeV neutron energy ⇒ transport + activation/transmutation

(2) Gas Dynamic Trap Neutron Source

- Nuclear assessment & design of test assembly
- Irradiation characteristics: dpa & gas production
- Shielding analysis

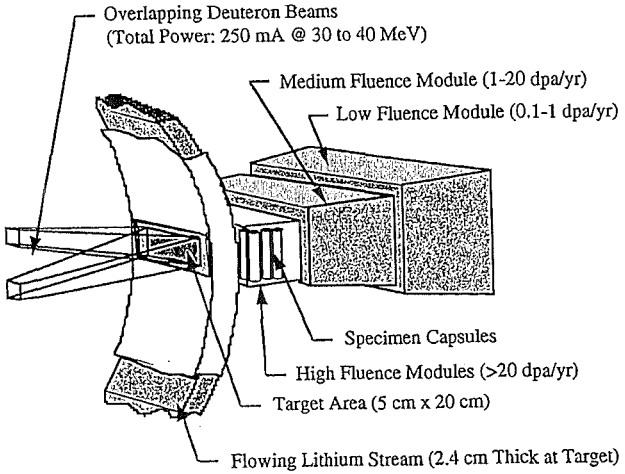

Interface of IFMIF facilities in Test Cell

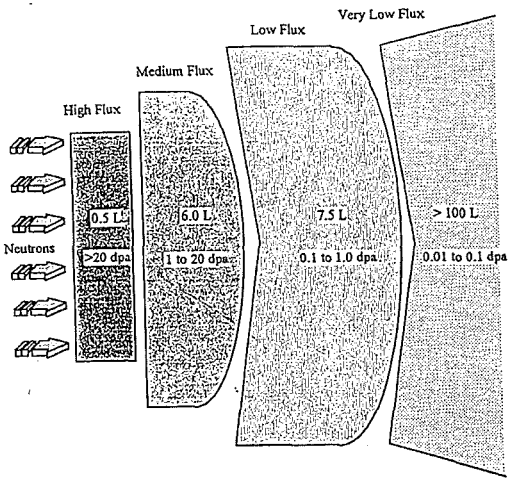

Test Cell Configuration

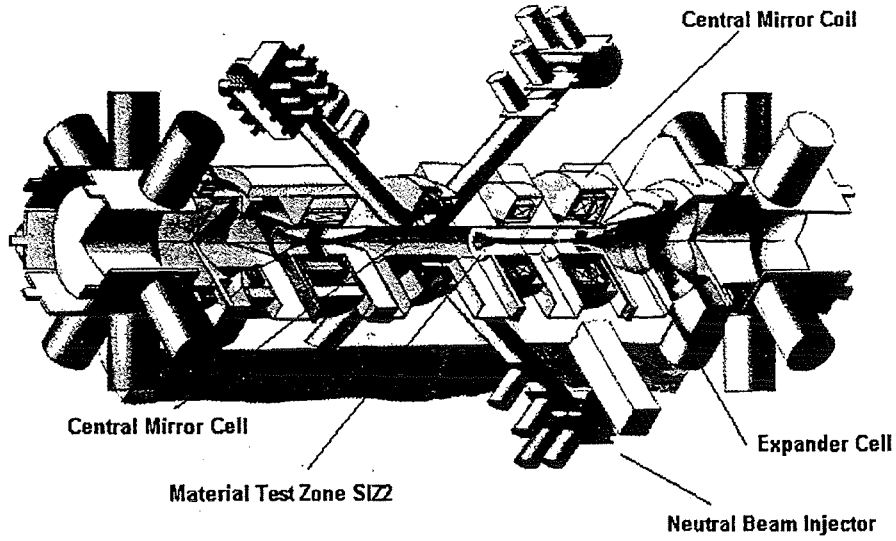

Gas Dynamic Trap (GDT) Neutron Source

GDT - Neutron Source
Elevation view of the tubular test assembly

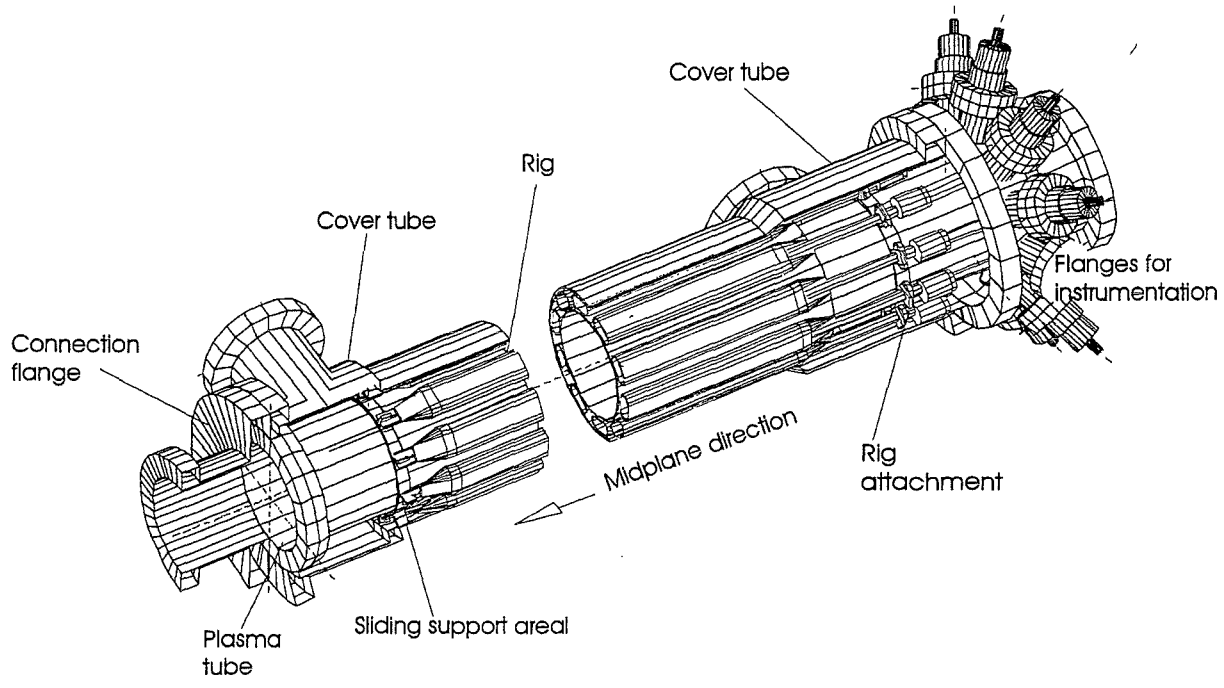

Fig.2 Comparison of first wall neutron spectra in ITER, IFMIF and GDT-NS

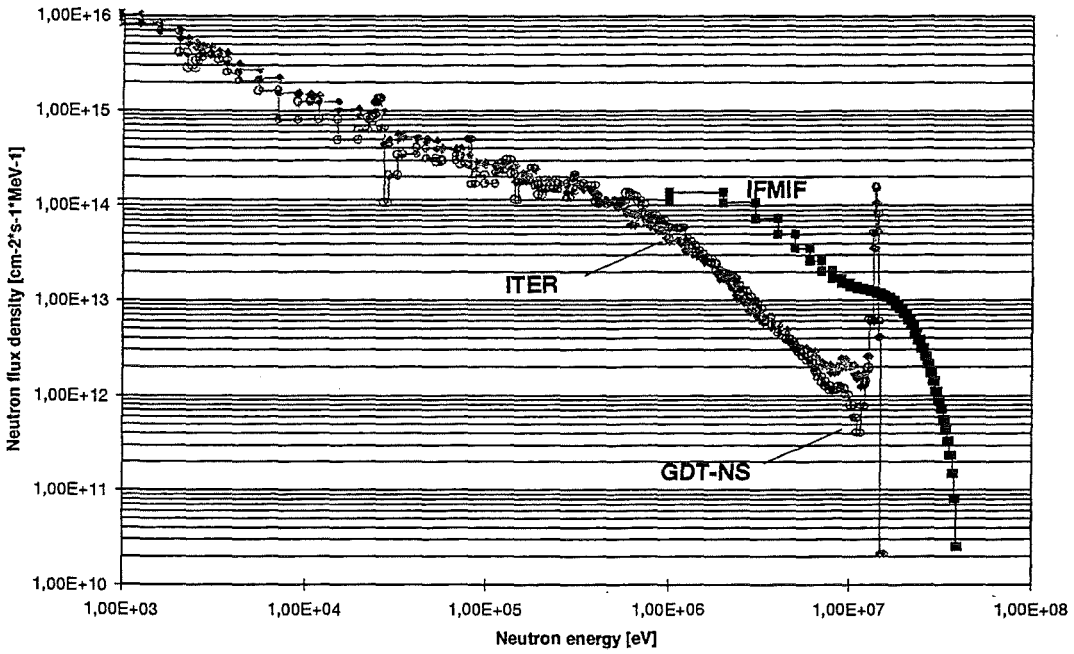

U. Fischer, 14.10.1997

Dpa rate in iron of GDT material test zone SIZ2

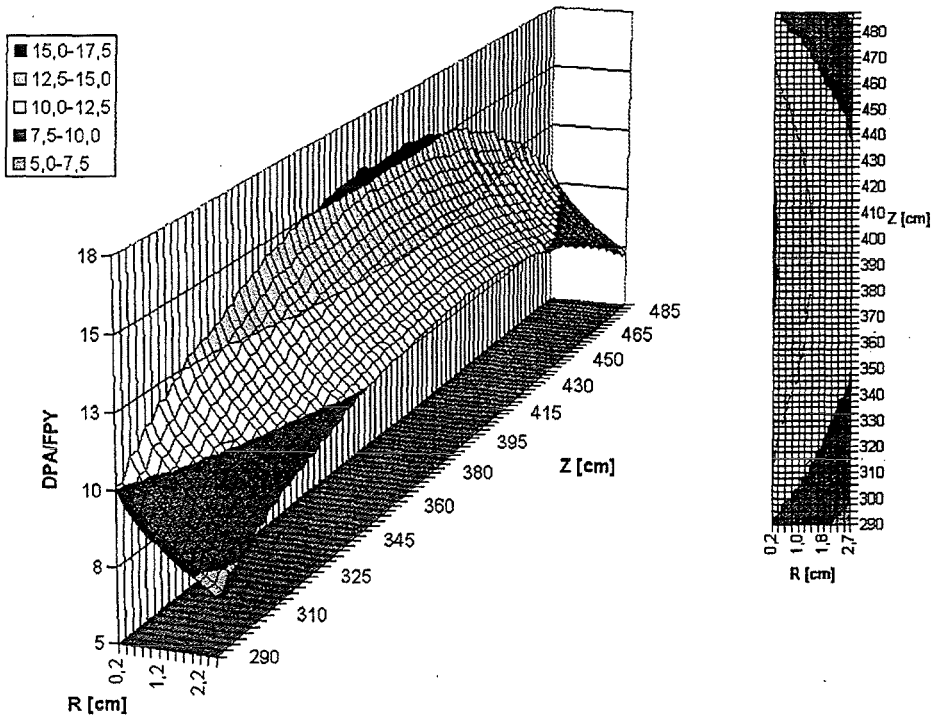

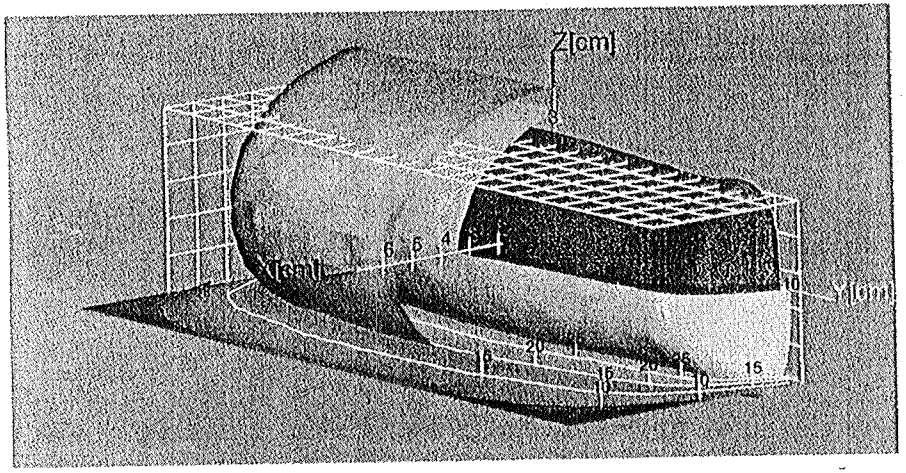

IFMIF DPA Isosurfaces

green = 20 dpa/fpy
yellow = 30 dpa/fpy
red = 40 dpa/fpy

Development Goals for Applications in Fusion Neutronics

- **Full MC based sensitivity calculations**
  - Track length + point detector estimators
  - Secondary distributions
  - No restrictions in geometry

  ⇒ MC based assessment of data related uncertainties in design calculations (tokamak)

  ⇒ Checking against experiments (uncertainty)

  ⇒ Use of double randomization technique ?

- **Use of CAD-generated geometry models**

  ⇒ easy & flexible transition of technical drawing to MC model

  ⇒ easy model modifications

- **Full 3d- burn-up calculations**

  ⇒ 3d activation system MCNP/FISPACT (existing)

  ⇒ feed back of nuclide inventory to into MCNP

Co-workers at FZK

E. Daum, M. Sokcic-Kostic, D. Leichtle, H. Tsige-Tamirat, E. Wiegner, P. Wilson, D. Woll, U. v. Möllendorff, A. Möslang

Co-operations

EU: ENEA Frascati & Bologna, TU Dresden, CEA Saclay & Cadarache, UKAEA Culham, ECN Petten, IRK Vienna

International: ITER JCT, JAERI Tokai-mura, ASIPP Hefei, University Jerusalem, University of Ljubljana, INP/IPPE Obninsk, BINP Novosibirsk, IAEA/NDS

Projects

Nuclear Fusion Project (FZK)

European Fusion Technology Programme (EU)
(EFF, ITER, Long-term Programme on Demo Blanket Development & Materials)

FENDL (IAEA/NDS)

U. Fischer, A. Möslang, A. A. Ivanov: Assessment of the Gas Dynamic Trap Mirror Facility as Intense Neutron Source for Fusion Material Test Irradiations, 6. IAEA Technical Committee Meeting on Fusion Power Plant Design and Technology, Culham, 24 - 27 March 1998

Y. Wu, U. Fischer, Integral Data Tests of the FENDL-1, EFF-2, EFF-3 and JENDL-FF-Fusion Nuclear Data Libraries, Forschungszentrum Karlsruhe, Wissenschaftliche Berichte FZKA-5953, Februar 1998.

U. Fischer et al.: International Benchmark Tests of the FENDL-1 Nuclear Data Library, Fusion Engineering & Design 37 (1997),9-21.

H. Tsige-Tamirat, U. Fischer, Three-dimensional Activation and Afterheat Analyses for the Dual Collant Breeder Blanket, Forschungszentrum Karlsruhe, Wissenschaftliche Berichte FZKA-5675, Januar 1996.

U. Fischer, M. Dalle Donne, Three-dimensional Neutronics Analysis of the European HCPB Blanket Test Module in ITER, 4th Int. Symp. on Fusion Nuclear Technology, Tokyo, Japan, April 6 - 11, 1997.

H. Freiesleben, W. Hansen, D. Richter, K. Seidel, S. Unholzer, U. Fischer, Y. Wu, Neutron and Photon Flux Spectra in a Mock-up of the ITER Shielding System, 4th Int. Symp. on Fusion Nuclear Technology, Tokyo, Japan, April 6 - 11, 1997

E. Daum, U. Fischer, A. Yu. Konobeyev, Yu. A. Korovin, V.P. Lunev, U. von Möllendorff, P. E. Pereslavtsev, M. Sokcic-Kostic, A. Yu. Stankovsky, P. Wilson D. Woll: Neutronics of the High Flux Test Region of the International Fusion Materials Irradiation Facility (IFMIF), FZKA-5868 (1997)

Workshop on „Monte Carlo Methods and Models for Applications in Energy and Technology",
Forschungszentrum Karlsruhe, May 12-14, 1998. http://inrwww.fzk.de/mc-workshop

Monte Carlo Methods and Models for Applications
in Energy and Technology

Workshop to be held at Forschungszentrum Karlsruhe, May 12-14, 1998

Monte Carlo Sensitivity Analysis of Deep-Penetration Benchmarks to Iron Cross Sections

R. L. Perel, J.J. Wagschal and Y. Yeivin

Racah Institute of Physics
The Hebrew University of Jerusalem
91904 Jerusalem, Israel

ABSTRACT

The evaluation of radiation damage in stainless-steel reactor pressure vessels requires reliable iron cross sections. However, cross sections in general, and those of iron in particular, in even the more recent evaluated-cross-section libraries are not yet reliable enough to satisfy the needs of user communities. In the analysis of any problem involving the calculation of physical quantities (?responses?) which are functions of cross sections (?parameters?), an essential element is the evaluation of the partial derivatives, i.e. the sensitivities of each response to every parameter. Sensitivities are necessary for determination of uncertainties in the calculated responses, for assessment of consistency of all the given (differential and integral) data, and for adjustment.

We have recently formulated an algorithm for Monte Carlo calculation of point- detector sensitivities to material parameters, and applied this algorithm to evaluate the sensitivities in three different types of deep penetration benchmark experiments characterized by measurement of the neutron leakage (or a functional of it) from an iron sphere driven by a (pulsed or continuous) neutron source at its center. The experiments analyzed were: Livermore iron spheres pulsed by 14 MeV neutrons, and the Czech NRI and the NIST iron spheres, driven by Cf-252 sources. Following a brief description of the experiments, the sensitivity analyses of the time-of-flight spectrum of leakage from the Livermore pulsed sphere, the energy spectrum leaking from the NRI sphere and of various fission-rate ratios in the neutron field outside the NIST sphere are elaborated. As one of the results of the analysis, we propose alternative experiments, which are more sensitive to differences in some important iron cross sections.

Last modified: Thu Apr 2 13:53:28 1998

Monte Carlo Sensitivity Analysis of Deep-Penetration Benchmarks to Iron Cross Sections

Reuven L. Perel
Jehudah J. Wagschal
Yehuda Yeivin

Racah Institute of Physics
The Hebrew University of Jerusalem
91904 Jerusalem
Israel

Iron-Sphere Leakage Experiments:

Experiment	Source	Response measured
Livermore pulsed sphere	14-Mev - pulsed	Flux time of flight spectrum
Czech sphere	Cf-252 - continuous	Flux energy- spectrum
NIST sphere	Cf-252 - continuous	Energy × flux energy-spectrum Fission rate ratio

Sensitivity analysis:

- Guidance for planning experiments
- Evaluation of cross sections
- Adjustment

Main Iron Isotope: Fe-56

Elastic scattering:

maximal energy loss: 6.9%
(for E=1.5 MeV: ≈ 100 keV)

1st level inelastic scattering:

Q-value: -847 keV

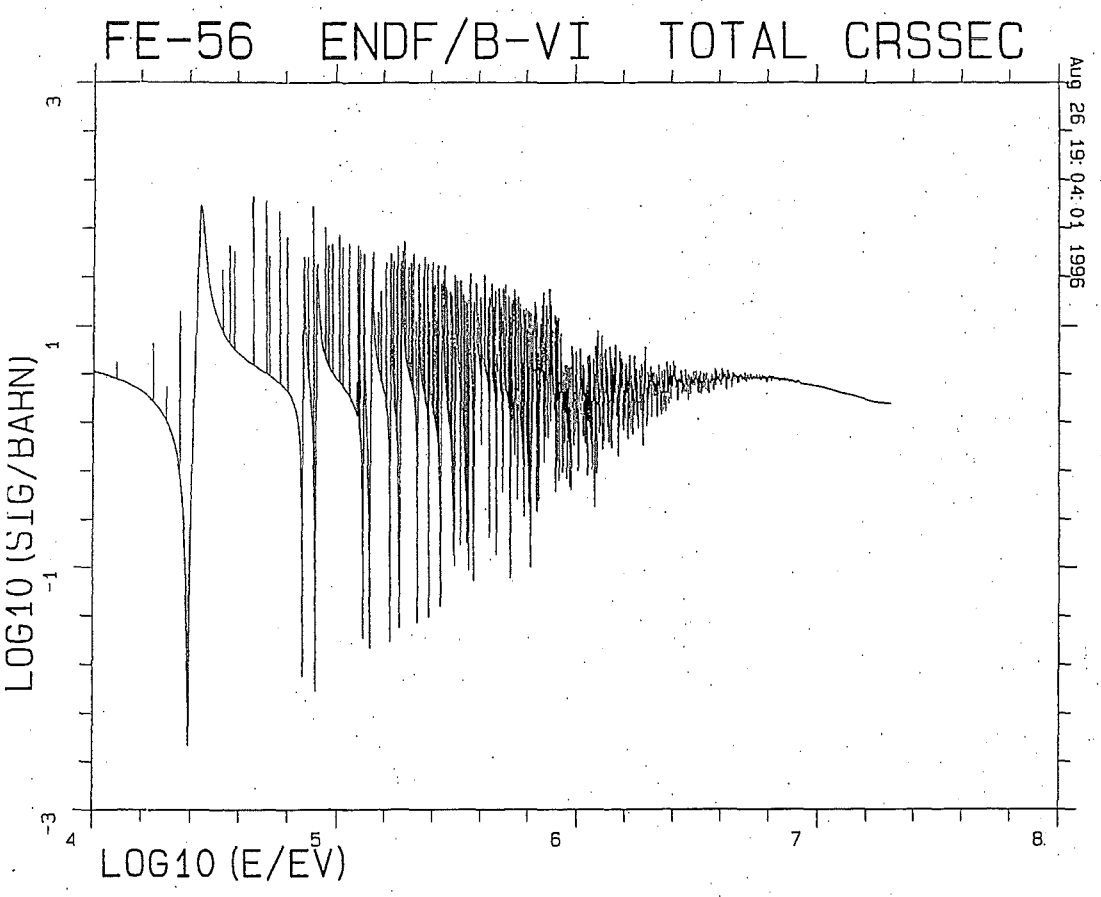

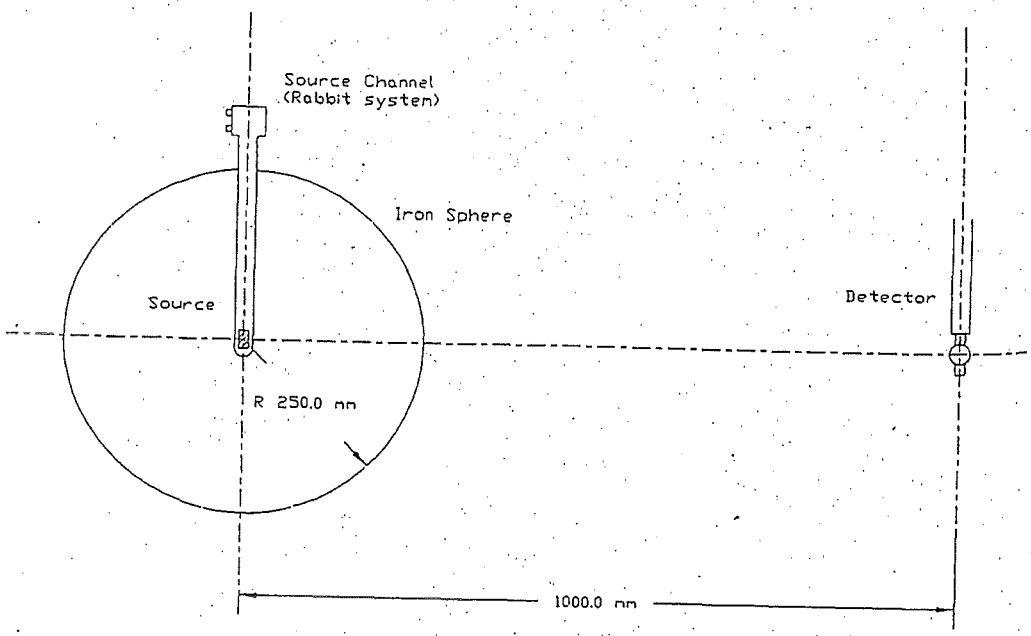

Fig. 1. Experimental setup.

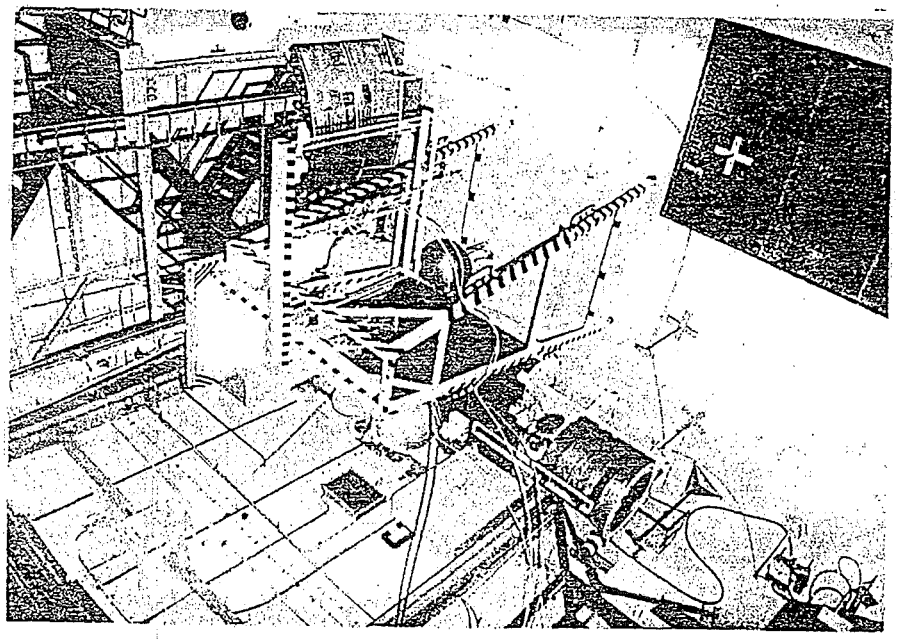

Fig. 11 Laboratory of neutron measurements in LR-0 reactor hall, iron cylindrical (alab) assembly, iron sphere of 50 cm diameter in measurement position (height 200 cm)

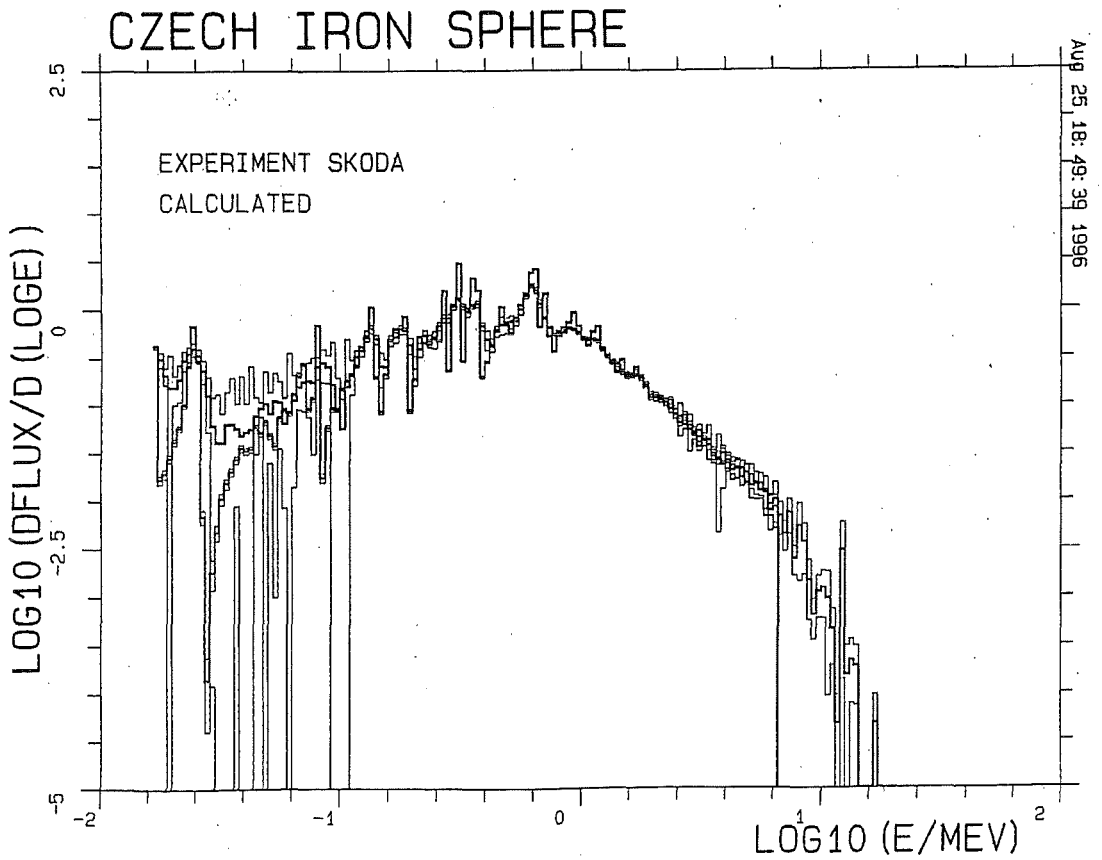

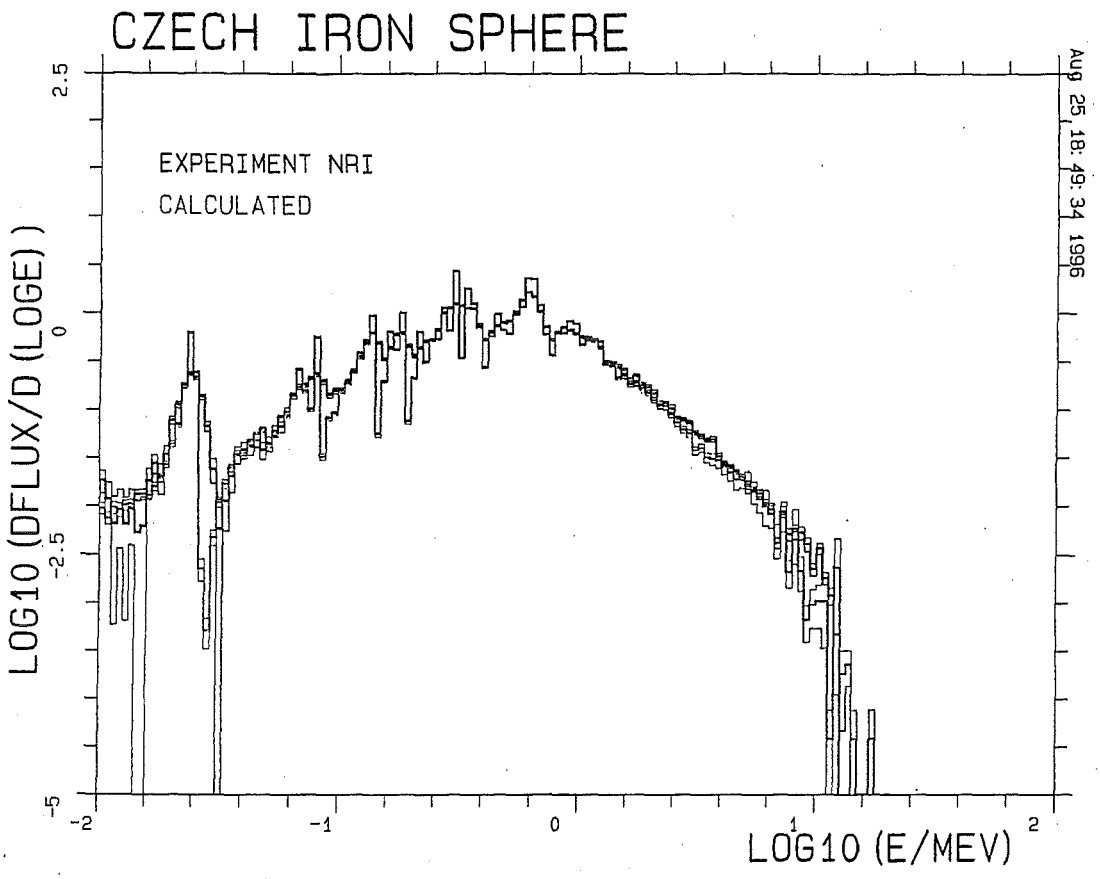
CZECH IRON SPHERE
EXPERIMENT NRI
CALCULATED
Aug 25 18:49:34 1996
LOG10 (DFLUX/D (LOGE))
LOG10 (E/MEV)
2.5
0
-2.5
-5
-2
-1
0
1
2

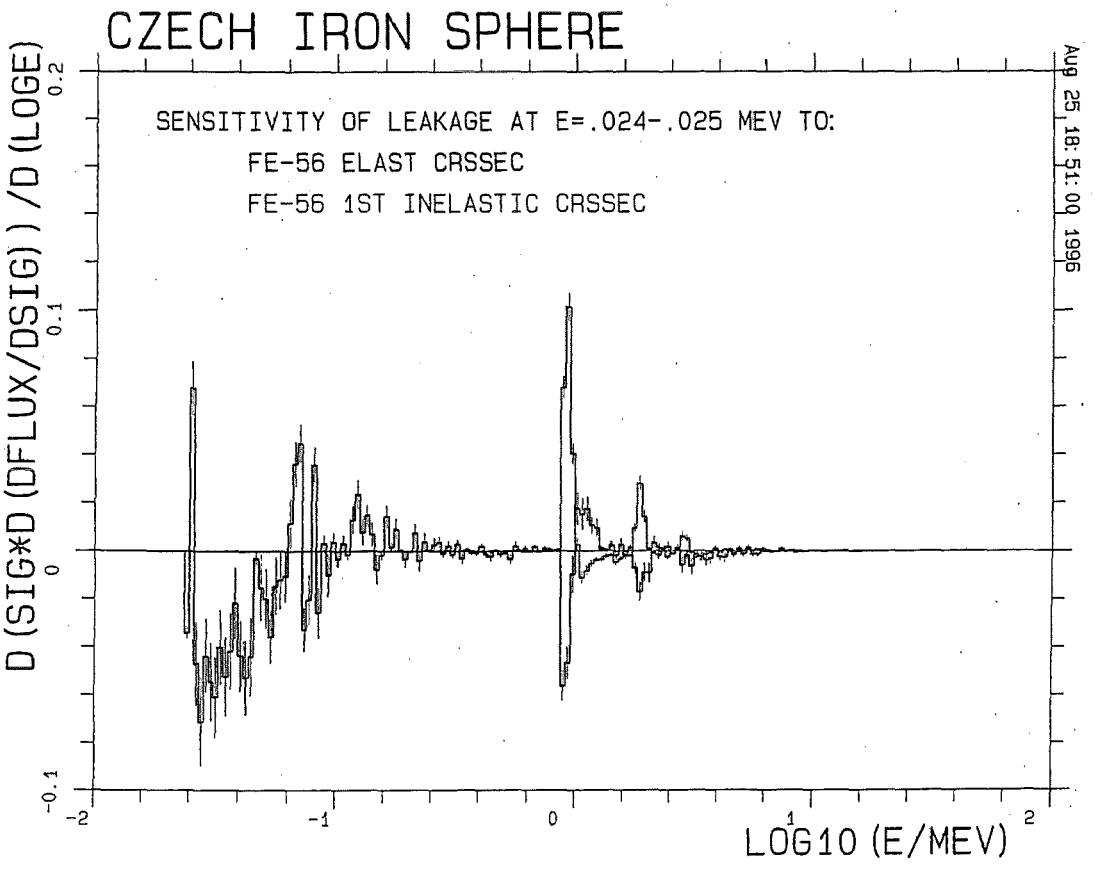
CZECH IRON SPHERE
SENSITIVITY OF LEAKAGE AT E=.024-.025 MEV TO:
FE-56 ELAST CRSSEC
FE-56 1ST INELASTIC CRSSEC
Aug 25 18:51:00 1996
D (SIG*D (DFLUX/DSIG)) /D (LOGE)
LOG10 (E/MEV)
0.2
0.1
0
-0.1
-2
-1
0
1
2

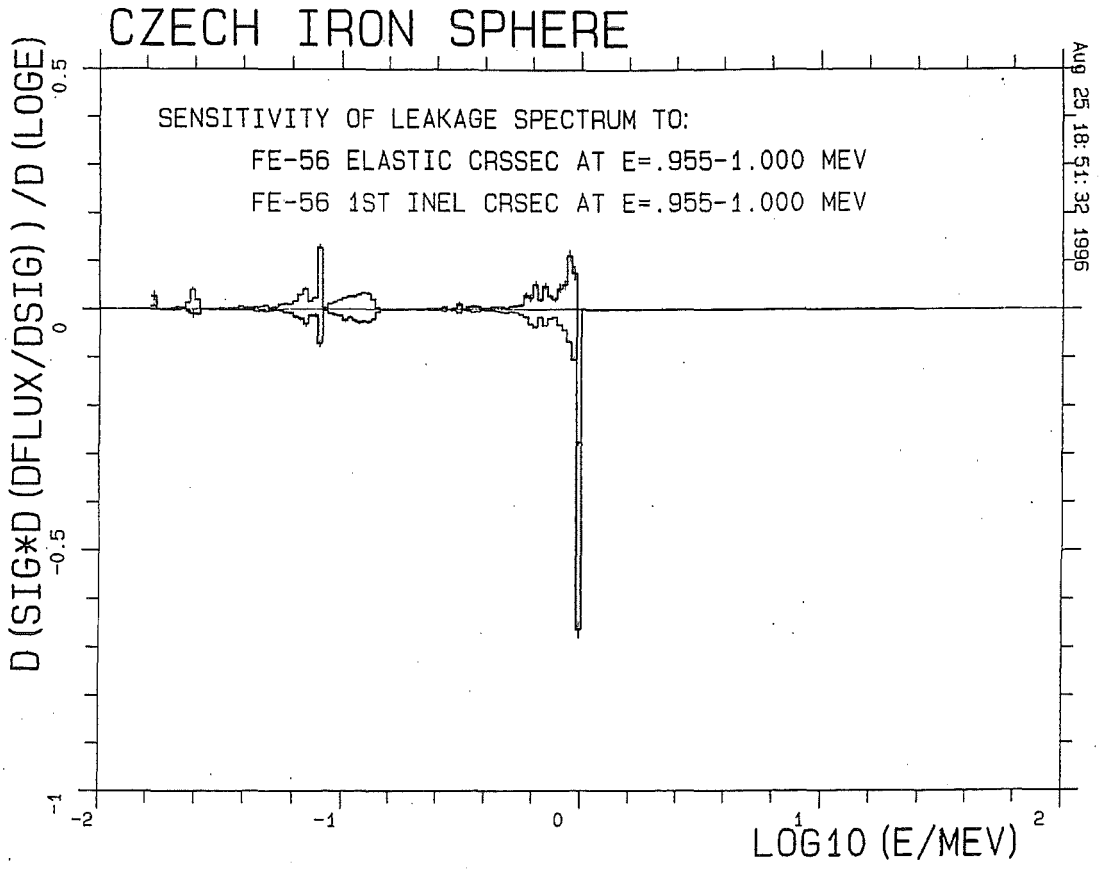
CZECH IRON SPHERE
SENSITIVITY OF LEAKAGE SPECTRUM TO:
FE-56 ELASTIC CRSSEC AT E=.955-1.000 MEV
FE-56 1ST INEL CRSEC AT E=.955-1.000 MEV
Aug 25 18:51:32 1996
D (SIG*D (DFLUX/DSIG)) /D (LOGE)
LOG10 (E/MEV)
0.5
0
-0.5
-1
-2
-1
0
1
2

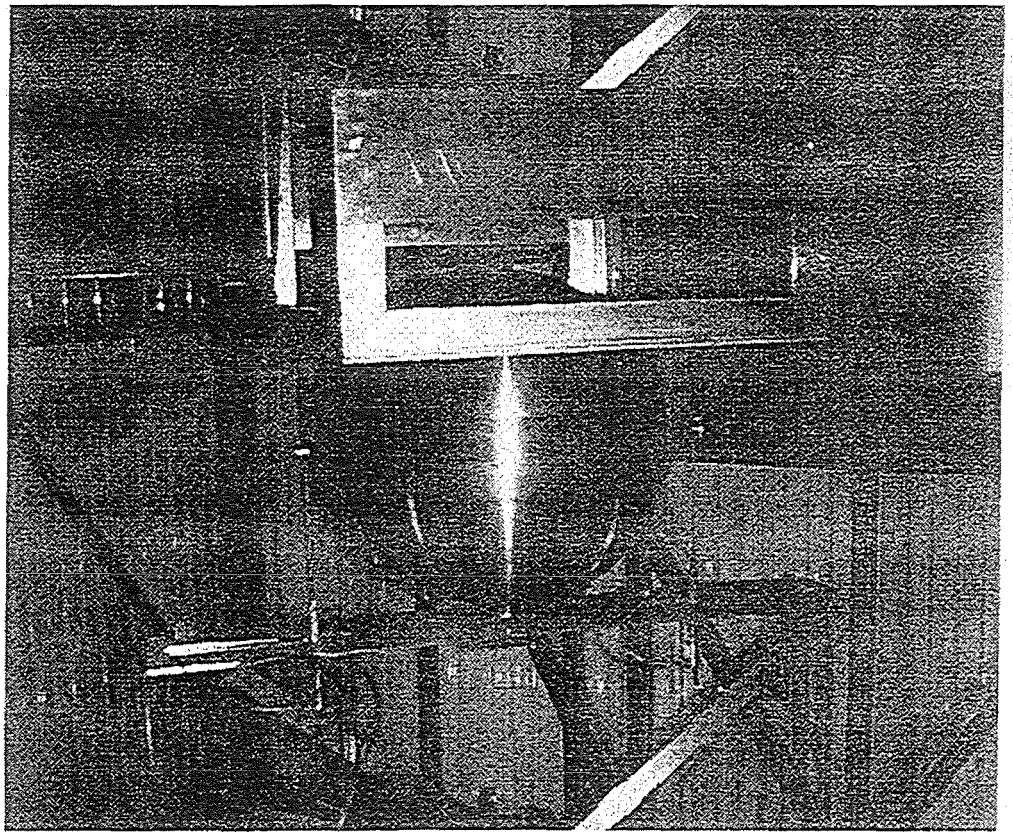

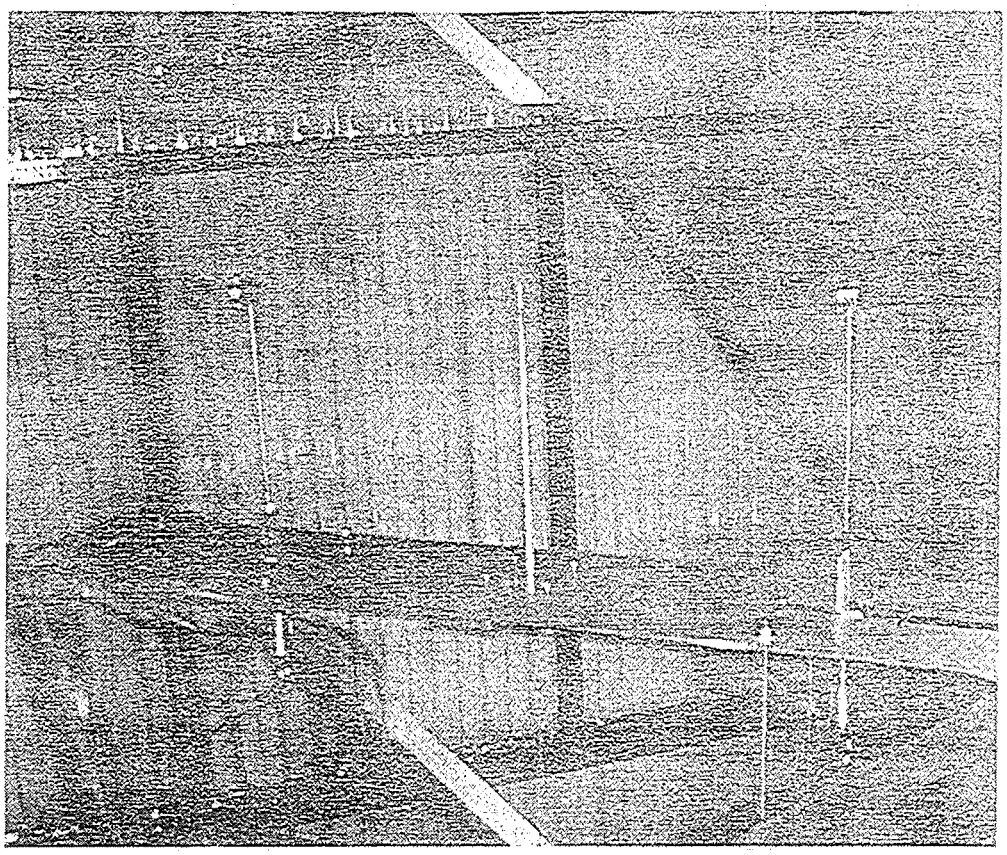

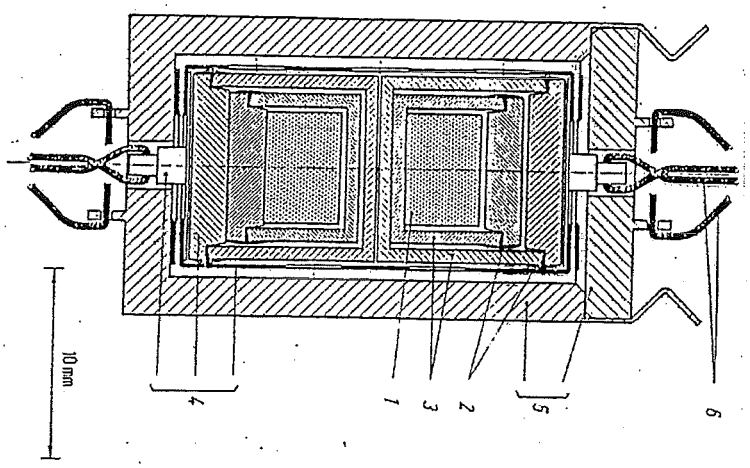
10mm
4
1
3
2
5
6

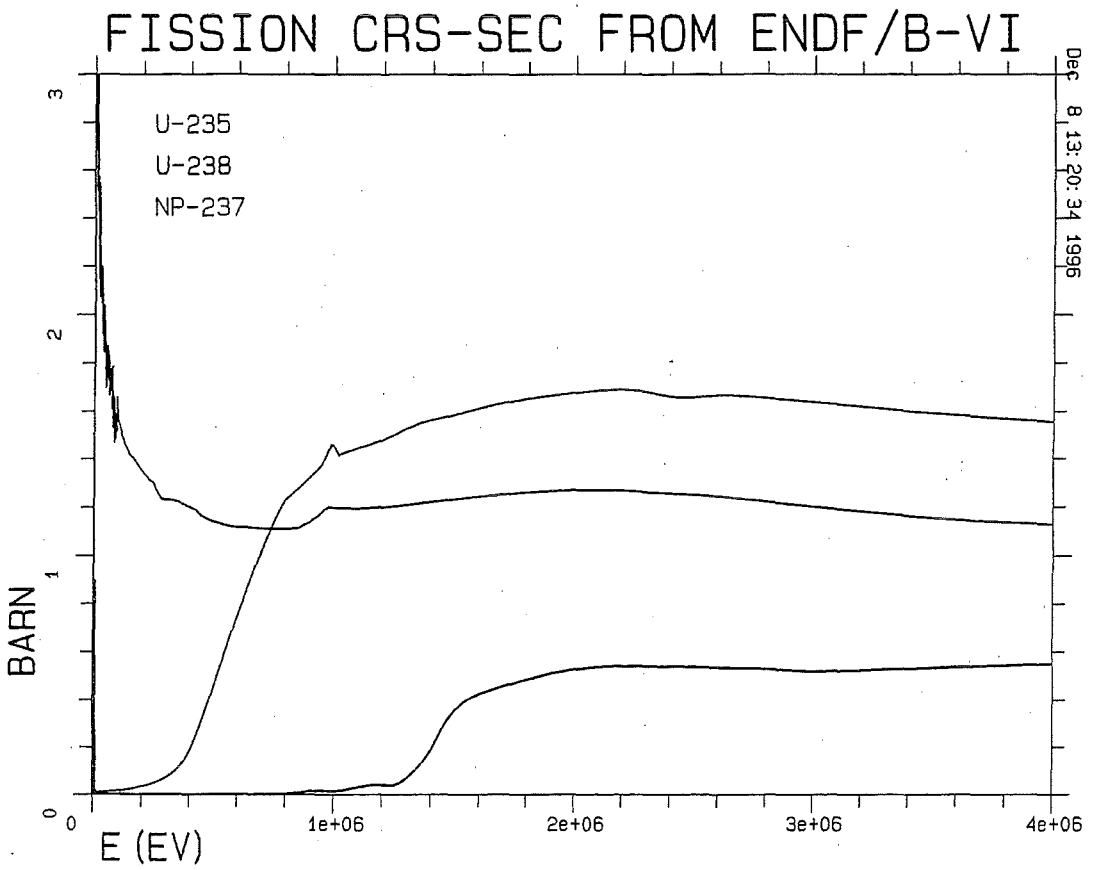

Relative Sensitivity of Reaction Rate Ratio:

$$\frac{\sigma}{(r_1/r_2)}\frac{\partial(r_1/r_2)}{\partial\sigma} = \frac{\sigma}{r_1}\frac{\partial r_1}{\partial\sigma} - \frac{\sigma}{r_2}\frac{\partial r_2}{\partial\sigma}$$

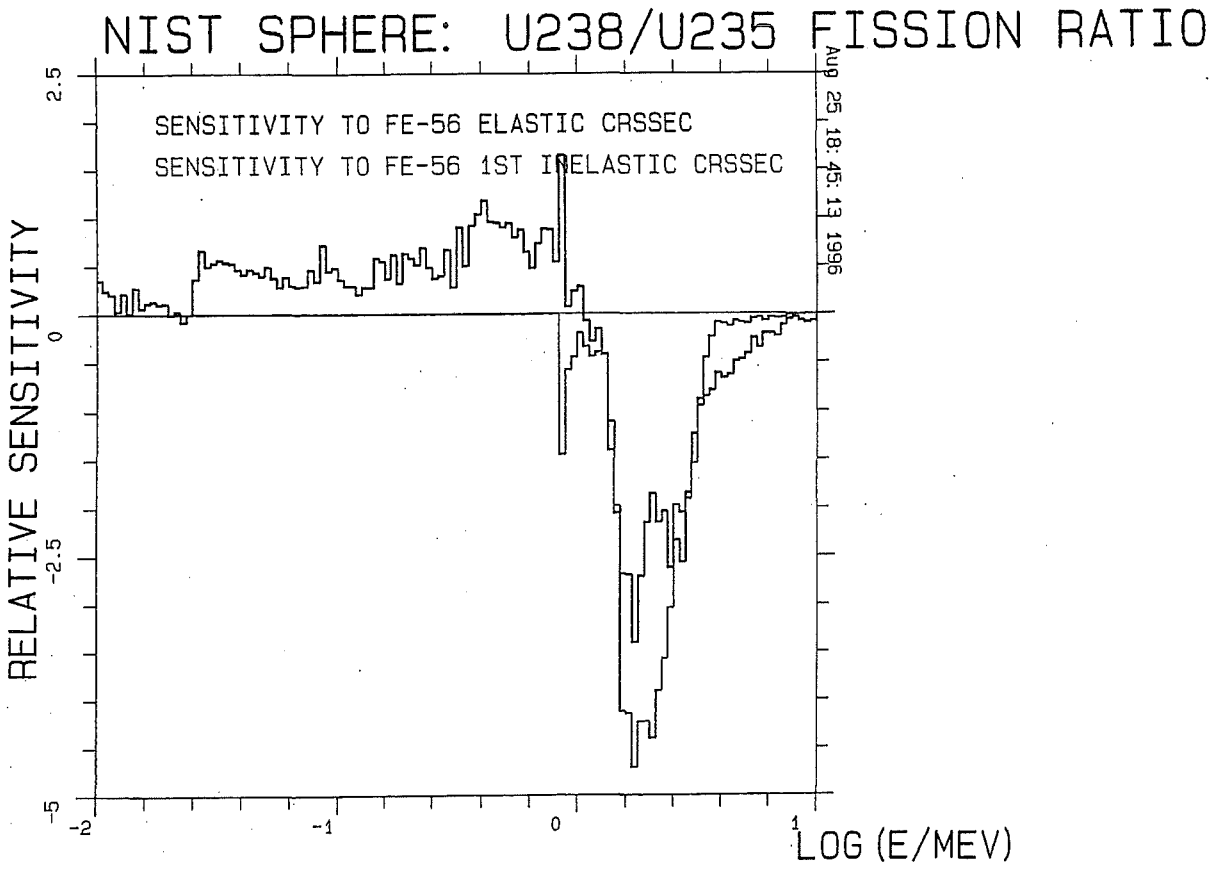
NIST SPHERE: U238/U235 FISSION RATIO
SENSITIVITY TO FE-56 ELASTIC CRSSEC
SENSITIVITY TO FE-56 1ST INELASTIC CRSSEC
Aug 25 18:45:13 1996
RELATIVE SENSITIVITY
2.5
0
-2.5
-5
-2
-1
0
1
LOG (E/MEV)

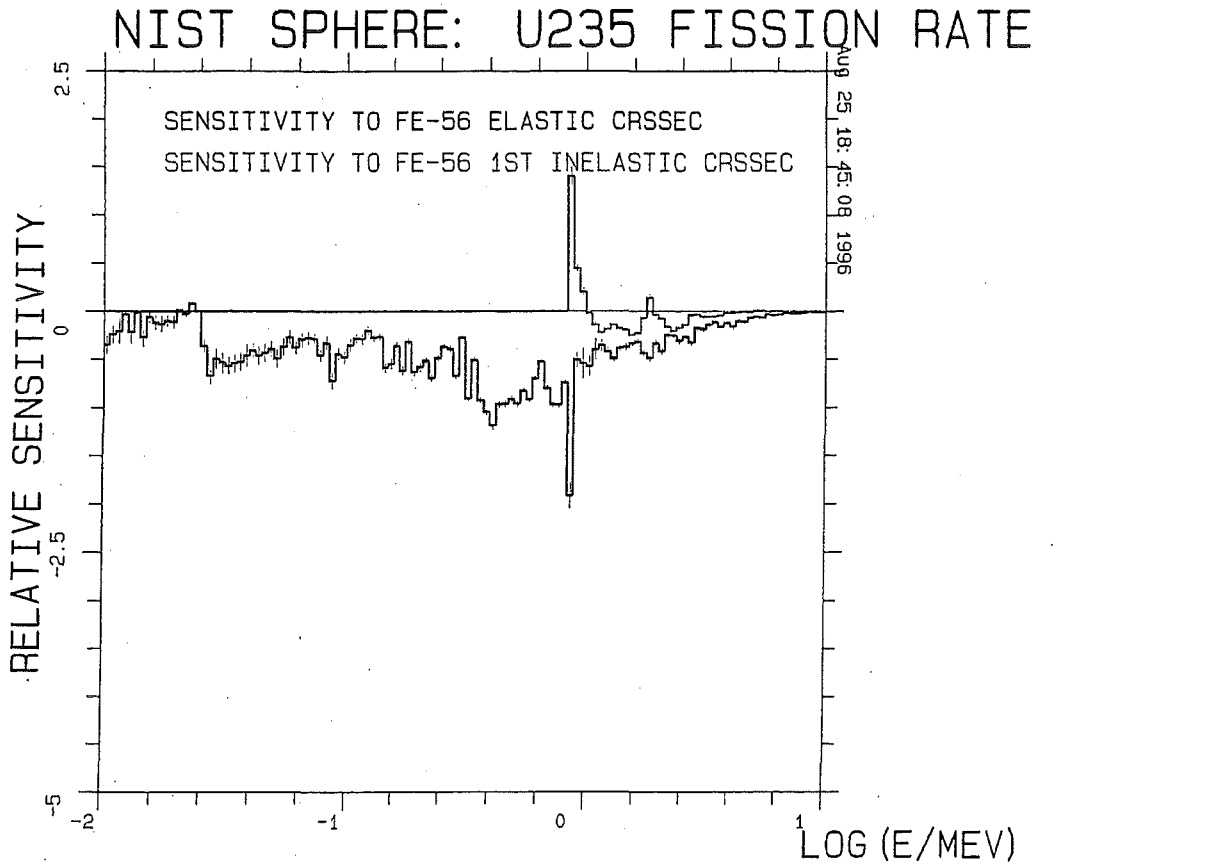
NIST SPHERE: U235 FISSION RATE
SENSITIVITY TO FE-56 ELASTIC CRSSEC
SENSITIVITY TO FE-56 1ST INELASTIC CRSSEC
Aug 25 18:45:08 1996
RELATIVE SENSITIVITY
2.5
0
-2.5
-5
-2
-1
0
1
LOG (E/MEV)

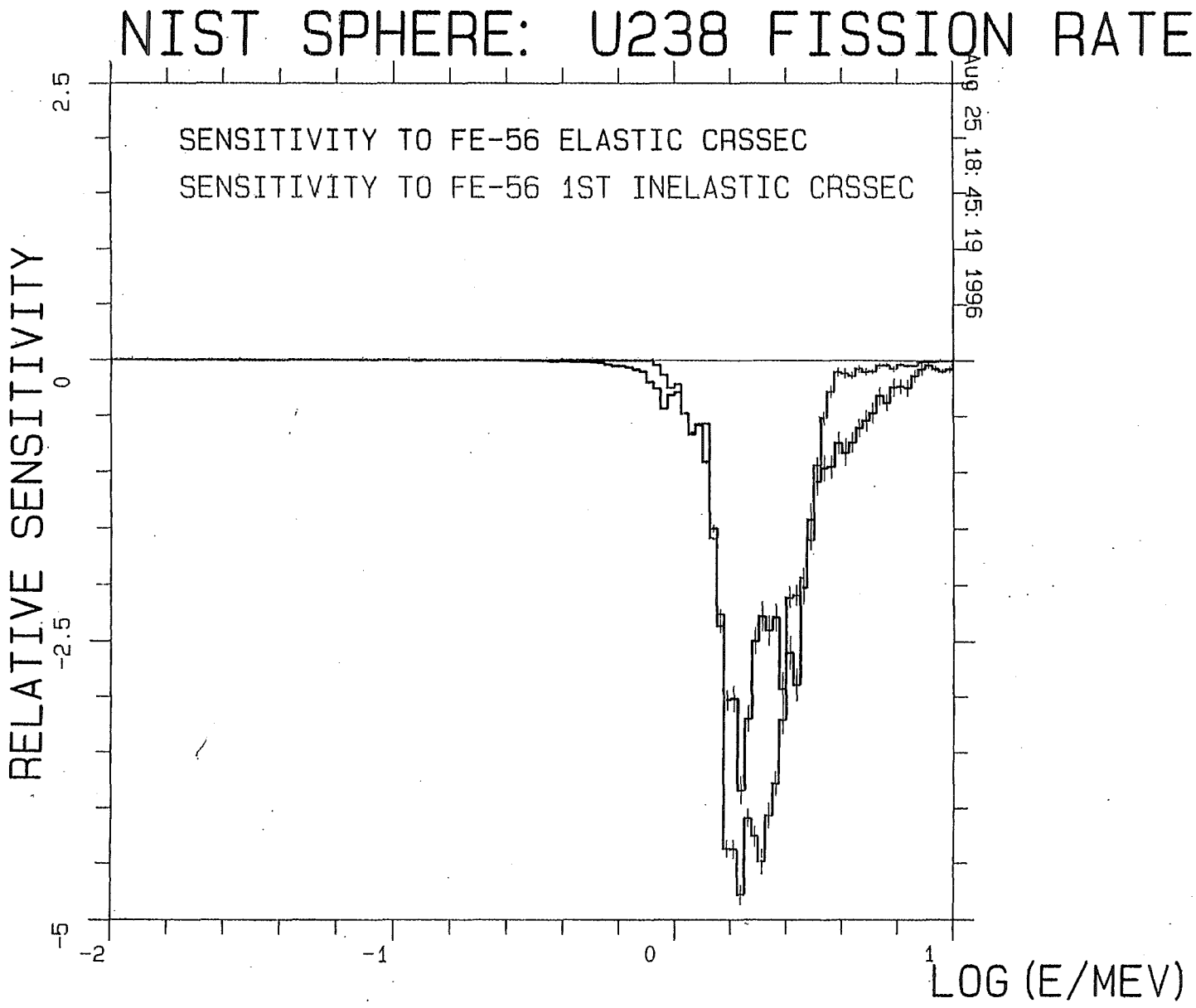
NIST SPHERE: U238 FISSION RATE
SENSITIVITY TO FE-56 ELASTIC CRSSEC
SENSITIVITY TO FE-56 1ST INELASTIC CRSSEC
Aug 25 18:45:19 1996
RELATIVE SENSITIVITY
2.5
0
-2.5
-5
-2
-1
0
1
LOG (E/MEV)

REFERENCES

1. M.C.G. Hall, "Cross Section Adjustment with Monte Carlo Sensitivities: Application to the Winfrith Iron Benchmark," Nucl. Sci. Eng., **81**, 423-431 (1982).

2. Judith F. Briesmeister, Editor, "MCNP™ -- A General Monte Carlo N-Particle Transport Code," Los Alamos National Laboratory Report LA-12625-M (March 1997).

3. R.L. Perel, J.J. Wagschal, and Y. Yeivin, "Monte Carlo Calculation of Point-Detector Sensitivities to Material Parameters," Nucl. Sci. Eng., **124**, 197-209 (1996).

4. H. Rief, "Monte Carlo Uncertainty Analysis," in *Uncertainty Analysis,* Y. Ronen, ed., pp. 187-215, CRC Press, Boca Raton (1987).

5. G.W. McKinney, "A Monte Carlo (MCNP) Sensitivity Code Development and Application," M.Sc. Thesis, University of Washington, (1984).

6. J.D. Densmore, G.W. McKinney, J.S. Hendricks, "Correction to the MCNP™ Perturbation Feature for Cross-Section Dependent Tallies," Los Alamos National Laboratory Report LA-13374-M (Oct. 1997).

7. P.F. Rose, Editor, ENDF/B-VI Summary Documentation. BNL-NCS-17541 (ENDF-201), 4th edition, National Nuclear Data Center, Brookhaven National Laboratory (1991).

8. E. Goldberg, L.F. Hansen, T.T. Komoto, B.A. Pohl, R.J. Howerton, R.E. Dye, E.F. Plechaty, and W.E. Warren, "Neutron and Gamma-Ray Spectra from a Variety of Materials Bombarded with 14-MeV Neutrons," Nucl. Sci. Eng., **105**, 319-340 (1990).

9. B. Jansky, Z. Turzik, M. Marek, "Reference Neutron Spectra Based on ^{252}Cf Sources used in NRI Rez," NRI-UJV 10368 R,D, Nuclear Research Institute Rez plc, Czech Republic (Dec. 1994).

10. J.S. Nico, J.M. Adams, C. Eisenhauer, D.M. Gilliam and J.A. Grundl, "^{252}Cf Fission Neutron Transport Through an Iron Sphere," in *Ninth International Symposium on Reactor Dosimetry*, Prague (September 1996).

Monte Carlo Methods and Models for Applications in Energy and Technology

Workshop to be held at Forschungszentrum Karlsruhe, May 12-14, 1998

A review of the applications of MCNP in neutronics for Fusion Technology at ENEA FRASCATI

Luigino Petrizzi

Associazione EURATOM-ENEA sulla fusione, C. R. Frascati
Via E. Fermi 27, Frascati ROME, ITALY

In our laboratories there is a group making extensive use of transport codes to calculate the nuclear radiation fields for several kind of applications. These are confined essentially in the frame of Fusion Technology; it is not mean a restriction as many examples will show.

Between the used transport codes, the Monte Carlo code MCNP has grown in significance, along the years, due its capability to handle complex geometry models, generally in 3-D, the use of continuous energy nuclear data and the powerful means to treat deep penetration problems, as required in most of the applications. The designers too, as in ITER, suggest explicitly MCNP as reference tool. It has also a solid background in documentation and quality assurance and its development has followed and still today follows strictly the computer and software technology development. These items, too, have contributed to the increase of its significance compared to the other methods and codes. At the moment, about 80% of our computer time is spent for MCNP runs, in our laboratory.

An overview is given of the different fields in which MCNP has been used, in the last years:

- In the design of the reference Breeding Blanket for the ITER machine. Neutronics has played a key role in the selection of the final design which has the main goal to breed > 0.8, satisfying all the thermal constrains.
- In the shielding analyses of ITER respect to the Toroidal Field Coils. The powerful variance reduction techniques have allowed the proper treatment of the deep penetration problem (till 2 meters of materials to cross). Moreover the capability to handle complex geometries has allowed the analyses of the streaming through any single penetration (ports and gaps).
- In the analysis of the experiments performed with the Frascati Neutron Generator (FNG) facility. The experimental results obtained in different configurations can be compared with calculated ones to validate the code itself or the nuclear data used. A big amount of work has been published which has involved many laboratories. A general satisfactory agreement has been found with all the main experimental data, (within 20-30 % for all nuclear responses at 100 cm of depth). In some cases the electron transport capability of MCNP have been used in these kind of calculations.
- In the diagnostic system of the multi-collimator in JET and in ITER. MCNP has been used as calibrating method. Strong source biasing has been required in this case to reach reasonable accuracy.
- In the design of IGNITOR machine, for the analysis of nuclear loads and of activation components.
- For the Long Term activity (DEMO reactor), the analysis supporting the design of the ITER Test Module (ITM).

MCNP has shown satisfactory capabilities to handle these problems. It will be shown also how the latest version MCNP4B with the multiprocessing capability (PVM) together with the available SP2 machine in Frascati (16 processors) has given greater impulse and more power to our analyses capability.

Last modified: Thu Apr 30 15:02:35 1998

Presented by: dr. Luigino PETRIZZI ,
Associazione EURATOM-ENEA sulla fusione, C. R. Frascati, Via E. Fermi 27, Frascati ROME, ITALY

The C.R. ENEA Frascati laboratories are dedicated mainly to the Fusion Technology, all the activities are grouped in one big *division.*
A subsystem of it is the neutronic *section*, it has the scope to develop research with neutrons for the technological development of fusion. It is divided in two subgroups: one is working on the experimental activity and the other on calculation essentially. The last develop an ensemble of activities all together called "Computing Methods for Neutron Transport".

The group makes extensive use of transport codes to calculate the nuclear radiation fields for several kind of applications. There are Sn codes: ANISN, DORT; Monte Carlo codes: MORSE (now out of use), MCNP (version 4B). Other codessuch as ANITA (now out of use), FISPACT are used to calculate from the neutron fluxes the activation induced in irradiated materials. An other code used is the system NJOY, capable to prepare cross section data in ENDF format to be used in transport codes. This was done in the past for preparing MCNP library from the European Fusion File (EFF).

Between the used transport codes, the Monte Carlo method and the code MCNP in particular has grown in significance, along the years. It is capable to treat complex geometry models, as needed in many fusion technology applications. It makes use of continuous energy cross section data, avoiding any of the problems connected withmultigroup data preparation, resonance treatment and similar. MCNP has also very powerful and tested variance reduction tools which give a big help the deep penetration problems, as required in many applications. Its reliability is very well known. In the ITER design, it isexplicitely suggested the use of MCNP as reference, and most of the work performed is in ITER frame. The code has also a solid background in documentation and quality assurance and its development has followed and still today follows strictly the computer and

A REVIEW OF THE APPLICATIONS OF MCNP IN NEUTRONICS FOR FUSION TECHNOLOGY AT ENEA FRASCATI
ENEA FUSION DIVISION
C. R. Frascati NEUTRONICS SECTION

software technology development. Now the RAM, the hard-disk capacity (Giga Bytes), the multiprocessing capability lets Monte Carlo calculations run for very complicated models in times comparable to the cpu spent by Sn 1-D calculations ten years ago. About 80% of our computer time is spent for MCNP runs, in our laboratory.

At the moment the latest version of MCNP the 4B is installed in our machines. Three workstation IBM RISC 6000 are available to our section in exclusive use: one, the oldest is used actually as disk or as server, because its available RAM is too low for any our applications. The other two RISC, a 41T and the newest 43P are used full time for short (1 hour) calculation. For very hard applications we have available in a large computing centre, in common use with all the other laboratories, an SP2 AIX IBM machine, with 16 nodes available. Each single node is equivalent in computing power to twice a 41T and 1.5 times a 43P. The SP2 is a system thought for parallel application. We have installed the multiprocessing version of MCNP on it. The gain in computing power is linear with the number of nodes available (each node has the same speed). In theory the gain that we can have is 30 times respect to a normal 41T machine, if all the 16 nodes are available. Actually not all the nodes are available at the same time. A queuing system, called Load Leveler, administrates the work. Classes are defined, with limited number of nodes available and limited time. A factor of ten has been experienced. This is very effective in our capacity to run problems with very hard variance reduction. An analysis which requires 1 month of computing time, in 3 days on the SP2 is done!! And still, the computing centre administrators are working for an improvement of the SP2 system.

An overview will be given of the applicationsof MCNP done in our group, in the last five years. These are confined essentially in the frame of Fusion Technology. For each of these applicationsemphasis will be given to the peculiar features of the MCNP code, which had relevance for the application.

1. **In the design of the reference Breeding Blanket for the ITER machine. Neutronics has played a key role in the selection of the final design which has the main goal to breed > 0.8.**

The first effort has been the modelling. Full description3 dimensional MCNP model of ITER machine, starting from the general model, developed inside the JCT during the summer 1995.The general model reproduces ITER, according to the TAC 8 design assumptions.
Taking advantage of the symmetry of the system a 9° degree slice has been modelled. In toroidal direction there are: 1 inboard module and one and half outboard modules, 2 cm gaps (toroidal and poloidal) are in between the modules.

The neutron source is simulated by a user supplied FORTRAN subroutine in which, reading an external data file, a set of co-ordinates x,y,z are generated. The algorithm has been firstly developed by M.Sawan (Wisconsin Un.) The probability associated to each set of co-ordinates are derived from a map of the neutron source neutron power, equivalent to the D-T interactions density map.

Calculations have been performed for the original ITER Joint Central Team(JCT) proposal of breeding blanket in which toroidal-poloidal shells of alternate materials follow the first wall profile. In the modelling of the breeder blanket layout, we tried to avoid any material dilution, reducing the uncertainty due to modelling and material homogenisation. The JCT proposal has showed a TBR performances under the assigned goal, in the reference coverage, due to the presence of headers which reduces the breeder coverage to a critical point.

The calculations have been performed also for the alternative European (EU) blanket proposal based on unit cellsa beryllium bed is confined in between two cooling poloidal radial plates where breeder rods are placed in proper radial-toroidal positions. The basic cell is repeated in toroidal direction filling the blanket module.
The internals of each module have been described in great detail, close as much as possible to the actual unit cell layout. This work has been possible thanks to the powerful "repeated structure" capability of MCNP (U, FILL, TRCL cards), together with a FORTRAN routine which *automatically* writes the model input, for cell and surfaces. This routine has the advantage to be adaptable: the side wall thickness, the number of unit cell per toroidal length, the breeder thickness are adjustable parametersIn

A REVIEW OF THE APPLICATIONS OF MCNP IN NEUTRONICS FOR FUSION TECHNOLOGY AT ENEA FRASCATI
C. R. Frascati FUSION DIVISION NEUTRONICS SECTION

this way a design modification can be easily taken into account. To have an idea of the complexity of the final model of the breeding blanket, more than 1000 cells were necessary. Such an effort would be really impossible without the help of an automatically input generator.

The results obtained for the EU proposal look promising (0.95 in the new reference coverage, and an extended thickness).
The TBR analyses is completed also by nuclear heating calculations, very important for the designers to check the thermal-hydraulics consistency.

The TBR calculations performed on the two designs were the basis for a selection exercise done in October 1997 in S. Diego in which the ITER Director (dr. Aymar) selected the EU proposal as the reference ITER design for the Breeding Blanket.

2. In the shielding analyses of ITER.

In the body of the neutronic analyses performed for the Breeding Blanket there is also the assessment of its shielding capability towards the Toroidal Field Coil (TFC) system. The nuclear loads on the TFC should be below assigned limits. This is a second strong requirement for the Breeding Blanket. A full 3-D shielding analysis has been performed using the Weight Window Generator (WWG) of MCNP. This powerful variance reduction technique has allowed the proper treatment of the deep penetration problem (till 2 meters of materials to cross).Many days of CPU on SP2 were necessary to reach a sufficient statistical error (one month for a full map of the machine).

Moreover the capability to handle complex 3-D geometries has allowed the analyses of the streaming through any single penetration (ports and gaps). A detailed analysis has been performed for the Shielding Blanket of ITER to study the effect of the streaming of the radiation through the gaps in between the modules. This had the scope to give to the designers the information of how much the bulk shielding performances can be reduced by the gaps penetrating the blanket.

3. In the analysis of the experiments performed with the Frascati Neutron Generator (FNG) facility.

FNG is a well known fusion facility. Many experiments have been performed in different configurations. All of them have been oriented to ITER. The work has been performed through international collaborations, and many laboratories and universities have been involved. The main objective of all the experiments was to compare the experimental results (E) obtained in different configurations with calculated ones (C). Discrepancies between Experiments and Calculations ($C/E \neq 1$) are assigned to the nuclear data used, assuming that the uncertainty due to the modelling and the code itself is negligible.

A model of the FNG facility has been set-up and distributed among also the other labs collaborating to the same task.
A proper source routine has been written by M.Pillon to sample in a proper way the neutron source. The processes of damping of the D beam in the Tritiated target, its straggling, and kinematics of the nuclear D-T have been described in detail.

In many calculations performed the WWG generator and energy cuts were used as the maintool of variance reduction. Their parameters depend heavily on the particular quantity to be calculated.

A REVIEW OF THE APPLICATIONS OF MCNP IN NEUTRONICS FOR FUSION TECHNOLOGY AT ENEA FRASCATI
C. R. Frascati FUSION DIVISION NEUTRONICS SECTION

A general satisfactory agreement has been found with all the main experimental data, (within 20-30 % for all nuclear responses at 100 cm of depth).
In some cases the electron transport capability of MCNP have been used in restricted local portion of the model.

4. In the diagnostic system of the multi-collimator in JET and in ITER.

MCNP has been used as calibrating method. Strong source biasing has been required in this case to reach reasonable accuracy.

5. In the design of IGNITOR machine, for the analysis of nuclear loads and of activation components.

In this case neutron fluxes have been calculated in selected places, in conjunction of the code FISPACT doses have been calculated outside the cryostat to verify the requirement <100 μSv/h.

Workshop on Monte Carlo Methods and Models for Applications in Energy and Technology
12-14 May 1998 Forschungzentrum Karlsruhe

The following features of MCNP have been experienced and gave help in solving problems:

- Full 3-D model with complex geometry
- Repeated structure, TRCL, FILL, LIKE, U cards
- User supplied source sampling routines
- Variance reduction: WWG, CUT, source bias.
- Electron transport, locally
- X-ray polarised transport
- PVM

A REVIEW OF THE APPLICATIONS OF MCNP IN NEUTRONICS FOR FUSION TECHNOLOGY AT ENEA FRASCATI
C. R. Frascati FUSION DIVISION NEUTRONICS SECTION

6. **For the Long Term activity (DEMO reactor), the analysis supporting the design of the ITER Test Module (ITM).**

The shielding capability of the ITM object towards the TFC, for the water cooled liquid breeder option, has been verified. This work has been performed through a collaboration with CEA.

7. **Through a collaboration with CNR Institute of Space Astrophysics MCNP has been used in the design of a detector for measuring hard X-ray.**

In this case the only photon transport capability of MCNP has been used.
The designed detector is a polarimeter based on the Compton scattering of linearly polarised photons. A modification of the subroutines of MCNP treating the Compton scattering has been necessary to handle properly this problem.

1. Design of the reference Breeding Blanket for ITER

   Viewgraphs of the model and more significative results

- For the former Joint Central Team proposal
- For the European Home Team proposal then choosed as the reference

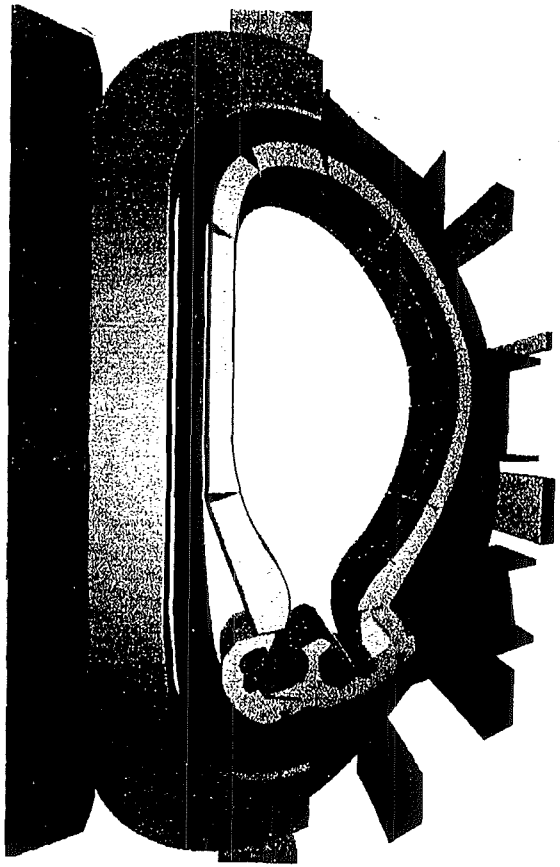

Fig 1.a poloidal section of the breeding blanket model (with new top and bottom header)

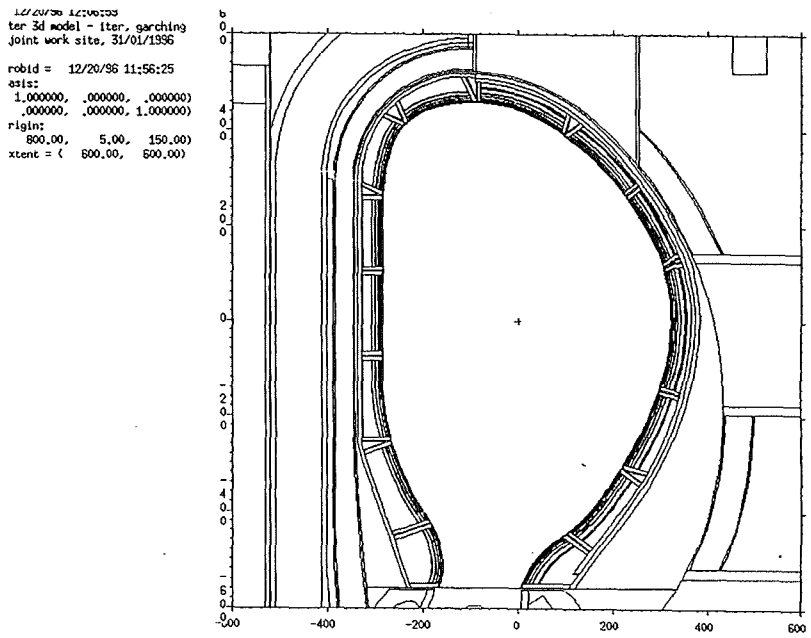

Fig. 1b. As 1a, detail of the top and bottom header (module #4)

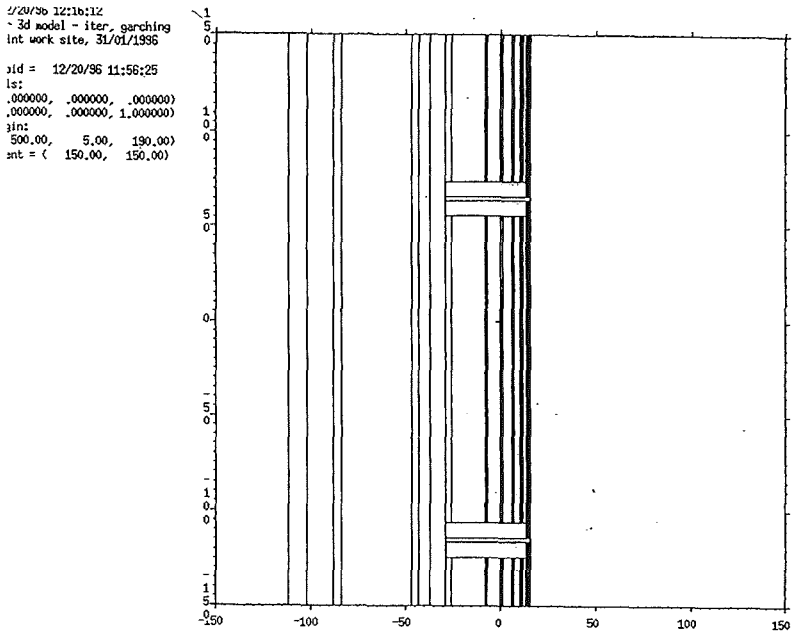

Fig. 2a Cross section of the inboard blanket (*poloidal* header can be easily seen)

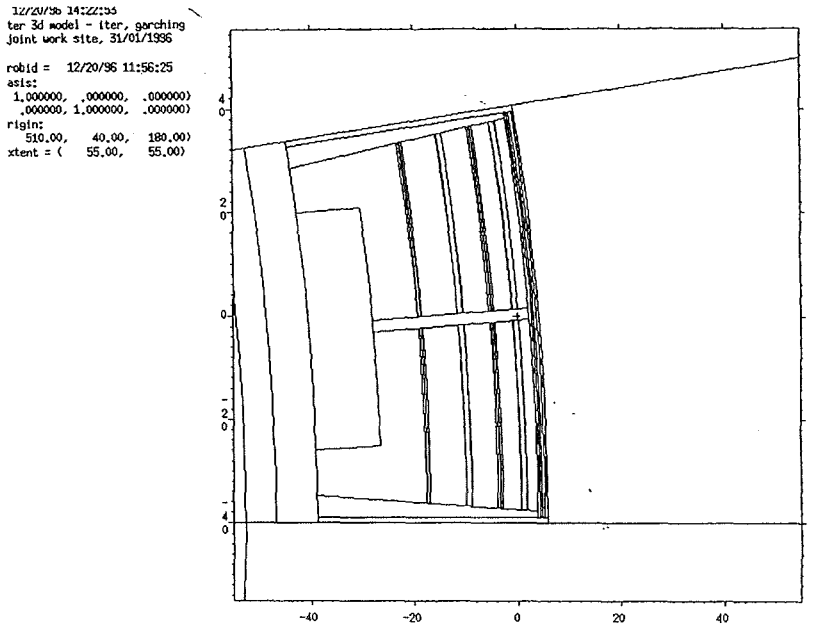

Fig. 2b Cross section of the outboard blanket (module #9)

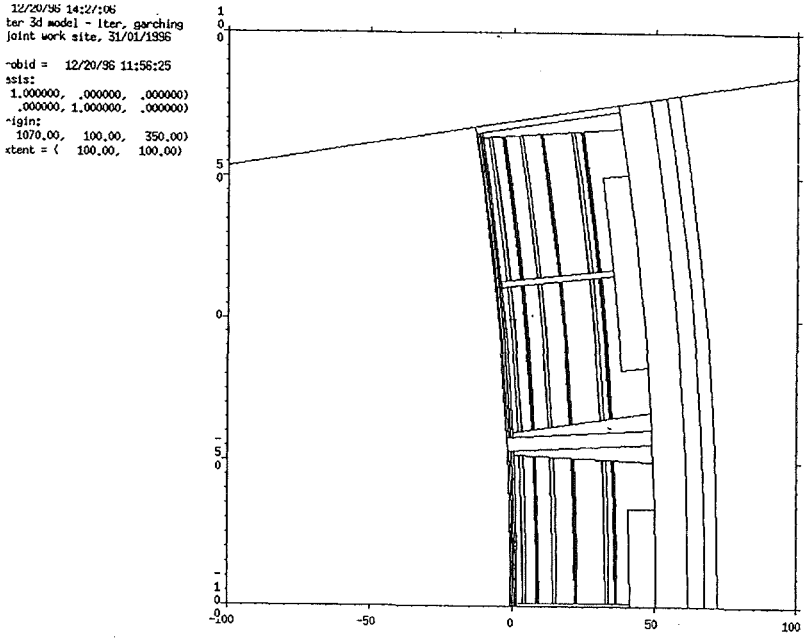

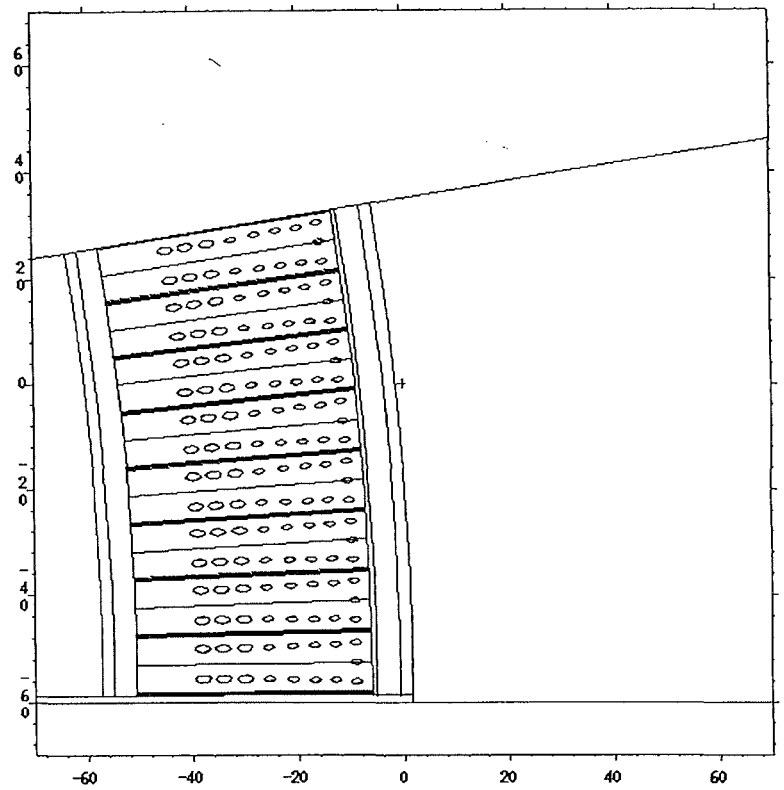

Horizontal section of one breeding module (inboard at z=590 cm, module #11)

3D power densities on mod #19

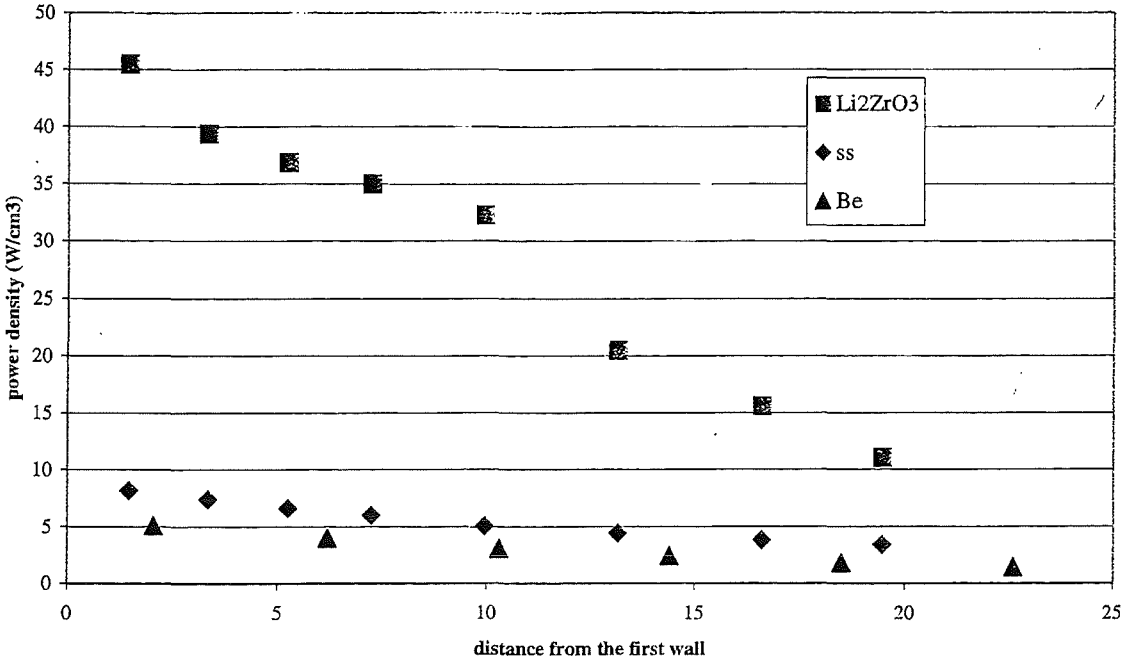

Radial Build of the Breeding Blanket Section

Region by Function	Materials	Zone Thickness-cm (porosity) Inboard	Outboard
Tile	Be	0.5	0.5
First Wall	Steel - Water - Steel	0.5 - 0.4 - 0.5	0.5 - 0.4 - 0.5
Multiplier	Be	2.0 (0.15)	1.6 (0.15)
Breeder	Steel - Li_2ZrO_3 - Steel	0.1 - 1.0 (0.3) - 0.1	0.1 - 1.0 (0.3) - 0.1
Multiplier	Be	3.5 (0.15)	3.0 (0.15)
Coolant	Steel - Water - Steel	0.3 - 0.3 - 0.3	0.3- 0.3 - 0.3
Multiplier	Be	5.0 (0.15)	4.3 (0.15)
Breeder	Steel - Li_2ZrO_3 - Steel	0.1 - 1.0 (0.3) - 0.1	0.1 - 1.0 (0.3) - 0.1
Multiplier	Be	6.8 (0.15)	5.4 (0.15)
Coolant	Steel - Water - Steel	0.3 - 0.3 - 0.3	0.3 - 0.3- 0.3
Multiplier	Be	-	8.6 (0.15)
Breeder	Steel - Li_2ZrO_3 - Steel	-	0.1 - 1.0 (0.3) - 0.1
Multiplier	Be	-	1.7 (0.3)*
Coolant	Steel - Water -Steel	-	0.3 - 0.3 - 0.3
Total radial thickness, cm		23.4	32.8

3-D MCNP results

model including updates suggested by JCT (details of headers and side walls)

	Zone	*Module #*	***Reference Coverage***	*Extended Coverage*	*Full Coverage*
Baffle	IB	1	-	*0.021*	*0.021*
		2	**0.037**	0.037	0.037
		3	**0.035**	0.035	0.035
		4	**0.033**	0.033	0.033
		5	**0.028**	0.028	0.028
		6	**0.027**	0.027	0.027
		7	**0.038**	0.038	0.038
	OB	8	**0.080**	0.080	0.080
		9	**0.098**	0.098	0.098
		10	**0.105**	0.105	0.105
		door 11	- **0.042**	- 0.042	*0.089* 0.042
		door 12	- **0.040**	- 0.040	*0.089* 0.040
Limiter		13	-	*0.112*	*0.112*
Limiter		14	-	*0.093*	*0.093*
Baffle		15	-	*0.051*	*0.051*
Total			**0.563**	0.840	0.929

Module No.	Reference Coverage & Reference Thickness	Full Coverage & Reference Thickness	Breeding Zone ΔR (cm) in Enlarged Thickness	Reference Coverage & Enlarged Thickness	Full Coverage & Enlarged Thickness
1	0	0.012	+9	0	0.015
2	0.019	0.020	+9	0.022	0.023
3	0.023	0.024	+10	0.027	0.028
4	0.022	0.022	+9	0.027	0.027
5	0.024	0.025	0	0.024	0.025
6, 7, 8	0.074	0.076	0	0.074	0.076
9	0.022	0.022	+4	0.024	0.024
10	0.020	0.020	+4.5	0.023	0.023
11	0.022	0.023	+4.5	0.025	0.026
12	0.031	0.033	0	0.031	0.032
Total IB	0.257	0.276		0.277	0.299
13	0.037	0.037	0	0.037	0.037
14	0.041	0.042	0	0.043	0.044
15	0.048	0.049	+7	0.055	0.056
16	0.063	0.064	+7	0.072	0.074
17	0.062	0.064	+7	0.073	0.075
18	0.031	0.033	+7	0.036	0.037
19	0 0.031	0.094 0.032	+7	0 0.035	0.108 0.036
20	0.030	0.032	+7	0.035	0.037
21	0.060	0.061	+7	0.070	0.071
22	0.060	0.061	+7	0.069	0.070
23	0.050	0.051	+7	0.056	0.057
24	0.043	0.043	+7	0.052	0.052
25	0.037	0.038	+7	0.042	0.043
26	0	0.032	+7	0	0.038
Total OB	0.593	0.733		0.675	0.835
Global TBR	**0.850**	**1.009**		**0.952**	**1.134**

2. Shielding anlyses of ITER

Viewgraphs of the model and more significative results

- For the shielding blanket: analyses focussed on the effect of the gaps in between the modules

- For the breeding blanket: analyses focussed on the shielding capability towards the components behind the blanket till the Toroidal Field Coils (TFC)

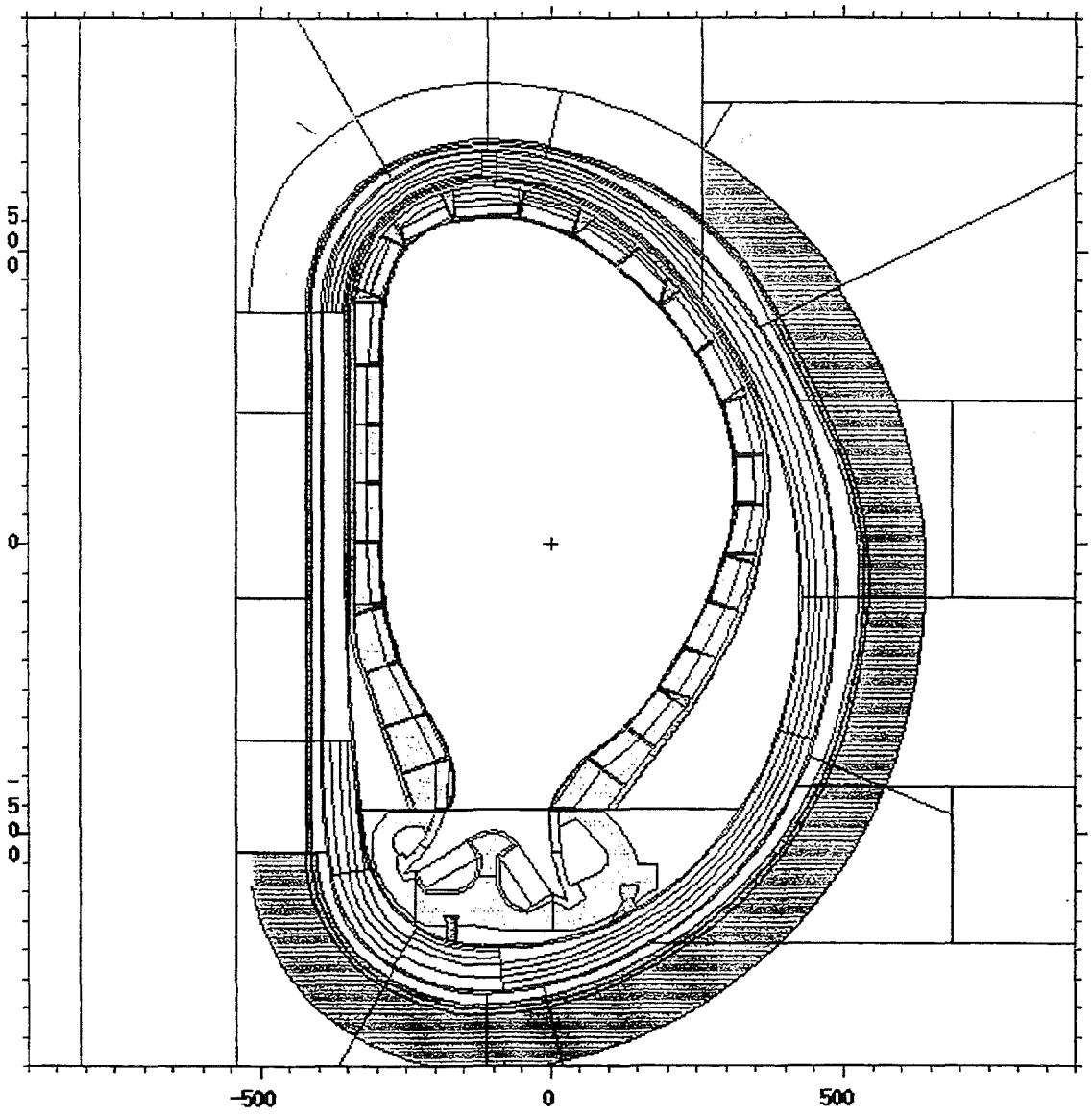
500
0
-500
-500
0
500

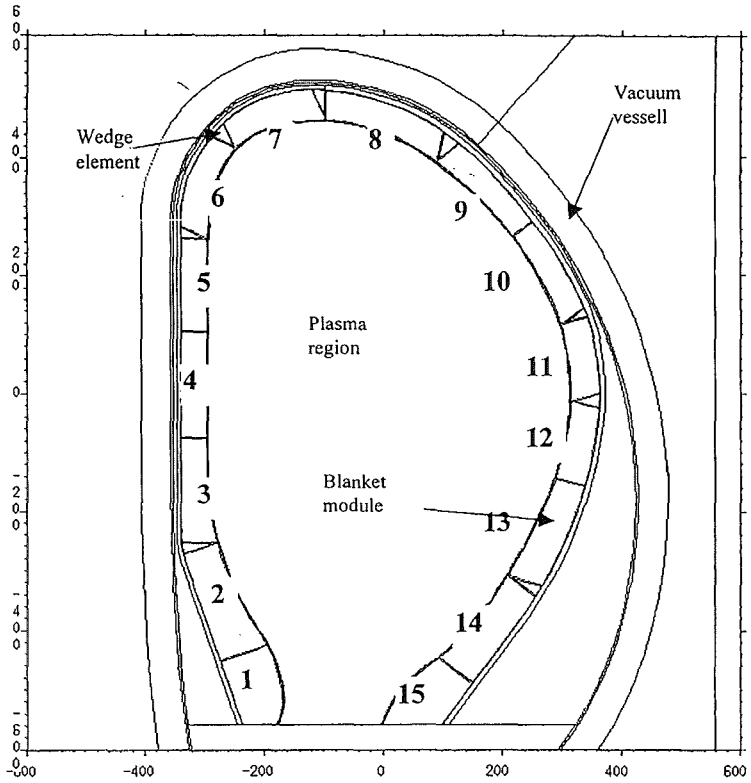

figure 2.1: vertical section with poloidal module number

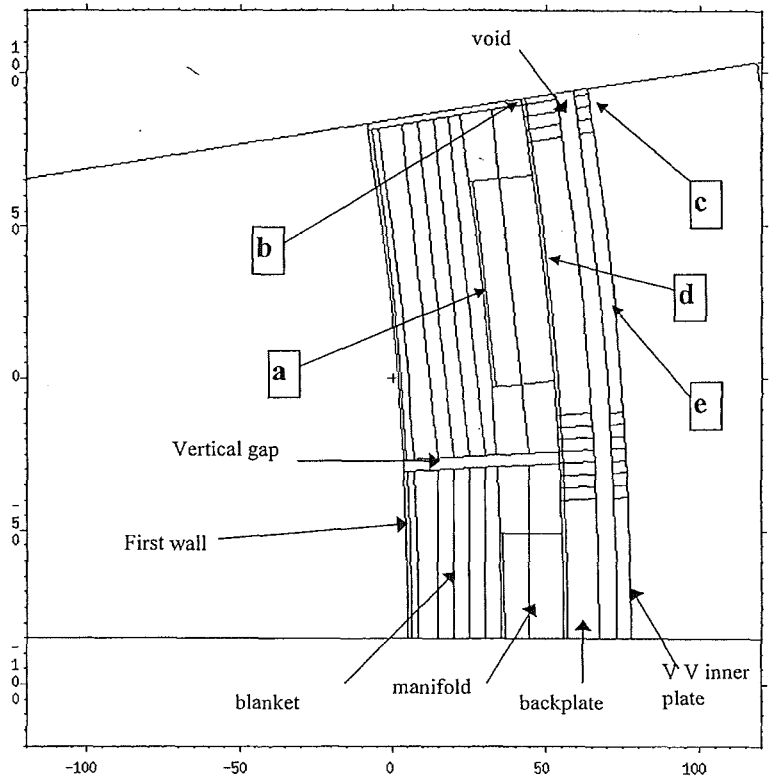

figure 2.2: horizontal section of outboard blanket at midplane with scoring cells signed (a through e)

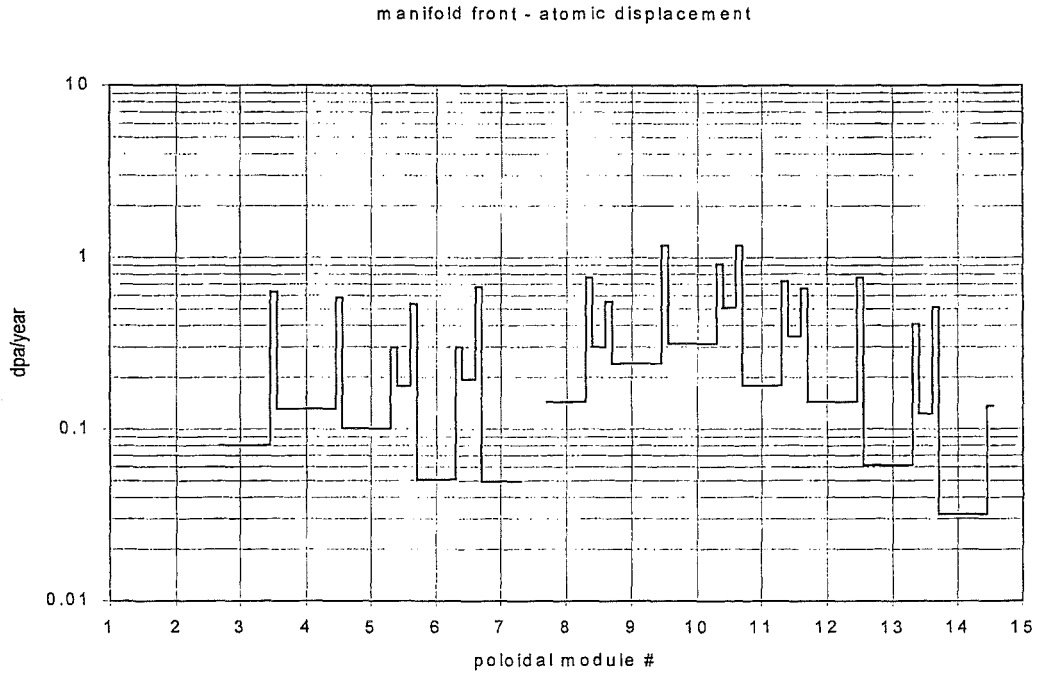

figure 2.5

54

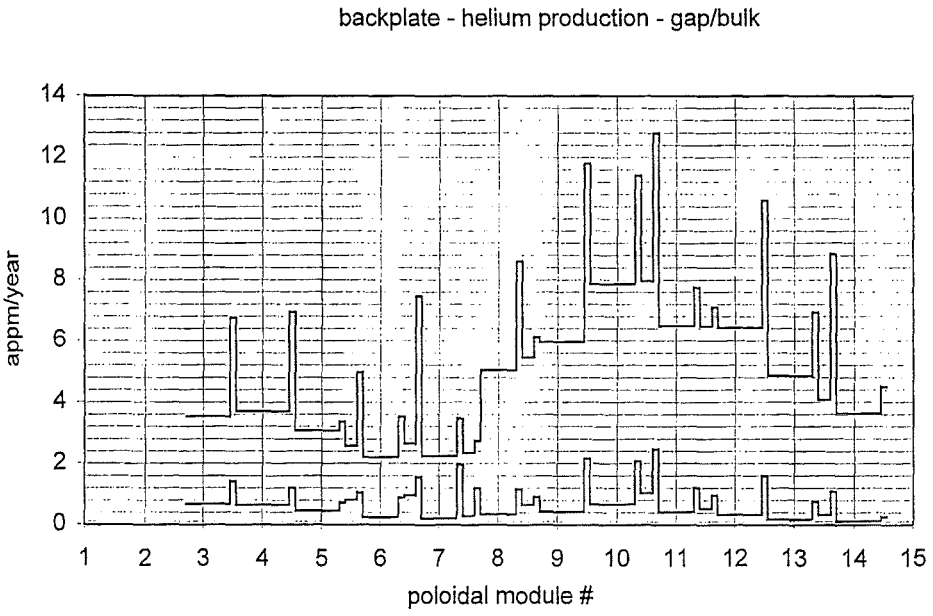

figure 2.9

60

Shielding analyses of the breeding blanket for ITER

Calculations have been performed by means of MCNP code (version 4A) /1/, using a full 3-D model, inclusive of the Toroidal Field Coil system and the breeder blanket layout. Hard variance reduction technique has been required to reach a satisfying statistical error in the scoring cells. Radiation loads in topical points behind the breeder blanket have been calculated along all the poloidal contour and compared to the required limits. The highest radiation values have been recorded behind the inboard blanket at midplane where, even the neutron wall loading is lower, the reduced thickness cannot damp the radiation to values lower than the outboard. In the following table radiation loads calculated in case of breeder blanket vs limits are reported (as the S. Diego meeting).

	ITER EU breeding blanket	Radiation load limits [GDRD]
Peak dose to electrical insulator (Epoxy) [rad]	$2.0 \cdot 10^8$	$3 \cdot 10^8$
Peak nuclear heating in the coil case [$mWcm^{-3}$]	0.14	2
Peak nuclear heating in winding pack [$mWcm^{-3}$]	0.05	1

Other required physical quantities, related to the radiation loads, are below:

- **Helium** production in the **breeder back plate** (appm 3 years) 5.6 (inboard)
- **Hydrogen** production ,, ,, 4.4
- **Dpa** in stainless steel ,,, ,, (dpa 3 years) 0.38

- **Helium** production in the **first layer** of **vacuum vessel** (appm 3 years) 1.65
- **Hydrogen** production...,, ,, ,, ,, 1.79
- **Dpa** in stainless steel ,,, ,, (dpa 3 years) 0.19

- **Helium** production in the **second layer** of **vacuum vessel** (appm 3 years) 5.5e-3
- **Hydrogen** production...,, ,, ,, ,, 8.1e-3
- **Dpa** in stainless steel ,,, ,, (dpa 3 years) 5.1e-4

The total amount of heat deposited by the radiation on the TFC system is estimated to be less than 8 kWatt on the 20 coils when the limit is 17 kWatt (calculations to be finished in ten days).

J. Briesmeister, Ed., "MCNP, A General Monte Carlo N-Particle Transport Code, Version 4A" LA-12625-M, (1993).

Shielding analysis

- Focussed on the shielding capability towards the TFC (GDRD requirements). Other quantities such as the dpa, helium production in the backplate have been measured too.
- A more complicated model has been required with the addition of splitting surfaces
- Variance reduction has been applied (WWG of MCNP) to reach a statistical error of 5% (benefit from the PVM)

- The total power [redacted] on the 20 TFCs is 6 kW (with ports shielded) lower than the limit (17 kW).

3. Analysis of the experiments performed with the Frascati Neutron Generator (FNG)

Viewgraphs of the model and more significative results

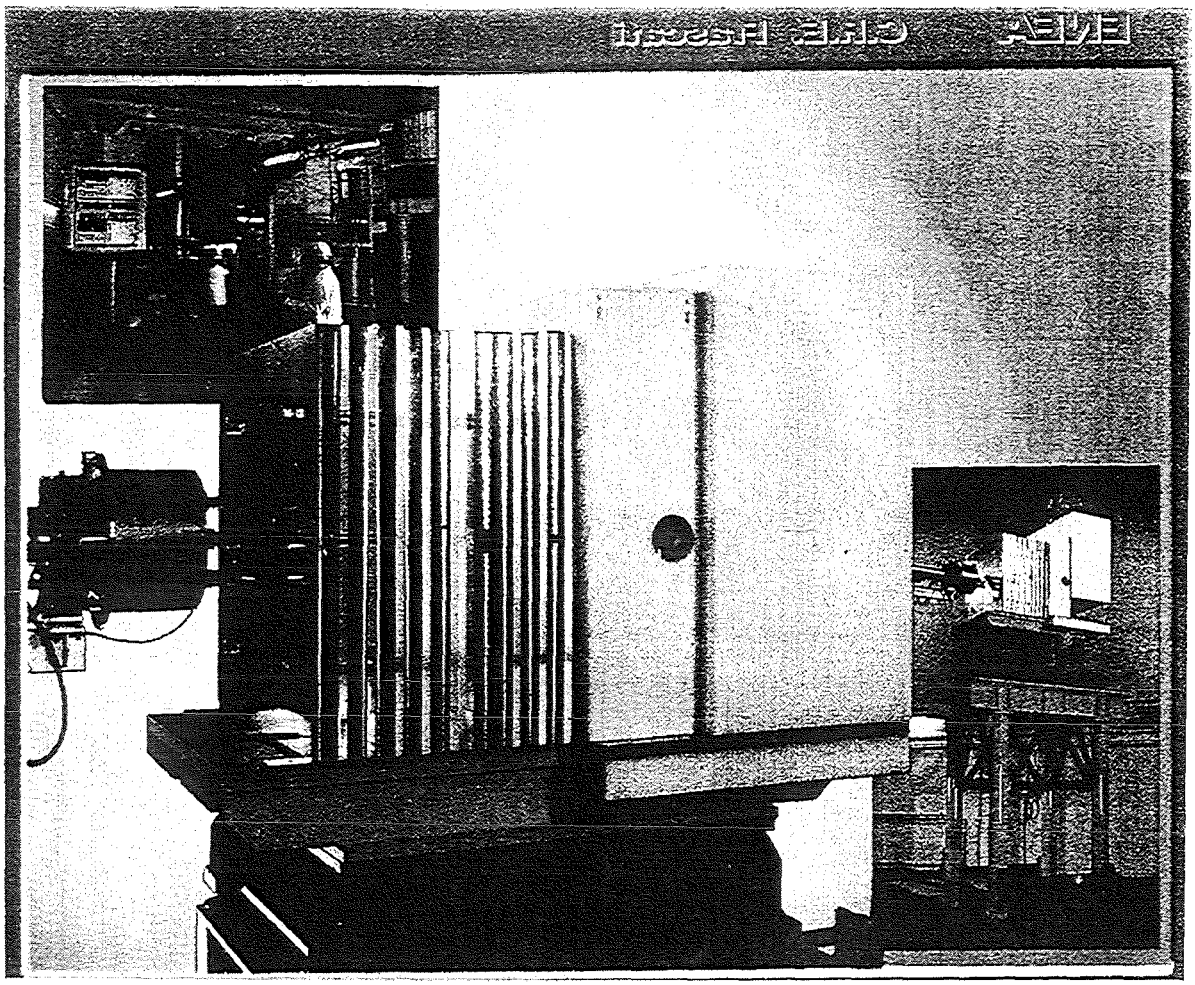

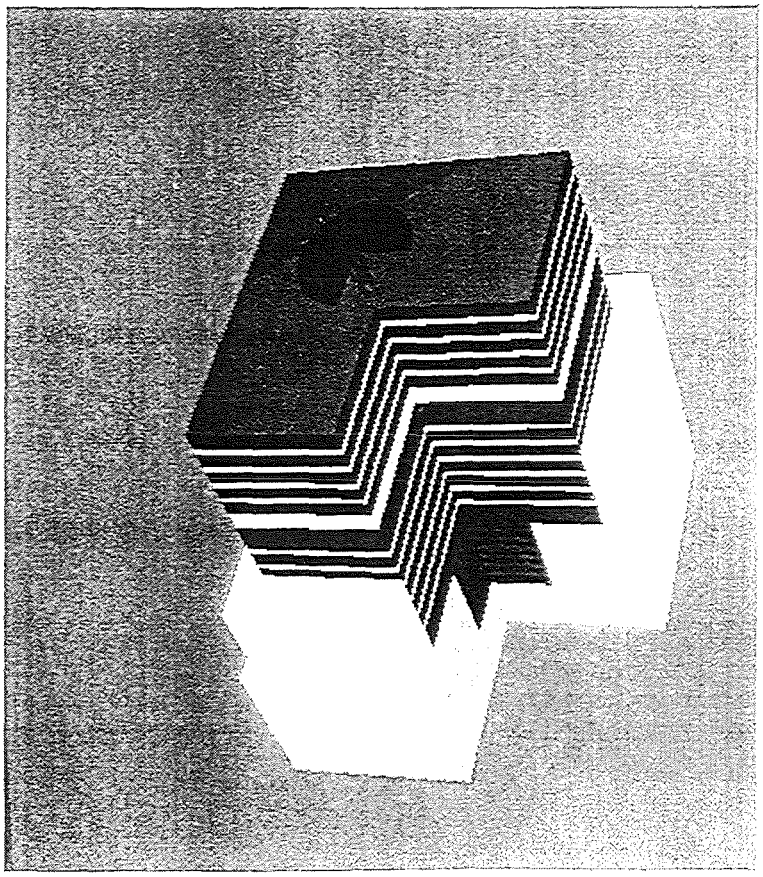

Results

MEASUREMENTS AND ANALYSIS OF NUCLEAR HEATING

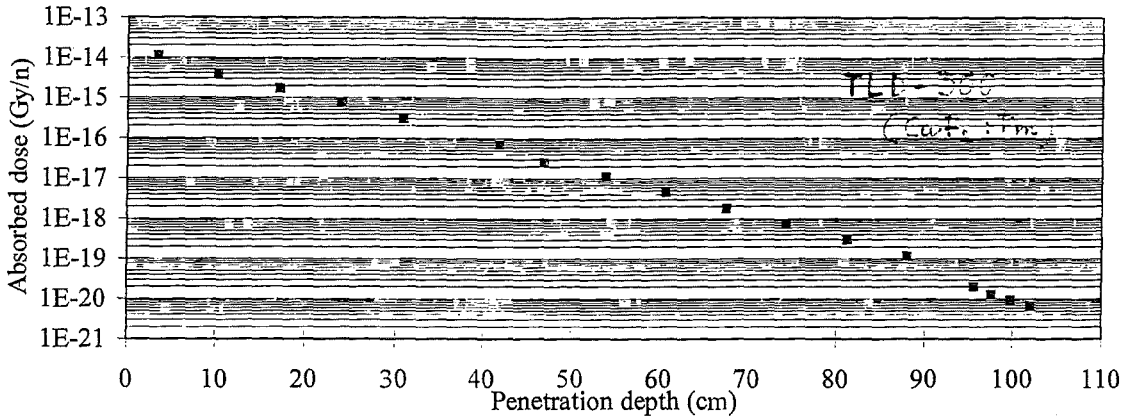

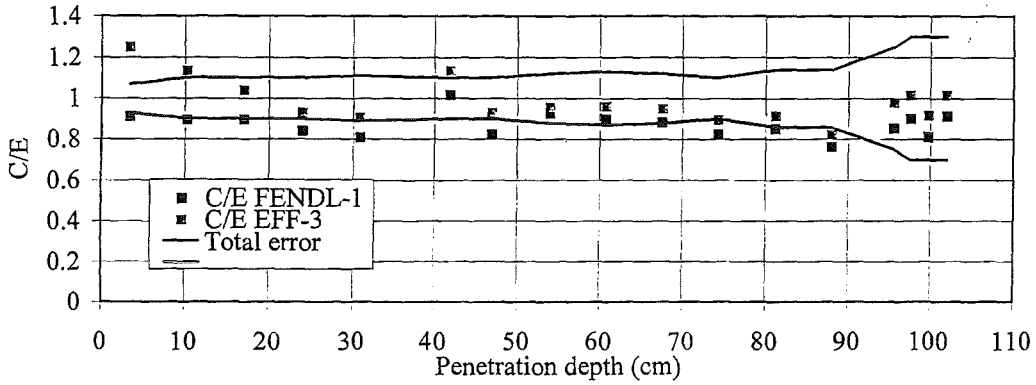

Results and discussion

REACTION RATES MEASUREMENTS AND ANALYSIS (examples)

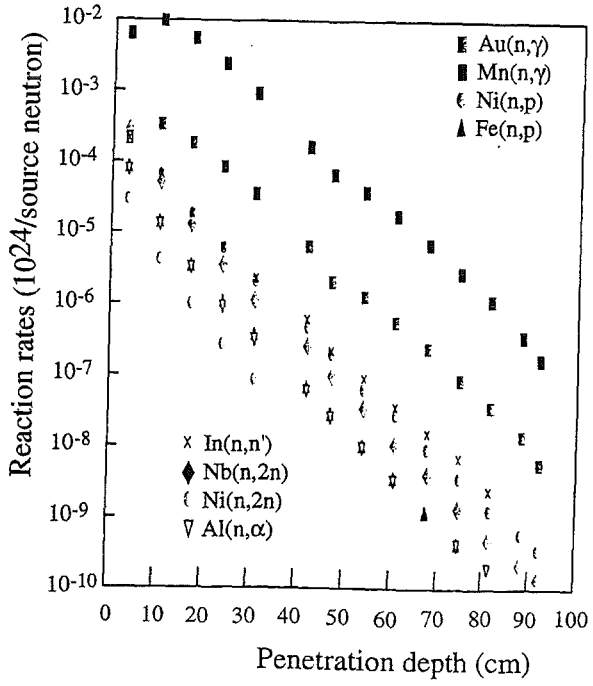

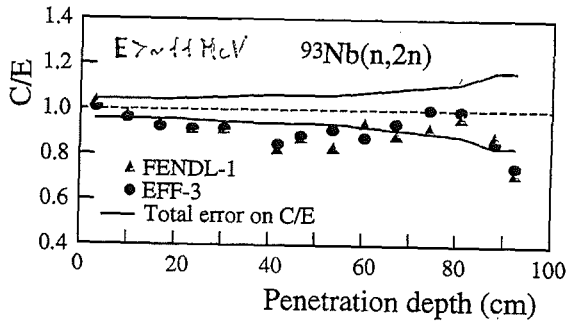

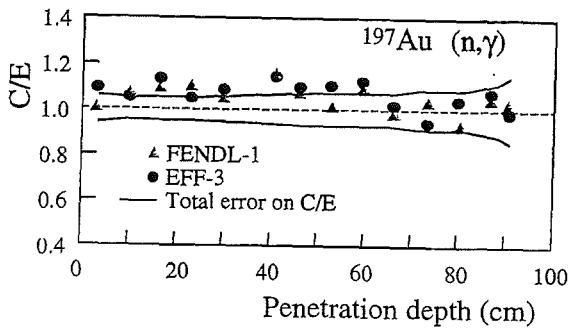

4. Design of the diagnostic system of the multi-collimator in JET and in ITER

   Viewgraphs of the system and the model and summary of the results

Calibration of the neutron profile monitor diagnostic at JET by means of the Monte Carlo code for Neutron and Photon transport MCNP.

Massimo Rapisarda

Associazione Euratom-ENEA sulla Fusione
Frascati Research Centre, via E. Fermi 27, 00044
Frascati (Rome) Italy.

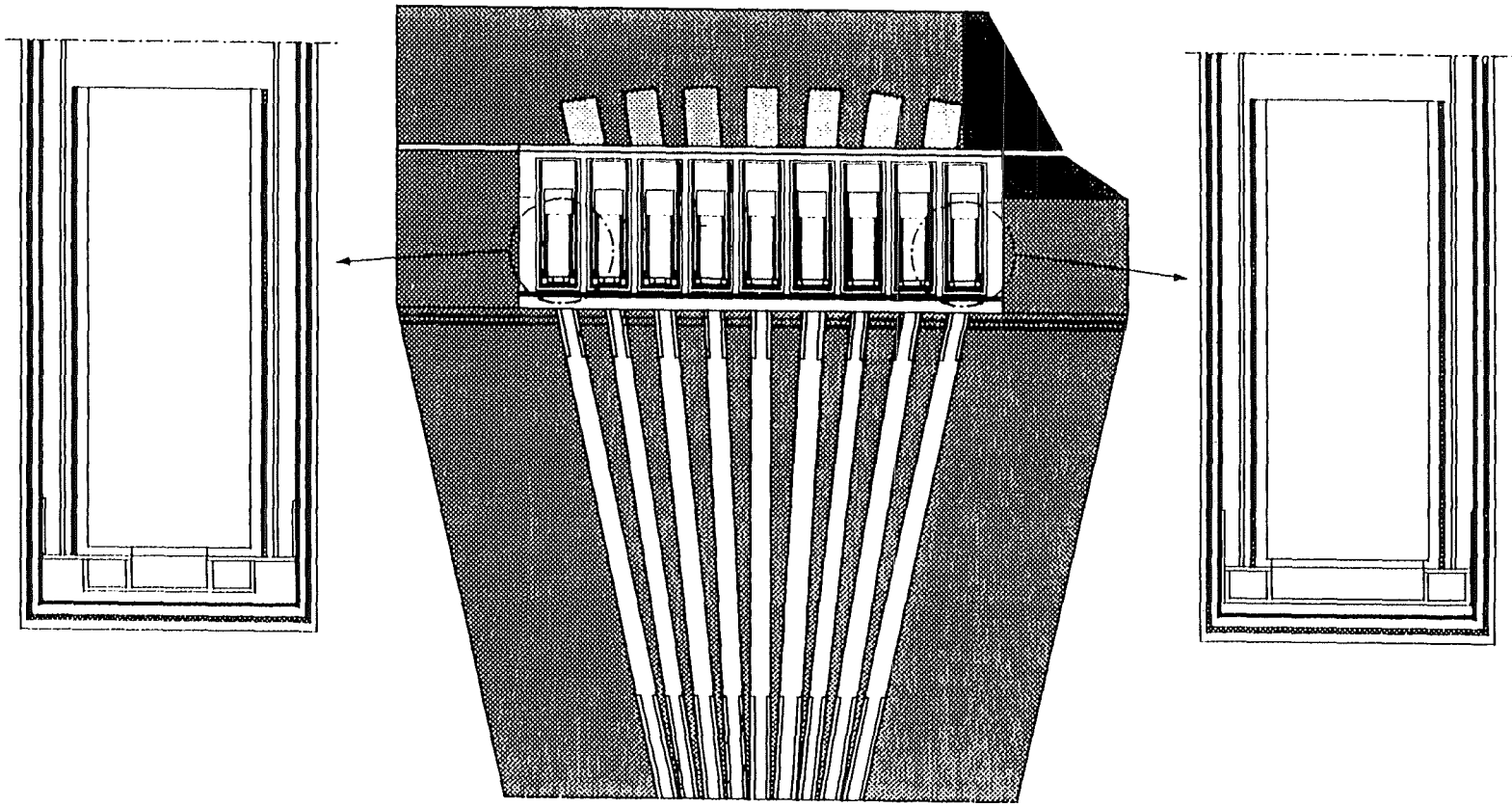

MCNP model of the vertical camera assembly, showing the detailed description of the scintillator cases.

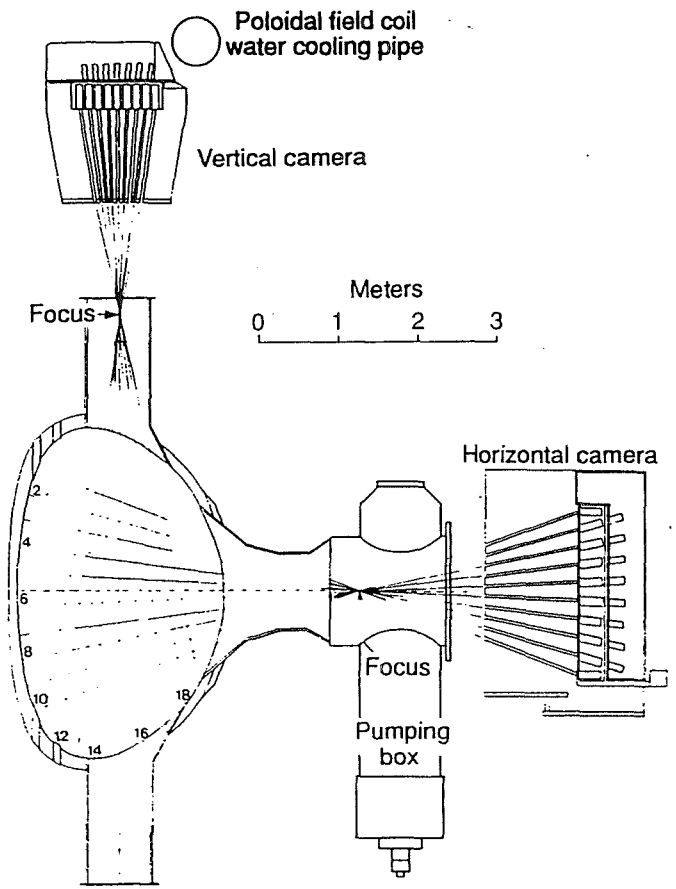

Fig. 2. Schematic of the JET neutron emission profile monitor collimation geometry. The direct line-of-sight chords illustrate the overall viewing extent within the JET vacuum vessel.

FROM: ADAMS ET AL. NUCL. INSTR. AND METH. A329 (1993) 277

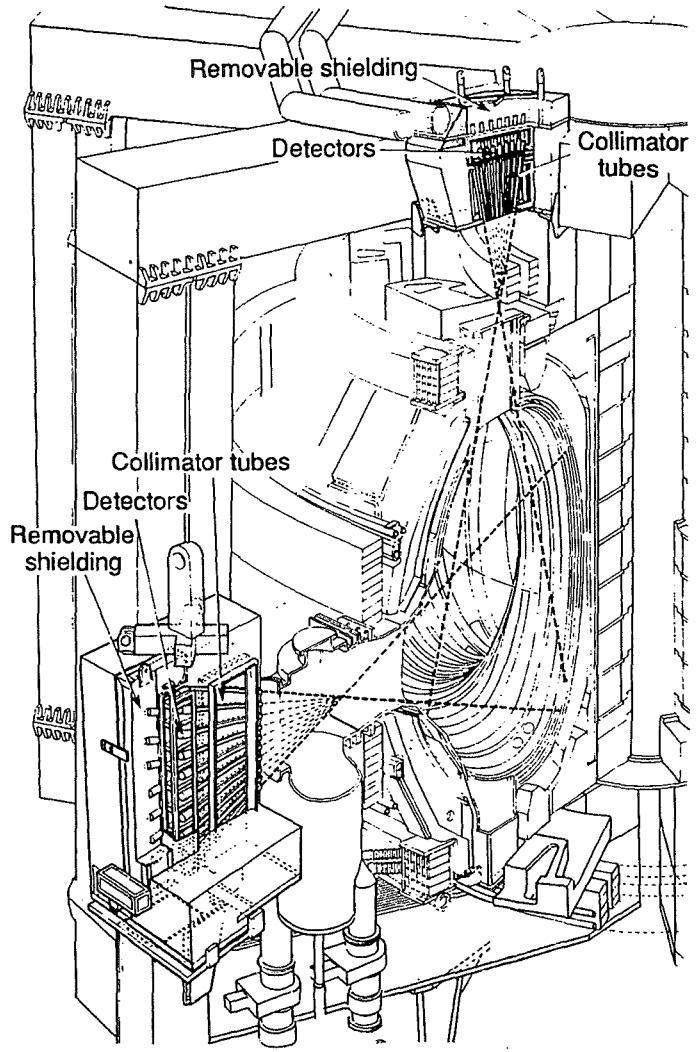

Fig. 1. Artist's impression of the JET neutron emission profile monitor. The location of the two bulk shield assemblies are shown relative to the main structure of JET.

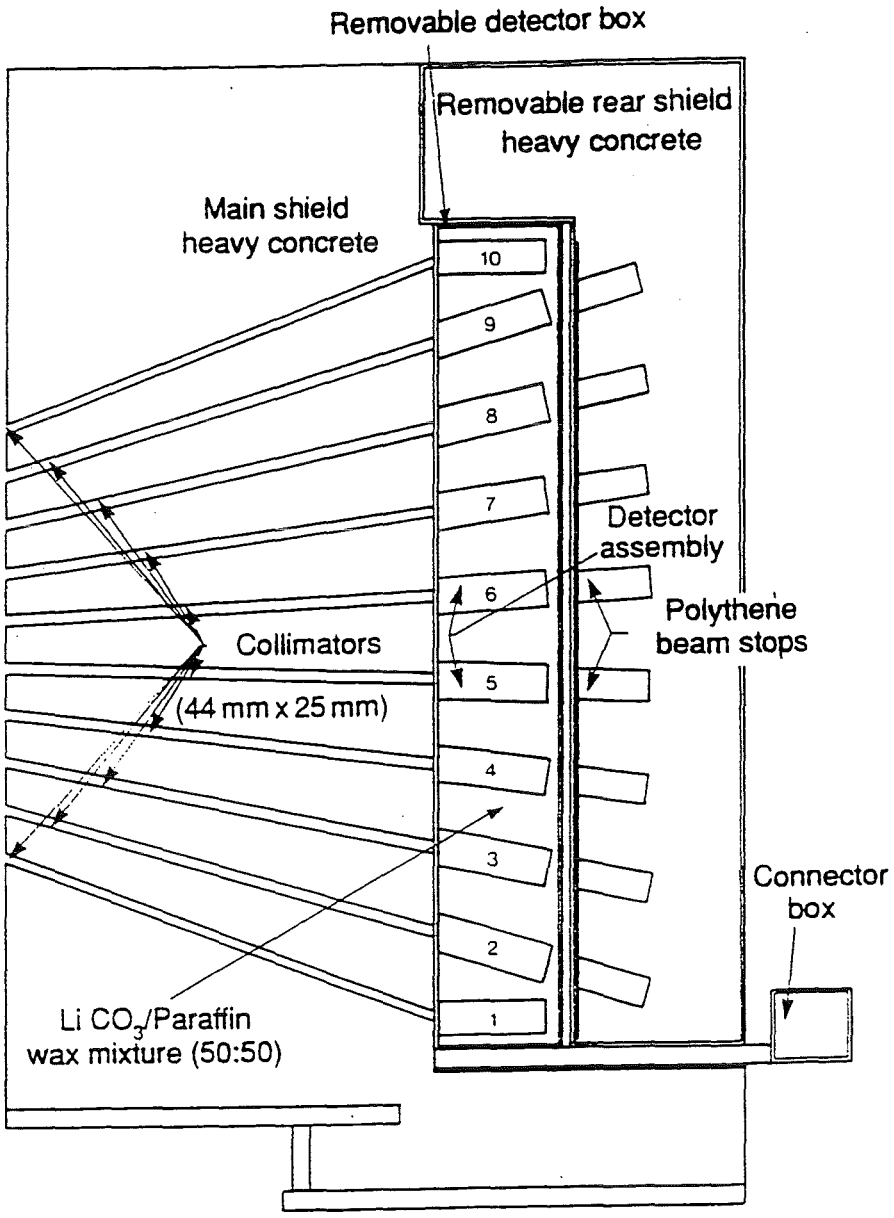

Fig. 3. Horizontal camera shield assembly (32 tonnes). The location of the removable detector box and rear shield are shown relative to the main bulk shield in which are embedded the 10 collimator channels. The removable rear shield contains the neutron beam dumps for 8 of the 10 channels.

Table 1.

Low Yield (2.45 MeV neutrons)							
Horizontal camera				Vertical Camera			
ch.	Real	Optic.	Real / Optic.	ch.	Real	Optic.	Real / Optic.
1	67.6	82.9	0.82 ± 1.6%	11	5.8	6.6	0.85 ± 5.8%
2	69.5	84.9	0.82 ± 1.6%	12	8.1	9.1	0.89 ± 4.9%
3	71.5	85.7	0.83 ± 1.6%	13	13.8	14.9	0.93 ± 3.8%
4	73.2	87.7	0.83 ± 1.6%	14	19.7	22.4	0.88 ± 3.2%
5	74.9	89.5	0.84 ± 1.6%	15	30.1	33.8	0.89 ± 2.6%
6	75.1	89.3	0.84 ± 1.6%	16	37.8	42.2	0.90 ± 2.3%
7	74.0	88.6	0.84 ± 1.6%	17	40.9	46.6	0.88 ± 2.2%
8	71.9	86.0	0.84 ± 1.6%	18	41.2	47.7	0.86 ± 2.2%
9	69.0	85.1	0.81 ± 1.6%	19	36.1	42.5	0.85 ± 2.3%
10	68.1	82.7	0.82 ± 1.6%				

Table 2.

High Yield (2.45 MeV neutrons)							
Horizontal camera				Vertical Camera			
ch.	Real	Optic.	Real / Optic.	ch.	Real	Optic.	Real / Optic.
1	14.6	16.7	0.87 ± 2.6%	11	5.9	6.6	0.89 ± 4.6%
2	14.2	16.1	0.88 ± 2.6%	12	8.3	9.3	0.89 ± 3.9%
3	23.0	27.9	0.82 ± 3.8%	13	13.8	14.9	0.93 ± 3.1%
4	24.0	29.7	0.81 ± 3.8%	14	27.3	35.1	0.78 ± 4.1%
5	22.5	28.7	0.78 ± 3.8%	15	24.9	31.7	0.79 ± 4.1%
6	24.1	29.1	0.83 ± 3.8%	16	26.5	31.9	0.83 ± 4.1%
7	24.3	28.3	0.86 ± 3.8%	17	24.3	31.1	0.78 ± 4.1%
8	24.0	28.6	0.84 ± 3.8%	18	27.2	33.2	0.82 ± 4.1%
9	14.4	16.4	0.88 ± 2.6%	19	26.1	31.7	0.82 ± 4.1%
10	14.7	16.7	0.88 ± 2.6%				

Table 3.

High Yield (14 MeV neutrons)							
Horizontal camera				Vertical Camera			
ch.	Real	Optic.	Real / Optic.	ch.	Real	Optic.	Real / Optic.
1	15.5	16.7	0.93 ± 2.2%	11	6.2	6.6	0.94 ± 5.0%
2	15.3	16.1	0.95 ± 2.2%	12	8.6	9.3	0.92 ± 3.5%
3	26.3	27.9	0.94 ± 3.3%	13	14.2	14.9	0.95 ± 3.5%
4	28.4	29.7	0.96 ± 3.3%	14	32.4	35.1	0.92 ± 3.5 %
5	26.0	28.7	0.91 ± 3.3%	15	30.1	31.7	0.95 ± 3.5%
6	28.0	29.1	0.96 ± 3.3%	16	32.5	31.9	1.02 ± 3.5%
7	27.2	28.3	0.96 ± 3.3%	17	30.8	31.1	0.99 ± 3.5%
8	27.0	28.6	0.94 ± 3.3%	18	31.7	33.2	0.95 ± 3.5%
9	15.3	16.4	0.93 ± 2.2%	19	30.8	31.7	0.97 ± 3.5%
10	15.6	16.7	0.93 ± 2.2%				

Table 4.

D-T (14 MeV neutrons)							
Horizontal camera				Vertical Camera			
ch.	Real	Optic.	Real / Optic.	ch.	Real	Optic.	Real / Optic.
1	7.30	7.28	1.00 ± 2.2%	11	6.10	6.54	0.93 ± 2.5%
2	6.94	6.89	1.01 ± 4.8%	12	1.73	1.51	1.15 ± 4.5%
3	5.52	5.47	1.01 ± 4.8%	13	1.98	1.50	1.32 ± 4.5%
4	6.04	5.85	1.03 ± 4.8%	14	7.27	6.26	1.16 ± 4.5%
5	5.33	5.62	0.95 ± 4.8%	15	7.27	6.18	1.18 ± 4.5%
6	5.91	5.86	1.01 ± 4.8%	16	7.39	6.43	1.15 ± 4.5%
7	5.52	5.42	1.02 ± 4.8%	17	7.14	6.05	1.18 ± 4.5%
8	5.66	5.72	0.99 ± 4.8%	18	7.57	6.54	1.16 ± 4.5%
9	7.06	7.09	1.00 ± 2.2%	19	7.23	6.19	1.17 ± 4.5%
10	7.37	7.45	0.99 ± 2.2%				

5. Design of IGNITOR machine

Viewgraphs of the model and an example of the results used for the safety analysis

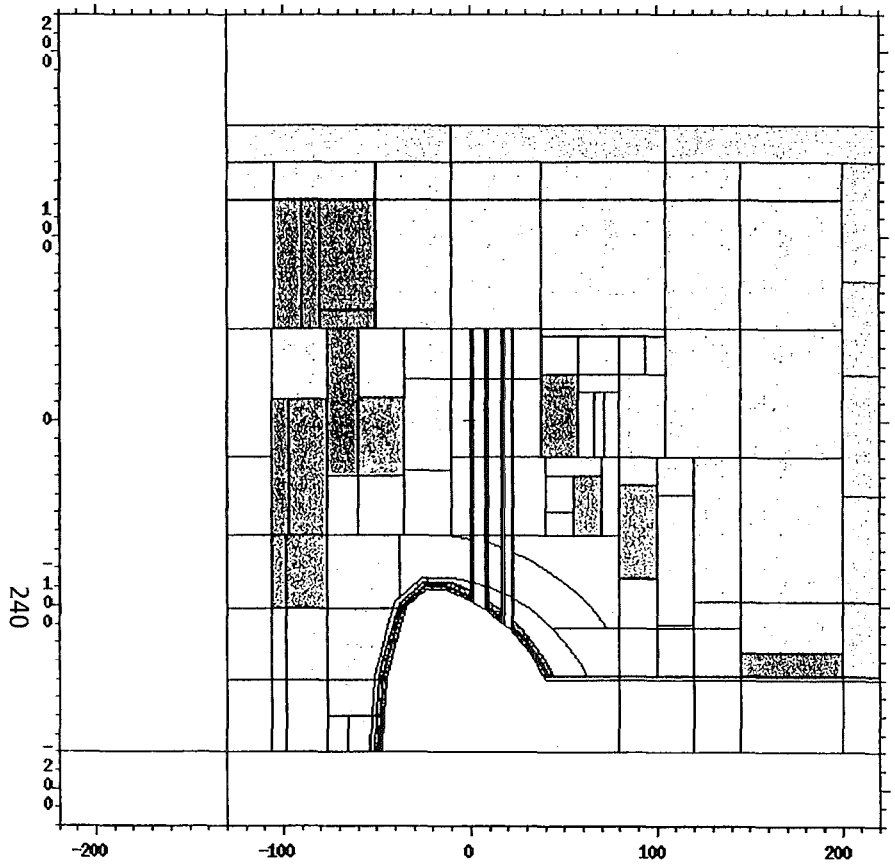
200
100
0
-100
-200
-200
-100
0
100
200

240

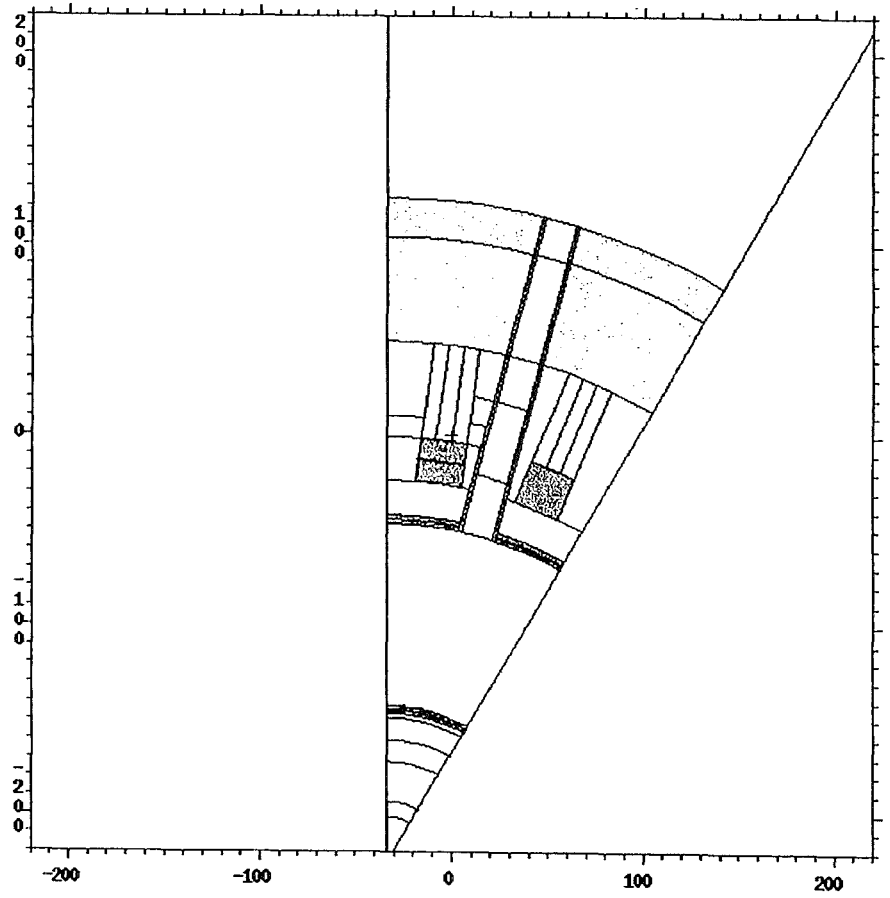
200
100
0
-100
-200
-200
-100
0
100
200

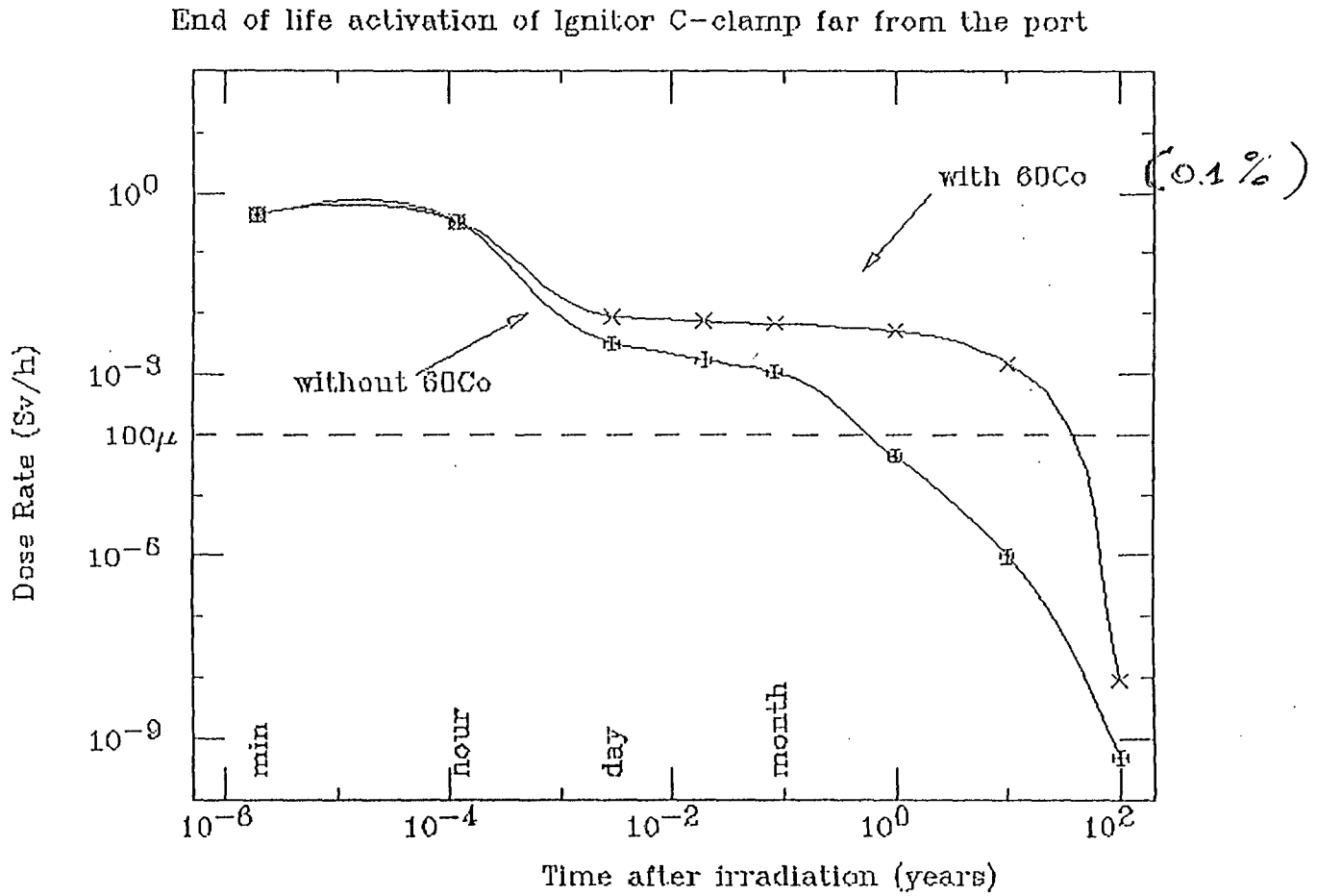
End of life activation of Ignitor C-clamp far from the port
with 60Co
(0.1 %)
without 60Co
Dose Rate (Sv/h)
10^{0}
10^{-3}
100μ
10^{-6}
10^{-9}
min
hour
day
month
10^{-6}
10^{-4}
10^{-2}
10^{0}
10^{2}
Time after irradiation (years)

Fig. 4

6. Shielding calculation for the design of the ITERT Test Module (ITM) Activity for the Long Term (DEMO reactor)

Some viewgraphs of the model and a short summary of the obtained results

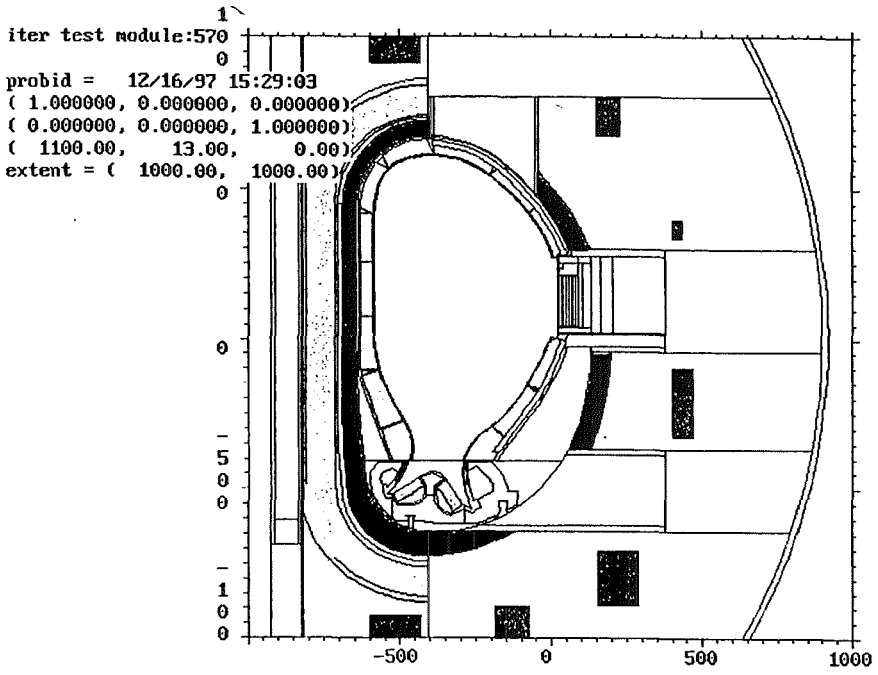

Fig. 1. Vertical cross section of the ITER model, modified to include the port and the TBM.

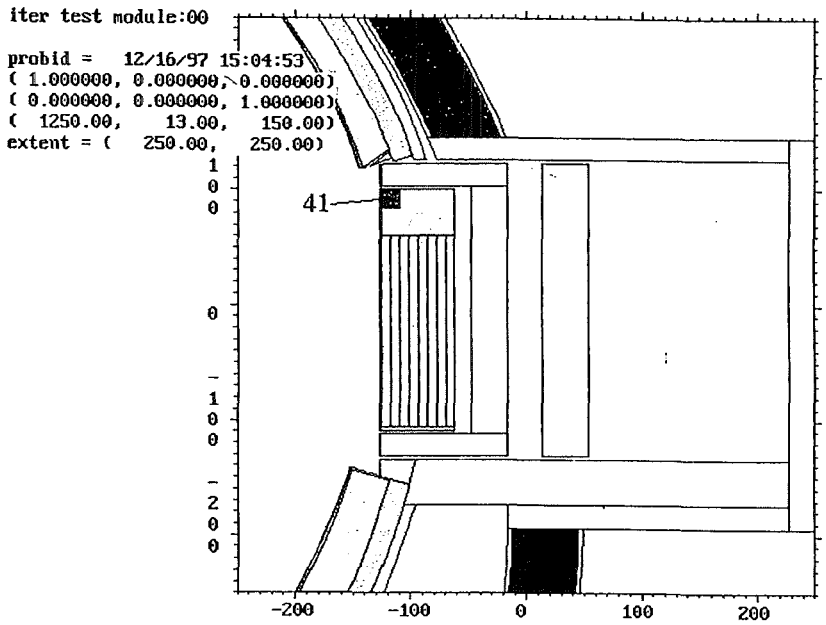

Fig. 2 Close up of the TBM in the port, showing the gaps for the mechanical tolerances.

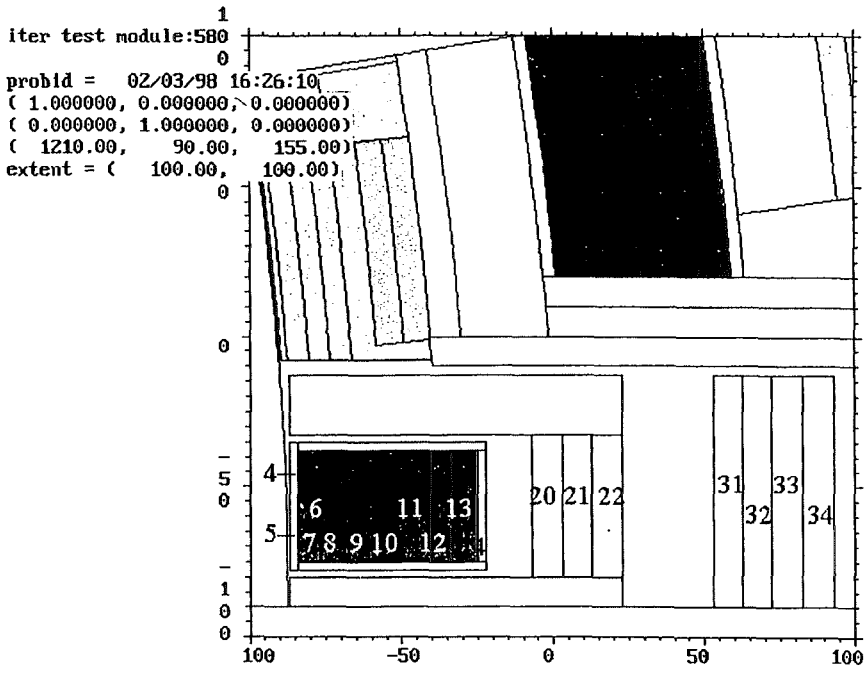

Fig. 3. Horizontal section of the TBM and the back shield at z = 150 cm (middle of the port) showing the layers in the components.

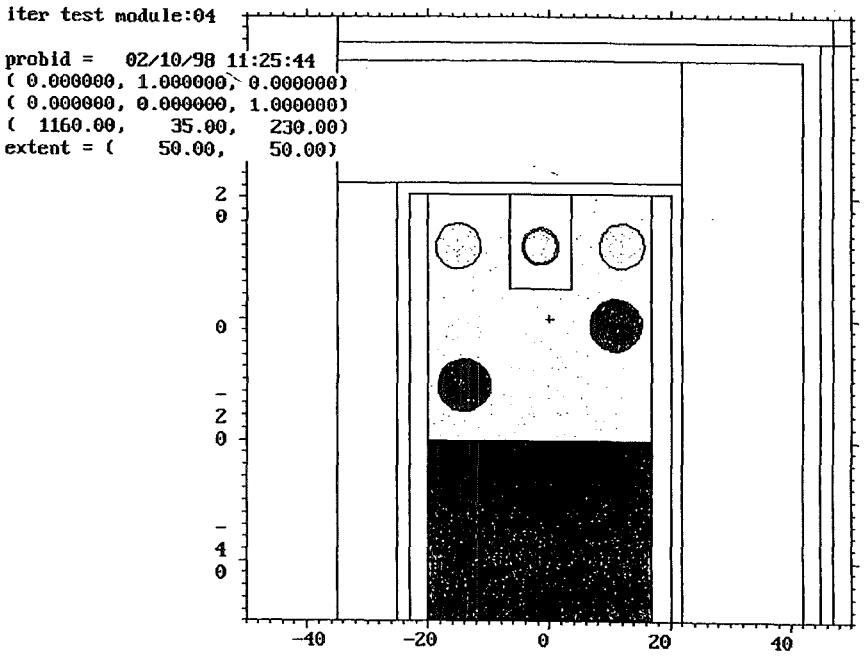

Fig. 4. Vertical cross section of the TBM intersecting the indentation, the water nozzles and the Lib ducts in the top part of the module.

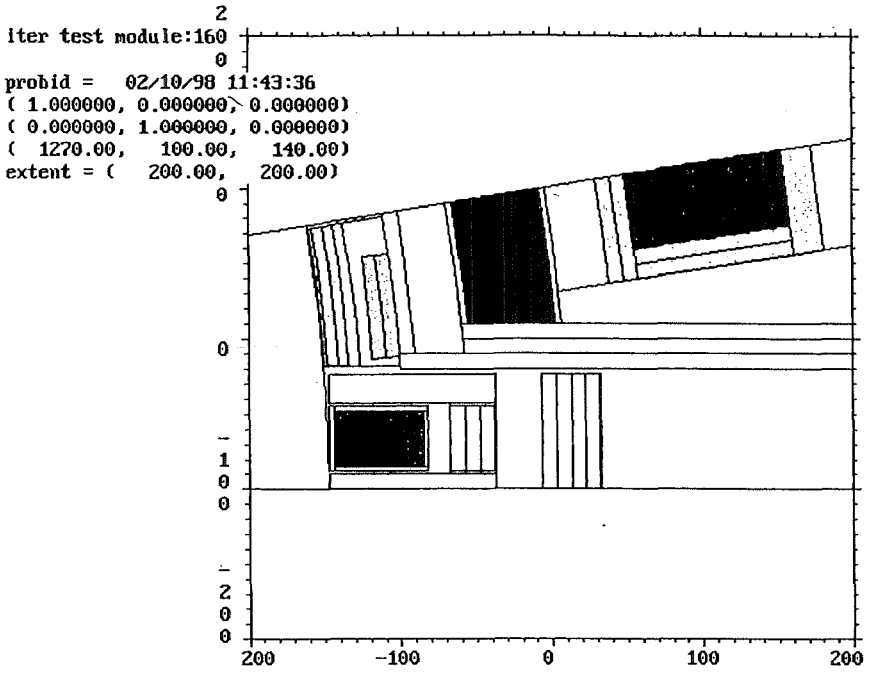

Fig. 5. Horizontal cross section of the model showing the relative positions of the magnet and of the TBM.

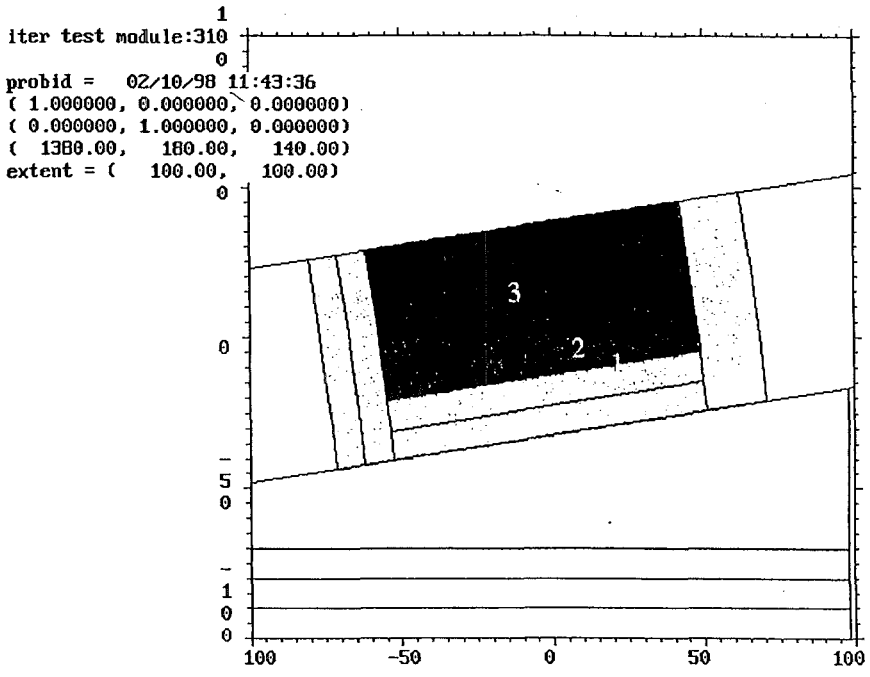

Fig. 6. Enlargement of the section of the magnet showing the three layers where the energy deposition is calculated

In the back of the steel frame:

Cell 20	Cell 21	Cell 22
n.h.: 0.1 W/cm^3 ± 10 %	n.h.: 0.07 W/cm^3 ± 11 %	n.h.: 0.04 W/cm^3 ± 14 %

In the additional back shield:

cell 31	cell 32	cell 33	cell 34
15 mW/cm^3 ± 15 %	6 mW/cm^3 ± 24 %	4.5 mW/cm^3 ± 22 %	2.3 mW/cm^3 ± 28 %

In the water tank and ducts in the top of the module (see figs. 2 and 4) :

cell 41	cell 42	cell 43	cell 44
5.4 W/cm^3 ± 20 %	1.1 W/cm^3 ± 30 %	1 W/cm^3 ± 40 %	0.7 W/cm^3 ± 30 %

Conclusions.

The insertion of the TBM in the horizontal port of ITER does not alter the shielding around the Toroidal Field Coils enough to pose at risk its functioning. Provided that the characteristics of the module are those described above, and that an additional steel shield of 40 cm is located in the back of the module there is no reason to worry for the nuclear heating in the magnet.

This result does not depend significantly on the choice of the TBM composing material because the geometry of this experiment interposes large masses between the plasma source and the magnet in any case. A possible source of worries, the presence of lead in the module, which generates many gamma rays when hit by neutrons, is neutralised by the thick and massive materials between the module and the coil.

The 3 cm mechanical gap around the frame of the module results too thin to weaken the shielding of the magnet, although it can be a serious source of radiation towards the experimental pit. Neutron streaming through such openings can be conspicuous if the gaps are straight, but, since simple modifications in the design can blind the neutron paths, there is no reason to worry for their contribution to the level of radiation in the pit (the radiation passing through the module and its case is the real unavoidable source of problems).

Finally, it must be noticed that, once the geometrical model of the assembly has been perfected and the distribution of the *weight windows* assessed, it is relatively easy to modify details or material compositions to perform again the calculation, should minor variations in the TBM assembly intervene.

7. Collaboration with CNR Institute
   Application of MCNP in astrophysics

Pergamon

Radiat. Phys. Chem. Vol. 48, No. 4, pp. 403–411, 1996

0969-806X(95)00472-6
0969-806X/96 $15.00 + 0.00

TREATMENT OF COMPTON SCATTERING OF LINEARLY POLARIZED PHOTONS IN MONTE CARLO CODES

GIORGIO MATT,[1] MARCO FEROCI,[1] MASSIMO RAPISARDA[2] and ENRICO COSTA[1]
[1]Istituto di Astrofisica Spaziale, C.N.R. and [2]Divisione di Neutronica, E.N.E.A.-C.R.E., Via Enrico Fermi 21-27, I-00044, Frascati, Italy

(Received 13 April 1995; accepted 29 November 1995)

Abstract—The basic formalism of Compton scattering of linearly polarized photons is reviewed, and some simple prescriptions to deal with the transport of polarized photons in Monte Carlo simulation codes are given. Fortran routines, based on the described method, have been included in MCNP, a widely used code for neutrons, photons and electrons transport. As this improved version of the code can be of general use, the implementation and the procedures to employ the new version of the code are discussed.

1. INTRODUCTION

While many efforts have been devoted so far in developing Monte Carlo codes able to deal with the radiative transfer of unpolarized photon beams (see Andreo, 1991 for a review), the problem of treating the polarization-dependent photon–particle interactions has not received yet the deserved attention despite its well recognized importance (e.g. Fernandez *et al.*, 1993). On the contrary, any treatment of photon transfer problems in which Rayleigh and/or Compton scattering plays an important role should in principle include the polarization dependence of the angular distribution of scattered photons, unless the geometry of both the matter and the incident radiation is perfectly spherical. In fact, even for unpolarized incident beams, the scattering process produces linearly polarized photons, which in turn produce an azimuthally anisotropic distribution of subsequent scattered photons or photoelectrons. We recall in Section 2.1 the relevant equations for Compton scattering when polarization effects are taken into account. For the sake of simplicity our treatment will neglect the distribution of the electron momenta, and therefore the Compton profile (see Ribberfors and Berggren, 1982). This is ignored also in the MCNP code (Briesmeister, 1993) with which we will deal in the following.

We have developed computational routines to deal with the polarization-dependent Compton scattering in Monte Carlo simulations. The routines were originally developed for astrophysical studies (Matt, 1993 and references therein) in situations where only scattering by free electrons was relevant and, therefore, they do not include any form factor. For Compton scattering by bound electrons and Rayleigh scattering, the polar scattering angle should instead be determined accordingly to the proper form factors. Radiation transport codes in the public domain often include detailed descriptions of such functions. Assuming, as it is usually done, that the form factors are independent of polarization, we can therefore restrict ourselves to deal, for bound electrons, with the azimuthal scattering angle only. This needs to be done for Compton scattering alone because, as far as the azimuthal distribution is concerned, Rayleigh scattering can be considered as a particular case of Compton scattering. The formulae for the polar (for free electrons) and azimuthal scattering angles as a function of the random generated number can be found in Section 2.2, along with a simple formalism for easily treating the transport of polarized photons and evaluating the degree and angle of polarization of the emerging photon distribution.

The majority of the most widely used photon transport codes do not include polarization effects (Fernandez *et al.*, 1993). Weisskopf *et al.* (1989) and Costa *et al.* (1990) used Monte Carlo programs to optimize the geometry of polarimeters for X-ray astronomy based on Thomson scattering (e.g. Novick, 1974). These codes, however, are rather specific in their purposes and are not in the public domain. It could therefore be worthwhile to include the treatment of polarization effects in widely used, multi-purpose public codes. This has recently been done for the EGS4 code by Namito *et al.* (1993) and for the GEANT3 package by Swinyard *et al.* (1991). The improved version of GEANT3, however, is not public and, moreover, it is not suitable for low energy X-rays transport (Brun *et al.*, 1987), due to its low energy (10 keV) cut-off and the lack of the atomic form factors.

We have implemented our routines in the Monte Carlo program for neutrons, photons and electrons transport MCNP. Our first goal was to study the capability of a hard X-ray polarimeter of a new concept, based on the Compton scattering in

ELSEVIER

Nuclear Instruments and Methods in Physics Research A 366 (1995) 161–172

NUCLEAR INSTRUMENTS & METHODS IN PHYSICS RESEARCH Section A

Design of a scattering polarimeter for hard X-ray astronomy

E. Costa[a], M.N. Cinti[a], M. Feroci[a,*], G. Matt[a], M. Rapisarda[b]
[a]*Istituto di Astrofisica Spaziale-CNR, Frascati, Italy*
[b]*Divisione di Neutronica –ENEA-CRE, Frascati, Italy*

Received 9 February 1995; revised form received 18 April 1995

Abstract
The design of a new hard X-ray Compton scattering polarimeter based on scintillating fibres technology is presented and studied in detail by means of Monte Carlo calculations. Several different configurations and materials have been tested in order to optimise the sensitivity in the medium/high energy X-ray band. A high sensitivity over the energy band 20–200 keV is obtained for a two material configuration. The advantages deriving from employing a new scintillating material, the YAP ($YAlO_3$), are also discussed.

1. Introduction

Since the first observation of a celestial X-ray source, Sco X-1, performed with a sounding rocket about 30 years ago [1], the improvement in the imaging and spectroscopic techniques for X-ray astronomy have been spectacular (see Ref. [2] for a recent review), and further important developments are expected in the near future. In order to have a more complete picture of the mechanisms responsible for the X-ray emission in cosmic sources, it would be very important to add polarimetric informations to the spectroscopic, imaging and temporal ones (e.g. Refs. [3], [4]). Unfortunately, the intrinsic difficulties in the X-ray polarimetric techniques and the limited collecting area of most telescopes flown so far prevented an extensive search for polarisation in X-ray sources. Actually, the X-ray polarisation is known at present for only one source, the Crab Nebula [5].

Only one X-ray polarimeter is at present scheduled for near future missions. SXRP (Stellar X-Ray Polarimeter [6]), on board the satellite Spectrum-X-Γ (to be launched in 1996), will be able to search for linear polarisation as low as a few percent in many galactic X-ray sources, in the energy band ~6–20 keV plus two narrow bands around 2.6 and 5.2 keV.

It would be very interesting to extend polarimetric measurements in the hard X-ray band (say, above 20 keV), both for the intrinsic astrophysical interest of such energy region, and because it would permit the use of balloons instead of the much more expensive and complex satellites, a use which is prevented at lower energies by atmospheric absorption.

In this paper we present the basic design and the simulated performances of a polarimeter for the hard X-ray band. This polarimeter is based on the well-known dependence of the angular distribution of the Compton scattering on the linear polarisation of the incident photons, but the proposed geometry and detection technique is of a new conception.

Because hard X-ray concentrators are still in their childhood, the geometrical area of the detector should be as large as possible in order to collect a sufficient number of photons. On the other hand, after the photon has suffered two or more scattering processes the information on the initial polarisation is largely lost; this limits the scale of the scatterer, in the direction perpendicular to that of the incident photons, to thicknesses of, at most, one mean free path. A possible way to reconcile these two opposite requirements is to increase the number of scattering elements and to use each scatterer as a detector too.

With regard to the working energy band, an absolute upper limit is set by the weakening of the dependence of the angular distribution of the scattered photons on the polarisation of the incident ones, which occurs around $m_e c^2$. The lower limit is determined by the photoelectric absorption. Given the strong dependence on Z of the photoabsorption cross section, the scattering material should be chosen with an atomic number as low as possible.

The paper is organised as follows: in Section 2 the basic physics and formalism involved are reviewed. In Section 3 the fibre polarimeter concept is presented. Section 4 is devoted to the description of the simula-

* Corresponding author. Tel. +39 6 9424589, fax +39 6 9416847, e-mail feroci@saturn.ias.fra.cnr.it.

SSDI 0168-9002(95)00460-2

REFERENCES

ITER Breeding Blanket

" ITER Design Description Document DDD G-16 WBS 1.6B Tritium Breeding Blanket System" ITER Breeding Blanket Meeting San Diego CA Oct. 1997

ITER Shielding Analysis

" ITER Nuclear Analysis" R.T. Santoro, L. Petrizzi et al. Presented at 19 SOFT (Symposium on Fusion Technology) Sept. '96 Lisbona

"Three-Dimensional Neutronics and Shielding Analyses for the ITER Divertor" M.E. Sawan, L. Petrizzi et al June 1996, Presented at the 12 Topical Meeting on the Technology of Fusion Power, Reno NV

"3-D Shielding Analyses of the Vertical and Mid-Plane Ports in ITER" L. Petrizzi, R.T. Santoro et al. June 1996, Presented at the 12 Topical Meeting on the Technology of Fusion Power, Reno NV

FNG neutronics analyses

"Shielding Neutronics Experiment" Final. Report on Eu contribution to ITER Task T218, P. Batistoni, L. Petrizzi et al., Nov. 1997

"Neutronics Shield Experiment For Iter At The Frascati Neutron Generator FNG", P. Batistoni, W. Daenner, L. Petrizzi et al. Presented at XVIII SOFT (Symposium on Fusion Technology) Sept. '96 Lisbona, published on Fusion Technology 1996

"Analysis of integral experiments on stainless steel shields for the validation of the FENDL library" V.Rado, P. Batistoni, L. Petrizzi. Fusion Engineering and Design 37 (1997) 39-48

"Analysis of the nuclear heating experiment for the ITER shielding blanket" L. Petrizzi, P. Batistoni, V.Rado proceedings of "Specialist' Meeting on Photon Production Data" held in Bologna Nov. 1994

"Integral data tests of the FENDL-1 nuclear data library for fusion applications" U. Fisher, P. Batistoni, L. Petrizzi, V.Rado. ENEA/RTI/ERG/FUS/NEU(96)01

Neutron Collimators

"Calibration of the neutron profile monitor diagnostic at JET by means of the Monte Carlo code for Neutron and Photon transport MCNP". M.Rapisarda. 4th Int. Conf. on Applications of Nuclear Techniques: "Neutrons and their applications". Crete, Greece, June 12-18 1994.

"Calculations of neutron streaming effects through the ports of the ITER fusion reactor." M.Rapisarda and P.Batistoni 5th Int. Conf. on Applications of Nuclear Techniques : "Neutrons in research and industry", Crete June 9-15 1996.

."A Neutron Camera for ITER" PF.B. Marcus, J.M. Adams, D.S. Bond, P.Batistoni, T. Elevant, N.P. Hawkes, O.N. Jarvis, L. Johnson, L. de Kock, M. Loughlin, M. Rapisarda, G. Sadler, P. Stott, C. Walker, N. Watkins Rev. Sci. Instrum. 68, No. 1 (1997) 514-519.

Test Blanket Module for ITER

"The Thermo-Mechanical Design of the Water Cooled Pb17Li Test Blanket Module for ITER" C. Nardi, M. Fütterer, F. Lucca, A. Palmieri, T. Pinna,M.T. Porfiri, M. Rapisarda, M. Roccella. SOFT-20 – Marseille (France) 7-11 September 1998 – Topic H

"Neutronic shielding analysis of the TBM." M.Rapisarda 1998 Conference on Computational Physics, Granada 2-5 Sept.

Astrophysics applications in collaboration with CNR

"Monte Carlo simulation of the materials and filling gas of the Imaging Proportional Counters for SXRP (Stellar X-Ray Polarimeter)". M.Feroci, E.Costa, M.Rapisarda S.P.I.E. 1743, 104 (1992).

"Background in Xenon filled X-Ray detectors".Nuclear Instruments and methods in Physics Research A, 371 (1996) 538-543. M.Feroci, E.Costa, J.Dwyer, E. Ford, P.Kaaret, M.Rapisarda, P.Soffitta.

"Design of a scattering polarimeter for hard X-Ray Astronomy". E.Costa, M.N.Cinti, M.Feroci, G.Matt, M.Rapisarda. Nuclear Instruments and methods in Physics Research A 366 (1995) 161-172.

"Treatment of Compton scattering of linearly polarized photons in Monte Carlo codes" G.Matt, M.Feroci, M.Rapisarda, E.Costa. .Radiation Physics and Chemistry, Vol.48, N.4, pagg.403-411 (1996).

"The Gamma Ray Bursts Monitor onboard Beppo-SAX: the Monte Carlo simulation for the response matrix" M. Rapisarda, L. Amati, M.N. Cinti, M. Feroci, and E. Costa, M. Orlandini, L. Nicastro, E. Palazzi, and D. Dal Fiume, P. Collina, G. Zavattini, and F. Frontera. Proc. SPIE Conference 3114 (San Diego, 1997).

Monte Carlo Methods and Models for Applications
in Energy and Technology

Workshop to be held at Forschungszentrum Karlsruhe, May 12-14, 1998

Monte Carlo Approach to Modelling of a Detection System for Gamma-Sources Embedded in Metal Truck Loads

M. Marseguerra, E. Zio

Dept. of Nuclear Engineering
Polytechnic of Milan-Italy
Via Ponzio 34/3, 20133 Milano, Italy

ABSTRACT

Although the use and disposal of radioactive materials is regulated by appropriate national and international agencies, the possibility that such materials could enter the recycling process as scrap cannot be overlooked. Several incidents occurred in recent years have demonstrated that, given the many varied uses of radioactive materials in modern industry and medicine, it is possible that these materials can find a way to a scrap processor's plant where recycling may lead to an internationally widespread contamination. This is a real problem that cannot be ignored.

To the authors' knowledge, this problem has been tackled primarily on an experimental basis. In this paper, we present a Monte Carlo approach to modelling of a detection system for scrap--iron loaded trucks. To estimate detectability limits for real situations, both homogeneous and inhomogeneous loads are considered, for various positions of shielded and unshielded sources.

Last modified: Thu Apr 2 13:49:26 1998

Workshop on
Monte Carlo Methods and Models for Applications
in Energy and Technology

Forshungszentrum, Karlsruhe, May 12-14, 1998

MONTE CARLO APPROACH TO MODELLING OF A DETECTION SYSTEM FOR GAMMA-SOURCES EMBEDDED IN METAL TRUCK LOADS

M. Marseguerra, Enrico Zio

Department of Nuclear Engineering
Polytechnic of Milan, Italy

STATEMENT OF THE PROBLEM

- Several incidents occurred in recent years have demonstrated tha radioactive materials from various uses can find a way into a scra processor's plant where recycling may lead to widespread contamina tion.
  - Auburn, NY (steel plant) $\Rightarrow$ 0.93 MBq of ^{60}Co
  - Juarez, Mexico (metal pellets stolen and sold as scrap metal) $\Rightarrow$ 2.59 MBq of ^{60}Co
  - Taiwan $\Rightarrow$ bad handling of ^{60}Co sources
  - Ireland $\Rightarrow$ 3.7 GBq of ^{137}Cs source of scrap melted into pellet- manufacts exported in England; widespread contamination o construction materials
- Radioprotection problem but also big economical burden (decontam- ination, lost revenue from production stoppage, decreased sales ...)
- Monitoring incoming scrap–loaded trucks at the foundry gate $\Rightarrow$ ex- perimental approach, so far.

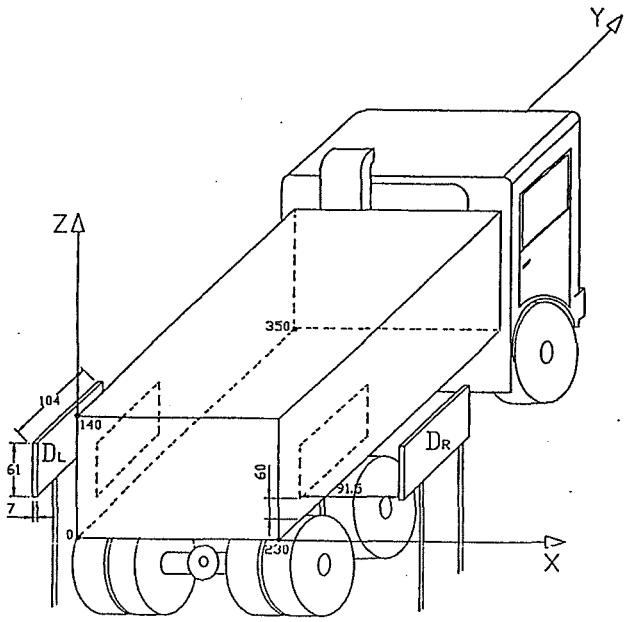

ure 1. Sketch of the truck and the detection system at the foundry gate. Note the two ector plates D_L and D_R which monitor the truck during its passage.

THE MODEL

Consider a γ flying in direction Ω from point P inside the truck loaded with scrap-iron

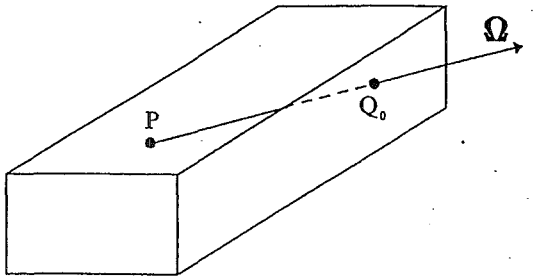

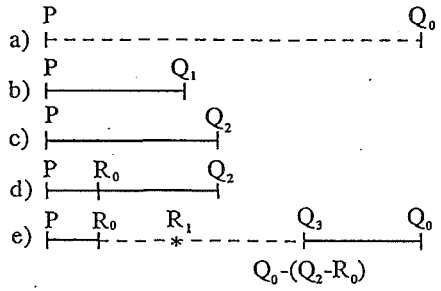

(Thick lines refer to solid iron)

Fig. a) : PQ_0 = Geometric chord within the truck loaded with scrap-iron.

Fig. b) : PQ_1 = Solid iron thickness corresponding to the scrap-iron thickness PQ_0

Fig. c) : PQ_2 = Random (uniform or triangular distributions) variation of PQ_1 within $\pm$ 10%

PR_0 = Sampled point of the γ interaction in case of infinite solid iron.

$PR_0 \geq PQ_2$: The γ flies out of truck without further interactions.

Fig. d) : $PR_0 < PQ_2$: The γ interacts at R_0 (in solid iron).

Fig. e) : The interaction point in scrap-iron must occur beyond R_0 and before $Q_3 = Q_0 - (Q_2 - R_0)$: its value R_1 is randomly (uniform or triangular distributions) sampled within (R_0, Q_3).

```
INPUT FILE FOR PROGRAM CAMION
24-OCT-97          12:16:50
FILE NAME : truck.dat

uck width along X  (cm) =                                    2.30000E+02
uck length along Y (cm) =                                    3.49700E+02
uck height along Z (cm) =                                    1.40000E+02
uck speed (Km/h) =                                           3.50000E+00
unting time (s) (it has a meaning only if VTRUCK=0) =        5.13977E+00
tection system dimension along Y (cm) =                      1.04100E+02
tection system dimension along Z (cm) =                      6.09600E+01
tection system thickness along X (cm) =                      5.71000E+00
tection system height from ground (cm) =                     6.00000E+01
e between truck side and detection system (cm) =             9.15000E+01
tection material density (g/cm^3) =                          1.03200E+00
tection energy threshold (MeV)          =                    0.00000E+00
 of detectors along Y =                                              2
mber of energy channels =                                          130
erage iron scrap density (weight/total volume) (g/cm^3) =    1.00000E+00
mber of randoms for scrap iron density randomization     =          2
nsity of solid iron (weight/volume of solids) (g/cm^3) =     7.80000E+00
urce characterization:
     N. points of X grid                                           5
     N. points of Y grid                                           8
     Z elevation                                             7.00000E+01
e sphere radius (cm)   R  =                                  3.00000E+00
     strength (photons/s) =                                  1.00000E+06
ergy (Mev) =                                                 1.30000E+00
rameter of solid material distribution =                     1.00000E-01
itial seed =                                                      7549305
```

Pb Shield	Source position	Mean counts/photon		Source strength (photon/s) for 500 counts in 4.67 s	
		Homog.	Heterog.	Homog.	Heterog.
R = 0 cm	centre ^{60}Co	$2.0 \cdot 10^{-4}$	$1.0 \cdot 10^{-3}$	$5.4 \cdot 10^{5}$	$1.1 \cdot 10^{5}$
	centre ^{137}Cs	$8.0 \cdot 10^{-5}$	$1.0 \cdot 10^{-3}$	$1.3 \cdot 10^{6}$	$1.1 \cdot 10^{5}$
	periphery ^{60}Co	$8.0 \cdot 10^{-3}$	$7.0 \cdot 10^{-3}$	$\underline{1.3 \cdot 10^{4}}$	$1.5 \cdot 10^{4}$
	periphery ^{137}Cs	$1.0 \cdot 10^{-2}$	$8.0 \cdot 10^{-3}$	$\underline{1.1 \cdot 10^{4}}$	$1.3 \cdot 10^{4}$
R = 3 cm	centre ^{60}Co	$8.0 \cdot 10^{-5}$	$4.0 \cdot 10^{-4}$	$\underline{1.3 \cdot 10^{6}}$	$2.7 \cdot 10^{5}$
	centre ^{137}Cs	$5.0 \cdot 10^{-6}$	$3.0 \cdot 10^{-5}$	$\underline{2.1 \cdot 10^{7}}$	$3.6 \cdot 10^{6}$
	periphery ^{60}Co	$3.0 \cdot 10^{-3}$	$3.0 \cdot 10^{-3}$	$3.6 \cdot 10^{4}$	$3.6 \cdot 10^{4}$
	periphery ^{137}Cs	$4.0 \cdot 10^{-4}$	$3.0 \cdot 10^{-4}$	$2.7 \cdot 10^{5}$	$3.6 \cdot 10^{5}$

Table I: Mean counts per photon for ^{60}Co and ^{137}Cs sources in central and peripheral position (from Figures 3 and 4 for ^{60}Co) and corresponding source strengths giving rise to a detectability limit of 500 counts on either one of the two side detectors. The underlined values identify the minimum and maximum source strengths and provide us with upper and lower limits of detectability.

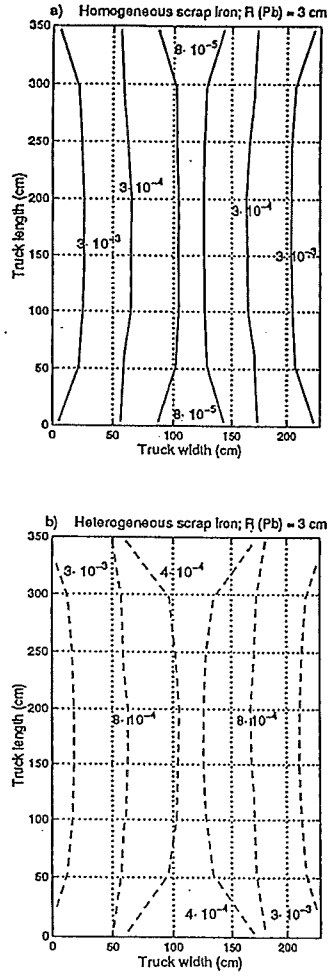

Figure 3. Count probability contour plots for a shielded (3 cm thick Pb) point source of ^{60}Co :
a) homogeneous scrap iron; b) heterogeneous scrap iron.

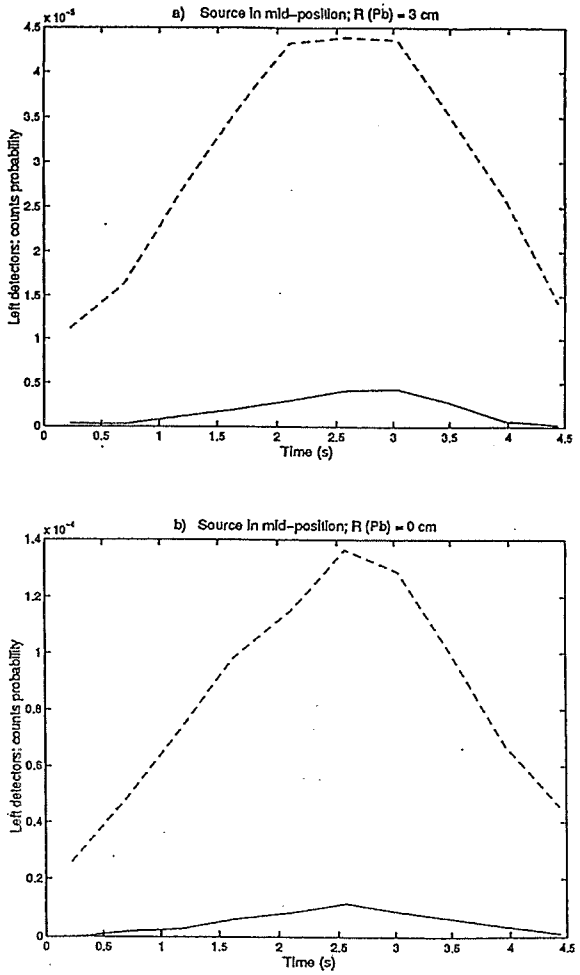

Figure 5. Time distribution of the left detectors count probability during the truck passage for a source in the mid-point of the truck container:
a) 3 cm thick Pb-shielded source; b) unshielded source.
Solid line = homogeneous load; dashed line = heterogeneous load.

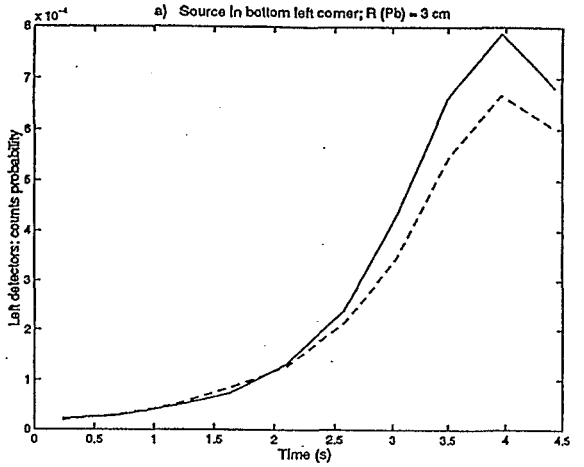

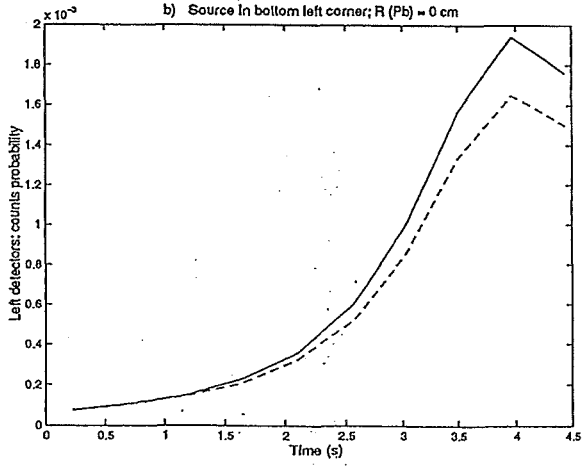

'igure 6. Time distribution of the left detectors count probability during the truck passage or a source in the bottom left corner of the truck container:
) 3 cm thick Pb-shielded source; b) unshielded source.
olid line = homogeneous load; dashed line = heterogeneous load.

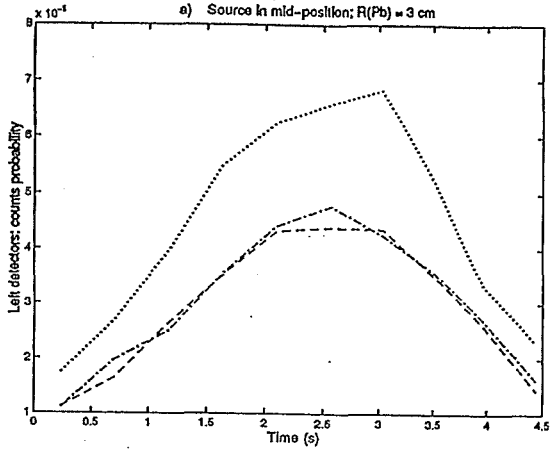

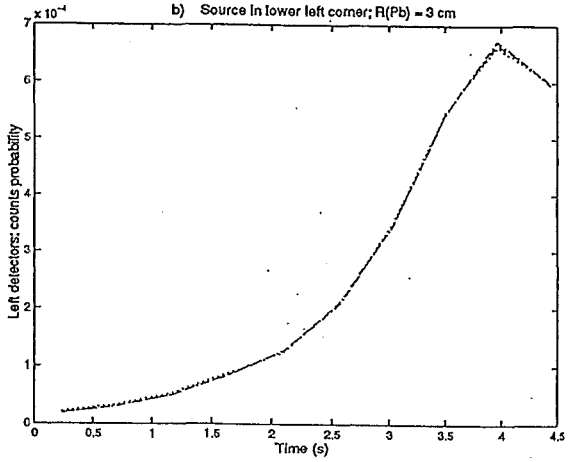

'igure 8. Time distribution of the left detectors count probability during the truck passage or a shielded (3 cm Pb-sphere) source in the mid point (a) and in the lower left corner b) of the truck container.
leterogeneity distribution parameter $\alpha = 0.1$ (dashed line); $\alpha = 0.3$ (dash-dotted line); $= 0.9$ (dotted line).

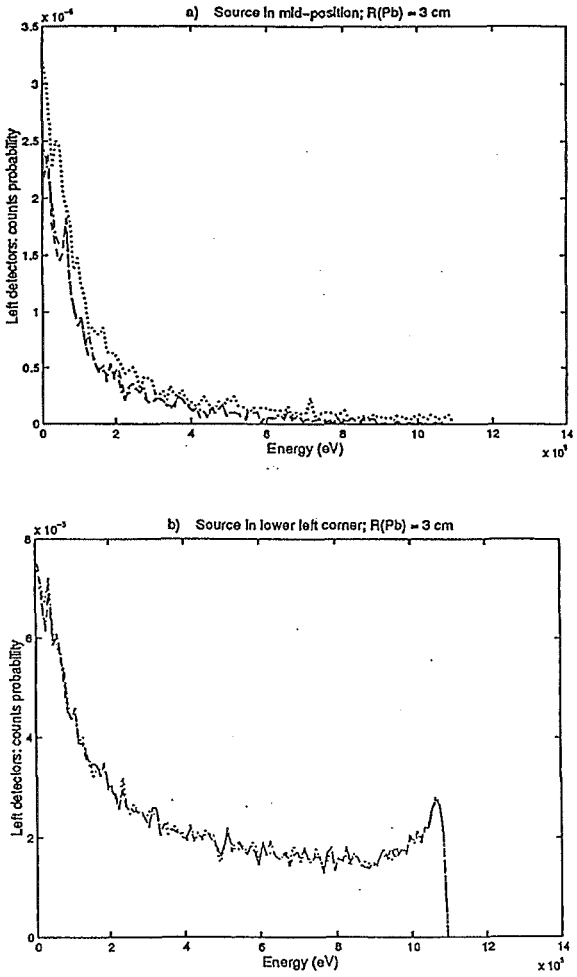

Figure 9. Left detectors energy spectra for a shielded (3 cm Pb–sphere) source in the mid-point (a) and in the lower left corner (b) of the truck container.
Heterogeneity distribution parameter $\alpha = 0.1$ (dashed line); $\alpha = 0.3$ (dash-dotted line); $\alpha = 0.9$ (dotted line).

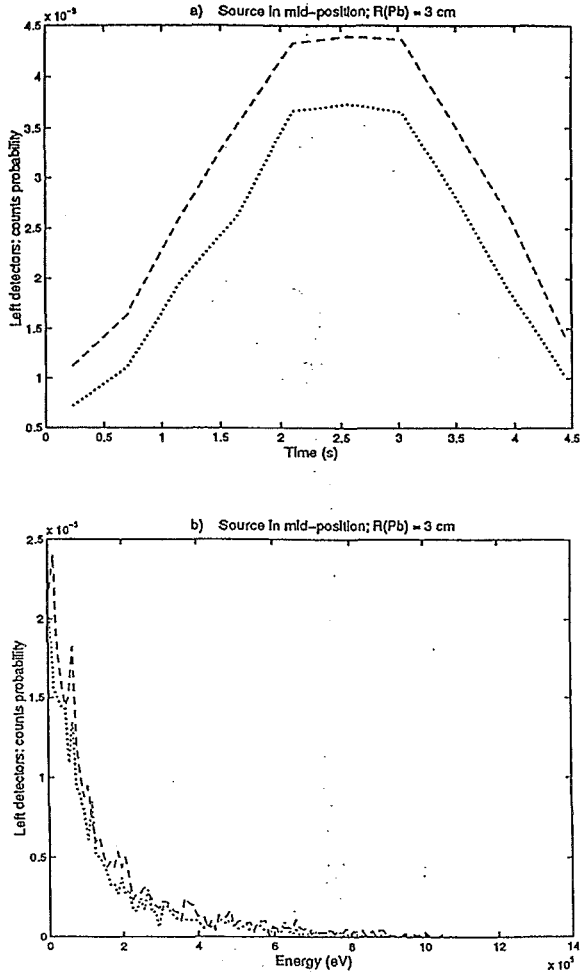

Figure 10. Left detectors count probability during the truck passage for a shielded (3 cm Pb–sphere) source in the mid point. Time distribution (a); energy spectrum (b). Heterogeneity distribution parameter $\alpha = 0.1$.
Dashed-line = uniform distribution; dotted line = triangular distribution.

CONCLUSIONS

- Inadvertent radioactive contamination of steel is a real issue of international importance.
- Sagefuards procedure are being established throughout the world.
- Limits of detectability must be established.
- Models can strongly aid the investigation and bring insights in support of the design of the detection systems.
- The Monte Carlo approach seems to be well suited to account for the main physical aspects of the problem and for treating the associated uncertainties.
- The crucial issue is the representation of the inhomogeneities and this inevitably introduces additional uncertainty and subjectivity: the Monte Carlo approach allows for sensitivity analysis to test the robustness of the underlying assumptions.

REFERENCES

1. INTERNATIONAL ATOMIC ENERGY AGENCY, "Nature and Magnitude of the Problem of Spent Radiation Sources", Vienna, IAEA-TECDOC-620, (1991).
2. J.O. LUBENAU and D.A. NUSSBAUMER, "Radioactive Contamination of Manufactured Products", *Health Physics*, Vol. 51, pp. 409–425, (1986).
3. K.L. MILLER, "It's Broken and It Needs To Be Fixed!", *Editorial in Health Physics*, Vol. 68, no. 4, pp. 439, (1995).
4. J.O. LUBENAU and G. YUSKO, "Radioactive Materials in Recycled Metals", *Health Physics*, Vol. 68, no. 4, pp. 440–451, (1995).
5. NUCLEAR REGULATORY COMMISSION, "Contaminated Mexican Steel Incident. Importation of Steel Into The United States That Had Been Inadvertently Contaminated With Cobalt-60 As A Result Of Scrapping Of A Teletherapy Unit", (1985).
6. E. MARSHALL, "Juarez: An Unprecedented Radiation Accident", *Nature*, 223, pp. 1152–1154, (1984).
7. F. CAMPI, Private Communications, (1997).
8. M. ANTONOPOULOS, Private Communications, (1997).
9. W.P. CHANG, C-C. CHAN and J-D. WANG, "^{60} Co Contamination in Recycled Steel Resulting in Elevated Civilian Radiation Doses: Causes and Challenges", *Health Physics*, Vol. 73, no. 3, pp. 465–472, (1997).
10. A. LAMASTRA, "The Changing Face of Radioactivity in Steel", *Spring Convention of the Association of Iron and Steel Engineering*, (1994).
11. J. O'GRADY, C. HONE and F.J. TURVEY, "Radiocesium Contamination at a Steel Plant in Ireland", *Health Physics*, Vol.70, no.4, pp. 568–572, (1996).

Monte Carlo Methods and Models for Applications in Energy and Technology

Workshop to be held at Forschungszentrum Karlsruhe, May 12-14, 1998

Simulation of Ge-Detector Calibration Using MCNP Code

J. Ródenas

Department of Nuclear Engineering
Polytechnic University
P. O. Box 22012, E-46071 Valencia, Spain

The determination of the activity deposed into the inner side of the process pipes of a LWR is very important to plan ALARA actions. These actions are focused on reducing the source term in order to decrease the collective doses received by exposed professional workers.

Nevertheless, the analysis using direct measurements presents the problem of the detector calibratior because they have to be done in places with difficult access and high dose rates. The experimental duplication of the source is not very easy, so it is more convenient to apply a calculation solution, such as the Monte Carlo method, for the detector efficiency calibration.

The detector geometry has been modelled with MCNP code and the detector response has been obtained using F8 tally, that is specific for pulse height determination. Thus, MCNP simulates the detection process to obtain spectrum peaks.

The procedure has been validated using different gamma sources in Laboratory. Several scenarios have been modelled including interposition of shielding plates and displacement of the source in respect to the detector. All sources used for validation have been considered as point sources. Comparison between experimental and calculated efficiencies shows a ratio LAB/MCNP with deviations less than 10% over the average, except in some few cases. Computer times are short and no serious problems have been found.

To model the actual situation a surface cylindrical source is introduced very close to the inner side of the pipe. The only allowed variance reduction for F8 tally is a bias in direction, but it is not sufficient. The relative error must be lower than 0.10 in order to ensure a reliable quality of the tally. However to accomplish that, a large amount of particles (up to 850000000 photons for longer distances and some energies) have to be started. That number of photons in any case has been lower than 375000000. Therefore, computing times become increased up to 1000 min. or more. Furthermore, when such a big number of photons is entered, a warning appears stating: "random number period exceeded, decrease stride". After this warning, if calculations are continued some fluctuations in the error are observed.

A possible solution is to calculate the number of photons entering a cell just in front of the detector, using another tally which permits more powerful methods of variance reduction. Results obtained with that tally would be considered as the source for the actual (F8) problem. This has not been modelled yet. Another possibility to decrease computing time might be to cut out the cylindrical source by an axial plane, disregarding the back side of the pipe. But unfortunately it is not allowed by the code.

Consequently, some powerful method of variance reduction is needed as well as a study on the random

number generation.

Last modified: Thu Apr 2 14:03:15 1998

Monte Carlo Methods and Models for Applications in Energy and Technology

Workshop held at Karlsruhe (Germany), May 12-14, 1998

SIMULATION OF Ge-DETECTOR CALIBRATION USING MCNP CODE

José Ródenas

Department of Nuclear Engineering

Polytechnic University of Valencia (Spain)

CONTENTS

- INTRODUCTION
- VALIDATION
- CALIBRATION FOR A PIPE
- PROBLEMS IN PIPE CALIBRATION
- CONCLUSIONS

INTRODUCTION

- *Dose reduction programs at Nuclear Power Plants include a measurement campaign to determine activities and doses in specific areas of the plant.*
- *A gamma spectrometry device is used for direct on-site measurements. The equipment includes a Germanium detector.*
- *On-site spectra acquisition is an essential tool to monitor the radionuclide concentration deposed into the inner side of the process pipes of the plant.*
- *The determination of this activity is very important to plan the ALARA actions that must be taken and to analyse its results.*
- *ALARA actions are focused on reducing the source term, in order to decrease collective doses received by exposed professional workers.*

Objectives of the Measurement Campaign

- *The objectives of evaluating gamma emissions at different points of the plant are:*
  - *To characterise the source term, in order to know its contribution to dose rate at a point.*
  - *Cost-benefit optimisation of a possible dose reduction action.*
  - *To assess the concentration tendency for certain radionuclides at points of interest.*
- *One of the most important purposes of the measurement campaign, included in the dose reduction program at NPPs, is to determine the average level of radioactive contamination (mainly caused by corrosion products), on specific plant component surfaces by using a direct on-site measurement, without taking samples.*
  - ➡ *activity deposed into the inner side of the recirculation loop pipes in a BWR (Cofrentes).*

4

CALIBRATION

- *The major problem in this kind of measurement work is the efficiency calibration of the spectrometry system.*
- *Measurements are performed in hard-to-access plant locations with high dose rates.*
- *As the experimental efficiency calibration becomes unpractical and too time consuming, and the experimental duplication of the source is not very easy...*
  - ➡ *it is more convenient to apply a computational solution, such as Monte Carlo method, for the detector efficiency calibration.*
- *MC provides a calibration method for those geometries, which cannot be handled in laboratory.*
- *The model can be used to scale experimental results for other geometries of the same type and can serve as a reference and flexible validation method of results to obtain maximum reliability.*

5

MC METHOD

- *Applying **Monte Carlo (MC) method**, the solution is searched by calculating random particle histories based on the particle cross section libraries and the geometrical information.*
- *Each particle history is calculated until the particle ceases to exist or it is transferred outside the problem range. In order to achieve a statistically reasonable and accurate result, **the amount of particle history simulations has to be fairly large**.*
- *MC method has been applied for the detector efficiency calibration using the **version 4A of MCNP code**.*
- ***MCNP** is an advanced MC simulation program, which contains all the necessary cross section data for neutron, photon and electron transport calculations.*
- *The version used is suitable for modelling the detector response, since it contains a **tally (F8) for detector pulse height determination**.*
- *MCNP simulates the detection process to obtain spectrum peaks.*

VALIDATION at UPV

- ***The computational calibration procedure was validated using gamma sources in laboratory.***
- ***All sources used for validation were considered as point sources.***
- *In a former stage, the efficiencies calculated by MCNP have been compared with the peaks measured in the Laboratory of Nuclear Engineering at the Polytechnic University of Valencia.*
- *It was considered:*
  - ***Three different distances between source and detector***
  - *for each distance **five scenarios (no shielding, stainless steel** and **lead** filters, both using **two different filter thickness**).*
- *Laboratory measurements as well as MCNP calculations have been performed for **two different energies**, resulting in **30 measurements** and the corresponding estimated efficiencies.*
- *MCNP/Lab ratio presented a deviation less than 10% over the average.*
- *The **comparison was relative** as they were not calibrated sources.*

VALIDATION at CNC

- *In a second stage, a validation using a Cs-137 source and the equipment of Cofrentes NPP (CNC) was performed.*
- ***Three studies were developed to analyse the influence of distance, shielding and off-centre on the calibration procedure.***
- **Distance.** *The source has been placed (without any interposed shielding) at different distances from the detector, lined up with the detector axis.*
- **Shielding.** *Stainless steel plates of different thickness have been interposed between the source and the detector, placed at a fixed distance and lined up as in the first case.*
- **Displacement.** *The source has been moved up on a perpendicular to the detector axis, maintaining the distance between the planes containing the source and the detector front side. (No shielding).*
- *Again the* ***comparison was relative*** *as they were not calibrated sources.*

8

DETECTOR SET

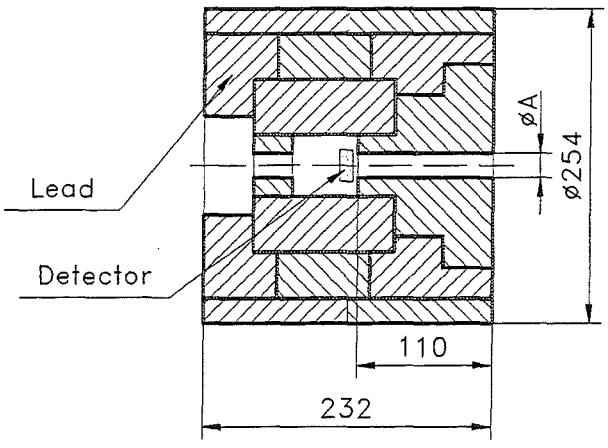

Collimator
A=10 mm
A=20 mm

9

DISTANCE ANALYSIS

DIST. (m)	Efficiency MCNP (B')	Normalised $B'' = B'/B_1$	Experim. E_i	Exp. Norm. $E' = E_i/E_1$	Ratio B''/E'
1	2.6663E-07	1	2.3639E+05	1	1
1.25	1.6971E-07	0.63649865	1.4907E+05	0.630610432	1.00933733
1.5	1.1752E-07	0.440744139	1.1100E+05	0.46956301	0.93862619
1.75	8.615E-08	0.323104225	8.4506E+04	0.357485511	0.90382467
2	6.5721E-08	0.246483768	5.7303E+04	0.242408731	1.0168106

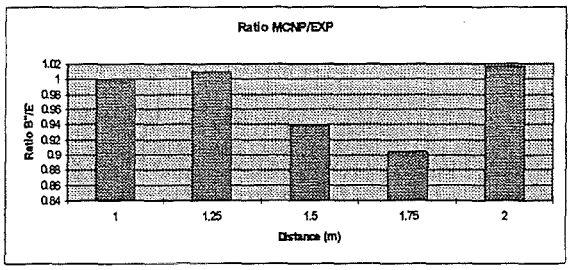

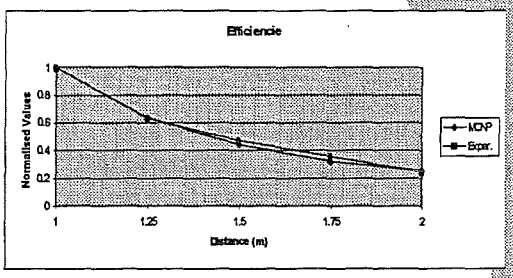

SHIELDING ANALYSIS

Thickness (cm)	Efficiency MCNP (B')	Normalised $B'' = B'/B_1$	Experim. E_i	Exp. Norm. $E' = E_i/E_1$	Ratio B''/E'
0	1.1752E-07	1	1.09E+05	1	1
0.5	8.7578E-08	0.745238095	8.16E+04	0.74774998	0.99664075
1	6.5643E-08	0.558582503	6.10E+04	0.55930712	0.99870444
1.5	4.947E-08	0.420957918	4.54E+04	0.41602969	1.01184584
2	3.7093E-08	0.315642303	3.38E+04	0.31008157	1.01793313
2.5	2.7762E-08	0.23624031	2.48E+04	0.2270461	1.0404949

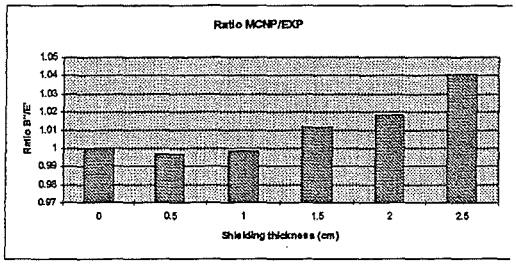

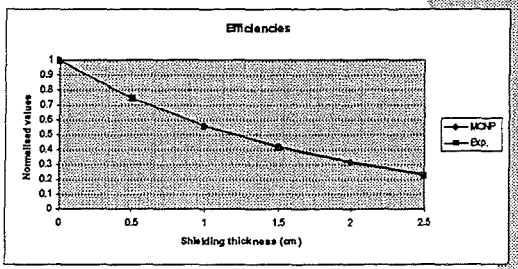

Diagram of Angles

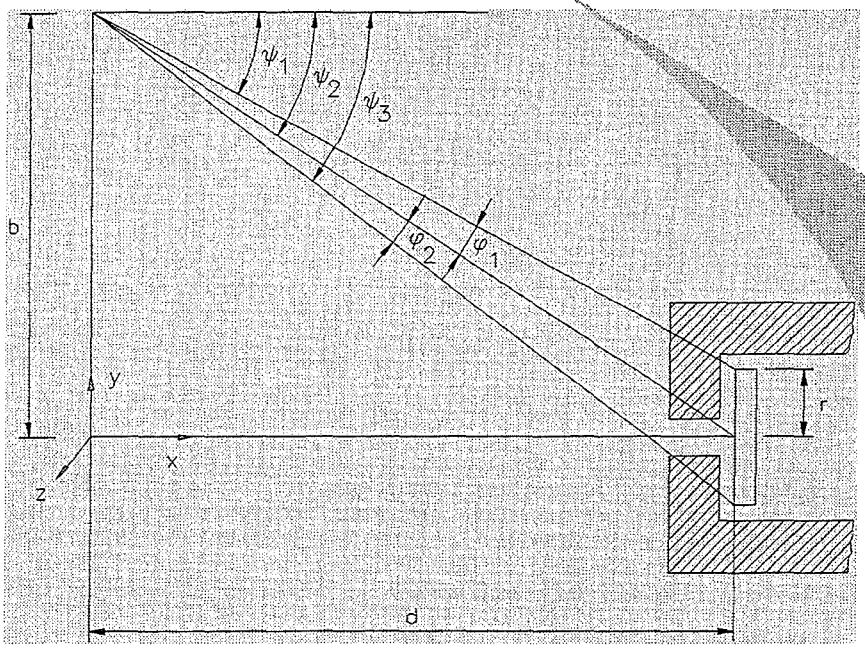

DISPLACEMENT ANALYSIS

Displac. (cm)	Efficiency MCNP (B')	Normalised B'' = B'/B$_i$	Experimental E$_i$	Exp. Norm. E' = E$_i$/E$_i$	Ratio B''/E'
0	1.1785E-07	1	111000	1	1
2	1.0546E-07	0.8948659	98445	0.88689189	1.00899096
4	8.6081E-08	0.73042146	81307	0.7324955	0.99716853
6	6.6701E-08	0.56597701	62297	0.56123423	1.00845062
8	4.7737E-08	0.40505747	45350	0.40855856	0.99143064
10	3.0325E-08	0.25731801	29200	0.26306306	0.97816092
12	1.6057E-08	0.13624521	16113	0.14516216	0.93857248

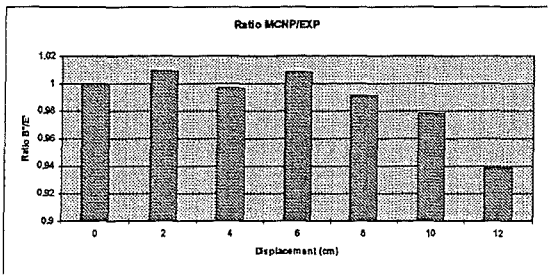

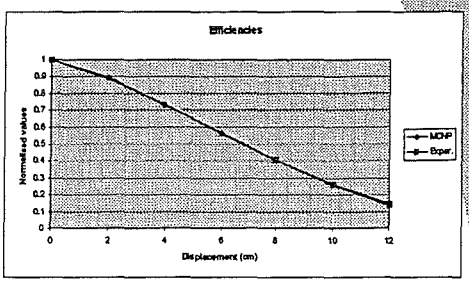

VALIDATION with CALIBRATED SOURCES

- *In a third stage, a validation using calibrated sources has been performed.*
- *The standard source was a 5 cm diameter filter where fission and activation products have been deposited and their activity has been exactly measured:*

  Cs-137 2.952 E+05 Bq

  Mn-54 3.504 E+05 Bq

  Co-60 6.713 E+05 Bq
- *The source has been simulated as a point source.*
- *Detector geometry model is the same as in previous cases.*
- *Calculations as well as measurements have been performed for both collimators, 10 and 20 mm.*
- *For each energy, efficiency results have been compared and the ratio MCNP/EXP represented*

ABSOLUTE CALIBRATION

10 mm Collimator

Isotope	Energy MeV	Efficiency MCNP (B')	Experimental E	Ratio B'/E
Cs-137	0.66166	2.6538E-07	1.99E-07	1.33354551
Mn-54	0.834	1.9091E-07	1.53E-07	1.24776873
Co-60	1.173	1.2384E-07	1.23E-07	1.00681472
Co-60	1.332	1.0737E-07	1.06E-07	1.01287921

20 mm Collimator

Isotope	Energy MeV	Efficiency MCNP (B')	Experimental E	Ratio B'/E
Cs-137	0.66166	9.7733E-07	8.53E-07	1.14575594
Mn-54	0.834	7.0032E-07	6.13E-07	1.14245031
Co-60	1.173	4.4952E-07	4.17E-07	1.0779966
Co-60	1.332	3.8694E-07	3.56E-07	1.08692317

COMPARISON of EFFICIENCIES

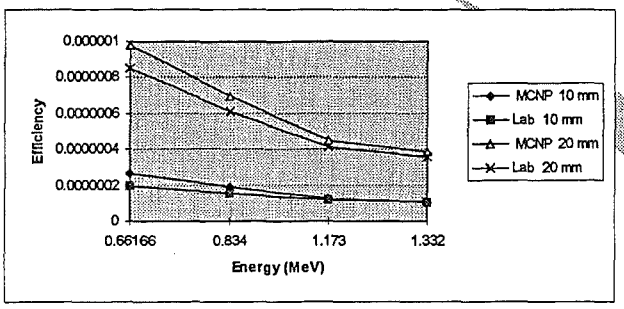

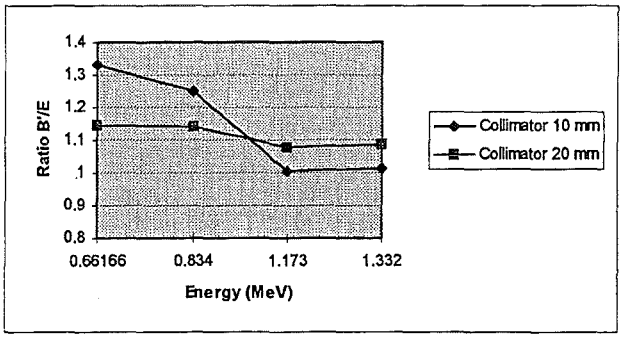

16

CALIBRATION for a PIPE

- ***The method is now applied to the assessment of surface contamination onto the inner side of the recirculation loop pipes in a BWR.***
- *A stainless steel pipe segment of 26 cm length and actual diameters has been modelled. Surface cylindrical source (representing deposed contamination) is introduced very close to the inner side of the pipe. To improve counting statistics, photons emitted towards the detector are preferentially counted.*
- *The pulse height obtained corresponds to one photon emission, that is, the efficiency in cps/Bq. Multiplying by the contaminated surface, the efficiency in cps/Bq/cm2 will be obtained.*
- *The actual surface contamination can be obtained just dividing the number of counts per second measured in the detector by the efficiency.*
- ***The simulation is repeated for several pipe-detector distances and each energy of interest, so a set of efficiency calibration curves can be obtained.***

17

MODEL of the PIPE

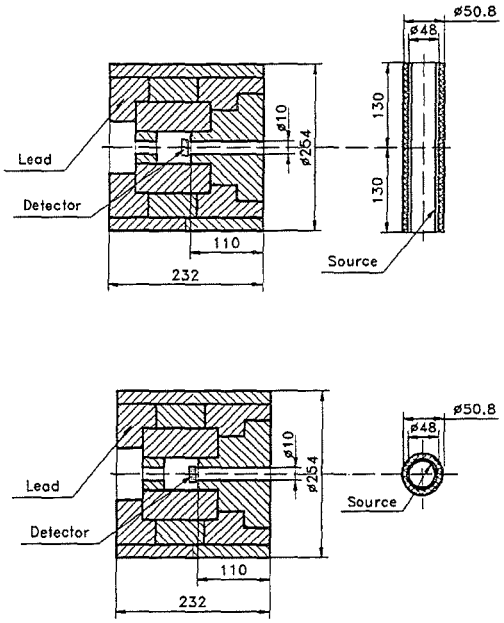

18

EFFICIENCY CURVES

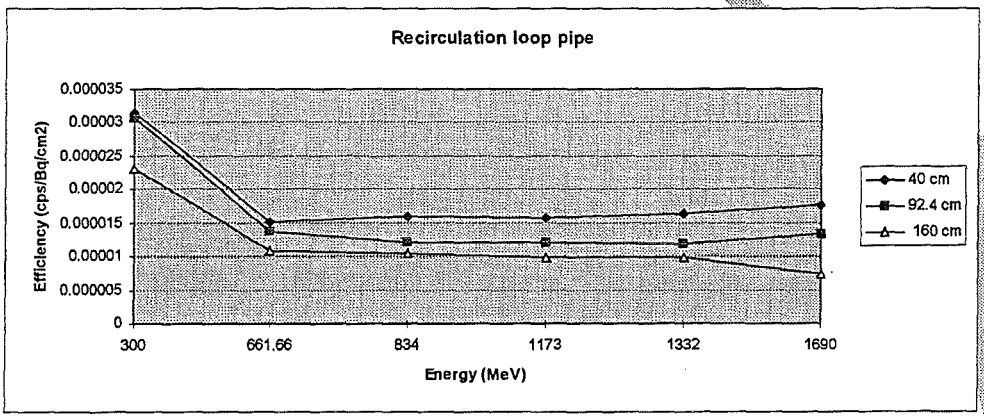

19

REMARKS

- *Variance reduction*
- *Relative error*
- *Number of particles*
- *Computing times*
- *Random number generator*

PROBLEMS

- *The only allowed variance reduction for F8 tally is a bias in direction.*
- **A large amount of particles have to be started to obtain a relative error lower than 0.10.** *Up to 850 x 10^6 photons in some cases, but never less than 375 x 10^6.*
  - ➡ **Computing times become increased up to 1000 min or even more.**
- *It appears a warning:* **"random number period exceeded, decrease stride".**
- *After this warning, if calculations are continued some fluctuations in the error are observed.*

Alternate Solution (1)

- *To calculate the number of photons entering a cell just in front of the detector, using another tally that permits more powerful methods of variance reduction.*
- *Results obtained with that tally would be considered as the source for the actual (F8) problem.*
- *This has not been modelled yet*

Alternate Solution (2)

- *To cut out the cylindrical source by an axial plane, disregarding the backside of the pipe. Unfortunately it is not allowed by the code.*
- *An alternate solution has been adopted to disregard photons emitted by the back half side of the source.*
- *A cylindrical surface closest to the inner side of the source has been modelled and the obtained cell, half a cylinder, was given an importance equal to 0.*
- *In this way, computing time is strongly reduced, up to 45 min for 350 x 10^6 photons, but relative error remains higher than 0.10.*

MISSING BACKSIDE

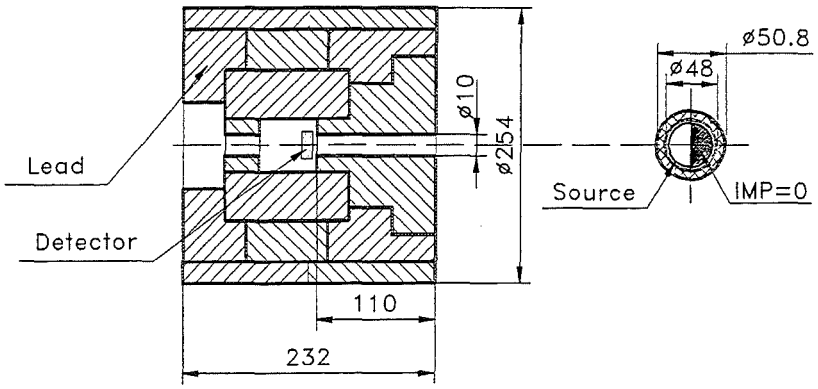

Alternate Solution (3)

- *Splitting the pipe by the plane XY, that is, the plane containing the detector axis, normal to the pipe axis.*
- *The upper side of the pipe is deleted and only the lower part is considered.*
- *In these runs, computing time decreased obtaining a similar value of the tally for 250 x 10^6 photons, with a relative error equal to 0.13.*

LOWER SIDE

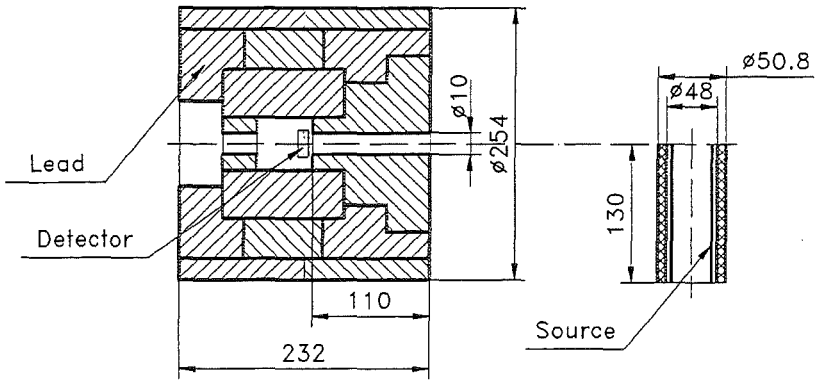

Energy cut-off card

- *In all runs a cell-by-cell energy cut-off card has been used.*
- *Lower energy cut-off was set to a few keV below the peak energy in all cells except detector, where it was set to 0.001 MeV.*
- *Nevertheless, two cases were run where the energy cut-off value was raised in the detector cell (e.g. up to 0.501 MeV for Cs-137 peak). In those cases a very peculiar behaviour was observed:*
  - *Computing time was increased.*
  - *Tally result was also increased.*
  - *Relative error decreased by a factor of two.*

CONCLUSIONS (1)

- *The detector efficiency can be determined by mathematical modelling with reasonable accuracy and reliability.*
- *MCNP code is a powerful and useful tool to obtain efficiency calibration, applicable to quantitative interpretation of the contamination measurements performed at NPPs.*
- *MCNP is a well validated program which may be used for validation of other computational methods.*
- *These computational methods have been scarcely applied so far, at least routinely, for detector efficiency calibration, but it is convenient to develop a work line in this sense.*

CONCLUSIONS (2)

- *When point sources are considered, calculations run quite well with reasonable computing times. On the other hand, relative error is always lower than 0.10, starting an acceptable number of photons.*
- *Nevertheless, when a surface source is considered, the number of photons to be started as well as computing time become highly increased. Furthermore, it appears the random number warning and some fluctuation on the relative error is observed.*
- *Some powerful method of variance reduction is needed as well as a study on the random number generation.*

REFERENCES

[1] "MCNP 4 A. Monte Carlo N-Particle Transport Code System", Los Alamos National Laboratory. Los Alamos, New Mexico, 1993.

[2] Tanner, V., Simbierowicz, P., Tiitta, A. "Efficiency calibration model for NPP surface contamination measurements (Final Report)", VTT Chemical Technology, December 1994.

[3] Iberdrola C.N. Cofrentes. Apoyo Técnico a la explotación. Equipo de espectrometría gamma aplicado a medidas de campo. P5090-OB-ES-005. Abril 95.

[4] Ródenas, J., Baeza, G., Serradell, V., Rius, V. "Simulación de la calibración de un detector de Germanio mediante el código MCNP 4A", XXII Reunión Anual SNE, Santander Octubre 1996.

[5] Ródenas, J., Rius, V. "Application of Monte Carlo method to the simulation of Ge-detector calibration", TOPSAFE'98, Valencia, 15-17 April 1998.

Appendix
INPUT FILE (1)

```
c Calibration for Ge detector
c ...activity measurements in RECIRCULATION LOOP PIPES
c collimator 10 mm
c Distance detector-pipe = 40 cm
c GEOMETRY
c DETECTOR CELLS
1 2 -5.32   -11 12 –13              imp:p=1 $detector
2 0          -4 1 –5                 imp:p=1 $ collimator 1st part
3 0         -6 5 -7 (11:-12:13)      imp:p=1 $ collimator 2nd part
4 0          -8 7 -9                 imp:p=1 $ collimator 3rd part
5 0          -10 -2 9                imp:p=1 $ collimator 4th part
6 1 -11.4   -3 1 -2 #2 #3 #4 #5 #1   imp:p=1 $ collimator shielding
c CELLS OF THE PIPE
52  8 -1.00    -34  35 -31           IMP:P=1 $ inside PIPE  (water)
53  3 -7.87    -34  35 -32  31 -39   IMP:P=0 $ half back PIPE
54  3 -7.87    -34  35 -32  31  39   IMP:P=1 $ half front PIPE
27  0   -39  32  38 -34 35 -36 37    IMP:P=0 $ gap behind PIPE
28  0    39  32 -1 -34 35 -36 37     IMP:P=1 $ gap between PIPE and collimator
29  0  1 -2 3  -34 35 -36 37         IMP:P=0 $ resonance box
8    0        34: -35: 36 :-37: -38: 2   imp:p=0 $ rest of universe
```

INPUT FILE (2)

```
c Surfaces of pipe
31 CZ 24.0665   $ inner side pipe
32 CZ 25.4      $ outer side pipe
34 PZ  13.00    $ top end pipe
35 PZ -13.00    $ bottom end pipe
c planes boxes
36  PY  25.4
37  PY  -25.4
38  PX -25.4
39  PX  0
c Surfaces detector
1  1 px 175        $ front plane collimator
2  1 px 198.2      $ back plane detector set (+ shielding
3  cx 12.7         $ exterior cylinder
4  cx 0.5          $ interior cylinder 1st part collimator
5  1 px 186        $ back plane 1st part collimator
6  cx 2.25         $ interior cylinder detector site
7  1 px 191        $ back plane detector site
8  cx 1            $ interior cylinder 3rd part collimator
9  1 px 194.2      $ back plane posterior 3rd part collimator
10 cx 4            $cylinder 4th part collimator
11 cx 1.275        $ cylinder detector
12 1 px 186.4      $ frontal plane detector
13 1 px 187.4      $ back plane detector
```

32

INPUT FILE (3)

```
c MATERIALS
m1 82000 1              $ lead
m2 32000 1              $ Germanium
M3 26000 1              $ Iron
M8  1000 0.67   8000  0.33          $ water
c vector (x,0,0) moving planes x y
tr1    -121 0 0
c source      Co-60 (1.17)
SDEF erg=1.173 POS=0 0 0 AXS=0 0 1 EXT=D2 RAD=24.0 VEC=1 0 0 DIR=D4 PAR=2
SI2 -13 -10 -7 -4 -2 0 2 4 7 10 13
SP2  0 1 1 1 1 1 1 1 1 1 1 1
SB2  0 1 1 2 4 8 8 4 2 1 1
SB4 -31  50.0
C Tallies
phys:p 100 1 0
f8:p,e 1
e8: 0 0.1 1.10 1.15 1.17 1.18 1.2
mode p e
CTME=200
c energy cut-off cell-by-cell except detector
elpt:p  0.001 1.169 11r
nps 375000000
print 126 130 140 160 30
```

33

Monte Carlo Methods and Models for Applications in Energy and Technology

Workshop to be held at Forschungszentrum Karlsruhe, May 12-14, 1998

Conceptual Design of Epithermal Neutron Beam for BNCT in the TRIGA Reactor Thermalizing Column

Marko Maucec, Bogdan Glumac

Josef Stefan Institute, Reactor Physics Divisior,
Jamova 39, 1111 Ljubljana - SLOVENIA

Activities on the field of Boron Neutron Capture Therapy research have been held in Slovenia since year 1994, when development of the epithermal neutron irradiation facility in one of the radial channels of "Josef Stefan Institute" (JSI) 250 kW TRIGA research reactor started. It proved out, that due to rather specific configuration, this option would not be suitable for BNCT experiments without extensive modifications, since the epithermal flux is approx. three orders of magnitude below the minimum therapy limit (10^9 n/cm^{2}s) containing rather high specific fast neutron as well as gamma doses.

Stimulated by the aforementioned facts, we initiated a new feasibility study of the utilizing the alternative epithermal neutron facility for BNCT in the thermalizing column (TC) of the TRIGA reactor. We particularly refer for the unique configuration of JSI TRIGA TC as the only reactor of this type in the world already having defined the irradiation room (the so called "dry cell") in a place, primarily devoted to the spent fuel storage pool. A special attention was devoted to the implementation of the fission converter of 30 W thermal power, which is already available at the Institute. The calculations prove that with the present fission converter it is possible to increase the epithermal flux for factor 2.4 and having increased the specific fast neutron dose for only 15% and gamma dose for 10%. The simple burn-up calculations and the estimation of the minimum air flow velocity of the force cooling system was also carried out.

An extensive parametric study of the moderating (Al_2O_3, AlF_3, FLUENTAL?, PbF_2, TEFLON? (CF_2)) and shielding materials (Pb, PbF_2, Bi, Pb(Li)) has been carried out in order to obtain the near optimum epithermal neutron beam performances. The advantage of raising the reactor power from 250 kW to at least 750 kW was also considered. The simulation results prove, that in the case of extended power level, we are able to assure a clean epithermal neutron beam (specific fast neutron dose 1.3×10^{-11} cGy cm^2/n$_{epi}$, specific gamma dose 2.3×10^{-11} cGy cm^2/n$_{epi}$) quite close to desired therapy limit (9×10^8 n/cm^{2}s) and consequently the irradiation times close to 1 h. Finaly, the approximate cost estimation of the optimized facility (Al/AlF_3 (pressed on 4.0 g/cm^3), PbF_2 reflector, Bi gamma shield and Pb collimator) has been carried out, on the basis of the extensive survey for the commercially available materials. It was estimated that the cost of elaboration should not exceed the amount of 60000 US$.

Last modified: Fri Apr 24 11:44:40 1998

BNCT in a TRIGA reactor thermalizing column

- feasibility study -

Marko Maučec, Bogdan Glumac

"Jožef Stefan" Institute, Reactor Physics Division
Ljubljana, Slovenia

Why did we pursue the study?

- inefficiency of the epithermal neutron irradiation facility installed in the radial channel
- intense utilisation of the thermal column for neutron radiography experiments

Reactor TRIGA Mark II - 250 kW

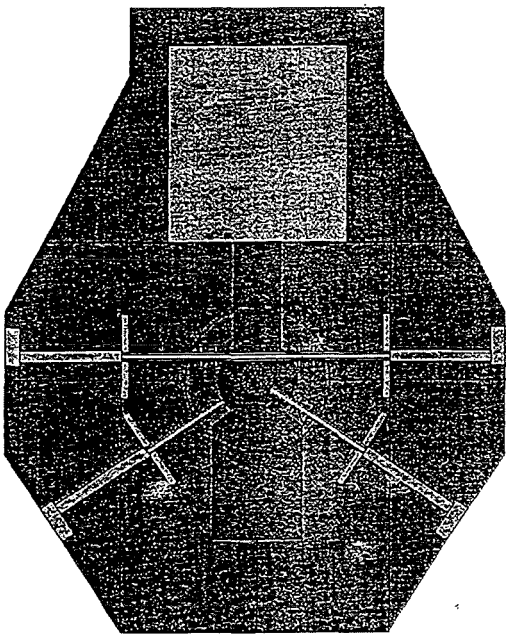

top view

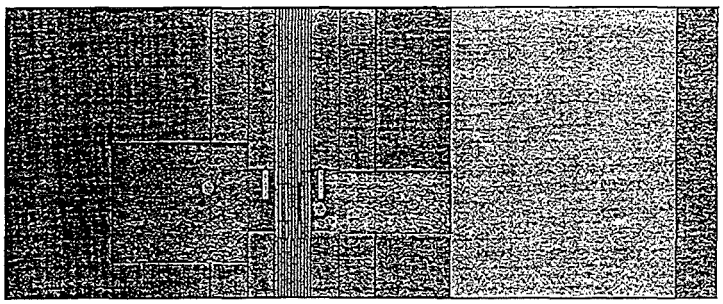

side view

Codes, methods and data

- MC transport code MCNP4B
- variance reduction methods: geometry splitting (initial), WWG (subsequent)
- cross-section data: ENDF/B-V and ENDF/B-VI evaluations
- flux-to-dose conversion factors: ICRP 51

What did we model and calculate?

- optimisation of the TRIGA reactor core
- utilisation of the neutron converter
- study of thermal neutrons absorbers
- study of reflector materials
- study of collimator materials
- study of gamma shielding
- study of epithermal neutron filters
- approximate cost estimation

Optimisation of the TRIGA reactor core

- 57 fresh fuel elements, 12% enriched
- excess reactivity: 4$ (2800 pcm)
- k_{eff} - 1.016 ± 0.002
- future plans: burned fuel elements and buildup of γ-dose

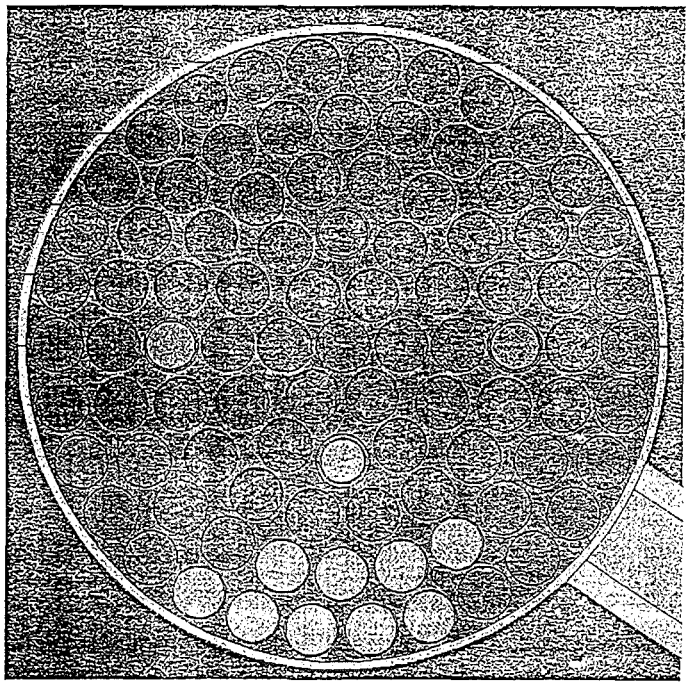

Normalisation of neutron source

- surface source option (SSW) on the Al clad of the core
- KCODE option: 1000 n/cycle and 2000 cycles (approx. $1.8 \cdot 10^6$ tracks)
- ν calculated for this TRIGA reactor core is 2.43
- n and γ tally normalisation factor at 250 kW - $2.1 \cdot 10^{16}$ n/cm^{2}s
- calculated for 500, 750 and 1000 kW

Characteristics of neutron converter

- m U^{tot} = 1468 g (m ^{238}U = 1174 g, m ^{235}U = 294 g, enrichment = 0.2)
- active part volume: 400.8 cm^3
- Φ_{term}= $9.8 \cdot 10^{11}$ n/cm^2s
- burnup estimation (10 y, 200 d/y, 8 h/d on 250 kW) less than 0.01%.
- energy released: 8 kW (at 250 kW)
- forced air cooling system - compulsory

Utilisation of neutron converter

Benchmark facility:

- 20 cm Al
- 30 cm AlF_3 (4 g/cm^3)
- 0.05 cm Cd
- 10 cm Bi
- Pb collimator
- 2.5 cm PbF_2 reflector
- 6 cm Li_2CO_3-poly neutron shield

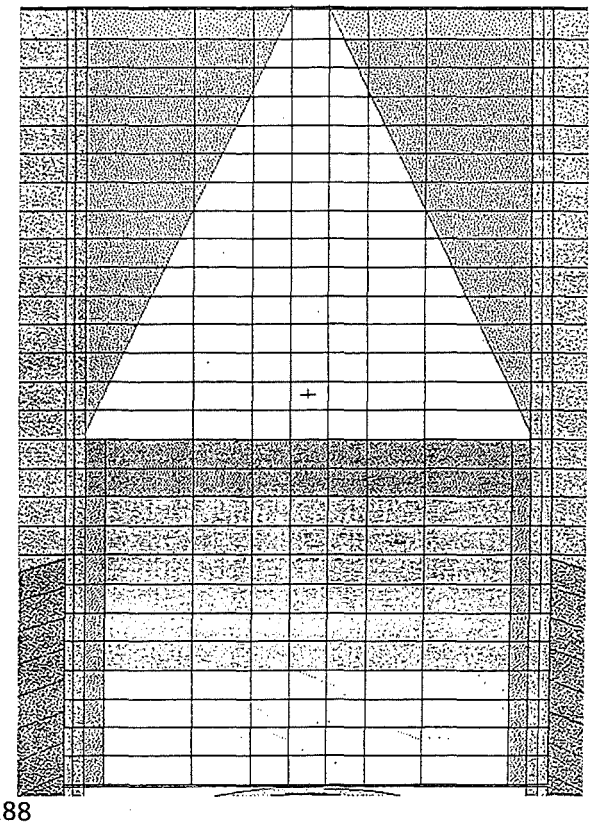

Utilisation of neutron converter

Efficiency of 8 kW fission converter:

- epith. n fluks Φ_{epi}: increase 2.4x
- D_{nfast} / Φ_{epi} = +15%
- D_{γ} = +10%
- D_{γ} / Φ_{epi}: decrease 2.3x
- J_{epi} / Φ_{epi} = +10%

Comparison between thermal neutron absorbers

	Cd	Gd	B_4C	Li_2CO_3-poly
Φ_{epi} (0.4eV-10keV) (10^9)	4.9	4.0	3.8	4.8
Φ_{th} (<0.4eV) (10^8)	0.6	0.65	0.7	7
Φ_{th} / Φ_{epi} ($x10^{-2}$)	1.22	1.67	1.83	14.4
Φ_{th} / Φ_{total} ($x10^{-2}$)	1.11	1.49	1.61	11.2
D_{γ} ($x10^{-3}$ Gy cm^2)	3.75	2.72	2.25	4.65
D_{γ} / Φ_{epi} ($x10^{-13}$ Gy cm^2)	7.6	6.8	6.0	9.7

Rel. err. Φ_{epi}: ±4%

Rel. err. D_{γ}/Φ_{epi}: ±11%

Comparison between reflector materials

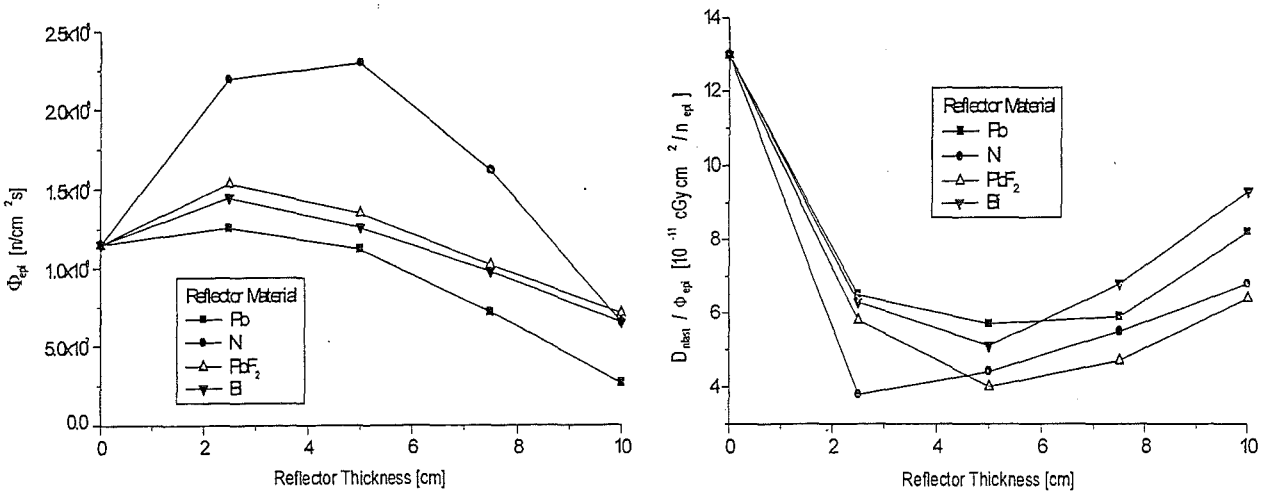

PbF_2 was selected for the reflector material

Comparison between collimator materials

M	Φ_{epi} (10^8 n/cm^{2}s)	D_{nfast}/Φ_{epi} (x10^{-13} Gy cm^2)	J_{epi}/Φ_{epi}
/	0.9	10.9	0.53
Pb	1.3	6.5	0.65
Ni	2.3	3.7	0.75
PbF_2	1.9	2.8	0.71
Bi	1.6	4.7	0.61

Rel. err. Φ_{epi}: ±4%

Rel. err. D_{nfast}/Φ_{epi}: ±8%

Pb and PbF_2 were selected as the collimator materials

Comparison between gamma shielding materials

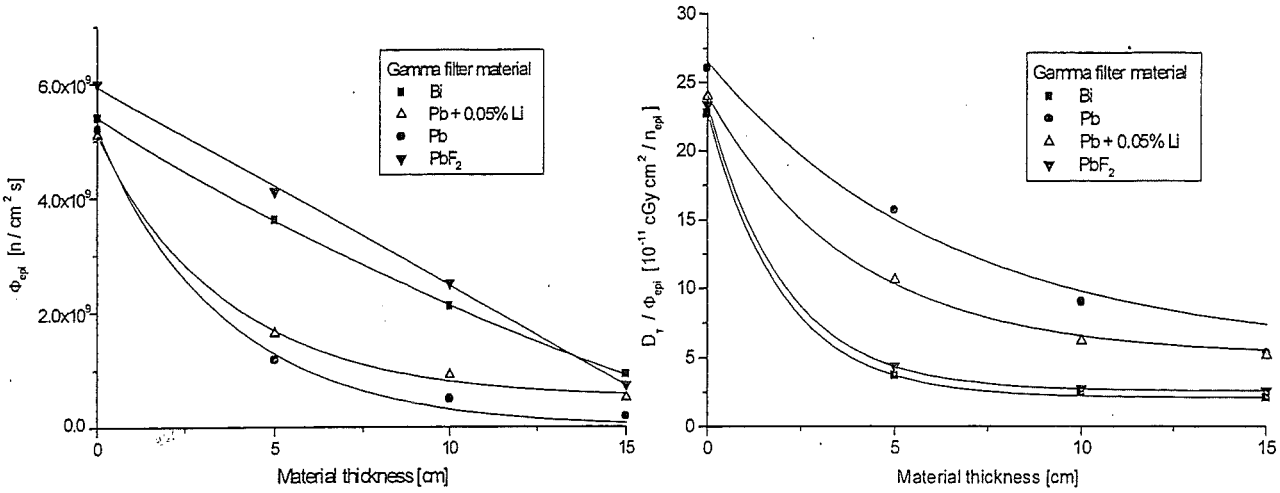

Bi was selected as the gamma shielding material

Efficiency of epithermal neutron filter materials

- Al_2O_3
- AlF_3
- PbF_2
- FLUENTAL® (69% AlF_3, 30% Al, 1% Li)
- Teflon® (CF_2)

☞moderation efficiency

☞availability & production

☞cost

Efficiency of epithermal neutron filter materials (d=50 cm)

Material / density (g/cm^3)	Φ_{epi} (0.4eV-10keV) (10^8 n/cm^{2}s)	D_{nfast}/Φ_{epi} (x10^{-13} Gy cm^2)	Specific cost (10^3 DEM/10^8 n_{epi})
Al_2O_3 (2.3)	2.1	17	15
Al_2O_3 (3.9)	0.8	4.7	>30
AlF_3 (2.8)	1.5	2.5	18
AlF_3 (4.0)	0.75	0.9	36
FLUENTAL®	1.25	1.8	100
PbF_2 (8.2)	1	3.5	84
Teflon® - CF_2 (2.2)	0.9	5.2	40

Proposed configuration

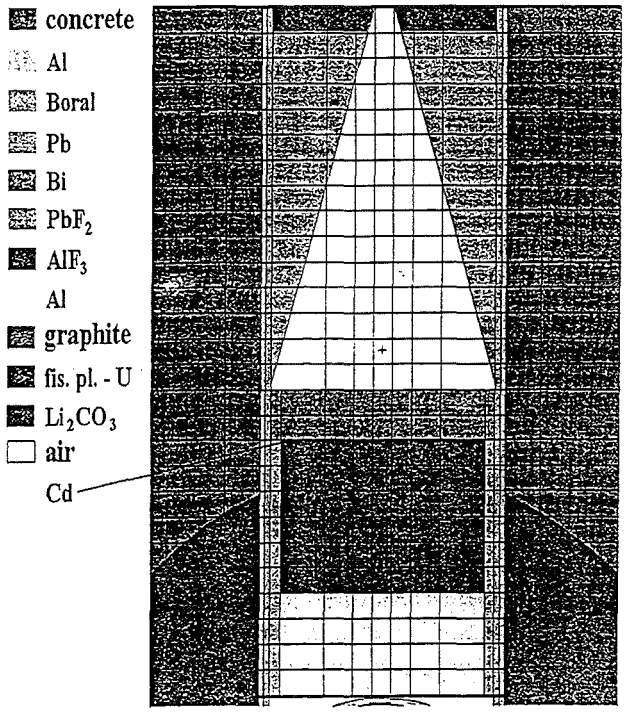

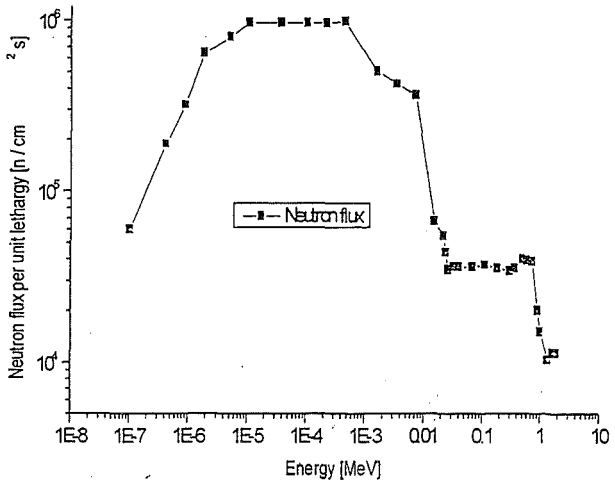

Averaged Relative errors in energy groups:

- thermal flux (E<0.4 eV): ±5 %
- epithermal flux (0.4 eV<E<10 keV): ±3 %
- fast flux I (10 keV<E<300 keV): ±10 %
- fast flux II (300 keV<E<20 MeV): ±15 %

Comparison to other BNCT facilities

Reactor	Power (MW)	Φ_{epi} (10^9 n/cm^{2}s)	D_{nfast}/Φ_{epi} (10^{-13} Gy cm^2)	D_γ/Φ_{epi} (10^{-13} Gy cm^2)	J_{epi}/Φ_{epi}
BMRR	3	1.8	4.3	1.3	0.67
MITR - II	5	0.2	13	14	0.55
HFR Petten	45	0.33	10.4	8.4	0.8
Musashi TRIGA	0.1	0.41	3.3	1.1	0.67
JRC TRIGA	0.25	0.45	4.3	12	0.64
BNL (core + f.p.)	10 + 0.05	1.4	4.6	<1	0.78
FiR TRIGA	0.25	3.5	2.6	1	N/A
JSI TRIGA	0.25 + 0.08	0.24	1.8	3.3	0.6
Therapeutic limits		>1	<5	<3	>0.5

Conclusions

- JSI TRIGA research reactor is the unique of its type, having the so called "dry cell"
- AlF_3 (4 g/cm^3) - irradiation characteristics comparable or better to other materials
- if reactor power is increased (750 kW or 1 MW), Φ_{epi} close to 10^9 n/cm^{2}s is achievable
- for 1 MW power, forced cooling system installation is compulsory
- cost estimation - less than 100.000 US$

Monte Carlo Methods and Models for Applications in Energy and Technology

Workshop to be held at Forschungszentrum Karlsruhe, May 12-14, 1998

Monte Carlo Calculation of Neutron Photo-Production in Radiotherapy Linear Accelerator High-Z Components

C. Ongaro, U. Nastasi, A. Zanini

Universita' di Torino
Ospedale S. Giovanni Antica Sede-Torino
INFN-Torino
ITALY

A non-negligible production of undesired neutrons is associated with high energy linear accelerators used in the cancer radiotherapy with photon beams. Neutrons are principally produced by giant resonance reaction in the high-Z components of the linear accelerator head. The accurate knowledge of such a photo-neutron spectrum is of crucial importance, in view of an optimization of cancer therapeutic treatment. Since the photoneutron production depends on the different treatment and machine characteristics and considering the difficulties to carry out direct measurements, Monte Carlo is a very appropriate method to accurately describe the neutron field.

At the Experimental Physics Department, University of Torino, a chain of Monte Carlo simulation codes has been implemented to obtain an accurate evaluation of the photo-neutron equivalent dose at the patient plane. A new Monte Carlo code, GAMMAN, for the evaluation of the photo-neutron production in thick high-Z layers has been developed, allowing to calculate the neutron spectrum and yield as well as the neutron angular and spatial distribution up to 30 MeV photon energies. Both the evaporation and the direct component are considered in the evaluation of the neutron energy spectrum and, weighting on the γ-n cross sections at the appropriate photon energies, the neutron spatial distribution has been randomly determined from the interaction points along each photon path of the electromagnetic shower, simulated with the EGS4 code.

GAMMAN has been inserted in POLAS, an user code, based on the EGS4 Monte Carlo transport routines, especially developed to accurately model the LINAC geometry and to calcuate the photon spectrum produced by the treatment unit. In particular, the effective photoneutron production in the 15 MeV MD-Mevatron (Siemens) accelerator in use at the "S. Giovanni Antica Sede" hospital (Torino, Italy), has been evaluated. The neutron equivalent dose at the patient plane can be then calculated by the code MCNP which transports the neutron data in the same LINAC geometry.

Last modified: Sat May 9 18:18:29 1998

MONTE CARLO CALCULATION OF NEUTRON PHOTO-PRODUCTION IN RADIOTHERAPY LINEAR ACCELERATOR HIGH Z COMPONENTS

C. Ongaro*, U. Nastasi°, A. Zanini°°

* University of Torino, V. P. Giuria,1 -10125 Torino, Italy
° Ospedale S. Giovanni A.S., V. Cavour 31 -Torino, Italy
°° INFN Sez. di Torino, V. P. Giuria,1 -10125 Torino, Italy

A chain of Monte Carlo simulation codes has been implemented to accurately describe the photoneutron production in high-Z elements, in view of applications to electron medical accelerators. The new Monte Carlo code GAMMAN has been developed to calculate the photoneutron spectrum and yield as well as the neutron angular and spatial distribution up to 30 MeV photon energies. GAMMAN has been coupled with the M.C. code PHOTO, that calculates the photon spectra in the complex geometry of medical accelerators, and with MCNP, for neutron transport, to obtain the effective photoneutron distribution at the patient plane.

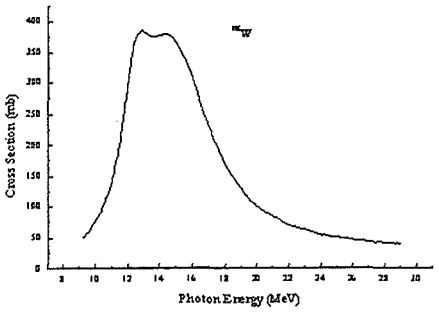

Cross Sections of ^{186}W, ^{197}Au, ^{181}Ta,

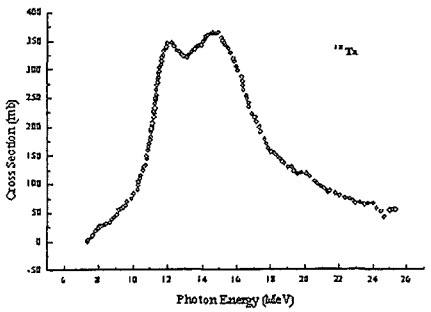

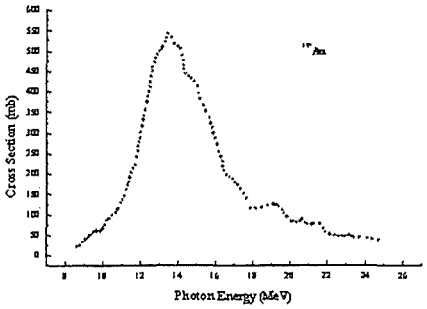

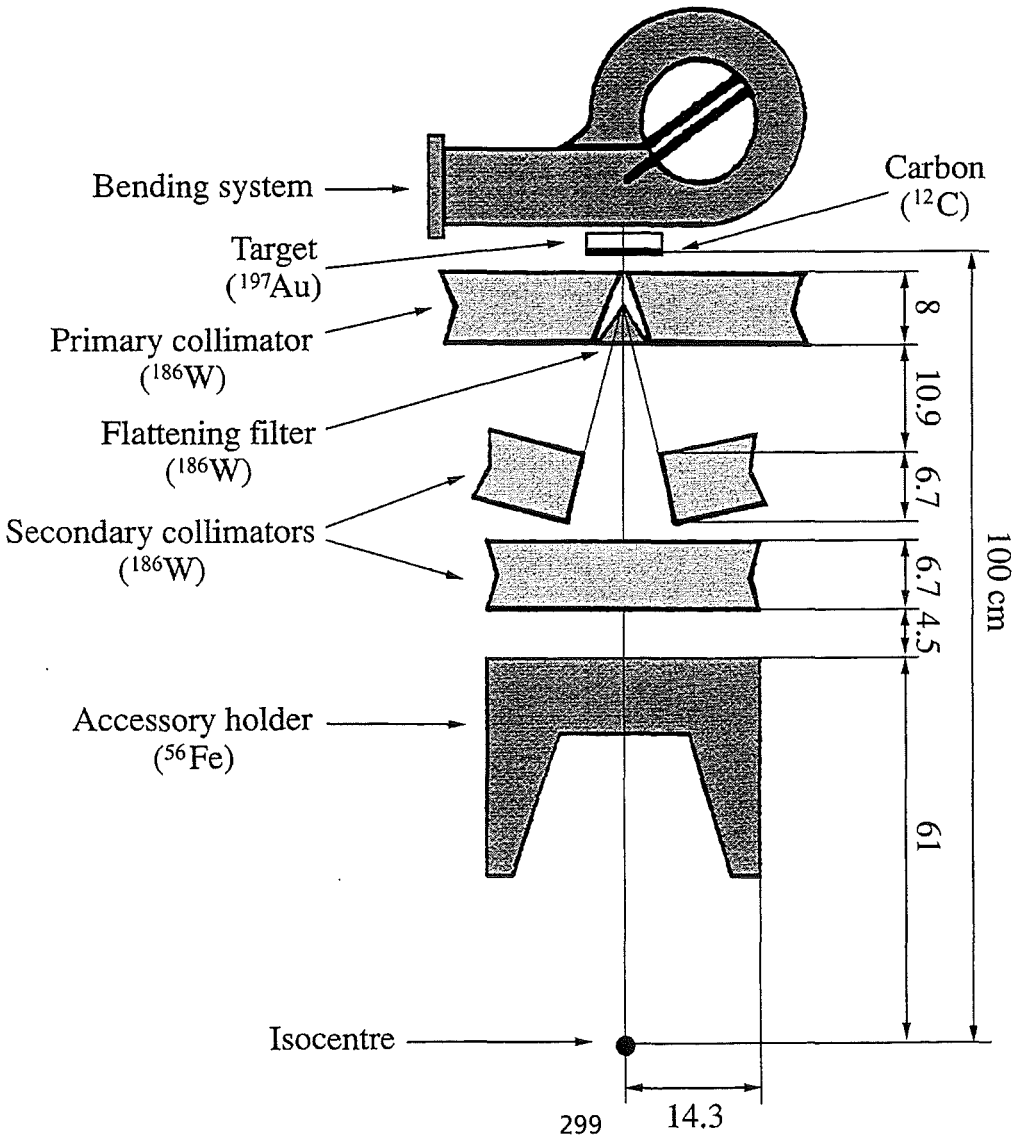

LINAC RADIOTHERAPY

The therapy treatment is planned to release the maximum gamma dose in the target volume, preserving the nearby area, in particular the most radiosensitive organs.

⇓

COLLIMATOR TECHNIQUE

⇓

SUPPLETTIVE FILTERS

⇓

MOVEBLE MULTILEAF

⇓

BEST ESTIMATION OF THE TARGET VOLUME

LEAKAGE NEUTRONS

Undesired neutrons are created by photons with **energy > 10 MeV in the high Z** components of medical accelerator head:

Target ^{197}Au	(E_{th} = 8.084 MeV)
Primary and secondary collimator ^{186}W	(E_{th} = 7.418 MeV)
Flattening filter ^{56}Fe	(E_{th} = 10.9 MeV)
Suppletive filter Pb	(E_{th} = 6.74 MeV)

$E_{mean,\ neutron}$ ~ 1-3 MeV (depending the Eg) ⟹ **High BIOLOGICAL EFFECTIVENESS**

Quite isotropic angular distribution ⟹ **DAMAGE to RADIOSENSITIVE ORGANS outside the treatment zone.**

⇓

SECONDARY MALIGNANCIES RISK

⇓

ACCURATE KNOWLEDGE OF PHOTONEUTRON SPECTRUM
required

⇓

NO DIRECT MEASUREMENTS
(overwhelming photon flux and pulsed nature of the radiation field)

⇓

SUITABLE MONTE CARLO CODE

RISK ESTIMATION from leakage neutrons

ICRP60 (1991)

⇩

New Quality and
weighting factors

ICRP74 (1996)

⇩

New Fluence to Equivalent
Dose conversion factors

⇓

- **AUGMERNTED NEUTRON RISK** (more than twice to respect to indication of ICRP21, in energy range 100 keV - 20 MeV)
- **NO CHANGE for PHOTONS**
- **LOWER EXPOSURE LIMIT/YEAR:** form 50 mSv/y to 20 mSv/y

For a therapeutic treatment consisting of **30 sessions of 2 Gy** gamma dose, the undesired neutron dose is estimated:

ICRP 21	ICRP 60
~ 60 mSv	**~ 100 mSv**

GAMMAN: M.C. photoneutron generation code

→ In view of determining the neutron field around the accelerators, the evaluation of the photo-neutron position and energy at the creation point is of crucial interest.

→ GAMMAN capabilities

- **Coordinates evaluation of the photoneutron starting point**
  Random calculation along each photon path
- **Photoneutron energy spectrum**
- **Photoneutron angular Distribution**

  1. **Evaporation neutrons** (according to Statistical Model)
     -Isotropic angular distribution

  2. **Direct neutrons** (En>2.5 MeV)
     - Anisotropic angular distribution according to

- **Both (g,1n) and (g,2n) reactions are taken into account**

$\sigma_{\gamma n}$ from "Atlas of photoneutron cross sections", B.L. Berman (1973)

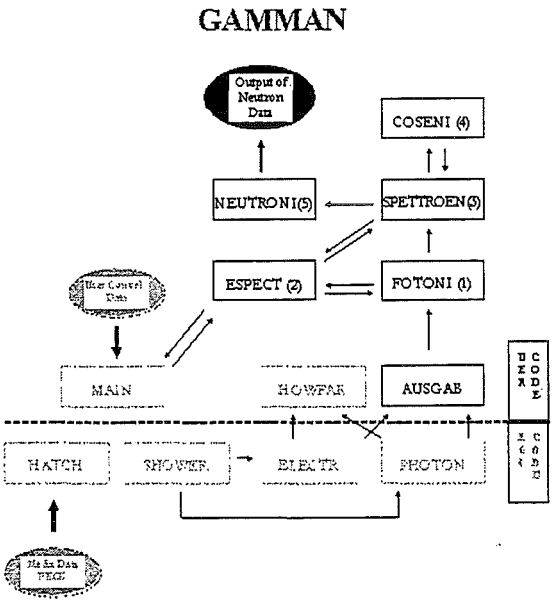

(1) choice of gamma step in which photoneutrons are produced
(2) acquisition of (γ,n) cross sections values
(3) calculation of neutron energy
(4) calculation of neutron cosines
(5) calculation of neutron position and output of results

Photoneutron energy spectrum

a - Evaporation neutrons

•In this gamma energy range (up to 30 Mev), neutrons are produced through giant-dipole-resonance (GDR).

•The spectrum of neutrons emitted from medium and high-Z elements is calculated from the statistical model of the compound nucleus

$$n \cdot dE_n = CE_n e^{-\frac{E_n}{T}} dE_n$$

$$T = (E_r / a)^{0.5}$$

E_r maximim residual nucleus energy

a empirical parameter depending on atomic weight A [1]

•Both (γ,1n) and (γ,2n) reactions are taken into account.

•Isotropic angular distribution

b- Direct neutrons

•The direct contribution is taken into account if $(E_g - E_{th}) > 2.5$ MeV

•The effect acquires importance as the incident gamma energy increases.

•A semi empirical method [2], which considers the dependence of the direct neutron fraction from E_g and A, has been used.

•Anisotropic angular distribution according to the function:

$$F(\theta) = 1 + C\sin^2(\theta)$$

C = experimental parameter [2]

Statistical weight

At the end of the generation process, each photoneutron is weighted by $w = \sigma_{\gamma,n}(E_\gamma) / \sigma_{tot}(E_\gamma)$

σ_{tot} is directly taken from EGS4 libraries; $\sigma_{\gamma,n}$ from "Atlas of photoneutron cross sections", B.L. Berman (1973)

NEUTRON POSITION

Coordinates evaluation of the photoneutron starting point

Because the cross section values for (γ,n) are more than 10^2 lower in respect to the photoelectric, Compton and pair effects, it is inconvenient to insert the photoneutron production in the standard procedure; at the same time the electromagnetic shower is not sensibly affected by the neutron production, as a consequence of this low probability.

⟹ In GAMMAN the neutron creation point i is chosen, for each history, between all n photon interaction points from the distribution

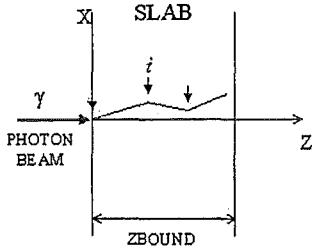

$$F(i) = \sum_{j=1}^{i} \frac{\sigma_{(\gamma,n),j}(E_{\gamma,j})}{\sigma_{TOT}}$$

$$\sigma_{TOT} = \sum_{j=1}^{n} \sigma_{(\gamma,n),j}$$

n = number of interection points

$E_{\gamma,i}$ is evaluated by EGS4, to take into account the electromagnetic shower during the transport in thick layers: energy spectrum and the spatial distribution of incident photons are altered.

Photoneutron spectrum from 24 MeV bremsstrahlung beam on ^{186}W slab (2.0 cm), compared with calculated data (Ref. 2)

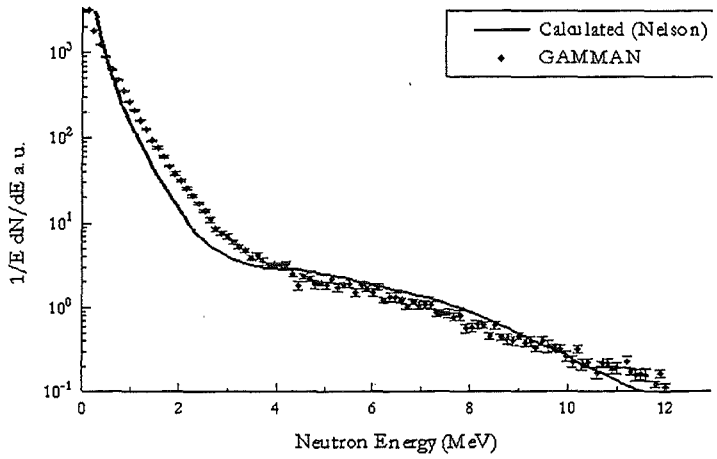

Photoneutron spectrum from 14 MeV quasi monochromatic photon beam on ^{181}Ta slab (0.55 cm), compared with experimental (Ref. 3) and calculated (Ref. 2) values.

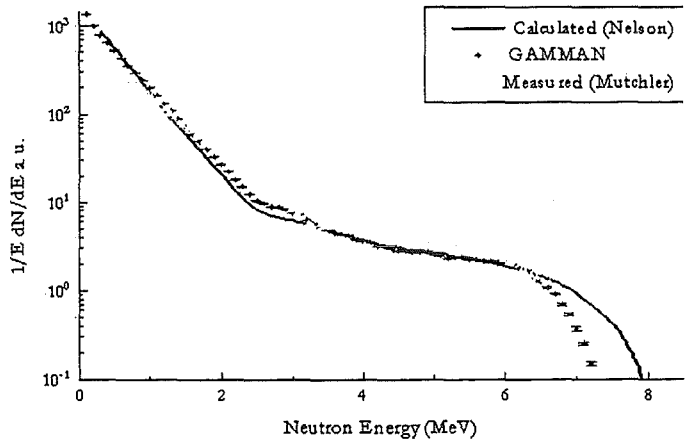

Photoneutron spectrum from 14 MeV quasi monochromatic photon beam on ^{186}W slab (0.556 cm), compared with experimental (Ref. 3) and calculated (Ref. 2) values.

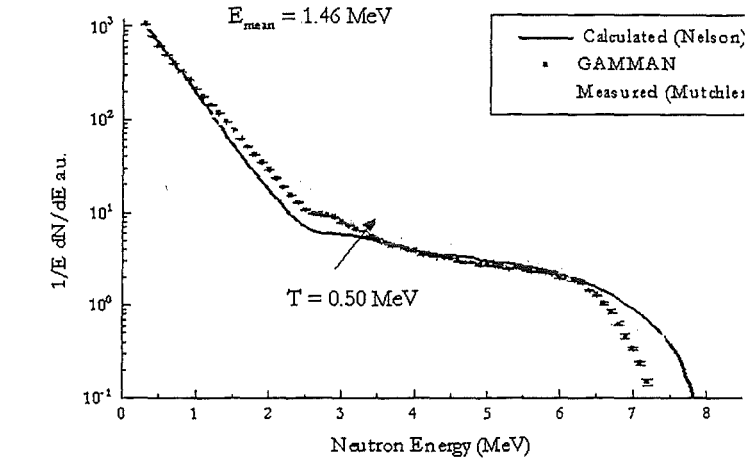

Photoneutron spectrum from 14 MeV quasi monochromatic photon beam on ^{186}W slab (0.556 cm), compared with experimental (Ref. 3) and calculated (Ref. 2) values.

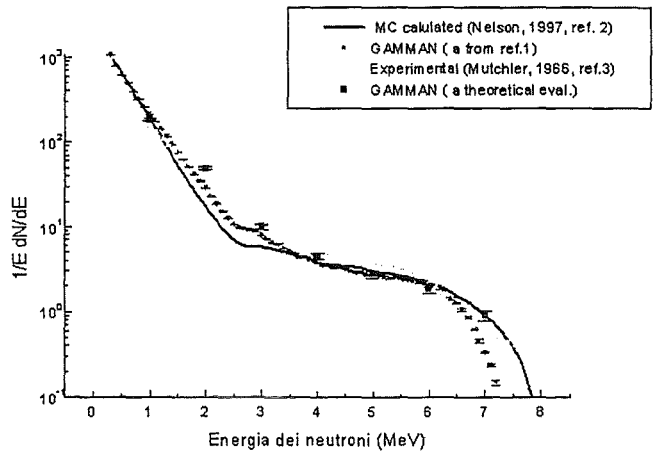

GAMMAN results, obtained by using *a* values taken from NCRP[1] and from a theoretical evaluation, have been also compared.

Comments to previous figures

- In all photoneutron spectra, calculated by GAMMAN, both the evaporated and the direct component are evident.
- Few experimental data are available on photoneutron production in thick layer.
- Experimental data are very old (1966, 1973).
- All pictures show a quite good agreement among GAMMAN and the other data, GAMMAN values lying between the calculated and the experimental ones.
- All pictures show, however, a certain disagreement between GAMMAN and the other calculated spectra[2] in the high neutron energy region, probably due to differences in cross sections.
- When using theoretical evaluation of *a* parameter in the GAMMAN calculation, the agreement improves.

Application to medical accelerators

For the application to the medical accelerators , GAMMAN has been inserted in POLAS, which simulates in 3D the electromagnetic shower in the accurate geometrical description of the accelerator head. The photoneutrons data, stored in a file are then processed through MCNP neutron transport code to obtain the effective neutron spectra at the patient plane.

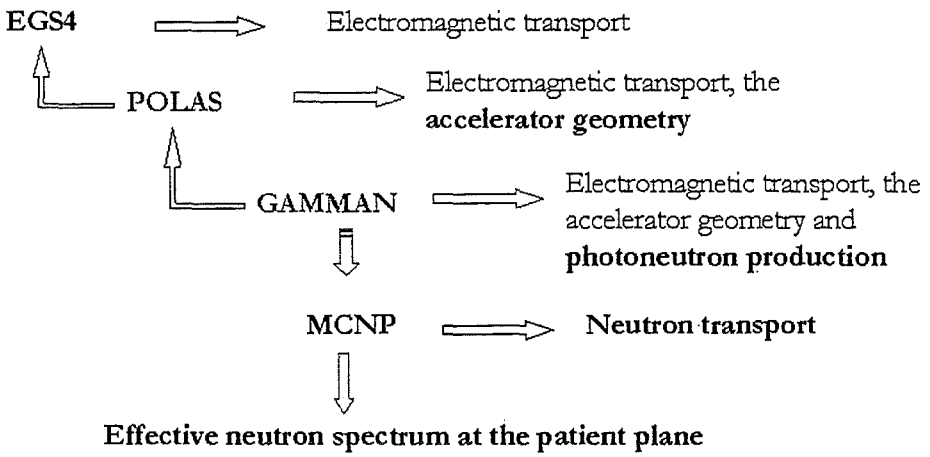

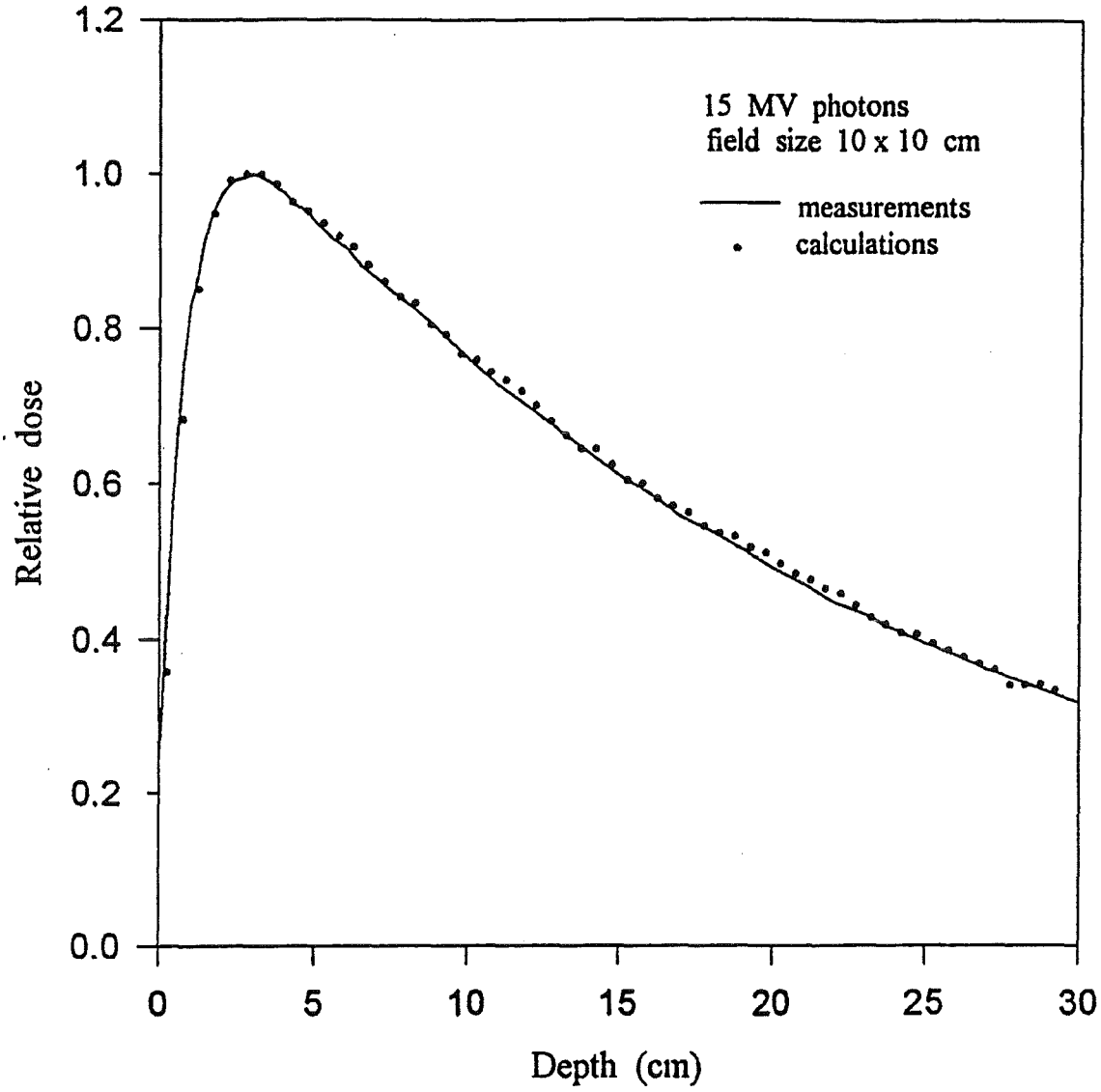

POLAS: PHOTON SPECTRA FROM 15 MeV e^- ON Au TARGET (0.09 cm THICK) of the MEVATRON SIEMENS MEDICAL LINAC

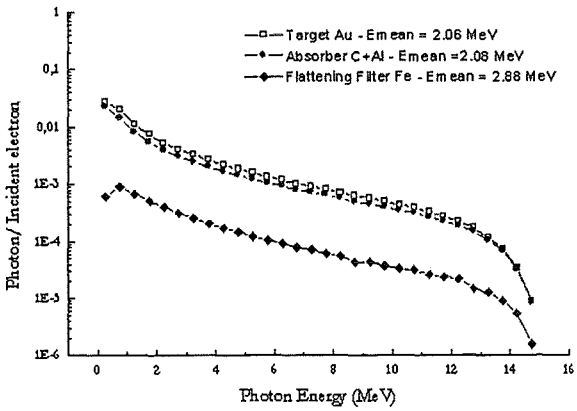

POLAS

Photon spectra produced in the linear accelerator

PLB: Measurements difficult to carry out

⇓

MONTE CARLO CODE

to simulate

RADIATION TRANSPORT

⇓

POLAS

- **EGS4 transport routines**
- **3D cylindrical geometry**

FEATURES

- Reproduces accurately **collimator shape**
- Evaluate **photon spectra** in any position inside the **gantry** and at the **patient** plane
- Evaluates the **absorbed dose** at the patient plane.

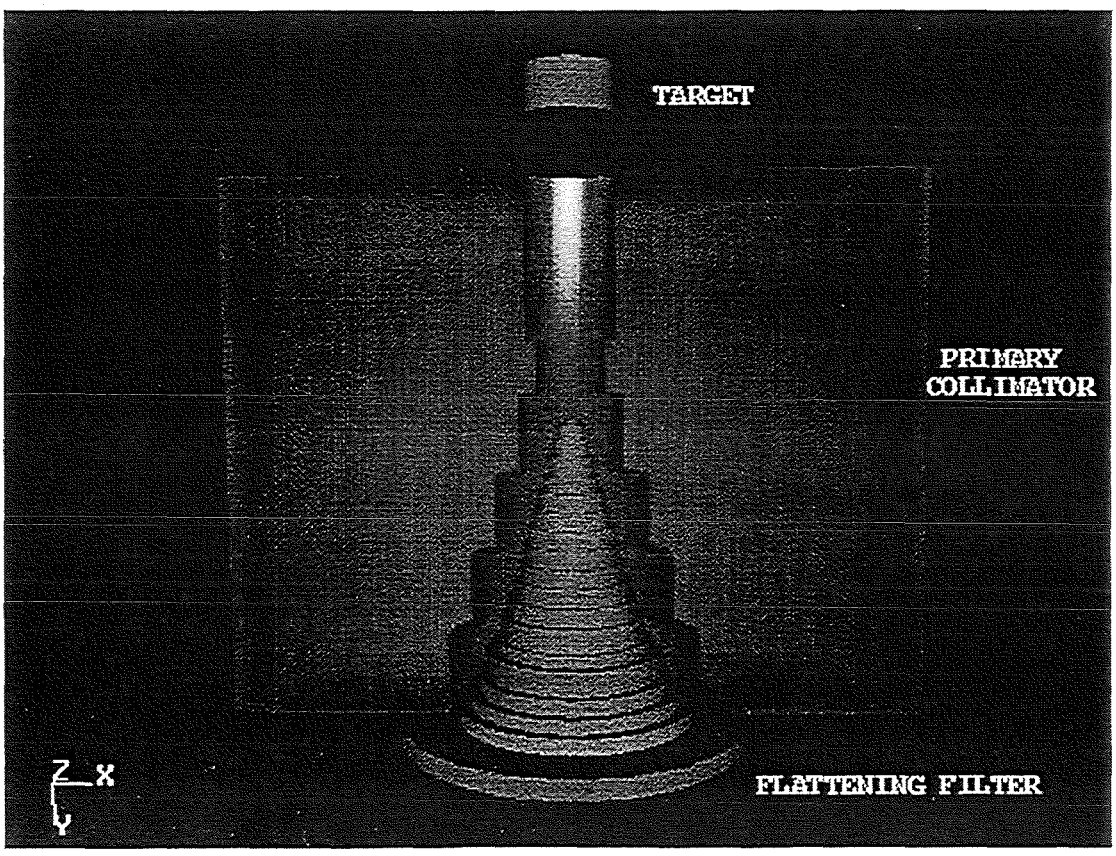

PHOTONEUTRON SPATIAL DISTRIBUTION OF IN THE Au TARGET (Mevatron Siemens 15 MeV)

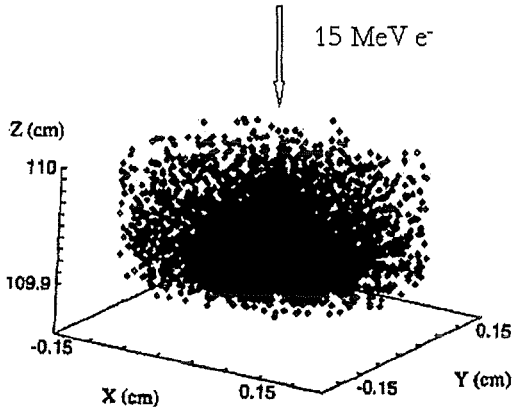

Spatial distribution of neutrons in the target (Au)

PHOTONEUTRON ENERGY SPECTRUM at the PATIENT PLANE (Mevatron Siemens LINAC, 15 MeV)

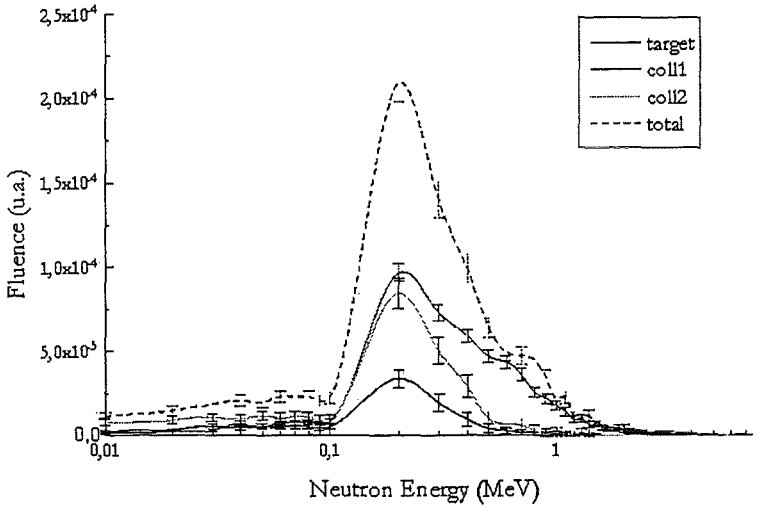

Application and Future Work

A reliable evaluation of the undesired photoneutron at the patiant plane in **LINAC RADIOTHERAPY TREATMENT** by using the Monte Carlo code chain (EGS4, POLAS, GAMMAN, MCNP4A).

- .**Shielding** of radiosensitive organs in view of the therapeutic treatment optimization.
- .Indication to industries for the **best choice of materials**, shape and size of the gantry components.
- .Accurate study of photoneutron generation in the additional filters; in particular , nowadays there are no information about the undue neutron dose equivalent released in the **conformal therapy by the multileaf technique** (in view of an evaluation of the best ratio risk-benefit).

References

1. NCRP Neutron Contamination from Medical Accelerators. NCRP Report 79., Bethseda, MD:NCRP Publications, (1984).

2. J.C.Liu, W.R.Nelson, K.R. Kase, X.S. Mao, Calculation of the Giant-Dipole-Resonance Photoneutrons using a Coupled EGS4-MORSE code, Rad. Prot. Dos., Vol. 70, pp 49-55 (1997).

3. G.S.Mutchler, The Angular Distributions and Energy Spectra of Photoneutrons from Heavy Elements, Ph.D. Thesis, M.I.T. (1966).

4. W.R. Nelson, A. Hirayama, D.W.Rogers, The EGS4 code system, SLAC - Report 265(1985).

5. G.F. Briesmeister, MCNP - A general Monte Carlo code for neutron and photon transport, Version 4A, Los Alamos, New Mexico, (1993).

6. J.M.Blatt, V.F.Weisskopf, Theoretical Nuclear Physics, J.Wiley and Sons, New York (1952).

Monte Carlo Methods and Models for Applications in Energy and Technology

Workshop to be held at Forschungszentrum Karlsruhe, May 12-14, 1998

Monte Carlo Simulation for Low Energy Electron Transport

A. Dubus

Service de Métrologie
Université Libre de Bruxelles
1050 Bruxelles - BELGIUM

Electron transport calculations appear in many different physics problems such as plasma physics, dosimetry, surface analysis,... We will describe here the applications of low energy (a few eV-a few keV) electron transport addressed in Brussels, i.e. surface analysis and electron emission from thin foils and from insulators.

Among the various surface analytical techniques, some (Auger Electron Spectroscopy: AES and X-Ray Photoelectron Spectroscopy: XPS) are based on the excitation of electrons by the incident particles (the emitted photoelectrons or Auger electrons being the measured signal). A precise description of electron transport is necessary to interpret correctly the measurements. Such a precise description can be obtained by using a Monte Carlo simulation.

Particle induced electron emission is known from the beginning of the century. However, there is still active research about particular kinds of experiments like electron emission from thin foils where forward and backward emissions are possible when the projectiles cross the foils, measurements of the statistical distribution of the number of emitted electrons, measurements of electron emission from insulators,...

Such problems are studied in Brussels from a theoretical viewpoint (but in strong relationship with an experimental viewpoint) using Monte Carlo simulation for the description of the transport. The accent will be put here as well on the physics of low energy electrons as on the technical viewpoint of the simulation

Last modified: Thu Apr 2 14:07:19 1998

MONTE CARLO SIMULATION FOR LOW ENERGY ELECTRON TRANSPORT

A. DUBUS, Université Libre de Bruxelles
Service de Métrologie Nucléaire (CP 165)
50, av. F. D. Roosevelt, B-1050 Bruxelles
(adubus @ ulb. ac. be).

STARTING POINT (1993) :

- ION BEAM INTERACTIONS WITH SOLID TARGETS
- NEUTRON TRANSPORT

→ ELECTRON TRANSPORT FOR LOW ENERGY (a few eV - a few keV) ELECTRONS EXCITED BY PARTICLES (e^-, H^+, ...) INCIDENT ON SOLID TARGETS

COMPUTATIONAL PHYSICS

MONTE CARLO SIMULATION = TOOL

3 APPLICATIONS TO ILLUSTRATE THE PHYSICS PROBLEMS :

1) IONS - NEUTRAL ATOMS INCIDENT ON THICK METALLIC TARGETS OR THIN CARBON FOILS : ELECTRON EMISSION

COLLABORATIONS : M. RÖSLER (BERLIN)
F.J. GARCIA de ABAJO (SAN SEBASTIAN)
J.C. POIZAT - J. REMILLIEUX (LYON)
H. ROTHARD (CAEN)
O. BENKA (LINZ)
K.O. GROENEVELD (FRANCFURT)

= ATOMIC COLLISIONS IN SOLIDS

2) ELECTRON SPECTROSCOPIES FOR SURFACE ANALYSIS

COLLABORATIONS : S. TOUGAARD (ODENSE)
A. JABLONSKI (WARSZAWA)

= SURFACE ANALYSIS

3) CHARGING EFFECTS IN INSULATORS

COLLABORATION : J.P. GANACHAUD (NANTES)

= PHYSICS OF INSULATORS

① INTERACTIONS OF "IONS" WITH SOLID TARGETS : ELECTRON EMISSION

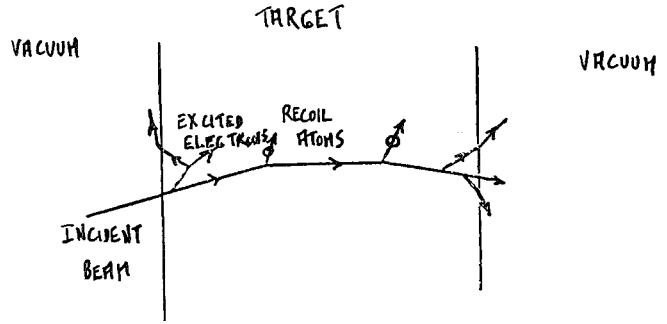

ELECTRON EMISSION KNOWN FROM I 1900

1°) TARGET : METAL, INSULATOR, THIN FOIL (CARBON), ...

2°) BEAM : H^+, He^+, He^{++}, Ar^{10+}, H^0, H^-, H_2^+, H_m^+, C_m^+, ...

ENERGY : H^+ 1 MeV ≠ Ar^+ 1 MeV

3°) MEASURED QUANTITY : YIELD (FORWARD, BACKWARD)
EMISSION STATISTICS

MONTE CARLO SIMULATION =

ANALOG SIMULATION

1°) CALCULATION OF CROSS SECTIONS

a) BEAM - TARGET :

COLLISIONS WITH ELECTRONS

IONIC CORES

CHARGE EXCHANGE ($He^{+} \rightarrow He^{++} + e^{-}$)

b) ELECTRON - TARGET :

COLLISIONS WITH ELECTRONS

(VALENCE, INNER - SHELL, COLLECTIVE)

"ELASTIC" COLLISIONS WITH IONIC CORES

↓

NO ENERGY LOSS BUT LARGE ANGLE DEFLECTION

c) RECOIL ATOMS

'NONLINEAR' EFFECTS : HIGH IONIZING DENSITY

⋮

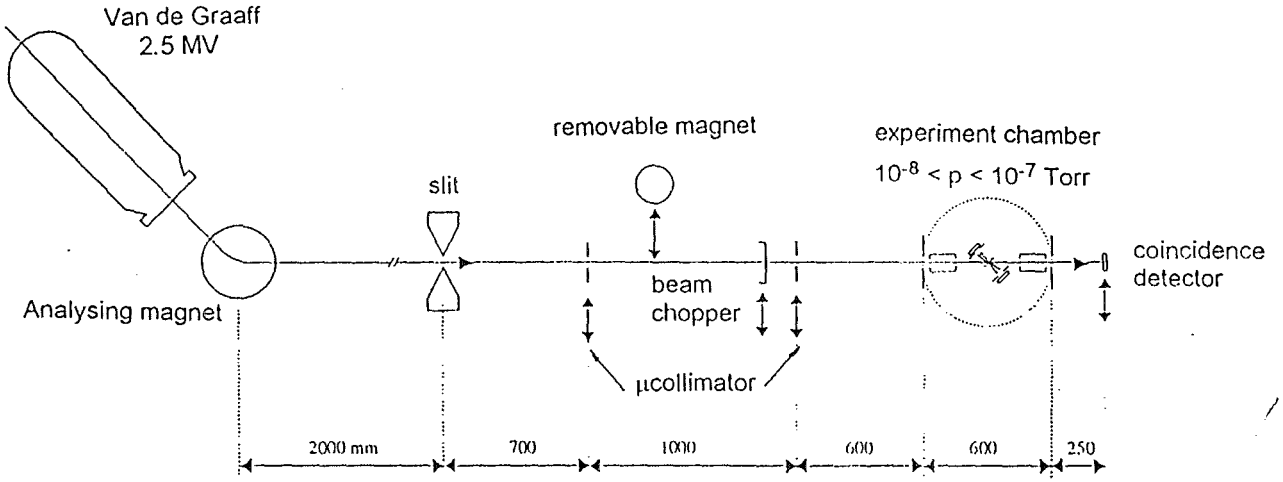

EXPERIMENTAL SET UP (IPN LYON)

⇒ MEASUREMENT OF EMISSION STATISTICS FOR $H^+ \rightarrow C$

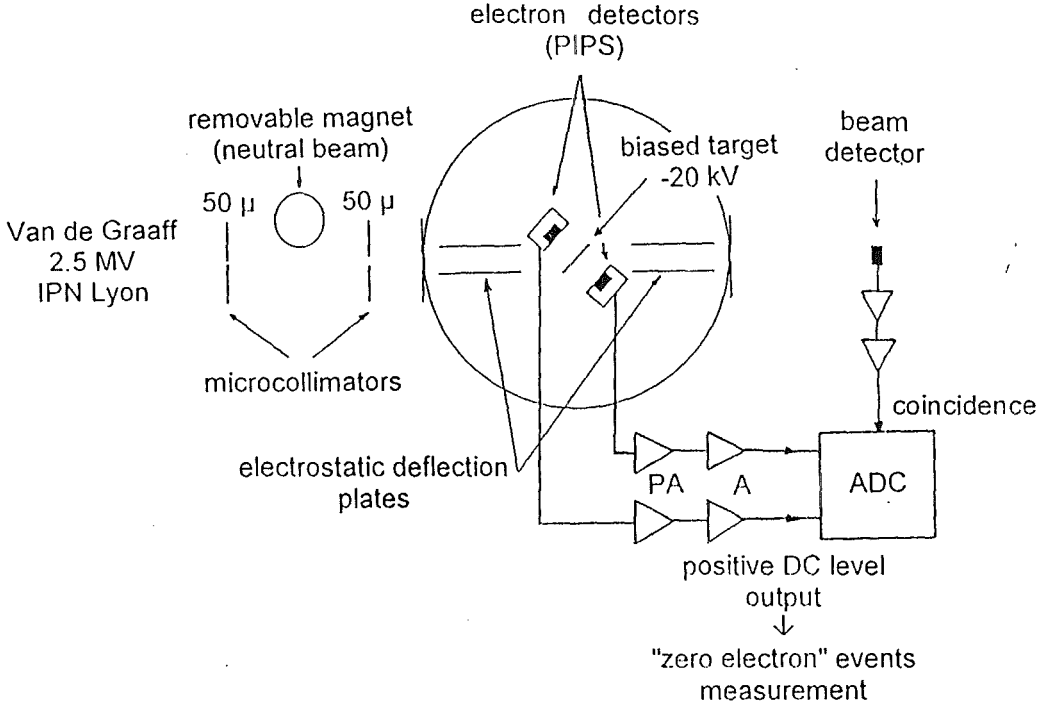

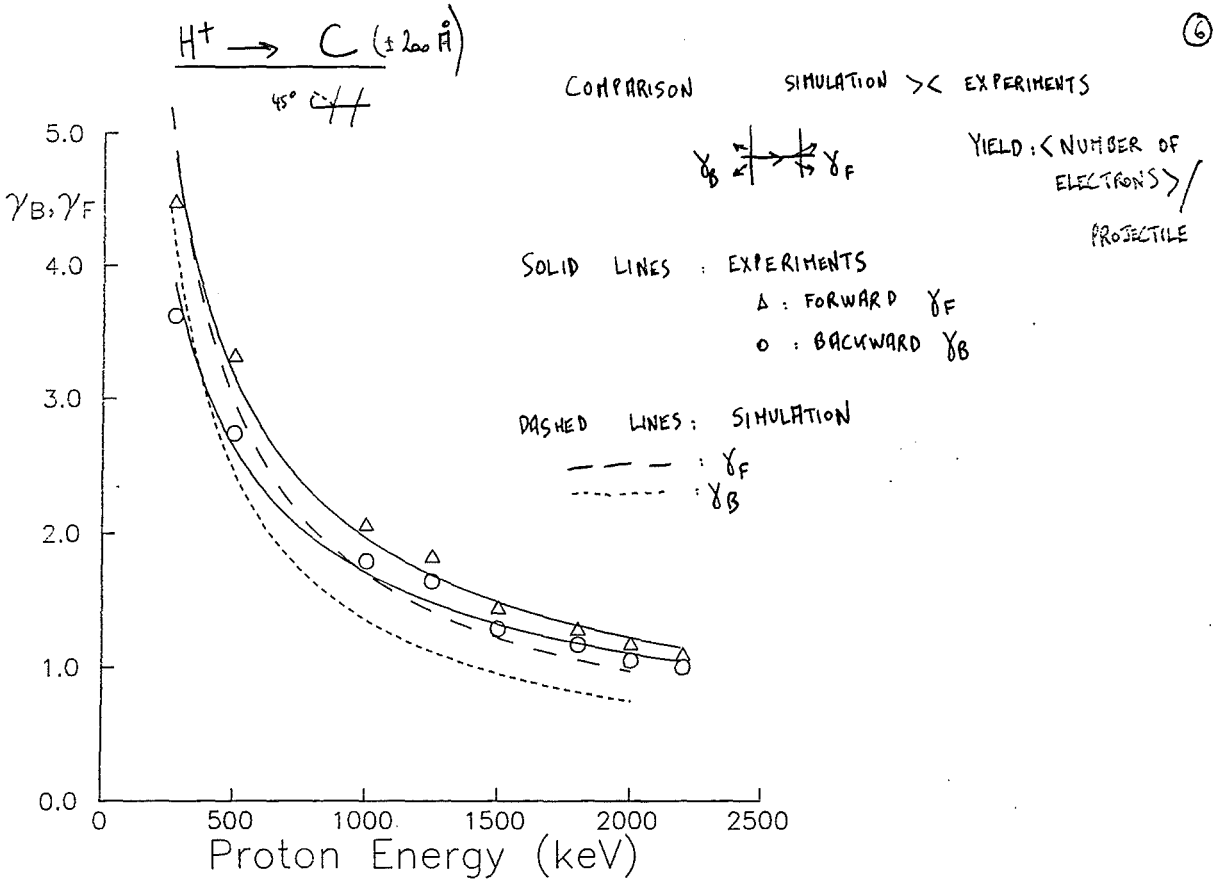

EMISSION STATISTICS

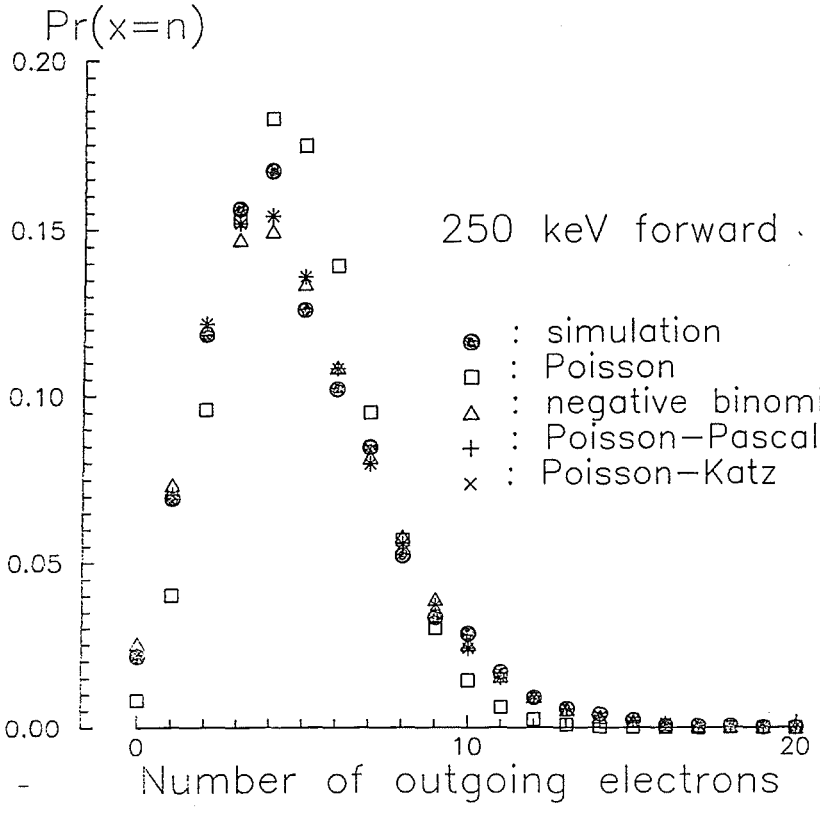

DISCRETE DISTRIBUTION

⇒ POISSON (1 PARAMETER)

⇒ NEGATIVE BINOMIAL (POLYA)

$$P(n) = \binom{k+n-1}{k-1} q^n (1-q)^k$$

(2 PARAMETERS)

⇒ POISSON - PASCAL (3 PARAMETERS)

POISSON - KATZ

IMPORTANT: DEVIATIONS WITH RESPECT TO A POISSON DISTRIBUTION

COMPARISON SIMULATION >< EXPERIMENTS ⑧

$H^+ \rightarrow C$

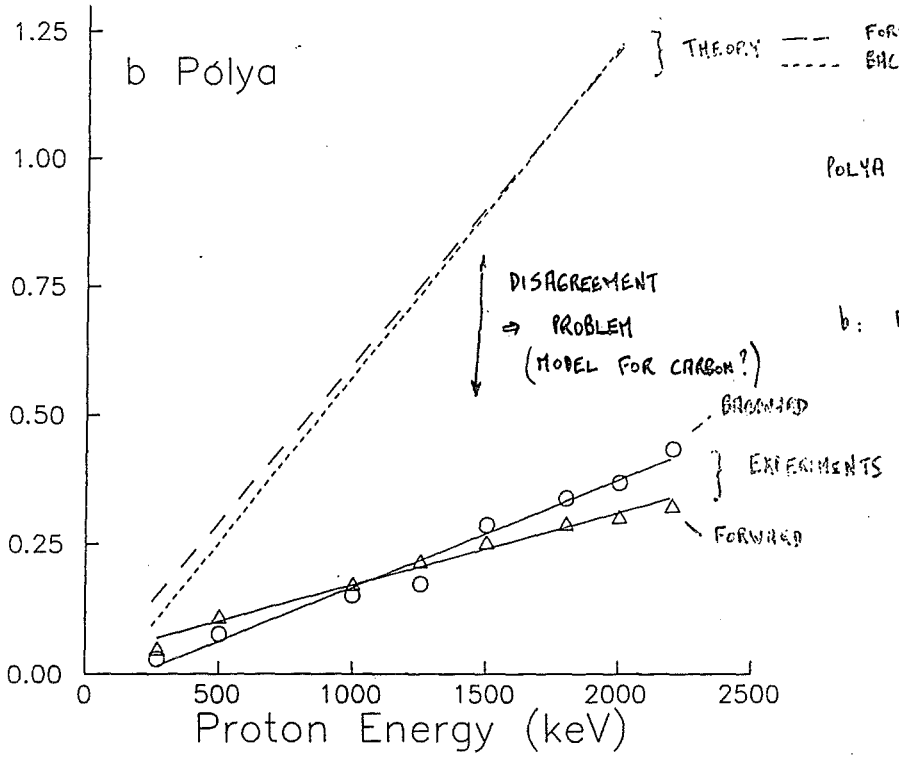

POLYA : $P_m(\mu, b) = \frac{\mu^m}{m!}(1+b\mu)^{-m-\frac{1}{b}} \prod_{i=1}^{m}[1+(i-1)b]$

b : DEVIATION WITH RESPECT TO POISSON

$H^+ \rightarrow C$ (BACKWARD EMISSION) ⑨

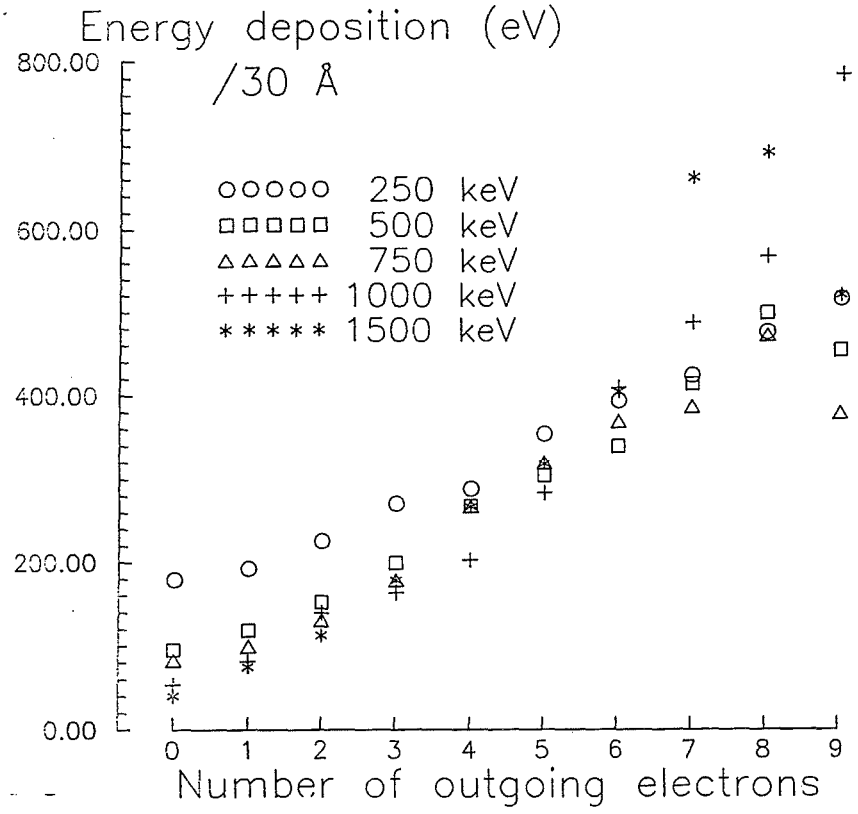

PROBLEM : ORIGIN OF THE DEVIATION WITH RESPECT TO POISSON : ?

CORRELATION BETWEEN ENERGY LOST BY THE PROTON IN A 30 Å ZONE WITH THE NUMBER OF EMITTED ELECTRON

$H^+ \rightarrow C$ (BACKWARD EMISSION)

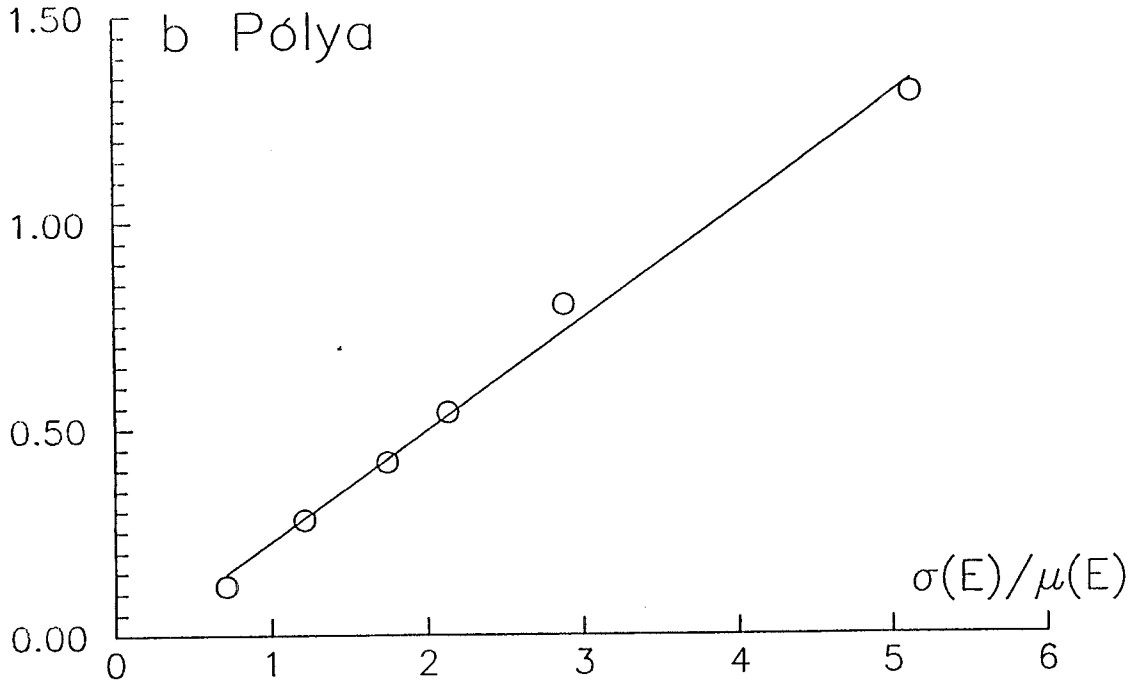

CORRELATION BETWEEN b POLYA PARAMETER AND $\frac{\sigma(E)}{\mu(E)}$ (STANDARD DEVIATION OF ENERGY LOST IN THE 3σ DEPTH ZONE)

FIRST EXAMPLE : H^+ (300 keV → 2 MeV)

⇒ NO CHARGE EXCHANGE

SECOND EXAMPLE : $H^\circ \rightarrow C$ ⇒ CHARGE EXCHANGE

$H^\circ \rightarrow H^+ + e^-$

MEASUREMENTS IN LYON IN COINCIDENCE WITH THE EXIT CHARGE STATE (H°, H^+)

$H^0 \rightarrow C$ (145 Å, 45°) OUTGOING H^0

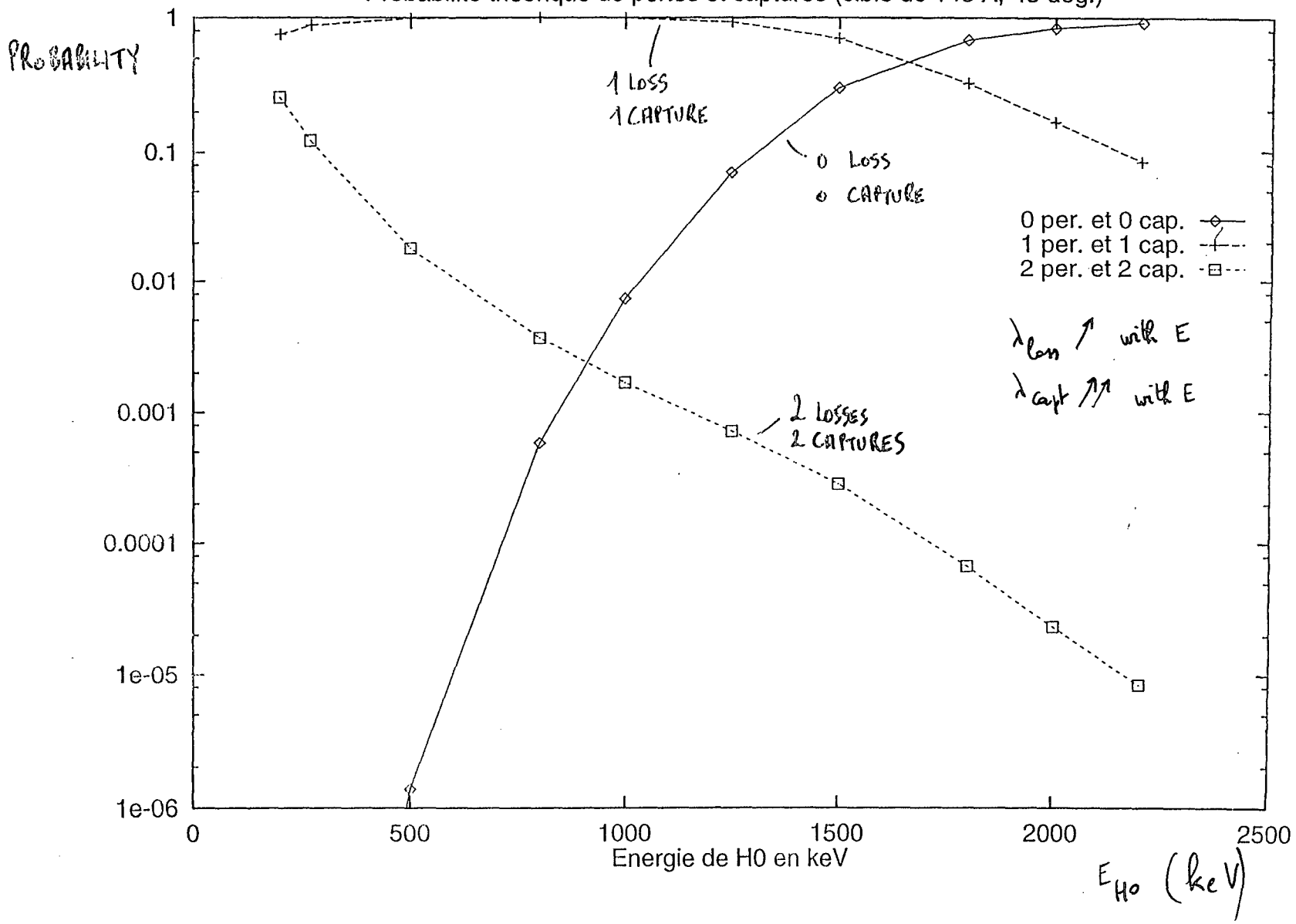

$H^0 \rightarrow C$

$H^+ \rightarrow C$

Monte Carlo Simulation >< EXPERIMENTS

BACKWARD YIELD γ_B

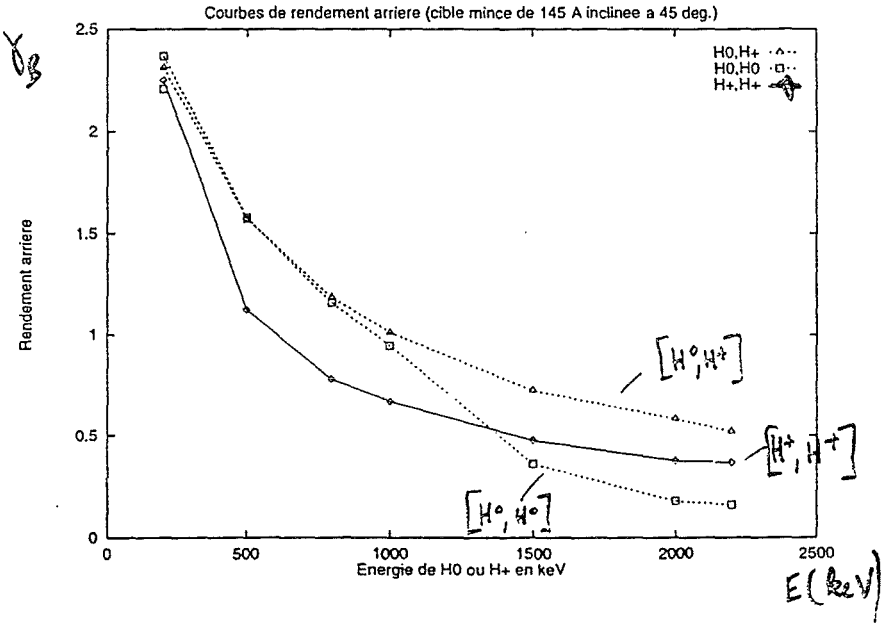

SIMULATION

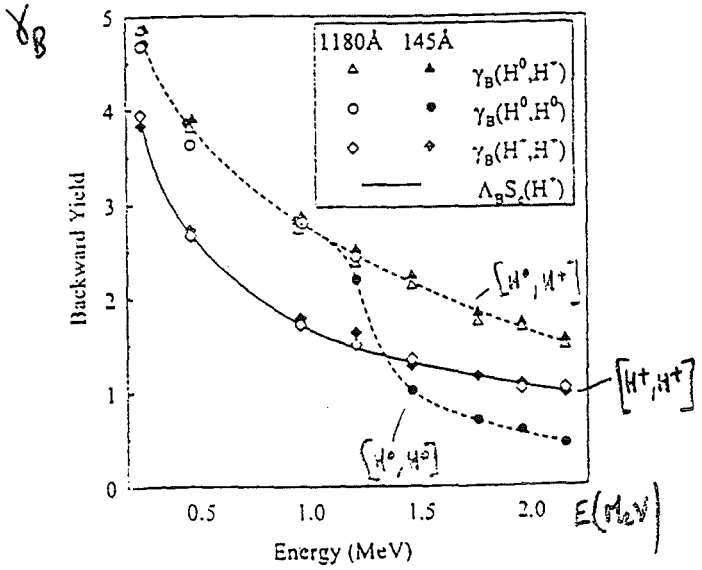

EXPERIMENTS

GOOD AGREEMENT THEORY - EXPERIMENTS

$[H^0,H^+] \simeq [H^0,H^0]$ FOR THE YIELD γ_B BELOW 1.0 MeV

ABOVE 1 MeV $[H^0,H^0]$ STRONG INFLUENCE OF ○ LOSS ○ CAPTURE

$H^0 \rightarrow C$

$H^+ \rightarrow C$

(14)

MONTE CARLO SIMULATION >< EXPERIMENTS

FORWARD YIELD γ_F

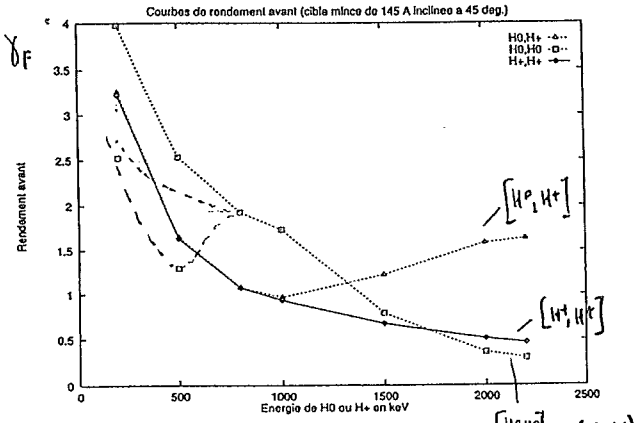

$[H^0, H^+]$

$[H^+, H^+]$

$[H^0, H^0]$ E(keV)

SIMULATION

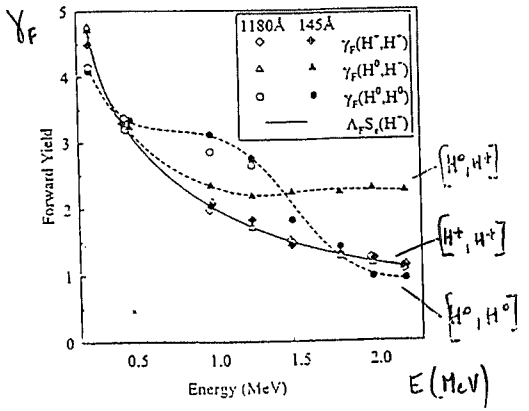

$[H^0, H^+]$

$[H^+, H^+]$

$[H^0, H^0]$

E(MeV)

EXPERIMENTS

a) $[H^0, H^+] > [H^+, H^+]$ ⇒ INCREASE DUE TO ELECTRON LOST $H^0 \rightarrow H^+ + e^-$

b) $[H^0, H^0] > [H^0, H^+]$: CAPTURE ⇒ AUGER PROCESS ⇒ CONTRIBUTION K-Shell

H^0
$H^+ \rightarrow C$

(15)

CORRELATION BETWEEN FORWARD AND BACKWARD EMISSION STATISTICS

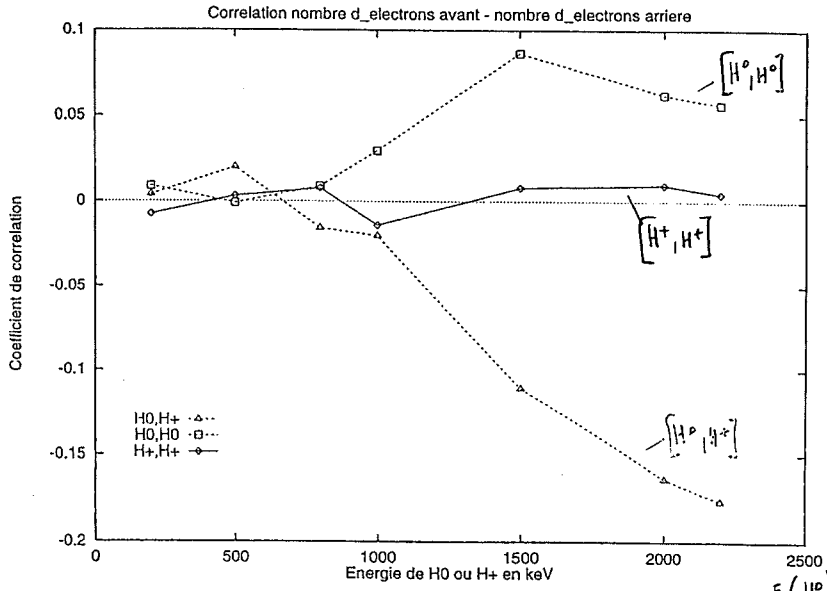

$[H^0, H^0]$

$[H^+, H^+]$

$[H^0, H^+]$

$E\left(\frac{H^0}{H^+}\right)$ (keV)

$[H^+, H^+]$: NO FORWARD - BACKWARD CORRELATION

$[H^0, H^+]$: INFLUENCE OF THE LOST ELECTRON

LOSS ⇒ ENTRANCE ⇒ $\gamma_B \nearrow$ $\gamma_F \searrow$

⇒ EXIT ⇒ $\gamma_B \searrow$ $\gamma_F \nearrow$ ⇒ NEGATIVE CORRELATION

$[H^0, H^0]$??

(16)

3rd EXAMPLE : $He^+, He^{++} \rightarrow Al$ (THICK TARGETS)

>< EXPERIMENTS (LINZ)

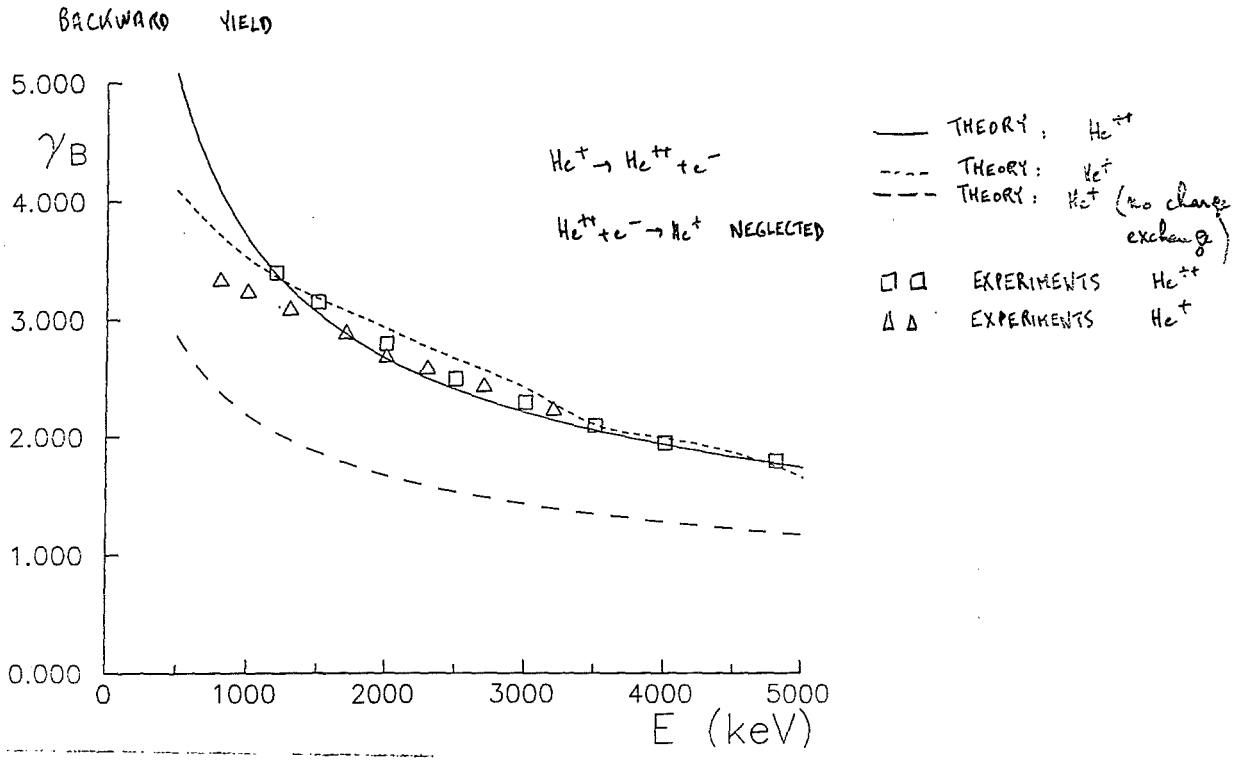

(17)

$He^+ \rightarrow Al$

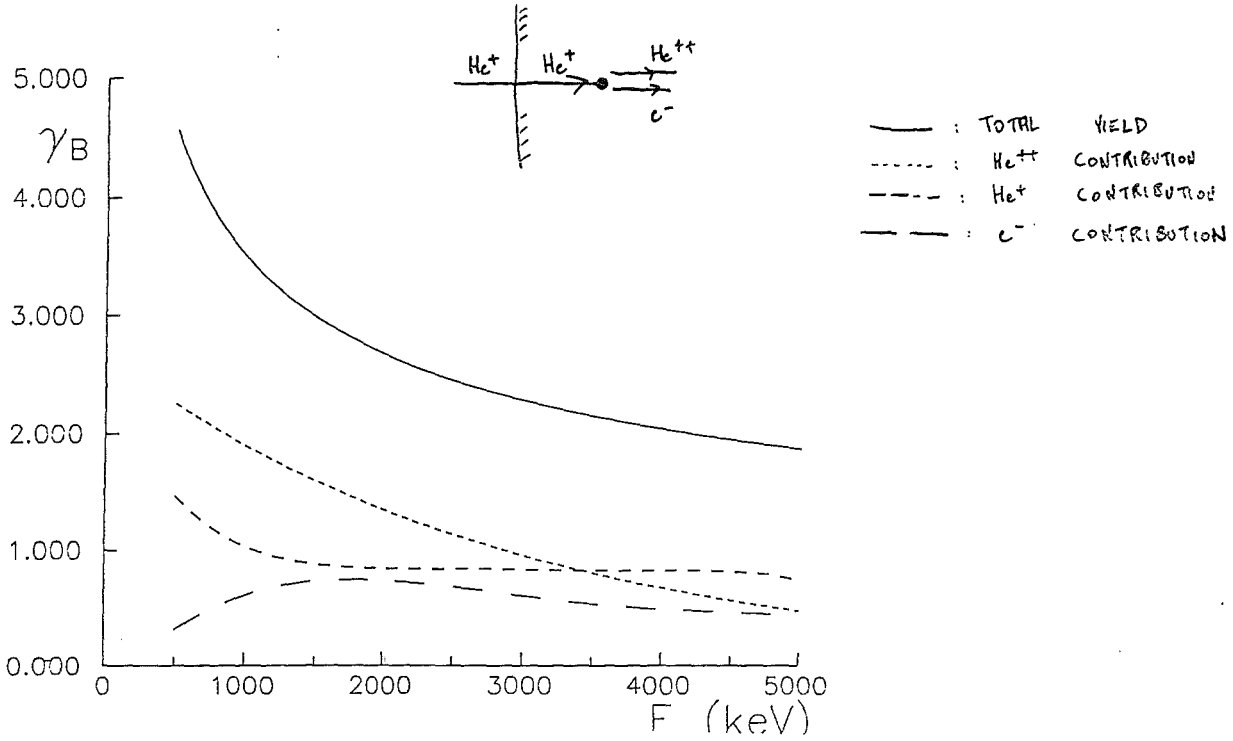

b POLYA PARAMETER FOR He^{++}, He^{+}, He^{+} (WITHOUT ENERGY LOSS)

$$P_n(\mu, b) = \frac{\mu^n}{n!} (1 + b\mu)^{-n - \frac{1}{b}} \prod_{i=1}^{n} (1 + (i-1)b)$$

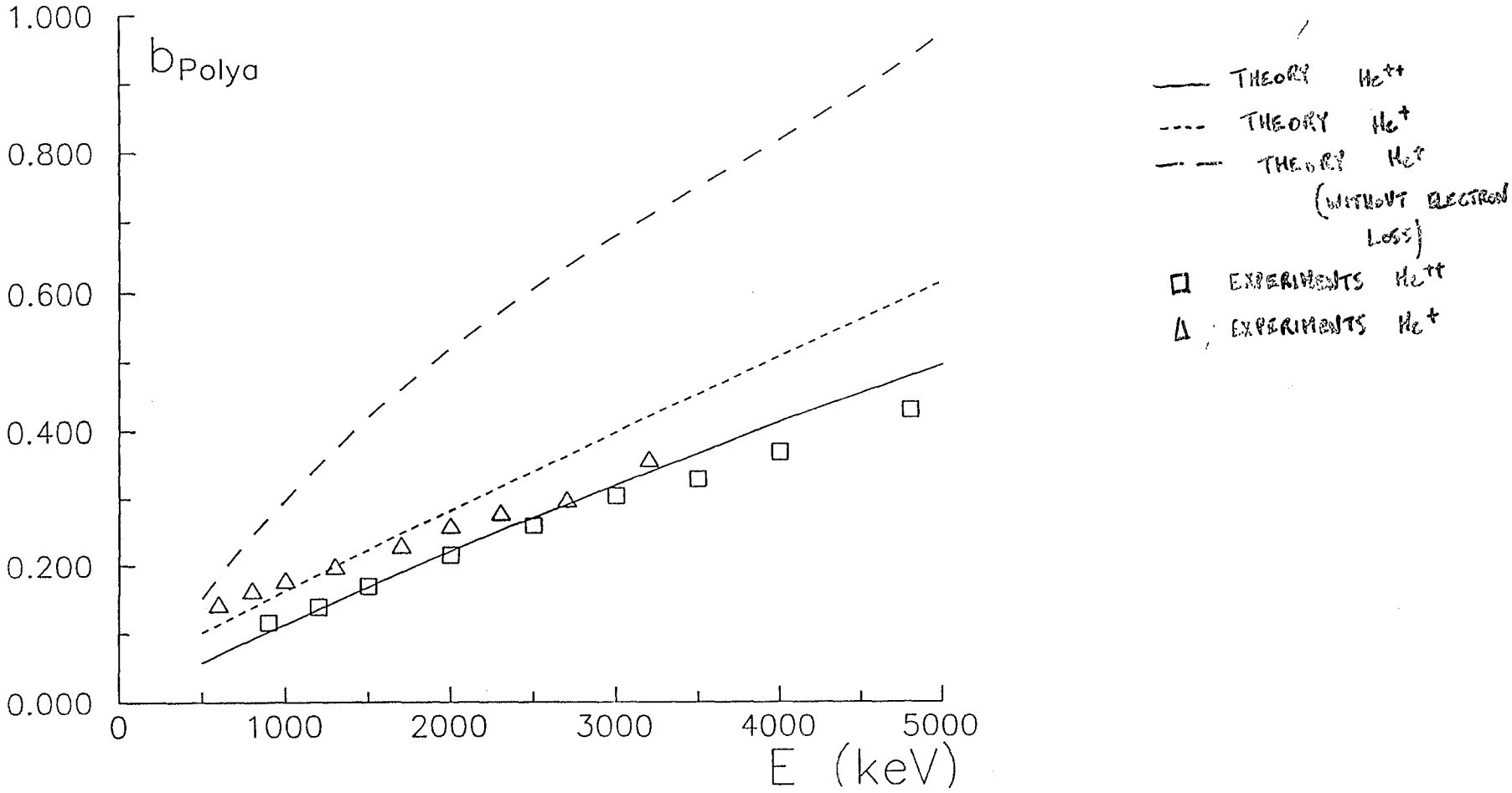

2nd APPLICATION : ELECTRON SPECTROSCOPIES FOR SURFACE ANALYSIS

BULK ≠ ANALYSIS → SURFACE ANALYSIS

⇓

IMPORTANT FOR TECHNOLOGICAL APPLICATIONS

MANY METHODS : SOME ARE BASED ON SMALL ELECTRON IMFP (A FEW Å FOR 5eV - 2000eV ELECTRONS) IN SOLIDS

1°) AES : AUGER ELECTRON SPECTROSCOPY

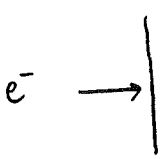

e^- ⇒ INNER-SHELL IONIZATION

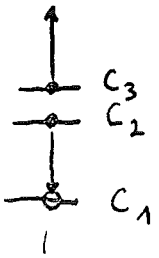

INNER-SHELL VACANCY

$C_1 C_2 C_3$ TRANSITION

2°) XPS : X-RAY PHOTOELECTRON SPECTROSCOPY

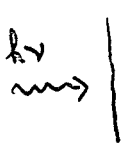

hν ⇒ INNER-SHELL IONIZATION

⇓

PHOTOELECTRON

FROM ± 1980 ⇒ INFLUENCE OF ELASTIC COLLISIONS (26)

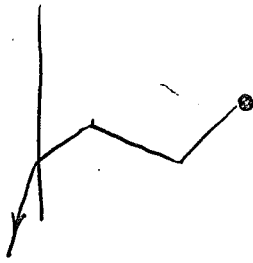

⇒ MONTE CARLO SIMULATION = BEST (?) TOOL

BRUSSELS : RECENT ACTIVITY IN COLLABORATION WITH S. TOUGAARD (ODENSE) AND A. JABLONSKI (WARSZAWA)

1°) ELASTIC ELECTRON BACKSCATTERING

⇒ COMPARISON OF MONTE CARLO SIMULATION WITH SEMI ANALYTICAL MODELS

ELASTIC BACKSCATTERING ⇒ A FEW COLLISION

⇒ COLLISION EXPANSION

MODELS : - 1 COLLISION

- OSWALD, KASPER, GRUHLER
  ⇒ COLLISION EXPANSION
  ANGULAR INTEGRALS EXACT

- DWYER
  WERNER, TILINN, HAYES } 1 EXA

+ TRANSPORT APPROXIMATION

$$\Sigma_{el}(\mu' \to \mu) = \frac{\Sigma_{tr}}{2} + \Sigma_p \delta(\mu - \mu')$$

ELASTIC ELECTRON BACKSCATTERING: ANGULAR CURRENT

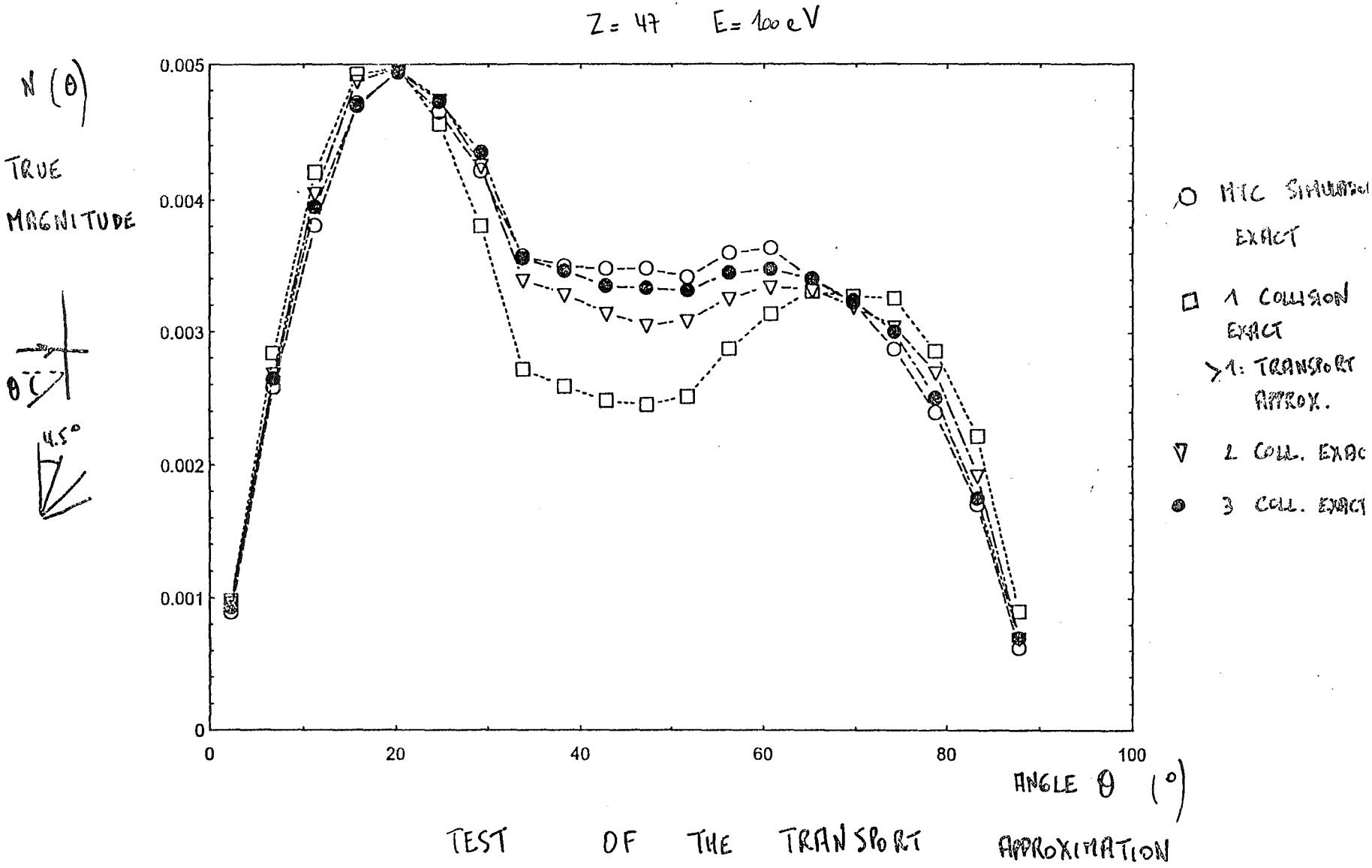

TEST OF THE TRANSPORT APPROXIMATION

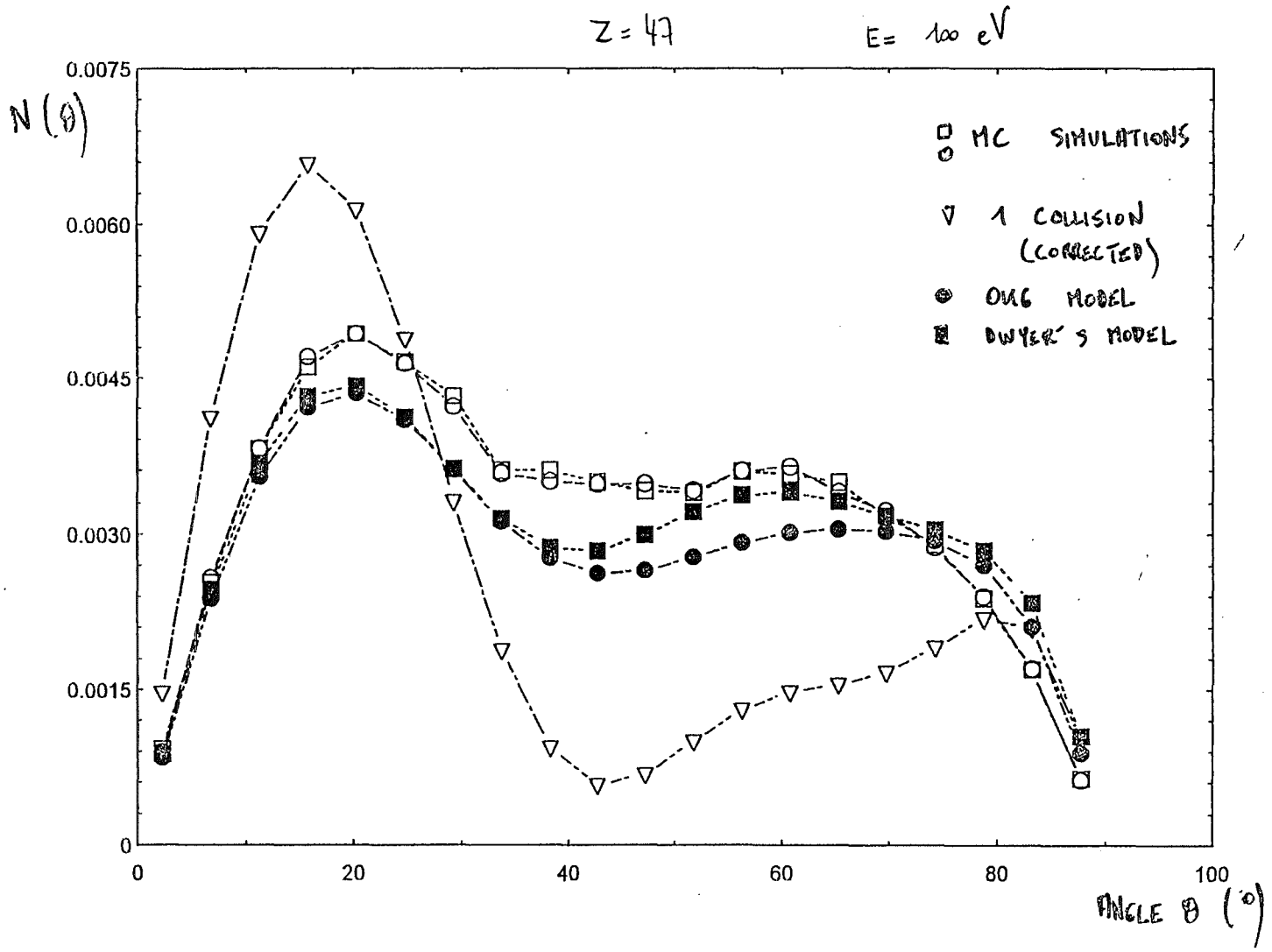

TEST OF THE MODELS : COMPARISON WITH MC SIMULATION

SOME SIMPLE VARIANCE REDUCTION TECHNIQUES

- NO INELASTIC COLLISIONS :

  SURVIVAL PROBABILITY $e^{-\lambda/\lambda_{in}}$

- AES SOURCE FAR FROM THE SURFACE

  $\Rightarrow$ BIASING OF THE SOURCE (ISOTROPIC)

  SPLITTING - RUSSIAN ROULETTE

3rd APPLICATION : CHARGING EFFECT IN INSULATORS

(S. BARTHOLOME THESIS)
COLLABORATION WITH
Prof. GANACHAUD (NANTES)

e^-
$h\nu$ → INSULATOR ⇒ ELECTRON EMISSION
H^+

⇓

CHARGING EFFECT

1) ELECTRON CASCADE

2) ELECTRONS - HOLES ⇒ POLARONS TRAPPED

3) TRAPPED POLARONS ⇒ ELECTRIC FIELD

⇓

DYNAMIC PROCESS (SELF-CONSISTENT)

e^- ⇒ . VERY QUICKLY : SURFACE : POSITIVE POTENTIAL

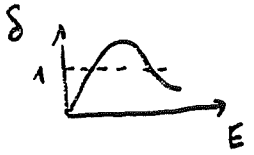

⇒ LOW ENERGY ELECTRONS ATTRACTED BACK

AND YIELD ≥ 1

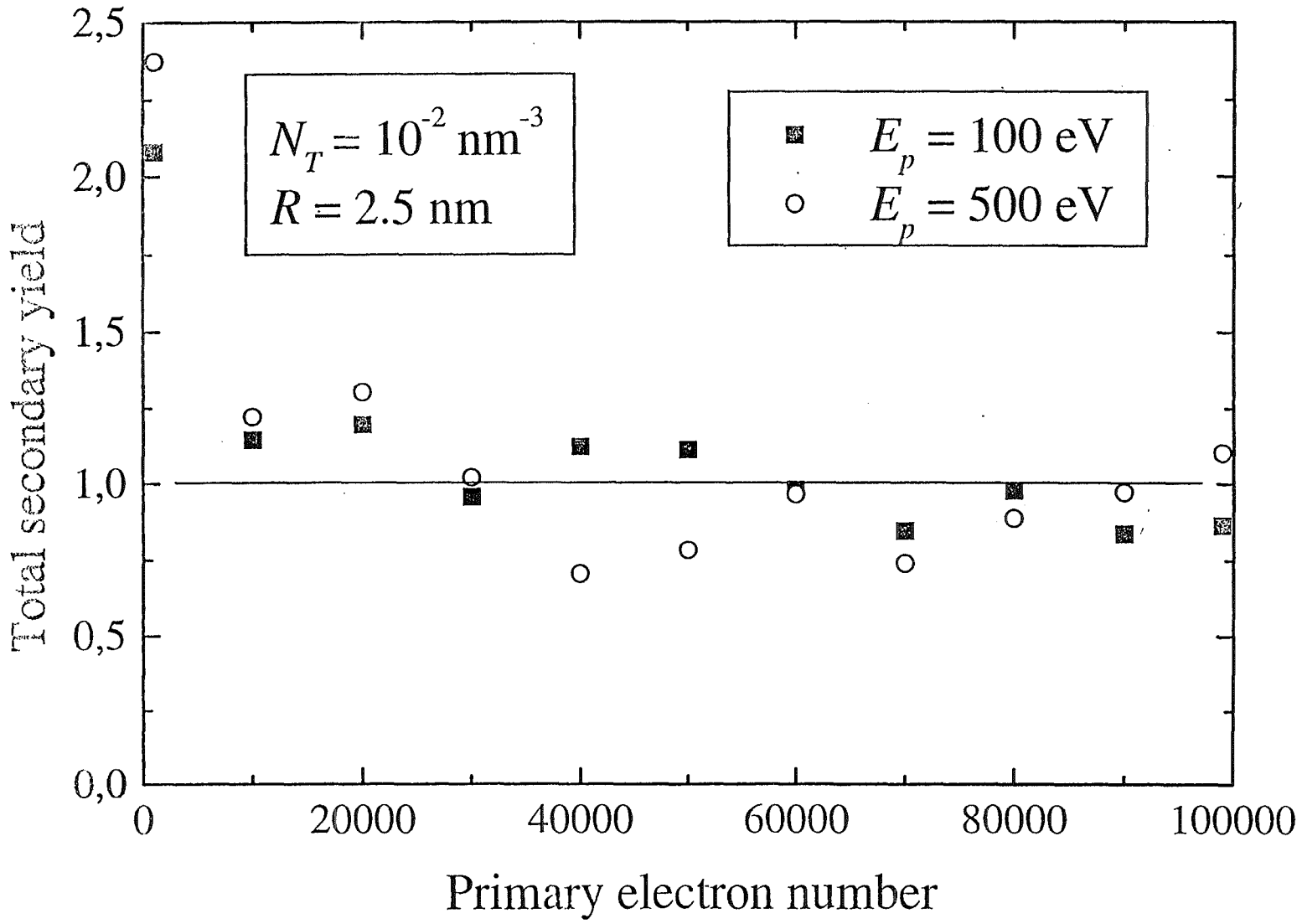
$N_T = 10^{-2}$ nm^{-3}
$R = 2.5$ nm
$E_p = 100$ eV
$E_p = 500$ eV
Total secondary yield
Primary electron number
2,5
2,0
1,5
1,0
0,5
0,0
0
20000
40000
60000
80000
100000

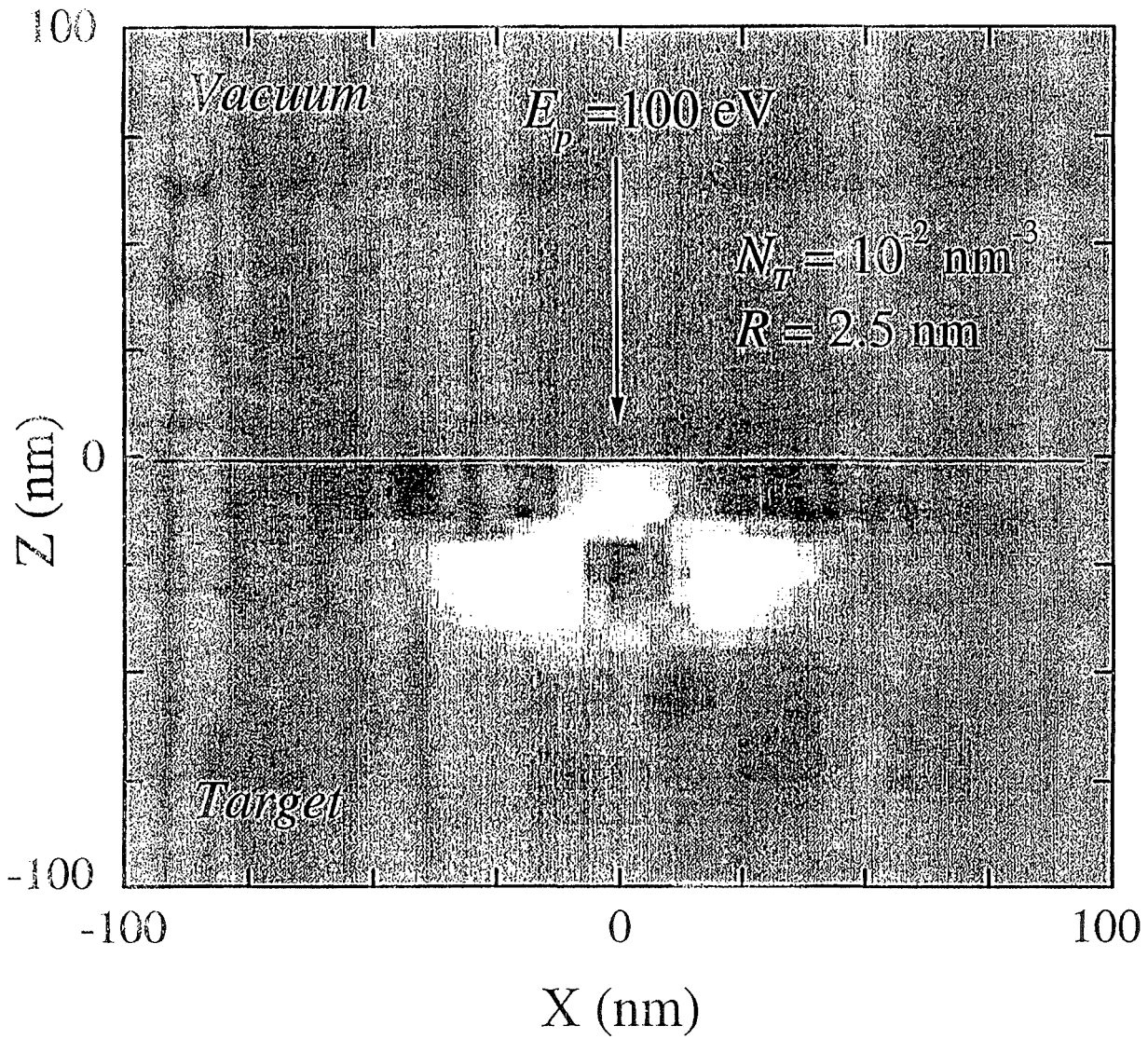

CHARGE DISTRIBUTION

BLACK ZONES: NEGATIVE

WHITE ZONES: POSITIVE

VERY NARROW BEAM

CONCLUSION

LOW ENERGY ELECTRON TRANSPORT ⇒ MONTE CARLO SIMULATION = BEST TOOL

FUTURE PROSPECTS :
- HIGH Z IONS
- CLUSTERS

⇒ COMPLICATED ANALOG SIMULATIONS

AES, XPS ⇒ MANY SYSTEMATIC CALCULATIONS

⇒ VARIANCE REDUCTION, ...

2nd IMACS SEMINAR ON MONTE CARLO METHODS

VARNA, BULGARIA, JUNE 1999.